Physiologically-based toxicokinetic modelling of lipophilic contaminants and plant secondary metabolites in dairy cows, calves and pigs

Dissertation zur Erlangung des akademischen Grades eines Doktors der Naturwissenschaften (Dr. rer. nat.)

Fachbereich Mathematik und Informatik

der Freien Universität Berlin

vorgelegt von

Jan-Louis Moenning

Berlin 2024

Die Arbeit wurde von Mai 2020 bis Januar 2024 am Bundesinstitut für Risikobewertung (BfR) in der Fachgruppe 84, Futtermittel und Futtermittelzusatzstoffe, unter der Betreuung von Dr. Jorge Numata erstellt.

Erstgutachter:	Prof. Dr. Max von Kleist
Zweitgutachter:	Prof. Dr. Ronette Gehring
Tag der Disputation:	09.07.2024

Table of Contents

1 Abstract

The determination of the transfer of undesirable substances and contaminants from oral exposure of farm animals into food of animal origin is essential to human risk assessment and management. The aim of this thesis was to develop physiologically-based toxicokinetic (PBTK) models that can be used to predict the concentration of specific contaminants in food of animal origin, based on the concentration in feed. Three groups of toxins were considered in the modelling approaches: polychlorinated dibenzo-p-dioxins (PCDDs) and polychlorinated dibenzofurans (PCDFs), for short "dioxins"; polychlorinated biphenyls (PCBs); and quinolizidine alkaloids (QAs). As the first two groups, dioxins and PCBs, are quite similar from a kinetic point of view, they have been evaluated together and separately from the QAs.

To gain a better understanding of the current state of research on the transfer of dioxins and PCBs to cow's milk, a review of the literature was first compiled and published in two parts. This showed that although many modelling approaches have been developed, sufficiently complex models are often based on limited data sets. Therefore, there is still an urgent need for PBTK models that have been validated with sufficient data to accurately predict the transfer of dioxins and PCBs into milk and tissue. Within the framework of this thesis, two well parameterised PBTK models were successfully developed on a broad basis of experimental measurements. The first published model is based on data derived from a PCB contamination incident and describes the distribution of three non-dioxin-like (ndl) PCBs in various tissues and milk of an adult cow during two lactations and one dry period as well as in their calves. This also includes the transfer of the investigated ndl-PCBs from the adult cow to her calf via placenta and milk. Of particular note is the ability of the model to distinguish between placental transfer and milk transfer through suckling with 10-14 % of the amount of congeners in calves at slaughter was due to placental transfer. Several parameters were derived for risk assessment quantifying theses transfer and distribution processes. The second published model uses data from a feeding study in which dairy cows were fed a mixture of numerous dioxins and PCBs at different time intervals during their negative energy balance (NEB) and positive energy balance (PEB) phases to assess the effects of different metabolic states on the transfer of contaminants into milk. This was done with a three-compartment model that was parameterised separately for the NEB and PEB phases and reliably predicts the concentration-time (ct) profile of the investigated contaminants in milk and blood. It is particularly worth mentioning that some of the parameters derived here were reported for the first time. Comparison of the parameters obtained in the different energy balance phases revealed that the transfer rates of the investigated contaminants are significant higher in the PEB phase than in the NEB phase. Significant differences were also found for other parameters such as β half-lives, but to a much lesser extent.

In the second part of the thesis, the knowledge gained from modelling approaches with dioxins and PCBs in cows was used to develop a model describing for the first time the transfer of three ndl-PCBs from feed into tissues of fattening pigs. The PBTK model was based on a

feeding study in which fattening pigs were fed with ndl-PCBs contaminated feed at different stages of their fattening period. The model consists of a liver and a fat compartment, which allows to describe the concentration of ndl-PCBs in the most relevant tissues for the consumer, i.e., muscle (based on its fat content) and liver. In addition, various transfer parameters were derived, which allows the quantification of the extent of transfer of these contaminants to these tissues under realistically changing feeding conditions and animal growth. The lowest transfer rate was obtained for PCB-28 with 9.57 % and the highest transfer rate was obtained for PCB-153 with 77.2 %.

In the final part of this thesis, QAs in dairy cows were investigated, which are kinetically completely different in their behaviour in comparison to dioxins and PCBs. QAs are potentially toxic plant secondary metabolites from lupins, a high-protein crop. Based on a feeding study in which dairy cows were fed subsequently with different amounts of QA-containing lupins, a PBTK model was developed to investigate the transfer of QAs into milk and its dose-dependency. As QAs are eliminated much faster from the body of the cows than dioxins and PCBs, aspects such as milking time and feeding time had to be taken into account. Since the ct-profile of QAs in milk during the depuration showed a biphasic behaviour, a three-compartment model was developed that induces a biphasic depuration phase in milk. This made it possible to describe the measured data quite well despite the high variability of the data points. The size of the experiment and the limited difference between the doses applies allowed no conclusion regarding a possible dose-dependent transfer. Several risk assessment parameters were derived, including transfer rates ranging from 1.05 % for angustifoline to 2.92 % for isolupanine and α-half-lives ranging from 0.26 d lupanine to 0.28 d hydroxylupanine. However, the very low concentrations covered by the β-half-lives are not expected to be relevant for risk assessment.

In summary, in the scope of this work, several PBTK models were successfully developed that describe and quantify the transfer of various contaminants to dairy cows, calves and fattening pigs. To make these models accessible to risk assessors, they will be implemented in the web tool BfR ConTrans.

2 Introduction

The transfer of environmental contaminants and its crucial role in risk assessment are central themes in understanding and addressing the multifaceted challenges posed by these substances with potentially negative effects on human health. The exposure of humans to environmental contaminants occurs through various pathways, as these substances traverse diverse environmental mediums. One such pathway is via the food chain. Subsequently, as contaminants can accumulate in food-producing animals and the products derived from them, the complexity of their journey necessitates a thorough investigation into their mechanisms and pathways of transfer from the environment via food producing animals and into the human food chain. Assessing contamination of food of animal origin becomes crucial in evaluating potential risks to human health, as the concentration of contaminants in the food chain directly impacts the extent of exposure. Therefore, comprehensive studies on the transfer dynamics, accumulation patterns, and exposure pathways are essential for assessing and managing the risk they pose.

Environmental contaminants are a growing concern for nature and humanity, since they can cause detrimental effects on the health of living beings [1]. Contaminants are defined as any physical, chemical, biological, or radiological substance or matter that adversely affects air, water, soil or living organisms [2]. They enter the environment either accidentally or deliberately, often but not always as a result of human activity. Some have been produced intentionally because of their useful industrial properties; others are simply by-products of industrial activity; still others occur naturally, and their abundance may or may not be altered by human activity [1-3].

A group of environmental contaminants that has come into the spotlight are persistent organic pollutants (POPs). POPs are organic chemicals that persist in the environment for a long time after release and often accumulate along the food chain until they may eventually reach concentrations that can have harmful effects on human health and the environment. They can be transported by air, water, soil organisms or migratory species and reach regions where they have never been produced or used [4-6]. Prominent members of this group include polychlorinated biphenyls (PCBs), polychlorinated dibenzo-*p*-dioxins (PCDDs) and polychlorinated dibenzofurans (PCDFs), Dichlorodiphenyltrichloroethane (DDT), poly- and perfluoroalkyl substances (PFAS) and many more (see [4] for a more exhaustive list).

Another important group of undesirable substances with potential negative health effects in humans are secondary plant and fungal metabolites, such as Δ^9-tetrahydrocannabinol, pyrrolizidine alkaloids, mycotoxins and quinolizidine alkaloids (QAs) [7]. Some of them can also be transferred from oral exposure of animals into foods of animal origin, thus becoming an exposure source for humans from the diet. This work is mainly concerned with QAs from lupins, a crop grown for its high protein content and used in dairy cow nutrition.

This work focuses on three groups of substances: PCDD/Fs, PCBs and QAs. Each of these groups consists of several congeners or compounds with a common base structure. Congeners

in chemistry are substances related to each other by origin, structure, or function. PCDD/Fs and PCBs have varying numbers and positions of the chlorine atoms. The compounds belonging to the group of QAs share a quinolizidine structure with various chemical groups attached.

2.1 Polychlorinated dibenzo-p-dioxins (PCDDs) and dibenzofurans (PCDFs)

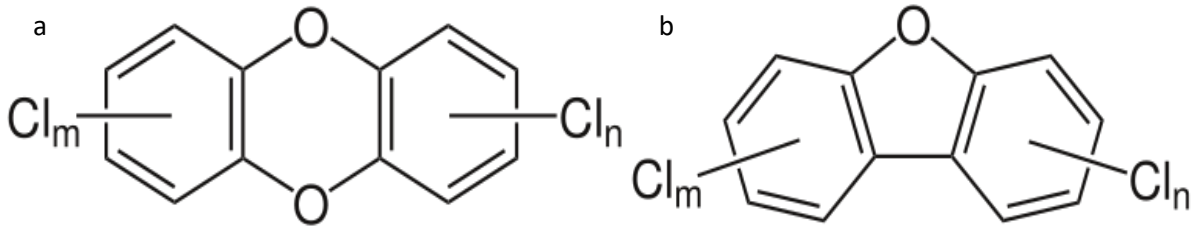

Figure 1: General structure of polychlorinated dibenzo-p-dioxins (PCDDs) (a) and dibenzofurans (PCDFs) (b).

PCDDs and PCDFs are two groups of tricyclic aromatic compounds giving rise to 75 and 135 congeners, respectively (Figure 1) [8]. They are also colloquially referred to as “dioxins”, as will also be done in this dissertation. The most extensively studied member is 2,3,7,8-tetrachlorodibenzo-*p*-dioxin (TCDD). It became known as a contaminant in Agent Orange, a herbicide used in the Vietnam War [9], and has the highest toxicity equivalency factor among the dioxins [10, 11].

The most striking chemical features of dioxins are their high lipophilicity (log K_{ow}>3) [12] and high chemical stability, resulting in long persistence in the environment. This is reflected as half-lives of several years in soil [13]. Some dioxins are the result of thermal processes that can occur naturally, such as in forest fires and volcanic activity. However, by mass, most dioxins were produced unintentionally as a result of human activity involving combustion processes, such as in industry or waste incineration [14-17]. Therefore, the concentration of dioxins in the environment also heavily depends on the geographic location, with higher concentrations near industrial and urban areas compared to rural areas [14]. Peak concentration of dioxins in the atmosphere were found around 1970-80s, when industries started reducing their emission of dioxins due to coming into force of policies regarding flue gas treatment [18]. Furthermore, the Stockholm convention on persistent organic pollutants of 2001 [4], which came into effect in 2004, requires the reduction or prevention of emission of dioxins into the environment as far as possible by applying the best available technologies. This likely caused a change in practices, so that nowadays the emission of dioxins from industrial sources is actually lower than from non-industrial sources [16, 19]. However, even if emission of dioxins could be completely stopped today, they would remain relevant for human health for many decades due to their persistence in the environment.

2.2 Polychlorinated biphenyls (PCBs)

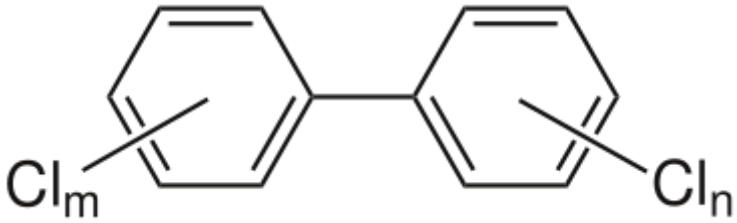

Figure 2: General structure of polychlorinated biphenyls (PCBs).

PCBs are double ring structures that are chlorinated to varying degrees. Depending on the number and position of chlorine atoms attached to the biphenyl structure, 209 different PCB congeners can be formed (Figure 2) [20]. However not all these congeners can be analytically quantified at once, so that frequently only a subset of these is analysed. In most cases, these are the 7 indicator PCBs (28, 52, 101, 118, 138, 153 and 180) and the 12 so called dioxin-like PCBs (77, 81, 105, 114, 118, 123, 126, 156, 157, 167, 169 and 189) [21]. Similar to dioxins, PCBs also exhibit high lipophilicity (log K_{ow}>3) [12] and long persistence in the environment, with half-lives in soil of several years [22]. The molecular conformation allows dividing PCBs into coplanar and non-planar. This molecular feature strongly correlates with the toxic mode of action of each congener, so that coplanar congeners have dioxin like (dl) action and non-planar ones have non-dioxin like (ndl) toxicity. This is discussed later in more detail. Unlike dioxins, PCBs are not natural substances, but were mostly deliberately produced commercially for their desirable chemical properties such as thermal stability, low water absorption and non-combustibility [23-25]. They were produced in large quantities between the 1930s and 1980s and were commonly used as mixtures marketed as Aroclor (Monsanto, USA), Clophen (Bayer, Germany), Phenoclor (Caffaro, Italy) or Kanechlor (Kanegafuchi, Japan) [26]. These mixtures were used in a wide range of products, including dielectric fluids in transformers and capacitors, heat transfer fluids lubricants [27] and paint [28]. Due to growing public awareness of PCBs adverse effects on human health and their ubiquitous presence in the environment their production was greatly reduced worldwide in the 1980s [29]. In addition, since 2004, the production of PCBs has been prohibited under the Stockholm Convention on POPs [4]. As a result of these efforts, environmental release of PCBs has been reduced in recent decades [26, 30]. However, due to their persistent nature; their use in products that are still in use today; and their appearance as by-products [31], they can still be found in the environment and affect human health.

2.3 PCBs and dioxins in humans

2.3.1 Effect of PCBs and dioxins on human health

Long-term exposure to dioxins and PCBs can have harmful effects on human health. With respect to their toxicity, dioxins and PCBs can be broadly categorized into two groups: dioxin-like (dl) PCBs and non-dioxin-like (ndl) PCBs. The toxicity of dl-PCBs is well studied, as it is strongly but not exclusively related to their ability to bind to the cytoplasmic Aryl hydrocarbon

receptor (AhR), a ligand-activated transcription factor [32-34]. In contrast, ndl-PCBs do not exhibit such affinity for AhR, because their non-planar structure does not fit into the specific pocket in the AhR [35].

AhR is expressed in various tissues and plays an important role in various biological processes. After binding, AhR is translocated from the cytoplasm to the nucleus, where it forms a complex with the AhR nuclear translocator (ARNT) [32, 34], among others, and regulates the expression of several target genes, including those encoding enzymes of the cytochrome P450 family 1, i.e. CYP1A1 and CYP1B1 (canonical pathways) [36-40]. Furthermore, it is known that AhR interacts with other receptor-mediated signalling pathways (non-canonical pathways), including nuclear factor-κB (NF-κB), nuclear factor erythroid 2-related factor 2 (NRF2), and estrogen receptor signalling [36-39]. As a result, AhR can play a significant role in regulating cell growth, differentiation [41], and immune response [38, 39]. Hence, any disruption or alteration in the activity of AhR can potentially have adverse effects on human health. Thus, it is not surprising that dioxins and dl-PCBs can cause developmental disorders, damage to the immune system, impairment of thyroid and steroid hormonal balance, and also cancer[42, 43]. The WHO classifies dioxins and dl-PCBs as “known human carcinogens” [44]. Furthermore, it has been discovered that men exposed in infancy or pre-puberty to TCDD may have impaired sperm quality, resulting in a reduced reproductive capacity [45]. Reduction in sperm quality is currently considered the most sensitive endpoint, and is thus basis for the Tolerable Weekly Intake (TWI) of 2 pg TEQ/kg body weight set by the European Union [46]. Besides their long-term effects, high doses of dioxins and dl-PCBs can have also acute toxic effects on e.g., liver and skin (chloracne) [47]. However, these acute effects require much higher doses not reached from the background contamination of the environment; such high doses are associated with local high release events such as the Seveso incident [48] or the Yoshu incident [49].

As the toxicity of dioxins and dl-PCBs is related to their affinity for the AhR and they occur as a mixture, their toxicity is in most cases not derived separately for each congener, but rather for the mixture. For this purpose, each congener is weighted with a toxic equivalency factor (TEF), which is directly related to its affinity for the human AhR. The toxicity of the mixture is then assessed using the TEF-weighted sum, which is presumably toxic equivalent (TEQ) amount of TCDD, which has TEF of one. The strongest affinity to AhR is associated with the congeners 2,3,7,8-TCDD and 1,2,3,7,8-PeCDD, and subsequently all other congeners are weighted with values less than one [11].

Since ndl-PCBs do not interact with AhR they cannot be assessed together with dioxins and dl-PCBs using a TEF. In general, ndl-PCBs are considered to be less toxic than dl-PCBs and are therefore less studied in this respect [50]. However, the toxic effects of some ndl-PCBs are known and the negative impacts on human health of others is under study [51]. In long-term animal studies, ndl-PCBs have shown adverse effects on the thyroid, liver, nervous system, immune system, endocrine system and reproduction [52]. Additionally, the International Agency for Research on Cancer (IARC) assessed PCB-153 as "possibly carcinogenic" in 2015 [53]. Because of the uncertainties surrounding the toxicity of ndl-PCBs, maximum levels for

these were not derived based on toxicological considerations but rather following the ALARA (As Low As Reasonable Achievable) principle [54].

2.3.2 Fate of dioxins and PCBs in humans

Generally, the primary exposure pathway for dioxins and PCBs in humans is through the consumption of high-fat foods, particularly animal products like meat, milk and eggs. Although other exposure pathways exist, such as inhalative [55-57] or dermal [58], their contribution to overall exposure is relatively insignificant compared to dietary intake. Indeed, more than 90% of human dioxins exposure occurs through food consumption [59]. Due to their lipophilic nature, most dioxins and PCBs are well absorbed from the gastrointestinal tract (GIT), as lipophilicity correlates well with permeation through the gut wall and subsequently with the extent of absorption [60]. After entering systemic circulation, these contaminants are strongly distributed into the adipose tissue leading to high bioaccumulation. Although slow [61], there are two possible routes of elimination of dioxins and PCBs from the human body, either via lipid excretion or metabolic degradation. Biotransformation occurs through complex metabolic pathways to hydroxylated, sulphated and glucuronidated and other metabolites. Hydroxylation occurs via the cytochrome P-450 (CYP) enzymes, in particular by CYP isoforms belonging to CYP1, CYP2 families. Interestingly, CYP enzymes induced by AhR are also involved in the metabolism of some congeners potentially resulting in an auto-induction of their metabolic degradation. Metabolism rates of PCBs are generally higher for congeners with fewer chlorine substitutions; however, the position of the substitution also plays a significant role in this respect [62]. In addition to metabolic degradation, these compounds can be eliminated from the human body through the excretion with fat. Fat is excreted mainly via feces, and it is possible that dioxins and PCBs diffuse through the intestinal wall and into the feces [63]. Bilary excretion may also contribute to excretion of these compounds into the feces, but this process is not dependent on the fecal fat concentration [64]. Another important pathway for the fat excretion is via lactation. During lactation, milk excretion is the most effective way for the mother to excrete fat and is therefore a very effective way of eliminating dioxins and PCBs from the body of the breastfeeding mother [65]. However, this also means that these lipophilic contaminants are transferred to the child through breast milk, presenting an exposure pathway [65, 66]. Since during breastfeeding infants consume mother's milk almost exclusively, it is crucial to make sure their concentration in mother’s milk is minimized. Indeed, the TWI for dioxins and dl-PCBs is set to ensure that the concentration in the nursing mother's milk is low enough to avoid adverse effects on their nursed children i.e., a reduction of their sperm quality [46].

2.4 Dioxins and PCBs in farm animals

Since human exposure to dioxins and PCBs occurs mainly through the consumption of fatty animal products, it is key to understand their transfer in farm animals.

As in humans, exposure to dioxins and PCBs in farm animals occurs predominantly orally. The main source of oral exposure is the feed, but passive uptake of soil can also play an important role, depending on the species and husbandry conditions [67]. In addition, other less common sources of oral exposure, such as licking contaminated paint [68], can also significantly increase the exposure of the animal. Once ingested, the congeners enter the GIT where they are absorbed mainly in the intestine. Non-absorbed congeners stay in the feces and get excreted from the animal's body. Although this principle holds true for all animals, there are major interspecies differences in the physiology/anatomy of the GIT and hence the fate of the contaminants. For example, cows and other ruminants have several stomachs, including a rumen, where many substances undergo biotransformation. However, in regard to dioxins and PCBs there is no evidence that degradation occurs in the rumen [69]. After they have reached the intestine, the contaminants are rapidly absorbed into systemic circulation. There is evidence that these compounds enter the bloodstream not only via first pass, but also enter the systemic circulation via the lymphatic system due to their high lipophilicity [70]. From the blood, the distribution of congeners into all tissues of the animal occurs, whereby the extent of distribution strongly correlates with the fat content of the respective tissue. This is also the reason why the current limits for dioxins and PCBs in animal meat are based on the fat content [54]. Once distributed into tissues, dioxins and PCBs can also be eliminated from the body; the elimination rates and also the routes are strongly species- and sex-dependent. However, there are two potential pathways that are present in all species and sexes: metabolic degradation in the liver and excretion together with fat e.g., via feces. In addition, there also exist species- and sex-dependent fat excretion pathways like milk excretion in mammals and the laying of eggs in chicken [71]. Milk excretion is the main route of fat excretion in dairy cows. A modern high yielding dairy cow can excrete over 10 000 L of milk , containing 350 kg of milk fat, in a single lactation period [72]. Although, the excretion of milk and the laying of eggs helps to reduce the body burden of these animals, milk and eggs are extensively used as human food and present therefore a major exposure source for humans. The growth of the animal can also help to reduce the concentration of contaminants in the animal's tissues by diluting them; this effect is particularly apparent in fattening animals slaughtered during or immediately after their main growth period, such as fattening pigs [73] and chickens [74] or calves [68].

To help reduce and to understand the exposure of humans with dioxins and PCBs, it is necessary to be able to predict the transfer of dioxins and PCBs from oral exposure into animal tissues or products for human consumption, such as milk. To do that it is essential to consider all relevant processes that influence their transfer. As there are several such processes involved, it is necessary to describe them comprehensively to ensure accurate predictions. This can be done by using so-called physiologically-based toxicokinetic (PBTK) models.

2.5 Quinolizidine alkaloids (QAs)

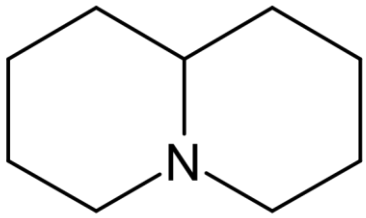

Figure 3: Quinolizidine base structure, always contained in quinolizidine alkaloids.

Quinolizidine alkaloids (QAs) are a group of toxins whose structure contains a quinolizidine ring. Almost 400 QAs have been identified (Figure 3) [75]. They are secondary plant metabolites and are mainly found in legumes. The highest occurrence of QAs is found in so-called primitive legumes of the genera *Lupinus, Ulex, Cytisus, Sophora, Genista* and *Orphanodendron* [75]. Lupins (*Lupinus*) in particular are of interest, as they have a long tradition as a source of protein in animal feed and therefore represents an alternative to soybeans. More than 500 lupin species have been identified, with varying levels of QAs [75-77]. They can be divided into bitter lupins, where the total QA content is up to 8% of the dry matter, and sweet lupins, where the total QA content should not exceed 0.05% of the dry matter [78]. Only the latter are to be used in animal feed, where it is also recommended that the total QA content should not exceed 0.02% of the dry matter [7, 79].

QAs are weakly basic, which favours their vascular permeability, enabling them to be transferred into milk. As QAs have toxic effects and can therefore have a negative impact on human health, they are important for risk assessment. However, past investigations had mainly been done with the QAs sparteine and lupanine. QA toxicity is related to the inhibition of acetylcholine receptors and voltage-gated ion channels at the motor end plates of neurons in the central and peripheral autonomic nervous systems. This may result in acute toxic effects, such as respiratory depression, vomiting and tachycardia [7,79]. However, no toxic endpoint has been identified for chronic exposure [7].

Limited data are available on kinetics of QAs, mostly for sparteine and lupanine. In cattle, QAs have been shown to be absorbed from the gastrointestinal tract, but the velocity and extent of absorption appears to be conger-specific [7, 80-82]. They are eliminated from the cow's body much more rapidly than dioxins or PCBs, with half-lives measured in hours rather than days or months [7, 80-82].

2.6 Physiologically-based toxicokinetic (PBTK) Models

PBTK models are mathematical models that describe the fate of toxic chemicals through the body based on the principles of kinetics describing the absorption, distribution, metabolization and elimination of these toxic chemicals [83]. Alternatively, when considering pharmaceutical products, such models are called physiologically-based pharmacokinetic (PBPK) models, which are conceptually the same. PBTK and PBPK models (PBK models for short) take into account the physiology of the organism, the properties of the chemical, and

the exposure route to predict the distribution of the chemical throughout the body and its elimination from the body.

The development of PBK models can be traced back to the 1930s, when researchers began to use mathematical modelling to study the distribution and elimination of drugs in the body [84, 85]. In the early years of PBK modelling, the approach was severely limited by the computational capabilities of the time, which only allowed the use of low complexity models under certain conditions such as steady state [85].

As computer technology advanced, so too did the capabilities of PBK modelling. With better computational capabilities, not only more complex models could be used, but also more complex procedures for deriving them could be applied, such as fitting approaches or Quantitative/Qualitative Structure Activity Relationship (QSAR) methods to derive model parameters [86]. This trend continues until today, especially with use of more sophisticated machine learning approaches and will probably also continue into the future.

Today, PBK models are widely used in toxicology, pharmacology, and environmental health. They are used to predict the local internal exposure of chemicals (as an aid to understand potential toxicity), optimize drug-dosing regimens, and evaluate exposure scenarios. With ongoing advancements in computational power and data availability, PBK models continue to evolve and improve, providing a valuable tool for understanding the complex interactions between chemicals and the body.

At the core of a PBK model is a system of differential equations that represent the flow of chemicals between different compartments of the body, such as the blood, organs, and tissues. These equations are based on physiologically relevant parameters such as blood flow rates, tissue volumes, and chemical-specific properties such as binding affinity [87]. The complexity of these models can vary greatly, from simple, linear, one-compartment models with very limited physiological representation, to very complex models with many non-linearly interacting compartments representing many different parts of the body. For low complexity models, the distinction between a toxicokinetic (TK) model and **PB**TK model can be hard to make, as the transition is fluid. The decision on how complex a model for a compound should be depends on many different factors, such as the purpose of the model e.g., which tissues or processes need to be predicted; another factor is the available data, as more complex models require more data; the last factor is what processes have a significant effect on the overall kinetics of the compound.

In the case of dioxins and PCBs, it is known that two-compartment TK models are sufficient to describe the concentration-time curve of milk in feeding studies of lactating cows accurately [88]. This is mainly due to the highly lipophilic nature of dioxins and PCBs, which causes them to accumulate in fat tissue, from which they are only slowly released. Therefore, dioxins and PCBs inside the animal can be broadly divided into two compartments i.e., those contained in fatty tissue and those not contained in fatty tissue. This two-compartment behaviour can be observed particularly well during the depuration phase after exposure of the animal. The concentration-time profile will resemble a biexponential function, i.e.

$$C(t) = C_0 e^{\lambda_0 t} + C_1 e^{\lambda_1 t} \quad (1)$$

with $C_0, C_1 > 0$, $\lambda_0, \lambda_1 < 0$ and $C(t)$ being the concentration at time t after start of depuration. Visually, under semi logscale this is characterized by an initial rapid decline followed by a slower, sustained decline.

However, despite the fact that the concentration-time curve of dioxins and PCBs can be accurately described by a two-compartment PBTK model, there are several reasons why a more detailed model may be useful. One reason could be that the concentration in a specific edible tissue needs to be predicted and therefore needs its own compartment. Another reason for using a more complex model may be to improve the estimation of model parameters. This makes it easier to specify model parameters based on the animal's physiology and the contaminant's chemical properties. This can also make it easier to account for changes in the physiological properties of the animal e.g., due to the growth of the animal or extrapolate between animals (e.g. different breeds).

Conversely, a less complex model, i.e., one compartment model, can also be used, as it requires even less data. However, doing so will result in a generally less accurate model for dioxins and PCBs (one that may be accurate for some tissues and time points, but inaccurate for others). Therefore, such models should only be used if the paucity of the data makes it necessary.

The most challenging part of developing such a model is usually the estimation of the model parameters. These parameters include those describing only compound unspecific physiological processes, such as blood flows or compartment volumes, which are reusable for different compounds but also compound specific parameters such as partition coefficients or clearance rates. As the compound specific parameters have to be estimated separately for each compound, they tend to be the most difficult to estimate. However, much effort has been put into developing methods to estimate these parameters experimentally via in vitro or vivo experiments, but also from purely in silico methods, such as QSAR [86]. However, in silico prediction of parameter such as metabolic degradation remains a big challenge up to this day.

In general, these models can become very complex. However, it should always be kept in mind that "everything should be as simple as it can, but not simpler" (often attributed to Einstein) and "all models are wrong, but some are useful" (quote from George Edward Pelham Box, British Statistician, 1919-2013). This means that not all processes need to be accounted for in such a model if they do not add any relevant improvement to the predictive capabilities of the model. In the case of dioxins and PCBs, the elimination is so slow that processes like milking and feeding can be considered as a continuous rather than discrete events. Including the time of milking would not improve the model significantly. In contrast to dioxins and PCBs, other undesirable substances such as QAs are eliminated from a cow's body relatively quickly [7], making it important to consider the exact exposure time and milking time.

3 Objective

Predicting the concentration of contaminants in food is a necessary prerequisite for risk assessment to estimate the potential risk from human consumption of contaminated food caused by oral exposure of the animals with undesirable substances. One possible tool to achieve this is PBTK modelling, which allows a dynamic time-dependent prediction of the content in specific tissues and concentrations in products of animal origin.

The main objective of this work is to develop such PBTK models for PCBs, dioxins and QAs in farm animals. As the main route of elimination of PCBs and dioxins is strongly linked to fat excretion such as lactation, an important focus is on developing PBTK models for lactating dairy cows. The developed PBTK models allow to describe the transfer of PCBs and dioxins from animal feed into edible products of these animals such as milk or muscle tissues. To this end, a comprehensive review was carried out to summarize the available literature describing the transfer of dioxins and PCBs from feed to milk of cows. The knowledge gained is then used to develop two PBTK models for lactating cows. One of these models focuses on the transfer of many different PCBs and dioxins into milk of high yielding dairy cows, where it is also investigated whether the metabolic status of the animals have meaningful impact on the overall transfer. The other model goes one step further and additionally describes the transfer via milk and placenta into the calf, but only for a small subset of these PCBs. In the second part of the study, core concepts regarding the transfer of dioxins and PCBs into cows were adapted to a monograstic species, namely fattening pigs. This adaptation enabled the derivation of PBTK models describing the transfer of dioxins and PCBs into the edible tissues of fattening pigs.

Finally, a PBTK model for a group of undesirable substances that are physicochemically different from PCBs and dioxins, i.e., QAs from lupins, is derived. QAs are not known to accumulate [7] in the animal, but they are transferred into the milk of dairy cows.

4 Mathematical background

4.1 Analytical solution of first-order TK models

As already mentioned in the introduction, TK models are typically described via compartment models, which in turn can be described in terms of differential equations. In the following case we assume first-order kinetics, i.e.

$$\dot{A}_i(t) = \sum_{j=1, j\neq i}^{m} A_j(t)\, a_{j\to i} - A_i(t)\left(k_i + \sum_{j=1, j\neq i}^{m} a_{i\to j}\right) + I_i(t) \tag{2}$$

for all $i \in \{1, \dots, m\}$ describing the amounts in the m compartments with $I_i(t), a_{j\to i}, k_i \geq 0$ for all $i, j \in \{1, \dots, m\}$. Here $A_i \geq 0$ describes the amounts in compartment i; $a_{j\to i}$ describes the transition rate from compartment j to i; k_i describes the elimination rate in compartment i; and $I_i(t)$ is the input into that compartment from outside the system (e.g., via feed) at time $t \in \mathbb{R}$. If one assumes that $I(t) = (I_1(t), \dots, I_m(t))^T \equiv 0$, then it can be deduced that the system is never gaining mass such that

$$\sum_{i=1}^{m} \dot{A}_i(t) = -\sum_{i=1}^{m} A_i(t) k_i \leq 0. \tag{3}$$

The system described in equation (2) can also be described via matrices, i.e.

$$\dot{A}(t) = MA(t) + I(t) \tag{4}$$

with $M = \left(m_{i,j}\right)_{i,j\in\{1,\dots,m\}} \in \mathbb{R}^{m\times m}$ being the transition matrix, where

$$m_{i,j} = \begin{cases} -\left(k_i + \sum_{l=0, l\neq i}^{m} a_{i\to j}\right) & if\ i = j \\ a_{j\to i}\ else \end{cases} \tag{5}$$

and $A(t) = (A_1(t), \dots, A_m(t))^T$ the amount vector.

The solution for equation (4) is given by

$$A(t) = \int_0^t e^{M(t-\check{t})} I(\check{t})\, d\check{t} + e^{Mt} A(0) \tag{6}$$

for a starting vector $A(0)$ [[89], Chapter 4.7]. If one assumes again $I(t) \equiv 0$, then equation (6) becomes

$$A(t) = e^{Mt} A(0) = \sum_{i=1}^{m} e^{\lambda_i t} v_i \alpha_i \tag{7}$$

for some $\alpha_i \in \mathbb{C}$ and $v_i \in \mathbb{C}^m$ is the eigenvector associated to the eigenvalue $\lambda_i \in \mathbb{C}$ of M with $Re(\lambda_i) \leq 0$ [Theorem 10.11 (i), [90]]. If one assumes that M is invertible then for $I(t) \equiv const.$ equation (6) becomes

$$A(t) = A^* + e^{Mt}(A(0) - A^*), \tag{8}$$

where A^* is the solution in steady state, i.e.

$$0 = MA^* + I \tag{9}$$

$$\Leftrightarrow A^* = -M^{-1}I. \tag{10}$$

The assumption that M is invertible is true if and only if M is outflow connected [Theorem 10.11 (ii), [90]], i.e. for every compartment $i \in \{1, \dots, m\}$ exist compartments $i_1, \dots, i_n \in \{1, \dots, m\}$ for some $n \in \mathbb{N}$ with $a_{i \to i_1}, a_{i_1 \to i_2}, \dots, a_{i_{n-1} \to i_n}, k_{i_n} > 0$.

In PBTK modelling, a common scenario involves slaughtering animals at the end of the study after a long depuration phase. This can provide valuable experimental data on the contaminant amounts in each model compartment at that specific time point. To derive model parameters from such data, it is essential to understand how the transition matrix influences the ratios between contaminant amounts in different compartments. For this, it is assumed that M is invertible and strongly connected (⇔irreducible), i.e. for all pairs of compartments $i, j \in \{1, \dots, m\}$ there exist $i_1, \dots, i_n \in \{1, \dots, m\}$ for some $n \in \mathbb{N}$ with $a_{i \to i_1}, a_{i_1 \to i_2}, \dots, a_{i_{n-1} \to i_n}, a_{i_n \to j} > 0$. Then a good assumption for this is that the system is in a pseudo steady state, i.e. the amount vector lives on $span(v_m)$, where $v_m \in \mathbb{R}^m_{+,0}$ is an eigenvector associated to the largest eigenvalue $\lambda_m \in \mathbb{R}_-$ of M [Theorem 10.2 (iii, iv), [90]]. This follows from equation (7), i.e.,

$$A(t) = e^{\lambda_m t} v_m \alpha_m + o\left(e^{\lambda_m t}\right). \tag{11}$$

Here, $\alpha_m > 0$ if $A(0) \in \mathbb{R}^m_{+,0}/\{0\}$. To see $\alpha_m > 0$ first note that for any $A(0) \in \mathbb{R}^m_{+,0}$ if $\alpha_m < 0$ than there exists a $t > 0$ so that $A_i(t) < 0$ for some $i \in \{1, \dots, m\}$ ↯. Therefore $\alpha_m \geq 0$ for any $A(0) \geq 0$. Next, let $A(0) \in \mathbb{R}^m_{+,0}/\{\mathbf{0}\}$ then $A(t) > 0$ for any $t > 0$ as M is strongly connected. Now let $e_1, \dots, e_m$ be the canonical base of $\mathbb{C}^m$ then $e_i = \sum_{j=1}^m v_j \beta_j^i$, where $\beta_j^i \in \mathbb{C}$ and $\beta_m^i \in \mathbb{R}^m_{+,0}$ for all $i, j \in \{1, \dots, m\}$ with at least $\tilde{\imath} \in \{1, \dots, m\}$ so that $\beta_m^{\tilde{\imath}} > 0$ as all the eigenvectors $v_1, \dots, v_m$ are also a minimal base of $\mathbb{C}^m$ and $v_m \in \mathbb{R}^m_{+,0}$. Finally let $A(t) = \tilde{A}(t_1) = \sum_{i=1}^m \tilde{A}_i(t_1)\, e_i = \sum_{i=1}^m e^{Mt_1} \tilde{A}_i(0)\, e_i = e^{\lambda_m t_1} v_m \sum_{i=1}^m \tilde{A}_i(0)\, \beta_m^i + o(e^{\lambda_m t_1})$, where $\tilde{A} = (\tilde{A}_1, \dots, \tilde{A}_m)$ is the solution of (7) with $\tilde{A}(0) = A(t_2) > 0$ for $t = t_1 + t_2$ and $t, t_1, t_2 > 0$. Here $0 < e^{\lambda_m t_1} \tilde{A}_{\tilde{\imath}}(0) \beta_m^{\tilde{\imath}} \leq \sum_{i=1}^m e^{\lambda_m t_1} \tilde{A}_i(0)\, \beta_m^i \overset{!}{=} e^{\lambda_m t} \alpha_m$.

□

4.2 Deriving transfer parameters

Beside this, the analytical solution of this problem can also be used to derive transfer parameters relevant for risk assessment. One very important parameter, the transfer rate during steady state (TR_{ss}) into some animal product such as milk, which describes the share of ingested contaminants that end up in the product. It can be derived using the steady state solution A^* defined in equation (10). For this let $i \in \{1, \dots, m\}$ be the compartment in which the excretion into the product of interest happens, e.g., udder, then

$$TR_{ss} = \frac{A_i^* k_i}{\sum_{j=1}^{m} I_j}, \tag{12}$$

where $I \in \mathbb{R}_{+,0}^m / \{\mathbf{0}\}$ is the constant input into the system. The other frequently sought parameters are the half-lives $\tau_i \in \mathbb{R}_+$ with $\in \{1, \dots, m\}$. It should be noted that in practise PBTK models are often of such a form that they induce eigenvalues λ_i, which do not have an imaginary component; otherwise the definition of half-lives can be problematic. Indeed this holds true if the longest circuit in the compartment model has at most length two [Theorem 12.6, [91]], i.e. there do not exist $n > 2$ distinct compartments $i_1, i_2, \dots, i_n \in \{1, \dots, m\}$ with $a_{i_1 \to i_2}, \quad a_{i_2 \to i_3}, \dots., a_{i_{n-1} \to i_n}, a_{i_n \to i_1} > 0$. Furthermore, assume that M is invertible ($\Rightarrow \lambda_i < 0$ for all $i \in \{1, \dots, m\}$) than the half-lives are given by

$$\tau_i = -\frac{\ln(2)}{\lambda_i}. \tag{13}$$

This follows directly from equation (7). However, a big problem with multiple half-lives describing the depuration of contaminant in a probe matrix μ, i.e.

$$A_\mu(t) = \sum_{i=1}^{m} e^{\lambda_i t} A_\mu^i \tag{14}$$

with $A_\mu^i \in \mathbb{R}$ with $i \in \{1, \dots, m\}$, is that A_μ^i has a significant influence on the shape of the curve. For example, some A_μ^i could be very small compared to the other so that the half-life τ_i becomes practically irrelevant for risk analysis even if τ_i itself is quite large. Therefore, it would be desirable to express the relevance of the individual τ_i half-lives. For the following, it is assumed that M is invertible and $A_\mu(0)$ is the steady state. The most straightforward way would be to normalize A_μ^i, i.e.

$$\overline{A_\mu^i} = \frac{A_\mu^i}{\sum_{j=1}^{m} A_\mu^j}. \tag{15}$$

However, the influence of these parameters on the shape of the curve can be quite hard to judge intuitively. Instead, it could be more useful to report the time intervals when each half life is the most relevant, i.e., the $\tau_{\tilde{\imath}}$ with $\tilde{\imath} = argmax_{i \in \{1,\dots,m\}} \left\{ \frac{d}{dt} A_\mu^i e^{\lambda_i t} \right\}$. In the case of biexponential decay, this could be expressed via the transition time $\tilde{t}$, i.e.

$$\frac{d}{dt}A_\mu^1 e^{\lambda_1 t}|_{t=\tilde{t}} = \frac{d}{dt}A_\mu^2 e^{\lambda_2 t}|_{t=\tilde{t}} \tag{16}$$

$$\Leftrightarrow \lambda_1 A_\mu^1 e^{\lambda_1 \tilde{t}} = \lambda_2 A_\mu^2 e^{\lambda_2 \tilde{t}} \tag{17}$$

$$\Leftrightarrow \tilde{t} = \frac{ln\left(\frac{\lambda_1 A_\mu^1}{\lambda_2 A_\mu^2}\right)}{\lambda_2 - \lambda_1}. \tag{18}$$

Then τ_1 is more relevant for $t < \tilde{t}$ and τ_2 for $t > \tilde{t}$ with $\tau_1 < \tau_2$.

An alternative to reporting multiple parameters describing the depuration phase would be to try to condense this information into one single parameter. This could be done with the mean residence time (MRT), which is the mean time a molecule of the contaminant stays in the system (based on [92]). Assuming again M is invertible, then it can be calculated as

$$MRT = \sum_{i=1}^{m} \pi_i \left(\int_0^\infty t e^{Mt} \bar{I} dt \right) k_i \tag{19}$$

$$= \sum_{i=1}^{m} \pi_i (\mathrm{M}^{-2}\bar{I}) k_i, \tag{20}$$

where $\bar{I}$ is the normalized input vector, i.e., $\sum_{i=1}^{m} \bar{I}_i = 1$ and π_i is the canonical projection into compartment i. In addition, $MRTln(2)$ could be interpreted as a type of average half-life.

4.3 Numerical ordinary differential equation (ODE) solver

Although the analytical solution in equation (6) of differential equation (2) can be very useful, it can be difficult to compute if the requirements of simplification ($I(t) \equiv const.$) for equation (7) are not meet. Furthermore, the problem to be solved often does not have the exact form described by equation (2) with the most common divergence from this being that M is not constant but rather time-dependent, as the animal physiology changes over time. In such cases, a different approach must be taken. One possibility without deriving a new analytic solution is by estimating M with a piecewise constant matrix $\widetilde{M}$. Then this problem can be solved again using the analytical solution described above. However, if this is also not satisfactory, e.g. when Michaelis-Menten kinetics are assumed instead of purely first-order kinetics [93], then a numerical approach will often become necessary for solving $\dot{A}(t) = f(t, A(t))$. Over the years, a variety of such methods have been developed, of which the Euler method is probably the best known [94].This method is based on the fact that that the derivative of a function defined as the limit, which is used to approximate it, i.e.

$$f(t, A(t)) = \dot{A}(t) \approx \frac{A(t+h) - A(t)}{h} \tag{21}$$

$$\Leftrightarrow A(t+h) \approx f(t, A(t))h + A(t). \tag{22}$$

for some small $h > 0$. Therefore, $A(t)$ approximated iteratively given some starting point $A_0 = A(0)$ and

$$A_{i+1} = f(t_i, A_i)h + A_i \tag{23}$$

for $h > 0$ and some $n \in \mathbb{N}$ with $hn = t$ and $hi = t_i$ with $i \in \{0, \dots, n\}$. Then $A_n \approx A(t)$. However, the Euler method is often not precise enough which is why other methods are also widely used such higher order Runge-Kutta methods [95].

4.4 Fitting algorithms

When developing PBTK models, it is often challenging to obtain direct estimates for a subset of $m > 0$ parameters. These parameters may be unavailable due to missing measurements or because they represent abstract concepts. In such cases, a common approach is to select parameter estimates $\tilde{p} \in \Theta \subset \mathbb{R}^m$ so that the model predictions closely match the measured data, i.e.

$$\tilde{p} \in argmin_{p \in \Theta}\{e(m(p), x)\}, \tag{24}$$

where m: $\Theta \rightarrow \mathbb{R}^n$ is the model prediction and e: $\mathbb{R}^n \times \mathbb{R}^n \rightarrow \mathbb{R}$ describes the difference between the measurements $x \in \mathbb{R}^n$ and a realisation of this model prediction.

However, finding this $\tilde{p}$ is often a non-trivial task, particularly as m is often a complicated function. Consequently, analytically solving this problem is often not feasible. Therefore, numerous numerical methods have been developed to approximate $\tilde{p}$. One of the most famous methods doing so is the Gauss-Newton method, which approximates a local minimum of r under the Euclid norm $\|\cdot\|_2$, i.e. it approximates

$$\tilde{p} \in argmin_{p \in S_\epsilon^m(\tilde{p})}\{\|r(p)\|_2\} \tag{25}$$

for some $\epsilon > 0$, where r: $\mathbb{R}^m \rightarrow \mathbb{R}^n$ is the residual. For this algorithm it is assumed r is twice differentiable in an open convex space around the local minimum $\tilde{p}$; the Jacobian matrix $J_r(\tilde{p})$ of r has full rank m, which requires among other that $n \geq m$ and $\|r(\tilde{p})\|_2$ is sufficiently small.

This method is an iterative approach, i.e., for a sufficiently close p^k to the local minimum a better candidate $p^{k+1} = p^k + d^k$ for some $d^k \in R^m$ is searched so that

$$f(p^k) > f(p^{k+1}), \tag{26}$$

where $f(\mathrm{p}) \coloneqq \|r(p)\|_2$. To choose an appropriate candidate for d^k, the second Taylor polynomial of f is considered, i.e.

$$f(p^k + d^k) \approx f(p^k) + \nabla f(p^k)d^k + {d^k}^{\mathrm{T}}\nabla^2 f(p^k)d^k \tag{27}$$

$$=: \mathrm{m}_{\mathrm{p^k}}(d^k), \tag{28}$$

Where ∇f is gradient of f and $\nabla^2 f$ its Hessian matrix. d^k is than chosen so that it minimizes locally $\mathrm{m}_{\mathrm{p^k}}$, which is equivalent to

$$0 = \nabla \mathrm{m}_{p^k}(d^k) \tag{29}$$

$$= \nabla f(p^k) + \nabla^2 f(p^k) d^k \tag{30}$$

and $\nabla^2 \mathrm{m}_{p^k}(d^k)$ is positive definite. The positive definiteness of $\nabla^2 \mathrm{m}_{\mathrm{p^k}}$ is derived from the following estimation

$$\nabla^2 f(p) = J_r(p)^T J_r(p) + \sum_{i=1}^{n} r_i(p) \nabla^2 r_i(p) \tag{31}$$

$$\approx J_r(p)^T J_r(p) \tag{32}$$

and the assumption that $J_r(p)$ has full rank m.

Therefore, d^k is given by

$$d^k = -\nabla^2 f(p^k)^{-1} \nabla f(p^k). \tag{33}$$

However, the computation $\nabla^2 f(p^k)$ can be computationally quite demanding and is therefore estimated by $J(p)^T J(p)$.

For more details see [96], where also the convergence of this algorithm is shown.

In practice, however, other algorithms are often used, of which the Levenberg-Marquardt method is the most popular. This algorithm is a combination of the Gauss-Newton method and the gradient descent method i.e., d^k is derived via the equation

$$-(J_r(p)^T J_r(p) + \lambda^k I) d^k = \nabla f(p^k) \tag{34}$$

for $\lambda^k > 0$ instead of equation (33) [97]. Hereby the choice of λ^k differs between implementations. The Levenberg-Marquardt method is often chosen over the Gauss-Newton method as it is more robust and tends to have better convergence [97-99].

However, both methods above have the problem that they only search for a local minimum. This means that there are potentially other minima that minimize $f(p)$ even further. This can be especially problematic if $f(p)$ has many minima, and the fitting method gets trapped in one local minimum. In such cases, global optimization methods are needed, which are more computationally expensive, but estimate the best parameter set on the whole parameter space Θ.

One such method is the differential evolution method, which is a population-based method that searches the entire parameter space in a probabilistic manner. The basic method is as follows. First, the crossover probability $CR \in [0,1]$, which controls the mutation rate, and the

differential weight $F \in [0,2]$, which controls the size of the mutation, must be chosen. The method is initiated by randomly drawing $ND > 3$ number of candidates of parameter sets $p^1, \dots, p^{ND}$ from the parameters space Θ. Next, for one of the existing candidates p^i, a potential new candidate $\tilde{p}$ is generated from the remaining population. For this, three randomly selected candidates $p^{l_1}, p^{l_2}, p^{l_3}$ are taken from the remaining population, i.e., $l_1 \neq l_2 \neq l_3 \neq i$. Furthermore, an index $R \in \{1, \dots, m\}$ is chosen at random, where a "mutation" is guaranteed occur. The values at each index $j \in \{1, \dots, m\}$ of the candidate $\tilde{p}$ are given by

$$\tilde{p}_j = \begin{cases} p_j^{l_1} + F\left(p_j^{l_2} - p_j^{l_3}\right) \text{ if } R = j \text{ or } CR > r \sim U(0,1) \\ p_j^i \text{ else,} \end{cases} \quad (35)$$

where $U(0,1)$ is the uniform distribution. Then, if $f(\tilde{p}) < f(p^i)$ replace p^i is replaced by $\tilde{p}$ and otherwise $\tilde{p}$ is discarded. This is continued until some termination condition is reached, such as number of evaluations or the size of the improvements. Note that the mutation operator $p_j^{l_1} + F\left(p_j^{l_2} - p_j^{l_3}\right)$ can also be swapped with other similar operators, see e.g., [100], where also some convergence criteria are shown.

4.5 Residuals

Besides the choice of the fitting method, the choice of the error function *e* is also important for finding the optimal parameters for a model. Most commonly, the least squares error function is used, i.e.

$$e(y, x) = \|r(y, x)\|_2^2 = \sum_{i=1}^{n} r_i(y_i, x_i)^2, \quad (36)$$

where $r: \mathbb{R}^n \times \mathbb{R}^n \to \mathbb{R}$ is called the residual describing the difference between the measurement and the predictions. Methods such as Gauss-Newton require the error function to have this form. To derive the residual from the given data for PBTK modelling there are several options. The canonical approach would be the pointwise distance, i.e.

$$r_i(y_i, x_i) = y_i - x_i. \quad (37)$$

for each $i \in \{1, \dots, m\}$. However, in PBTK modelling, the data are mostly in the form of concentrations or amounts, where the measured values change over orders of magnitude in the course of the study due to the exponential nature of these processes (see section 4.1). Therefore, often relative errors are used instead, as it is expected that the absolute error of the model should be lower at lower concentrations. Furthermore, because of this in the following it is assumed that all values are positive, i.e. $r : \mathbb{R}_+^n \times \mathbb{R}_+^n \to \mathbb{R}$. One common choice for this is to normalize the pointwise distance by the model prediction [73, 101], i.e.

$$r_i(y_i, x_i) = \frac{y_i - x_i}{y_i}. \quad (38)$$

However, a major problem with this approach is that the normalization itself depends on the model, so if the model does not represent the data well, the normalization does not make

sense in context of the data. For example, if the model over-predicts the measurements by a large factor $x_i \ll y_i$ than $r_i \approx 1$; but in contrast, if the model underpredicts the measurements $x_i \gg y_i$ than $r_i \gg 1$. In general, this tends to favor overpredictions. Alternatively, one could use the measurements for normalization, i.e.

$$r_i(y_i, x_i) = \frac{y_i - x_i}{x_i} \tag{39}$$

but this may cause the measurement inaccuracy to have an undesirably large influence on the residual and as with the previous residuals, this would cause the fitting method to favour underpredictions. Furthermore, in both cases the difference e induced by r does not fulfil the definition of a metric, i.e., since in general

$$e(x, y) = e(y, x) \tag{40}$$

does not hold true. Because of these shortcomings, a different residual is usually used in this work. It was opted for the log difference as the residual, i.e.

$$r_i(y, x) = \log(y_i) - \log(x_i) = \log\left(\mathrm{y_i}/x_i\right). \tag{41}$$

The log residual has the advantages of still considering the relative difference, while the error induced by it is a metric, as it is among other properties symmetric. Therefore, it does not favour higher values in one of its arguments over the other.

All the residuals presented so far have in common that residual at each point is independent of the point of measurement and are all measurements points are evaluated equally. In practice, however, this is often undesirable because there is often additional information about some of the measurement points, for e.g., when one measurement matrix (e.g. milk at several time points) has more measurement points than the other (e.g. muscle meat after slaughter), but the model should consider both matrices equally. To do this, so-called weights $\omega_i \in [0,1]$ with $\sum_{i=1}^{n} \omega_i = 1$ are added to the residual so that

$$e(y, x) = \|\tilde{r}(y, x)\|_2^2 = \sum_i \omega_i r_i(y_i, x_i)^2. \tag{42}$$

Therefore,

$$\tilde{r}_i(y_i, x_i) = \sqrt{\omega_i} r(y_i, x_i). \tag{43}$$

Thus, measurements at i with larger ω_i have more influence on the final parameter. In the case of the two matrices mentioned above the naïve choice for ω_i would be $\frac{m_1}{m_1+m_2}$ for all i describing matrix one and $\frac{m_2}{m_1+m_2}$ for all i describing matrix two, with m_1 and m_2 being the number of measurement in matrix one and two, respectively.

4.5.1 Dealing with censored data

Another common problem in deriving the residuals is partial censoring of the measurement results. This means that if a data point falls within a certain interval, the exact value of the measurement is unknown, but the interval containing the value is known. For concentration measurements, the most relevant case is left censoring of the data, because due to analytical

limitations it is not possible to reliably quantify or even detect substances below a certain threshold, i.e., limit of quantification (LOQ) and limit of detection (LOD). A common approach dealing with this is to simply replace LOQ-censored data with half the value of the LOQ. This approach may work well when using equation (37) for residues, as the absolute difference between the actual value and the replacement value is small. However, if one uses a residual that takes into account the relative distance, such as equations (41), this can be detrimental as the relative distance between the actual value and the replacement value can be quite large. Therefore, a more sophisticated approach is preferable. Such an alternative approach for censored data could be as follows:

Let $(a_1, b_1], \dots, (a_l, b_l]$ with $l \in \mathbb{N}$ and $a_1 \geq b_1 \geq \cdots \geq a_l \geq b_l \in \mathbb{R}$ be the censored intervals, e.g., $a_1 = LOQ$, $b_1, a_2 = LOD$ and $b_2 = 0$. Furthermore let r_i be the residuum that cannot account for censored data and $\overline{r_i}$ that can.

Case 1: $x_i \notin (a_1, b_1] \cup \dots \cup (a_l, b_l]$

Then nothing changes, i.e., $\overline{r_i}(y_i, x_i) := r_i(y_i, x_i)$

Case 2: $x_i \in (a_j, b_j]$ for some $j \in \{1, \dots, l\}$ and $y_i \in (a_j, b_j]$

Then $\overline{r_i}(y, x) := 0$ as the prediction would yield the same results as the measurement.

Case 3: $x_i \in (a_j, b_j]$ for some $j \in \{1, \dots, l\}$ and $y_i \notin (a_j, b_j]$

Then $\overline{r_i}(y_i, x_i) := \min\{r_i(y_i, a_j), r_i(y_i, b_j)\}$, where the minimum is chosen to ensure that $\overline{r_i}(\cdot, x_i)$ is continuous for every $x_i \in \mathbb{R}$.

An further alternative is to assume that the data is distributed according to some censored distribution, e.g., censored normal distribution [102]. Then the maximum likelihood estimation is used. However, this approach was not used in this work as it computationally more expensive, usually requiring to fully parametrize the distribution, i.e., also deriving variance in the case censored normal distribution.

4.6 Model confidence

For a proper risk analysis and risk communication, it is often not sufficient to derive only the optimal parameters $p \in \mathbb{R}^m$ ($m > 0$) from the data. It is also crucial to express the certainty of these parameters. Assuming that our parameters are multivariate normally distributed, this could be expressed by the covariance matrix Σ. For $n > 1$ samples x_i assume $f(\{x_i\}) \sim \mathcal{N}(p, \Sigma n)$ are independent, where f is the function that transforms a set of data points into a parameter estimate. Σ can be estimated by

$$\tilde{\Sigma} := \frac{1}{n(n-1)} \sum_{i=1}^{n} \left(f(\{x_i\}) - \bar{f}\right)\left(f(\{x_i\}) - \bar{f}\right)^T, \tag{44}$$

where

$$\bar{f} := \frac{1}{n}\sum_{i=1}^{n} f(\{x_i\}) \sim \mathcal{N}(p, \Sigma) \tag{45}$$

estimates p. However, the direct use of this approach in modelling presents some problems. First, a single data point is usually not sufficient to derive parameters; rather, a sufficiently large set of data points is required. Second, even if it is possible to derive such identically and independent distributed samples, the fitting algorithm on all samples $f(\{x_1, \dots, x_n\})$ will provide a better estimate of p than $\bar{f}$ as $f(\{x_i\}) \sim \mathcal{N}(p, \Sigma n)$ is presumably an imperfect assumption, which gets better with larger sample size $f(\{x_{i_1}, \dots, x_{i_l}\}) \sim \mathcal{N}(p, \Sigma n/l)$ for $0 < l \leq n$ and distinct $i_1, \dots, i_l \in \{1, \dots, n\}$.

To deal with this problem, several methods have been developed. One well-known method is the delete-d Jackknife method, which rearranges equation (45) so it is possible to use f on large subsets of $\{x_1, \dots, x_n\}$. The algorithm works as follows:

Let Z be the set that contains all possible subset of $\{x_1, \dots, x_n\}$ containing $n - d$ elements; therefore Z contains $\binom{n}{d}$ sets. Then calculate for each $\zeta \in \mathrm{Z}$ the optimal parameter estimate

$$p_\zeta := f(\zeta) \approx \frac{1}{n-d}\sum_{x \in \zeta} f(\{x\}). \tag{46}$$

Next calculate the average over all p_ζ's, i.e.

$$\bar{p} = \frac{1}{\binom{n}{d}}\sum_{\zeta \in \mathrm{Z}} p_\zeta. \tag{47}$$

Finally, Σ can then be estimated as follows

$$\tilde{\Sigma} := \frac{n-d}{d\binom{n}{d}}\sum_{\zeta \in \mathrm{Z}} (p_\zeta - \bar{p})(p_\zeta - \bar{p})^T \approx \frac{1}{n(n-1)}\sum_{i=1}^{n} \left(f(\{x_i\}) - \bar{f}\right)\left(f(\{x_i\}) - \bar{f}\right)^T. \tag{48}$$

Using this method, it is than assumed that $p \sim \mathcal{N}(f(\{x_1, \dots, x_n\}), \tilde{\Sigma})$ distributed.

A commonly used alternative to the jackknife method is bootstrapping. However, the jackknife method tends to perform better with small sample sizes [103].

4.7 Statistical methods

For proper risk assessment and management, it is often necessary to evaluate whether a certain criterion has a significant influence on a certain parameter relevant for risk assessment. To evaluate this, statistical tests are used, the most widely used of which is the student t-test [104]. There are two versions of this test: the one sample and two sample t-test. In the one sample t-test, it is tested whether the mean μ_0 of independent normal distributed $X_1^0, \dots, X_{n_0}^0 \sim \mathcal{N}(\mu_0, \sigma^2)$ is equal to certain value μ i.e., the null-hypothesis H_0 is $\mu = \mu_0$. In contrast, the two-sample t-test tests whether the means μ_1 and μ_2 of two sets of

independent normal distributed $X_1^1, \dots, X_{n_1}^1 \sim \mathcal{N}(\mu_1, \sigma^2)$ and $X_1^2, \dots, X_{n_2}^2 \sim \mathcal{N}(\mu_2, \sigma^2)$ are equal, i.e., the null-hypothesis H_0 is $\mu_1 = \mu_2$.

To test H_0, the test statistic has to be determined. If the variance σ^2 is given, then the test statistic

$$Z = \sqrt{n_0}\frac{\overline{X^0} - \mu}{\sigma} \tag{49}$$

or

$$Z = \frac{\overline{X^1} - \overline{X^2}}{\sigma\sqrt{\frac{1}{n_1} + \frac{1}{n_2}}} \tag{50}$$

is under H_0 standard normal distributed with

$$\overline{X^k} = \frac{1}{n_k}\sum_{i=1}^{n_k} X_i^k \qquad \text{for } k \in \{0,1,2\}. \tag{51}$$

However, σ^2 is usually unknown and has to be estimated as

$$S = \sqrt{\frac{\sum_{i=1}^{n_0}\left(X_i^0 - \overline{X^0}\right)^2}{n_0 - 1}} \tag{52}$$

or

$$S = \sqrt{\frac{\sum_{i=1}^{n_1}\left(X_i^1 - \overline{X^1}\right)^2 + \sum_{i=1}^{n_2}\left(X_i^2 - \overline{X^2}\right)^2}{n_1 + n_2 - 2}}. \tag{53}$$

Notably this results in the test statistic

$$T = \sqrt{n_0}\frac{\overline{X^0} - \mu_0}{S} \tag{54}$$

or

$$T = \frac{\overline{X^1} - \overline{X^2}}{S\sqrt{\frac{1}{n_1} + \frac{1}{n_2}}} \tag{55}$$

under H_0 being not standard normally distributed anymore. They are now t-distributed with $n_0 - 1$ degrees of freedom in the case of the one-sample t-test and $n_1 + n_2 - 2$ in the case of the two-sample t-test. H_0 is then accepted if the realisation of the T lies between the $\alpha/2$ and $1 - \alpha/2$ quantile of the respective t-distribution. Otherwise, it is rejected, meaning the difference is considered to be statistically significant. Here α is the significance level and is defined beforehand, often $\alpha = 0.05$. Assuming that H_0 is correct, α is the probability that H_0 gets nevertheless rejected. Noteworthy is that the assumption that X_1^k have to be normally distributed can be relaxed to only require that the μ_k and variance σ^2 exist if the sample size

is large enough due to the central limit theorem, i.e., the distribution of the mean $\overline{X^k}$ can be approximated by a normal distribution.

Furthermore, a slightly modified version of the two-sample t-test is the Welch test [105], which does not require the distributions X_1^1 and X_1^2 to have the same variance. Beside this there also exist many other tests, which try to determine significant differences using different assumptions such as unparametrized tests like the Wilcoxon test for one sample cases or the Wilcoxon-Mann-Whitney-Test for two sample cases [106, 107].

5 Publications

5.1 Transfer of dioxins and PCBs in dairy cows

5.1.1 Paper 1

Moenning, J.-L., et al., Transfer of polychlorinated dibenzo-p-dioxins and dibenzofurans (PCDD/Fs) and polychlorinated biphenyls (PCBs) from oral exposure into cow's milk – part II: toxicokinetic predictive models for risk assessment. Nutrition Research Reviews, 2023. 36(2): p. 484-497.

Nutrition Research Reviews, page 1 of 14 doi:10.1017/S0954422422000208

Transfer of polychlorinated dibenzo-*p*-dioxins and dibenzofurans (PCDD/Fs) and polychlorinated biphenyls (PCBs) from oral exposure into cow's milk – part II: toxicokinetic predictive models for risk assessment

Jan-Louis Moenning[1], Torsten Krause[2], Julika Lamp[2], Ronald Maul[2], Hans Schenkel[3], Peter Fürst[4], Robert Pieper[1] and Jorge Numata[1]*

[1]*Department Safety in the Food Chain, German Federal Institute for Risk Assessment (BfR), Max-Dohrn-Straße 8-10, Berlin 10589, Germany*

[2]*Department of Safety and Quality of Milk and Fish, Max Rubner-Institut, Hermann-Weigmann-Straße 1, Kiel 24103, Germany*

[3]*Department of Animal Nutrition, University of Hohenheim, Emil-Wolff-Str. 10, Stuttgart 70599, Germany*

[4]*Chemical and Veterinary Analytical Institute Münsterland-Emscher-Lippe (CVUA-MEL), Joseph-König-Straße 40, Münster 48147, Germany*

Abstract

Understanding the transfer of polychlorinated dibenzo-*p*-dioxins (PCDDs) and dibenzofurans (PCDFs) as well as polychlorinated biphenyls (PCBs) from oral exposure into cow's milk is not purely an experimental endeavour, as it has produced a large corpus of theoretical work. This work consists of a variety of predictive toxicokinetic models in the realms of health and environmental risk assessment and risk management. Their purpose is to provide mathematical predictive tools to organise and integrate knowledge on the absorption, distribution, metabolism and excretion processes. Toxicokinetic models are based on more than 50 years of transfer studies summarised in part I of this review series. Here in part II, several of these models are described and systematically classified with a focus on their applicability to risk analysis as well as their limitations. This part of the review highlights the opportunities and challenges along the way towards accurate, congener-specific predictive models applicable to changing animal breeds and husbandry conditions.

Key words: **Food safety: Pharmacokinetics: Compartment models: Ruminants: Carry-over**

(Received 3 February 2022; revised 7 October 2022; accepted 3 November 2022)

Introduction

Polychlorinated dibenzo-*p*-dioxins and dibenzofurans (PCDD/Fs, collectively and colloquially called 'dioxins') as well as polychlorinated biphenyls (PCBs) are persistent, bioaccumulative and toxic environmental contaminants. These substances may enter the animal food chain and have in the past led to feed and food contamination incidents affecting cattle[1–3], causing elevated PCDD/F and PCB levels in milk. At the same time, up to 50% of the PCDD/F and PCB human exposure, especially in infants and toddlers, can be attributed to consumption of milk and milk products[4,5]. Part I of this review covered the state of knowledge on data and transfer parameters from over 50 years of experimental studies; likewise, part I stressed the large variability and uncertainty found in the data and transfer parameters, explaining it in terms of factors stemming from the cow's metabolic state and factors stemming from the contaminants physicochemical properties[6]. Based on data from experimental studies and further *in silico* tools, predictive toxicokinetic models are generated as an aid to modern quantitative risk assessment and risk management. The present Review focuses on providing an overview of the models that have been developed to predict the concentration of PCDD/Fs and PCBs in cow's milk on the basis of the oral exposure of cows.

Modelling and simulation approaches have been used for a long time to describe the fate of xenobiotics (chemicals foreign to the body) across species[7]. Toxicokinetic models for bovines perform predictive estimations on the basis of mathematical equations that reflect the contaminants' fate and the cow's physiological processes. Toxicokinetic models are often based on particular animal feeding experimental data (*in vivo*), but unlike the raw data, they can be used to extrapolate to conditions different from the experiment. Models can in turn make use of *in silico* predictions of transfer subprocesses or model parameters (based on e.g. physicochemical properties) as well as *in vitro* and *ex vivo* laboratory

* Corresponding author: Jorge Numata, email: jorge.numata@bfr.bund.de

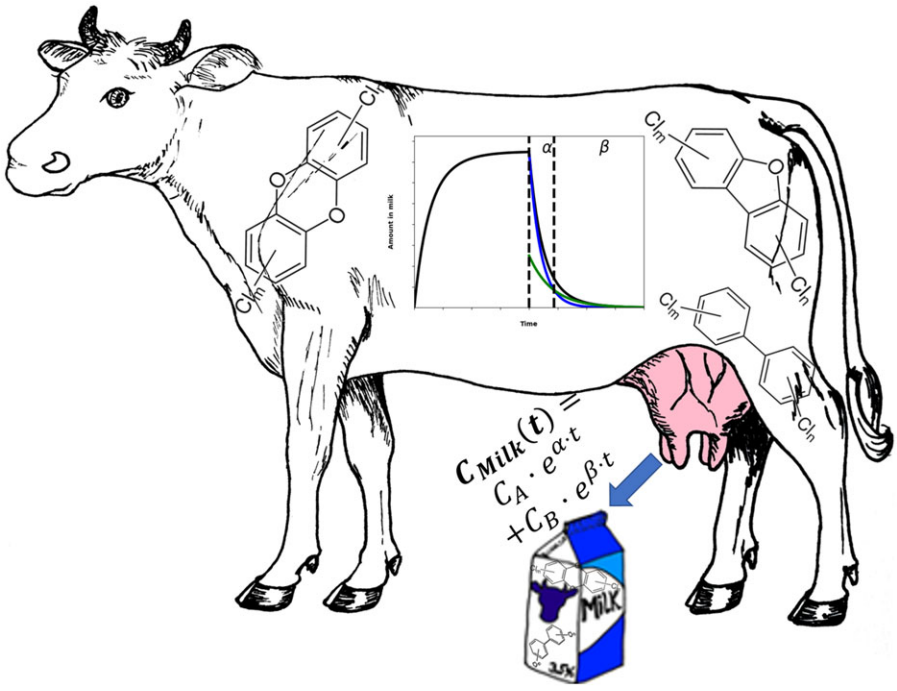

models[8] (providing information on tissue distribution and metabolism); this may become necessary to predict the transfer of substances for which little or no animal experimental data are available. Toxicokinetic models thus extract transfer information from those data and allow extrapolation to describe other situations of interest with a relatively small amount of additional data[9]. Furthermore, toxicokinetic models can be used in research as a basis to verify scientific hypotheses by implementing them into models or to predict processes that cannot be captured experimentally, providing deeper insight into the fate of contaminants in the organism.

Once the model is properly parametrised and validated, it allows a user to simulate contamination scenarios and predict their outcome, either in the form of transfer parameters or using easy-to-use implementations with graphical user interfaces such as EFSA TKPlate[10], RIVM/WFSR FeedFoodTransfer.nl and BfR ConTrans[11]. They are used in the contexts of human and animal health risk analysis (risk assessment and risk management) as well as in ecotoxicological and environmental risk analysis. The quantitative model predictions can help risk managers simulate courses of action and make informed decisions to ensure consumer health; likewise, model predictions help risk managers decide whether it is justifiable to preserve the affected livestock. Reliable data and models can help improve risk analysis in terms of consumer protection, financial repercussions and animal welfare.

Toxicokinetic models simulate the absorption, distribution, metabolism and excretion (ADME) of a toxic substance in an animal organism. The simplest models for cows are non-physiological and make predictions for transfer parameters without attempting to explicitly mimic the transport of a substance inside the animal tissues. Others use one to two compartments (bundling many tissues) and can, despite their simplicity, be quite successful in reproducing milk concentration data. The more complex models have as many as eight compartments mimicking (groups of) tissues such as the gastrointestinal tract, liver, udder, etc.

Many models are based on feeding experiments that yield a limited number of data points for a small subset of individuals. The fate of a contaminant in one particular cow depends not only on the chemical nature of the (mix of) contaminants, but also on the factors extensively discussed in part I as influences on transfer parameters, including the metabolic state of the cow, body fat content, milk yield and matrix of the contamination source[6]. A herd consists of many individuals, each of which may be in a different lactation cycle timepoint or metabolic state and have a different milk yield or body fat content[1,12]. After calving, cows reduce their fat deposits and can increase the flow of contaminants into the milk, causing milk concentrations to increase up to four times the levels determined during periods of maximum weight gain. However, for non-seasonal calving herds, variability averages out these individualities, so that the contamination of such herd milk may depend more on contaminant input than on the physiology of each individual cow[13]. This supports in principle the use of simpler models. At the same time, there are trends in the dairy industry (e.g. higher milk yields) that have a systematic effect on the properties of the herd. To generate and parametrise models that will be useful in future conditions, it is advisable to avoid oversimplifying the cow's physiology. This suggests the use of more complex models that capture the physiology of the cow more closely, so that these effects may be explicitly used in predictions.

Toxicokinetic models to predict PCDD/F and PCB transfer from feed into milk can thus widely vary in their complexity. Famous is the phrase attributed to George Box: 'All models are wrong, but some are useful'[14]. Table 1 provides an aid to balance model complexity and usefulness and to choose among

https://doi.org/10.1017/S0954422422000208 Published online by Cambridge University Press

Table 1. Summary of models discussed and their respective strengths and limitations

Model Type	Strengths	Limitations	Figures, Equations
Non-compartmental models	• Prediction of transfer parameters • Requires only some physico-chemical or molecular data on the contaminant and none from animals	• No physiological representation • No prediction of concentration/amount time profile • Low accuracy	Eqs. (14)–(17)
One-compartment models	• Approximate prediction of concentration/amount time profile • For parametrisation of the model, only one half-life and a transfer rate are needed (information often available)	• Simple physiological representation of the cow • Insufficiently describes the time after certain changes (e.g. different levels of contaminants in the feed or changed milk fat yield) due to the use of only one half-life	Figs. 2 and 9 Eqs (4)–(6), Eq. (40)
Two-compartment models	• Good prediction of concentration/amount time profile • If sufficient data are available, all necessary parameters can be derived by fitting to the concentrations in the milk only	• Limited physiological representation of the cow • Requires at least four parameters (normally two half-lives, transfer rate and e.g. mean residence time) • Complete two-compartment models rarely published for PCDD/Fs and PCBs in cows	Fig. 3 Eqs. (7)–(13)
PBTK models	• Accurate prediction of concentration/amount time profile • More detailed physiological representation of the cow, which can therefore be used to predict concentrations in specific tissues (e.g. blood and liver)	• Requires large amount of animal- and contaminant-specific information and assumptions • No clear improvement in accuracy for predicting concentration/amount-time profiles in milk compared to the two-compartment model	Fig. 5, Eqs. (18)–(23) Fig. 6 Fig. 8, Eqs. (36)–(43)
Fugacity models	• Accurate prediction of concentration/amount–time profile • More complex physiological representation of the cow, which can therefore be used to predict concentrations in specific tissues (e.g. blood and liver) • Emphasis on the diffusion limited process in the kinetics of these contaminants	• Requires a large amount of animal- and contaminant-specific information and assumptions • No clear improvement in accuracy for predicting concentration/amount–time profiles in milk compared with the 2-compartment model • Uses abstract, non-intuitive variables such as the fugacity capacity	Fig. 7, Eqs. (28)–(34)

the different available modelling approaches that we summarise in this review. Since different purposes require different models, this review provides a summary of the available approaches and their use.

The main focus of the review is to

- evaluate the availability of toxicokinetic models for all toxicologically relevant congeners (seven PCDDs, ten PCDFs and twelve dl-PCBs) as well as the indicator ndl-PCBs in terms of their applicability for risk assessment;
- appraise the available toxicokinetic models with respect to their capacity to make quantitative predictions for risk assessment and management.

We begin by introducing the mathematical tools used in kinetic modelling, starting with three key quantities to describe transfer: transfer rate (TR), transfer factor (TF) and biotransfer factor (BTF). These are discussed thoroughly in part I of this review in the chapter on kinetic parameters to characterise the feed-to-milk transfer behaviour[6], and we recall their mathematical definitions below in eqns. (1–3). The transfer rate (TR) describes the percentage of congener intake with the diet (mass or mole) that is excreted with the milk,

$$\mathrm{TR}[\%] = \frac{\mathrm{DailyExcretionViaMilk}\left[\frac{\mathrm{ng}}{\mathrm{d}}\right]}{\mathrm{DailyIntakeViaFeed}\left[\frac{\mathrm{ng}}{\mathrm{d}}\right]} \times 100\% \tag{1}$$

While TRs can be calculated for any given time period during an experiment or an incident, they reach a maximum when a steady state between constant intake and output is reached. The transfer factor (TF), also known as bioconcentration factor (BCF), is a dimensionless quantity describing the ratio of the congener concentration in milk (fat) to its concentration in the feed,

$$\mathrm{TF} = \frac{\mathrm{ConcentrationInMilkfat}\left[\frac{\mathrm{ng}}{\mathrm{kg}}\right]}{\mathrm{ConcentrationInFeed}\left[\frac{\mathrm{ng}}{\mathrm{kg}}\right]}. \tag{2}$$

Lastly, the biotransfer factor (BTF) is calculated on a whole milk basis instead of milk fat, deviating from the standard for TF. Moreover, the BTF is not dimensionless and has units of time/mass, such as [d/kg], and is not restricted to an exposure from a single source (e.g. feed) but can also account for contamination through multiple pathways

$$\mathrm{BTF}\left[\frac{\mathrm{d}}{\mathrm{kg}}\right] = \frac{\mathrm{ConcentrationInMilk}\left[\frac{\mathrm{ng}}{\mathrm{kg}}\right]}{\mathrm{TotalDailyIntake}\left[\frac{\mathrm{ng}}{\mathrm{d}}\right]}. \tag{3}$$

One- and two-compartment models: mathematical motivation

In general, during contamination incidents or feeding studies with a more or less constant exposure amount or dose D [ng/d], the concentration in milk C_{Milk}[ng/L] (usually in milk fat basis) will constantly increase and asymptotically converge towards a steady-state concentration C_{max}[ng/L] (Fig. 1). This kinetic behaviour can be most simply described with a one-compartment model (Fig. 2) as done in MacLachlan (2009)[15], which mathematically corresponds to the differential equation

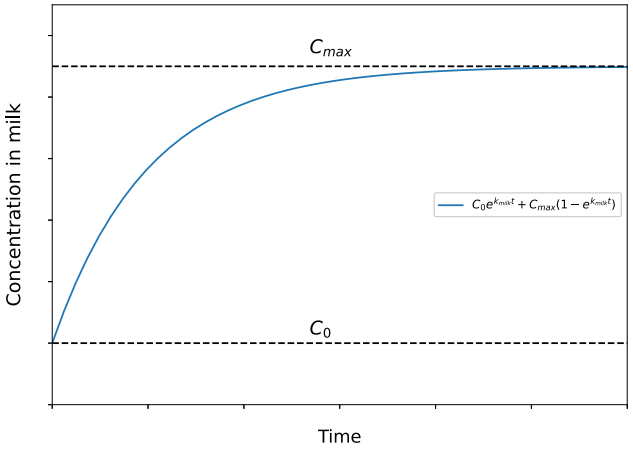

Fig. 1. Hypothetical plot of the assimilation phase of a one compartment model. The system starts the assimilation phase with an initial contamination of C_0 and converges asymptotically against its steady state C_{max}.

$$\mathrm{d}A_{\mathrm{Cow}}/\mathrm{d}t = F_{\mathrm{abs}}D - k_{\mathrm{Milk}}A_{\mathrm{Cow}}(t) \tag{4}$$

with the concentration in milk (hereafter, specifically in milk fat) thus given by

$$C_{\mathrm{Milk}}(t) = k_{\mathrm{Milk}}A_{\mathrm{Cow}}(t)/V_{\mathrm{Milk}}, \tag{5}$$

where k_{Milk} [1/d] is the milk excretion rate constant, V_{Milk} [L/d] is the milk fat yield, A_{Cow}[ng] is the amount of contaminant in the cow and F_{abs} [unitless] is mainly the fraction of dose absorbed into the cow but also accounts for all non-milk routes of elimination. F_{abs} can depend on multiple factors, such as the source of the contaminant (e.g. soil, grass, gelatine capsule) but also on the concentration itself as shown for pigs in Savvateeva et. al (2020)[16]. From eqns. (4) and (5), one can solve for the concentration in milk fat as

$$C_{\mathrm{Milk}}(t) = C_0e^{(-k_{\mathrm{Milk}}\,t)} + C_{\mathrm{max}}\left(1 - e^{(-k_{\mathrm{Milk}}\,t)}\right), \tag{6}$$

where C_0 [ng/L] is the initial concentration at time $t = 0$. Equation (6) represents the typical monoexponential behaviour of growing towards the asymptote $C_{\mathrm{max}} = F_{\mathrm{abs}}D/V_{\mathrm{Milk}}$ (Fig. 1) corresponding to accumulation until equilibrium in the cow. This suggests using the experimentally obtained steady-state concentration (or as an approximation, the maximum experimentally observed concentration) to estimate C_{max}, as was done in, for example, ref. [17]. The value of C_{max} is the result of the dynamic equilibrium between input and elimination. The transfer factor TF can be obtained using $\mathrm{TF} = C_{\mathrm{max}}/C_{\mathrm{feed}} = F_{\mathrm{abs}}W_{\mathrm{Feed}}/(\rho_{\mathrm{Milk}}V_{\mathrm{Milk}})$, where W_{Feed}[kg/d] is the feeding rate and ρ_{Milk}[kg/L] is the density of milk fat. Additionally, the transfer rate is given by $\mathrm{TR} = F_{\mathrm{abs}} \times 100\%$.

The depuration phase commences after removing the daily exposure to contaminants and is characterised by a decrease in the amount of contaminants in the cow with a concomitant decrease in their concentration in milk over time. For the

https://doi.org/10.1017/S0954422422000208 Published online by Cambridge University Press

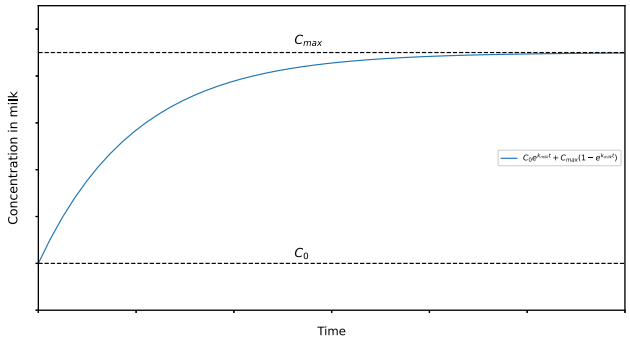

Fig. 2. The one-compartment model. Here it is assumed that the cow consumes a constant amount D of a contaminant, of which F_{abs} portion gets absorbed into the 'cow' compartment. Finally, the cow shows a continuous excretion of the contaminant into milk at the rate k_{Milk}.

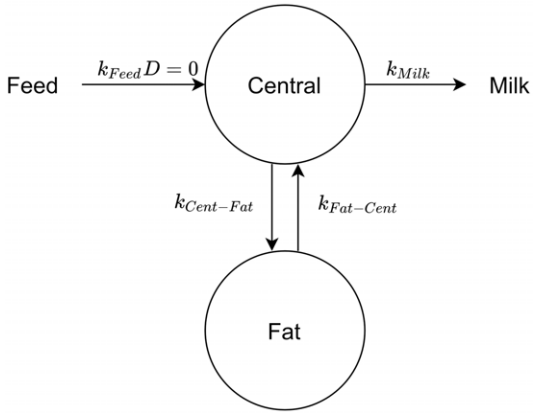

Fig. 3. A two-compartment model with input set to 0 and only a single output via milk. Here $k_{\text{Cent-Fat}}, k_{\text{Fat-Cen}}$ are the flow rates between the compartments, and k_{Milk} is the excretion rate via milk, which is assumed to happen continuously.

one-compartment model, the depuration behaviour of A_{Cow} is an exponential decrease to an asymptote C_0, with the same rate k_{Milk}. For PCDD/Fs and PCBs, the depuration phase is experimentally characterised by an initial fast depuration during the first few days and a slower second depuration over several weeks and months. This biphasic behaviour is a signature of the presence of a peripheral compartment (body fat, i.e. adipose tissue) that stores contaminants and releases them slowly. During the initial fast depuration phase, mainly the portion of the contaminant in tissue that is in rapid exchange with blood is excreted via milk fat. As a result, the equilibrium of contaminants between blood and body fat is disturbed, leading to a slow remobilisation and elimination of contaminants from body fat tissues into blood and therefore into milk fat. The biphasic nature of the depuration indicates that a single rate constant is not sufficient to capture the necessary behaviour. The simplest mathematical description such a biphasic depuration phase is a two-compartment model, as shown in Fig. 3 and corresponding to the differential equation system

$$\frac{dA_{\text{Cent}}(t)}{dt} = k_{\text{Fat-Cent}}A_{\text{Fat}}(t) - (k_{\text{Milk}} + k_{\text{Cent-Fat}})A_{\text{Cent}}(t), \quad (7)$$

$$\frac{dA_{\text{Fat}}(t)}{dt} = k_{\text{Cent-Fat}}A_{\text{Cent}}(t) - k_{\text{Fat-Cent}}A_{\text{Fat}}(t), \quad (8)$$

with again the concentration in milk fat given by

$$C_{\text{Milk}}(t) = k_{\text{Milk}}A_{\text{Cent}}(t)/V_{\text{Milk}}, \quad (9)$$

where A_{Cent} and A_{Fat} [ng] are the amounts in the central and fat compartments and $k_{\text{Fat-Cent}}, k_{\text{Cent-Fat}}, k_{\text{Milk}}$ [1/d] are the respective transition rates. During depuration phase the explicit solution for the concentration in milk fat C_{Milk} therefore has the form

$$C_{\text{Milk}}(t) = C_A \cdot e^{(\alpha \cdot t)} + C_B \cdot e^{(\beta \cdot t)}, \quad (10)$$

where $C_A + C_B$ [ng/L] is the concentration at the beginning of the depuration phase and α and β are the elimination rate constants, which are always negative. This is the well-known biexponential decay, that is, there are two half-lives that describe the time until the concentration in the milk fat is halved in the respective phase of elimination. Inspecting eqn. (10) suggests a simple method to obtain half-lives from experimental depuration data: plot the depuration phase on a semilogarithmic scale ($\ln(C_{\text{Milk}}(t))$) and estimate the initial slope (α) and terminal (β) slopes (Fig. 4). This simple method has been used, for example, by Fries *et al.* (1973) and Brambilla *et al.* (2008)[1,18]. More formally, the elimination rate constants can now be analytically determined, as they are equal to the eigenvalues of the induced transformation matrix (Supplementary Material Chapters 1 and 2), that is,

$$\alpha = \frac{1}{2}(-\sqrt{(k_{\text{Milk}} + k_{\text{Cent-Fat}} + k_{\text{Fat-Cent}})^2 - 4k_{\text{Milk}}k_{\text{Fat-Cent}}} - (k_{\text{Milk}} + k_{\text{Cent-Fat}} + k_{\text{Fat-Cent}})) \quad (11)$$

and

$$\beta = \frac{1}{2}(\sqrt{(k_{\text{Milk}} + k_{\text{Cent-Fat}} + k_{\text{Fat-Cent}})^2 - 4k_{\text{Milk}}k_{\text{Fat-Cent}}} - (k_{\text{Milk}} + k_{\text{Cent-Fat}} + k_{\text{Fat-Cent}})). \quad (12)$$

Thus, the elimination half-lives ($\tau_{1/2}$ [d]) for the depuration phase can be calculated as

$$\tau_{\frac{1}{2}\alpha} = \frac{\ln(2)}{-\alpha};\ \tau_{\frac{1}{2}\beta} = \frac{\ln(2)}{-\beta} \quad (13)$$

Here $\tau_{\frac{1}{2}\alpha}$ is the initial fast half-life, or 'α-half-life', of the contaminant, and is the result of the initial elimination from the central compartment at the start of depuration; $\tau_{\frac{1}{2}\beta}$ is the second slower half-life of the contaminant, which is often called 'β-half-life' or terminal-half-life, as it describes the latter and final phase of continuous elimination of the remobilised contaminant (e.g. Toutain and Bousquet-Mélou (2004)[19]).

Often models are proposed that comprise more than two compartments, which technically results in more than two half-lives. These additional compartments are introduced to

https://doi.org/10.1017/S0954422422000208 Published online by Cambridge University Press

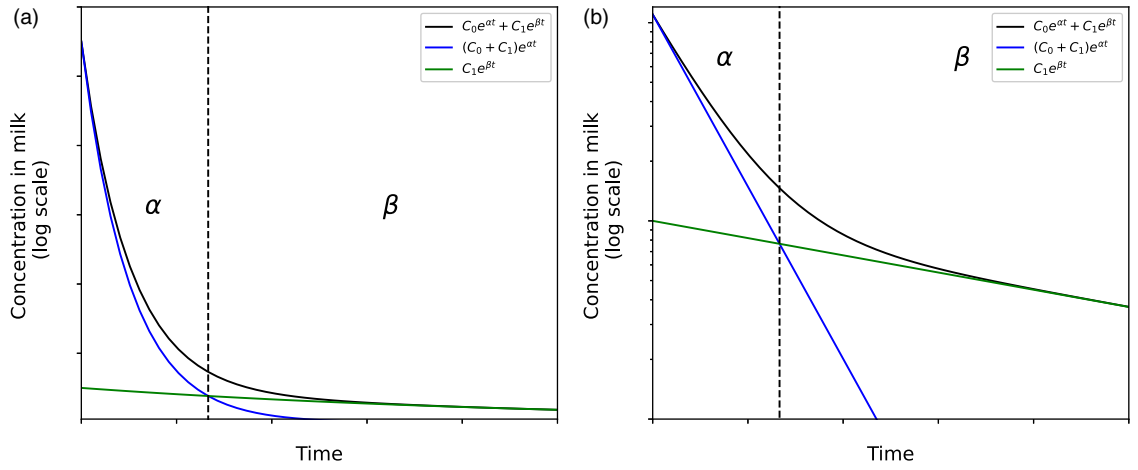

Fig. 4. Hypothetical plot of the depuration phase of a two-compartment model with a linear *y*-axis scale (left) and logarithmic *y*-axis scale (right). The system starts the depuration phase with initial contaminant concentration $C_0 + C_1$ and decreases double exponentially towards 0. Thereby it transitions from an almost monoexponential α depuration phase to an almost monoexponential β depuration phase.

reproduce the kinetics more precisely. However, the additional half-lives have a negligible effect on the shape of the concentration-time curve, effectively resulting in a biphasic behaviour that can be well described using only α- and β-half-lives.

Non-physiological approaches for calculating transfer parameters

Firstly, it should be noted that all three transfer parameters TR or eqn. (1), TF or eqn. (2) and BTF or eqn. (3) are conceptually similar, as all of them relate the input to the output of the contaminant (often in steady state) using different measurements of the contaminant (total amount, concentration in milk fat or concentration in milk). Therefore, it is possible to interconvert between them, as shown in part I of the review[6].

While TR, TF and BTF can be derived from experimental feeding studies or estimated from field observational data, there have been multiple attempts at predicting them for a contaminant using data from lactating cows that have not reached the steady state. One common strategy is to use experimental data from feeding studies where the cows did not reach steady-state conditions and estimate the steady-state concentration with the help of a non-physiologically based one-compartment model (Fig. 2) as presented by, for example, Connet and Webster (1987)[20]. For this purpose, they note that in such a model the concentration in milk fat (C_{Milk}) for a given constant concentration in feed (C_{Feed}) can be described by the differential equation

$$\frac{\mathrm{d}C_{\text{Milk}}(t)}{\mathrm{d}t} = k_{\text{ass}}C_{\text{Feed}} - k_{\text{eli}}C_{\text{Milk}}(t) \qquad (14)$$

with the rate constants $k_{\text{ass}}, k_{\text{eli}}$, which can be derived from the one-compartment model (eqns. 4 and 5). These are then fitted to the experimental data (Research Triangle Institute (RTI), 2005, Appendix A[17] for more details on fitting the data). The steady-state concentration is then given by $\frac{k_{\text{ass}}}{k_{\text{eli}}} \cdot C_{\text{Feed}}$ and subsequently $\text{TF} = \frac{k_{\text{ass}}}{k_{\text{eli}}}$.

Other approaches are not based on animal experimental data, but rather on physical chemistry, such as Travis and Arms (1988)[21], who proposed a relation between BTF and the octanol-water partition coefficient K_{ow} (see also the chapter on degree of chlorination and partitions coefficients in part I of the review[6]) using linear least-squares fitting such that

$$\log_{10}(\text{BTF}) = -8.085 + 0.992\,\log_{10}(K_{\text{ow}}). \qquad (15)$$

A geometric mean approach was discussed by Birak *et al.* (2001)[22] as an alternative to the linear square approach. The idea of Travis and Arms was further developed in RTI[17] as this method becomes increasingly inaccurate for higher values of $\log_{10}(K_{\text{ow}})$, which is especially relevant here, as PCDD/Fs and PCBs have rather high $\log_{10}(K_{\text{ow}})$ values. Therefore, they fitted the BTF data with help of a second-order polynomial resulting in

$$\log_{10}(\text{BTF}) = -3.56 + 1.07\log_{10}(K_{\text{ow}}) - 0.099\log_{10}(K_{\text{ow}})^2. \qquad (16)$$

For a more in-depth comparison of such methods using some form of fitting of $\log_{10}(K_{\text{ow}})$, see Takaki *et al.* (2015)[23]. Dowdy *et al.* (1996)[24] took a slightly different approach, as they noted that the experimentally derived $\log_{10}(K_{\text{ow}})$ values for the same contaminant can vary widely depending on the method used[25] and furthermore that the metabolisation rate of the contaminant should also be taken into account. Therefore, they developed a quantitative structure–activity relationship (QSAR) method, based on the Randic branching index[26] of a given contaminant's molecular structure to derive the 'normal path first-order Molecular Connectivity Index', ${}^1\chi_{pc}$. They presumed ${}^1\chi_{pc}$ determines the lipophilicity and the metabolic stability of the contaminant. Hence, they effectively used ${}^1\chi_{pc}$ instead of $\log_{10}(K_{\text{ow}})$ for linear square fitting, resulting in a formula that depends only on ${}^1\chi_{pc}$ to predict the BTF of a contaminant, that is,

https://doi.org/10.1017/S0954422422000208 Published online by Cambridge University Press

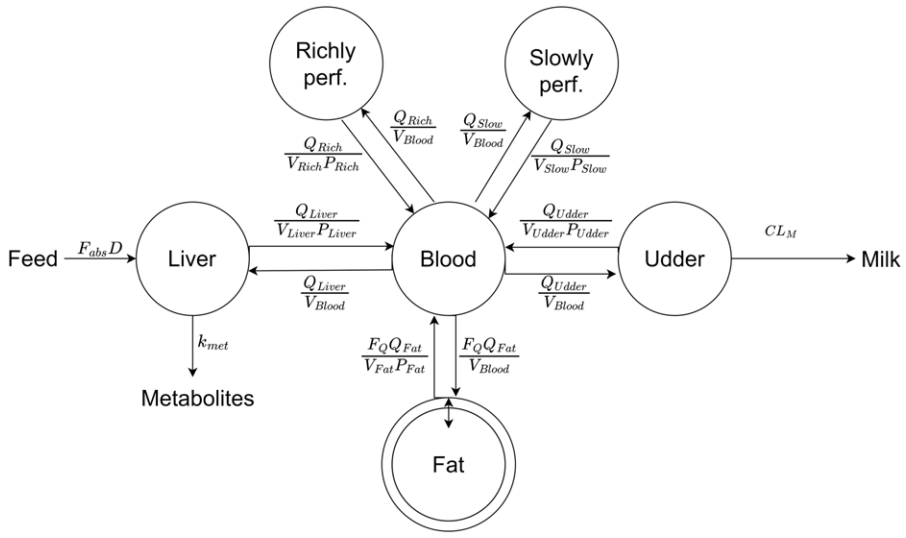

Fig. 5. Schematic depiction of the original six-compartment model derived in Derks et al. (1994)[27]. Here, Q_i[L/d] stand for the blood flow rate into/out of the compartment i, P_i [unitless] is the (compartment i)/blood partition coefficient and V_i [L] is the volume of compartment i. The compartments i are liver, richly perfused tissues, slowly perfused tissues, udder, fat and blood. For fat we have an additional constant F_Q [unitless] accounting for the fact that this compartment is diffusion limited. The input into this model happens continuously through the liver with D [ng/d] being the dose of contaminant fed to the cow daily and F_{abs} the fraction absorbed into the system. Metabolism of the contaminant takes place in the liver at the rate k_{met}[1/d]. Additionally, the contaminant is excreted in the udder via milk proportional to the amount of milk fat excreted $CL_{Milk}[L/d]$.

$$\log_{10}(\mathrm{BTF}) = -5.879 + 0.421^{1}\chi_{pc}. \qquad (17)$$

Models based on physiological approaches

The first physiologically based pharmacokinetic/toxicokinetic models (PBPK/TK) for PCDD/Fs and PCBs in lactating cows were published by Derks *et al.* in 1994[27] and McLachlan as early as 1992[28]. They used different modelling approaches, both of which are still in use today. Additional models for lactating cows focusing on general lipophilic/hydrophobic contaminants with similar physico-chemical properties for PCDD/Fs and PCBs were proposed by different authors and have since been used for PCDD/Fs and PCBs. These models are discussed below.

The classical PBTK approach by Derks

The most prominent model was published by Derks *et al.* (1994)[27]. It is a classical physiologically based toxicokinetic (PBTK) model that describes the ADME processes of a contaminant in an organism while taking into account various physiological and physico-chemical factors of an individual lactating cow. In a classical PBTK approach, the contaminant is distributed from one compartment to another, whereby the concentration-driven rate terms depend on several characteristics of the animal and contaminant, as well as on the compartments themselves. All the rate terms are combined into a system of mass balance equations that describes the amount of contaminant in each compartment over time, as well as the outflow in the form of metabolised contaminant and milk excretion. The PBTK model of Derks *et al.* (1994)[27] consists of six compartments (Fig. 5): blood, which connects all compartments; liver, in which metabolic degradation occurs; udder (represented only by udder fat), from which continuous excretion via milk fat occurs; body fat as peripheral storage compartment; and the remaining organs, which are divided into slowly (e.g. muscle, skin, bones) and richly blood-perfused (main internal organs except liver, e.g. kidney and gastrointestinal tract). The substance enters the system via the liver, so this model takes first-pass kinetics into account. The distribution between blood and each tissue compartment depends on three variables: the blood flow Q_i [L/d], the compartment volume V_i [L] (both of which depend on the physiology of the individual cow) and the partition coefficient P_i [unitless], which reflects the physico-chemical properties of the contaminant by describing the tissue–blood ratio of the contaminant in equilibrium. In addition, it is assumed that all transitions between the compartments are blood flow limited, except for the fat compartment, which is diffusion limited and is taken into account by multiplying the blood flow Q_F [L/d] by a constant $F_Q \leq 1$. Blood flow limited means that it is assumed that the amount of blood flow into the tissue is the limiting factor in the exchange of substances, that is, the blood within the tissue is immediately in steady state with the tissue. Diffusion limited means that we assume the limiting factor is the exchange of contaminant from blood to tissue and is not instantaneous (and by definition not instantly in steady state). The liver metabolism is accounted for with a first-order rate constant k_{met} [1/d] and the proportion that is absorbed from the GIT via first-pass into the liver is accounted for by a redefined F_{abs} [unitless]. The milk fat yield is now labelled CL_{Milk} [L/d], instead of the synonymous V_{Milk} from previous models to underline the fact that this variable serves the function of kinetic clearance of contaminant through the removal of udder fat (identical in concentration to milk fat). The assumption of continuous lactation throughout the day is made. The resulting differential equation system is

https://doi.org/10.1017/S0954422422000208 Published online by Cambridge University Press

$$\frac{dA_{Blood}}{dt} = \sum_{i \epsilon T}\left(\frac{Q_i A_i}{V_i P_i} - \frac{Q_i A_{Blood}}{V_{Blood}}\right) + F_Q \frac{Q_{Fat} A_{Fat}}{V_{Fat} P_{Fat}} - F_Q Q_{Fat} \frac{A_{Blood}}{V_{Blood}} \quad (18)$$

with $T = \{\text{Slow, Rich, Udder, Liver}\}$,

$$\frac{dA_{Fat}}{dt} = F_Q Q_{Fat} \frac{A_{Blood}}{V_{Blood}} - F_Q \frac{Q_{Fat} A_{Fat}}{V_{Fat} P_{Fat}}, \quad (19)$$

$$\frac{dA_{Liver}}{dt} = Q_{Liver} \frac{A_{Blood}}{V_{Blood}} + F_{abs} D - \frac{Q_{Liver} A_{Liver}}{V_{Liver} P_{Liver}} - k_{met} A_{Liver}, \quad (20)$$

$$\frac{dA_{Rich}}{dt} = Q_{Rich} \frac{A_{Blood}}{V_{Blood}} - \frac{Q_{Rich} A_{Rich}}{V_{Rich} P_{Rich}}, \quad (21)$$

$$\frac{dA_{Slow}}{dt} = Q_{Slow} \frac{A_{Blood}}{V_{Blood}} - \frac{Q_{Slow} A_{Slow}}{V_{Slow} P_{Slow}}, \quad (22)$$

$$\frac{dA_{Udder}}{dt} = Q_{Udder} \frac{A_{Blood}}{V_{Blood}} - \frac{Q_{Udder} A_{Udder}}{V_{Udder} P_{Udder}} - \frac{CL_{Milk} A_{Udder}}{V_{Udder}}. \quad (23)$$

The concentration in milk fat is thus given by

$$C_{Milk} = \frac{A_{Udder}}{V_{Udder}}. \quad (24)$$

Different methods have been used to obtain model parameters. Especially notable is the calculation of the partition coefficients P_i, which was discussed in detail by Derks (1994)[27] and van Eijkeren (1998)[29], as we summarise below. Blood flow and organ volume were directly derived from experimental data and k_{met}, F_Q and F_{abs} fitted to experimental data with numerical methods.

The determination of partition coefficients P_i was done differently in Derks (1994)[27] and van Eijkeren (1998)[29]. While Derks estimated the partition coefficient P_i by dividing the tissue concentration of the contaminant by the blood concentration at the end of the study, van Eijkeren *et al.* (1998) estimated the partition coefficients using the K_{ow} of the contaminant and various generic tissue component fractions[29]. But in MacLachlan 2009[30] it is noted that the latter method produces almost indistinguishable values for contaminants with $\log(K_{ow}) > 3$; since all PCDD/Fs and PCBs fulfill this property, the method incorrectly predicts the same partition coefficients and therefore almost identical distribution for each congener among the compartments. It is thus recommended to use better methods to predict the partition coefficient for PCDD/Fs and PCBs, for example, Graham *et al.* (2011)[31] or Endo *et al.* (2013)[32].

Derks *et al.* originally used their model to describe the dynamics of 2,3,7,8-TCDD in lactating cows[27], and other authors have since adapted it to describe other lipophilic contaminants. More recent studies[2,29,33] combined the udder fat and blood compartments into one blood compartment (Fig. 6), as the udder has a high blood flow Q_{Udder} compared with its small volume V_{Udder}, and therefore is almost instantly in equilibrium with the blood[29]; this modification introduces a milk/blood partition coefficient, P_{Milk}, which is conceptually similar to the now missing compartment udder/blood

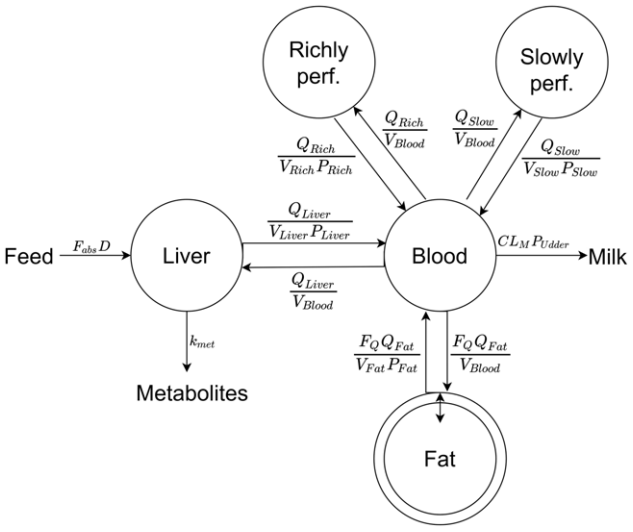

Fig. 6. Schematic depiction of the modified Derks (1994)[27] model with the udder included in the blood compartment. Here Q_i[L/d] stands for the blood flow rate into/out of the compartment i, P_i[*unitless*] is the partition coefficient between blood and compartment i and V_i[L] is the volume of compartment i. The compartments i are liver, richly perfused tissues, slowly perfused tissues, body fat, blood and milk. For body fat, there is an additional constant F_Q[unitless] accounting for the fact that this compartment is diffusion limited. The input into this model happens continuously through liver with daily contaminant dose D [ng/d] and fraction absorbed F_{abs} [unitless]. Metabolism of the contaminant takes place in the liver at the rate k_{met} [1/d]. Additionally, the contaminant from the blood can be excreted via milk proportional to the amount of milk fat excreted CL_{Milk} [L/d].

partition coefficient, that is, the concentration in milk fat is then given by

$$C_{Milk} = \frac{A_{Blood}}{V_{Blood}} P_{Milk}. \quad (25)$$

This only changes the equation system slightly (Supplementary Material Chapters 1–4 and Equation S10). Additionally, it is possible to use this model for beef cattle or calves (non-lactating) by also removing the udder compartment and setting $CL_{Milk} = 0$ and therefore having no milk excretion[33,34]. Such a model without milk excretion had already been used by Leung *et al.* (1990)[35] for the description of TCDD kinetics in rats.

The fugacity approach by McLachlan

A different approach was proposed in McLachlan (1992)[28]: a fugacity model to describe the dynamics of hydrophobic contaminants in a lactating cow; this was further developed in Rosenbaum *et al.* (2009)[36] and Tremolada *et al.* (2014)[13]. Such models are based on more general multimedia fugacity models (MFM) from environmental chemistry[37]. MFMs are often used to describe the fate of chemical contaminants across whole environmental compartments, and specifically the rates at which they move between phases. The transfer rate is proportional to the fugacity difference between the source and destination phases. The basis of the model is the mass balance equations for each phase including fugacities, fluxes and amounts, in this case, applied to a single organism with inputs and outputs. The fugacity (f) has units of pressure [Pa].

https://doi.org/10.1017/S0954422422000208 Published online by Cambridge University Press

A key concept is the fugacity capacity (Z_m) [mol/(m^{3}Pa)], which is conceptually the capacity of compartment m (a phase) to absorb a solute (contaminant). The fugacity capacities Z_m are calculated with the equilibrium partition coefficients of the chemicals, Henry's law and other physico-chemical equations. The concentration C_m of a chemical in compartment m is given by

$$C_m = Z_m f_m. \tag{26}$$

Note that conceptually Z_m is similar to the partition coefficient of the classical PBTK approach in the sense that

$$\frac{Z_m}{Z_i} = P_{mi}\left(= \frac{C_{m,ss}}{C_{i,ss}}\right) \tag{27}$$

as in equilibrium among compartments $f_{m,ss} = f_{i,ss}$ holds true.

The transport coefficients D [mol/(Pa·d)] describe processes, such as advective transport (of a substance by bulk motion, e.g. the ingestion of a contaminant with feed), transformation (e.g. metabolisation) and diffusion. D is defined for advective processes as the product of a volume flow rate [m^3/d] and a fugacity capacity Z [mol/(m^{3}Pa)]; D is defined for diffusive processes as the product of a conductance [m/d], an interface area [m^2] and a fugacity capacity; and for transformation D is defined as the product of a rate constant [1/d], a compartment volume V [m^3] and a fugacity capacity [mol/(m^3 Pa)][38]. One conceptual core difference to the classical PBTK approach is that blood flow is not considered a limiting factor for the distribution of the contaminant, that is, purely diffusion-limited kinetics are assumed.

The MFM proposed by McLachlan consists of three compartments (Fig. 7): the digestive tract as the entry point into the system; the blood, which distributes the substance throughout the body; and finally, body fat as the storage compartment. The substance can be excreted either from the digestive tract via the faeces or from the blood via milk. In addition, the substance can also be metabolised in the blood compartment or the digestive system.

An additional assumption is made, namely that the system is always in a 'pseudo-equilibrium', that is, from the knowledge of the fugacity in one compartment, all other fugacities can be calculated; importantly, only the fat compartment acts dynamically. This results in a mass balance equation system of the form

$$\text{Dose} = D_{\text{Exe}} f_{Dig} + D_{\text{Dig-Blood}}\left(f_{\text{Dig}} - f_{\text{Blood}}\right) + D_{\text{Dig-Meta}} f_{\text{Dig}}, \tag{28}$$

$$D_{\text{Dig-Blood}}\left(f_{\text{Dig}} - f_{\text{Blood}}\right) = D_{\text{Milk}} f_{\text{Blood}} + D_{\text{Blood-Fat}}\left(f_{\text{Blood}} - f_{\text{Fat}}\right) + D_{\text{Blood-Meta}} f_{\text{Blood}}, \tag{29}$$

$$D_{\text{Blood-Fat}}\left(f_{\text{Blood}} - f_{\text{Fat}}\right) = \frac{\mathrm{d}\left(V_{\text{Fat}} Z_{\text{Fat}} f_{\text{Fat}}\right)}{\mathrm{d}t}. \tag{30}$$

And therefore the concentration in milk fat is given by

$$C_{\text{Milk}} = \frac{D_{\text{Milk}} f_{\text{Blood}}}{\text{CL}_{\text{Milk}}}, \tag{31}$$

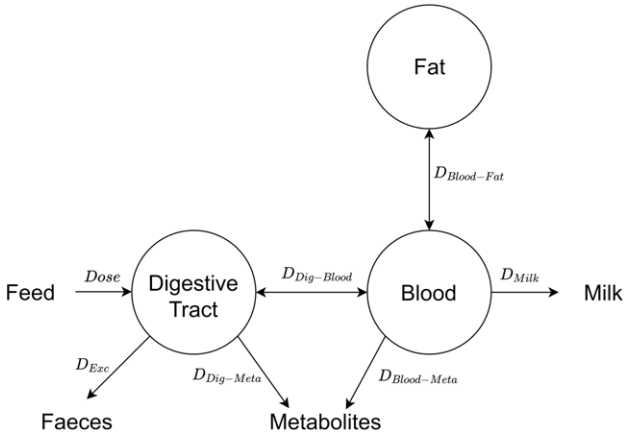

Fig. 7. Schematic depiction of the fugacity model proposed by McLachlan (1994)[38]. Here $D_{\text{Dig-Blood}}$ [mol/(Pa·d)] and $D_{\text{Blood-Fat}}$ [mol/(Pa·d)] are the transport coefficients between the compartments. The input into the system is given by dose [mol/d] into the digestive tract. Excretion can happen via faeces out of the digestive tract or via milk out of the blood with transport coefficients D_{Exc} [mol/(Pa·d)] and D_{Milk} [mol/(Pa·d)], respectively. Additionally, in both these compartments, the contaminant can be metabolised with transport coefficients $D_{\text{Dig-Meta}}$ [mol/(Pa·d)] and $D_{\text{Blood-Meta}}$ [mol/(Pa·d)], respectively.

where CL_{Milk} [mol/d] is the amount of milk fat excreted each day.

Owing to the pseudo-equilibrium assumption, there is only one linear differential equation, so the McLachlan (1994)[38] model mathematically behaves as a one-compartment model, thereby inducing only one half-life (no biphasic behaviour). With the help of various data sets, McLachlan was able to create formulas for all non-metabolic transport coefficients that depend only on the K_{ow} value and Henry's law H of the contaminant. To do that, it was assumed that the contaminant has to pass through a water and lipid layer to change from one compartment to another. For the metabolic transport coefficients $D_{\text{Blood-Meta}}$ and $D_{\text{Dig-Meta}}$, no satisfactory data were available and the respective factors were set to 0 in the simulations.

A similar approach with the same three compartments was later used in Tremolada *et al.* (2014)[13]. Here, the pseudo-equilibrium assumption was dropped so that a biexponential behaviour can be reproduced; the volumes of all three compartments (and not only the volume V_{Fat} of the fat compartment) were additionally considered. Furthermore, the input parameter Dose is also described in terms of fugacity, that is, $\text{Dose} = D_{\text{Grass}} f_{\text{Grass}} + D_{\text{Feed}} f_{\text{Feed}} + D_{\text{Soil}} f_{\text{Soil}}$. This results in the differential equation system

$$\frac{\mathrm{d}f_{\text{Dig}}}{\mathrm{d}t} = \frac{D_{\text{Grass}} f_{\text{Grass}} + D_{\text{Feed}} f_{\text{Feed}} + D_{\text{Soil}} f_{\text{Soil}} + D_{\text{Blood-Dig}} f_{\text{Blood}} - \left(D_{\text{Exc}} + D_{\text{Dig-Met}}\right) f_{\text{Dig}}}{V_{\text{Dig}} Z_{\text{Dig}}}, \tag{32}$$

$$\frac{\mathrm{d}f_{\text{Blood}}}{\mathrm{d}t} = \frac{D_{\text{Blood-Dig}}\left(f_{\text{Dig}} - f_{\text{Blood}}\right) + D_{\text{Blood-Fat}}\left(f_{\text{Fat}} - f_{\text{Blood}}\right) - \left(D_{\text{Milk}} + D_{\text{Blood-Meta}}\right) f_{\text{Blood}}}{V_{\text{Blood}} Z_{\text{Blood}}}, \tag{33}$$

https://doi.org/10.1017/S0954422422000208 Published online by Cambridge University Press

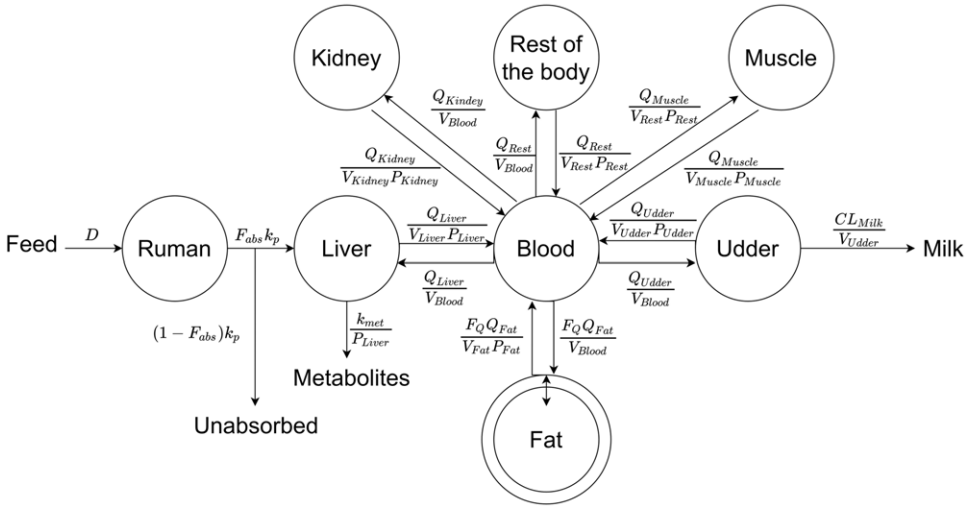

Fig. 8. Schematic depiction of the general eight-compartment model derived in MacLachlan (2009)[30]. Here Q_i [L/d] stand for the blood flow rates into/out of the compartment *i*, P_i [unitless] is the (compartment *i*)/blood partition coefficient, V_i [L] is the volume of compartment *i*. The compartments *i* are liver, richly perfused tissues, slowly perfused tissues, udder, body fat, blood and milk. For body fat there is an additional constant F_Q accounting for the fact that this compartment is diffusion limited. The input into this model happens continuously into the rumen, with *D* [ng/d] being the dose of contaminants in feed. From the rumen, the fraction F_{abs} [unitless] of contaminant gets absorbed at the rate k_a [1/d] into the main part of the system; the rest is excreted via the faeces. Metabolism of the contaminant takes place in the liver with the clearance CL_{Liver} [1/d]. Additionally, the contaminant can be excreted from the udder via milk, proportional to the amount of milk fat excreted CL_{Milk} [L/d].

$$\frac{\mathrm{d}f_{\text{Fat}}}{\mathrm{d}t} = \frac{D_{\text{Blood}}(f_{\text{Blood}} - f_{\text{Fat}})}{V_{\text{Fat}}Z_{\text{Fat}}}. \tag{34}$$

And the concentration in milk fat is again given by

$$C_{\text{Milk}} = \frac{D_{\text{Milk}}f_{\text{Blood}}}{\text{CL}_{\text{Milk}}}. \tag{35}$$

Here, the transport coefficients D_i were derived similarly as in McLachlan (1994)[38]. Additionally, the metabolic rate constants were calculated under the assumption that they are the sole reason for the discrepancy between measured excretion via milk + faeces and input of contaminants. Furthermore, it is assumed that the metabolic rate is also proportional to the lipid volume of the compartment and its fugacity capacity, that is, $D_{i-\text{Meta}} = k_i V_i Z_{\text{oct}}$ for a fitted k_i, where Z_{oct} is the fugacity capacity of octanol.

In this context, the CKow dynamic model of transfer to meat and milk for lipophilic contaminants proposed by Rosenbaum *et al.* (2009)[36] should be mentioned. At its core, CKow is a three-compartment model of the same structure as McLachlan (1994)[38], where the transition terms between the compartments are also derived similarly to McLachlan's, but instead of the fugacities of each compartment, they work with concentration of the contaminant, thereby eliminating the need of transforming fugacities into concentration in practical applications.

Generalised models for the transfer of lipophilic contaminants into milk

Generalised models for the transfer of lipophilic contaminants into cow's milk can also be used for PCDD/Fs and PCBs. One such generalised model was developed in MacLachlan (2009)[30]. This is a classic PBTK model with eight compartments (Fig. 8), which is similar in structure to the model developed by Derks in 1994, but with two major differences. The first difference is that the remaining tissues are not divided into poorly and richly perfused, but into muscle, kidney and other tissue compartments. The other difference is the addition of a rumen compartment, which creates a gradual passage (exponentially distributed input) to the intestine following first-pass kinetics via the liver; thereafter, the contaminant follows liver first-pass metabolism. While these generalisations make the model widely applicable, for PCDD/Fs and PCBs (because of their long half-lives), rumen lag before liver first-pass effect may not be so important to model explicitly[30].

The model can be written as the differential equation system

$$\frac{\mathrm{d}A_{\text{Rumen}}}{\mathrm{d}t} = (F_{\text{abs}} - 1)k_a A_{\text{Rumen}} + \text{Dose}, \tag{36}$$

$$\frac{\mathrm{d}A_{\text{Liver}}}{\mathrm{d}t} = Q_{\text{Liver}}\frac{A_{\text{Blood}}}{V_{\text{Blood}}} + F_{\text{abs}}k_a A_{\text{Rumen}} - \frac{Q_{\text{Liver}}A_{\text{Liver}}}{V_{\text{Liver}}P_{\text{Liver}}} - \frac{k_{\text{met}}A_{\text{Liver}}}{P_{\text{Liver}}}, \tag{37}$$

$$\frac{\mathrm{d}A_{\text{Blood}}}{\mathrm{d}t} = \sum_{i\in T}\left(\frac{Q_i A_i}{V_i P_i} - \frac{Q_i A_{Blood}}{V_{Blood}}\right) + \frac{F_Q Q_{Fat}A_{\text{Fat}}}{V_{\text{Fat}}P_{\text{Fat}}} - F_Q Q_{Fat}\frac{A_{\text{Blood}}}{V_{\text{Blood}}} \tag{38}$$

with $T = \{\text{Kidney, Muscle, Rest, Udder, Liver}\}$,

$$\frac{dA_{\text{Fat}}}{\mathrm{d}t} = F_Q Q_{\text{Fat}}\frac{A_{\text{Blood}}}{V_{\text{Blood}}} - \frac{F_Q Q_{\text{Fat}}A_{\text{Fat}}}{V_{\text{Fat}}P_{\text{Fat}}}, \tag{39}$$

$$\frac{\mathrm{d}A_{\text{Kidney}}}{\mathrm{d}t} = Q_{\text{Kidney}}\frac{A_{\text{Blood}}}{V_{\text{Blood}}} - \frac{Q_{\text{Kidney}}A_{\text{Kidney}}}{V_{\text{Kidney}}P_{\text{Kidney}}}, \tag{40}$$

$$\frac{\mathrm{d}A_{\text{Muscle}}}{\mathrm{d}t} = Q_{\text{Muscle}}\frac{A_{\text{Blood}}}{V_{\text{Blood}}} - \frac{Q_{\text{Muscle}}A_{\text{Muscle}}}{V_{\text{Muscle}}P_{\text{Muscle}}}, \tag{41}$$

https://doi.org/10.1017/S0954422422000208 Published online by Cambridge University Press

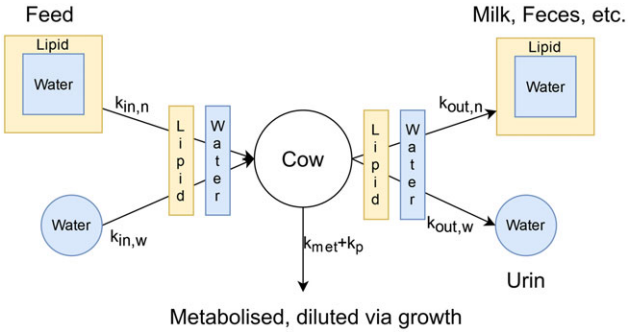

Fig. 9. Schematic description of the multitrophic level model of Hendriks *et al.* (2001)[39], adapted to the lactating cow[40]. The source of contamination could be feed, divided into water and lipid, or just water. The absorption rate of both, $k_{in,i}$ [1/d], is derived assuming that these contaminants must first pass through both water and lipid layers to enter the cow. The excretion of contaminants is divided into urinal excretion represented as water in the model on the one hand, and biomass excretion on the other (e.g. milk), which is further divided into water and lipid. The excretion rates $k_{out,i}$ [1/d] from the system are influenced by a water and lipid layer, as was the case for absorption. In addition, the reduction of the contaminant concentration in the cow's body can occur via metabolism or dilution of the biomass with the rate constants k_{met} [1/d] or k_p [1/d].

$$\frac{dA_{Udder}}{dt} = Q_{Udder}\frac{A_{Blood}}{V_{Blood}} - \frac{Q_{Udder}A_{Udder}}{V_{Udder}P_{Udder}} - \frac{CL_{Milk}A_{Udder}}{V_{Udder}}. \quad (42)$$

Thus, the concentration in milk fat is again given by

$$C_{Milk} = \frac{A_{Udder}}{V_{Udder}}. \quad (43)$$

Similar to the Derks model[27], the transition between each compartment depends on the blood flows Q_i[L/d], the compartment volumes V_i[L/d] (both of which depend on the properties of the individual cow) and the partition coefficient P_i[unitless], which reflects the physico-chemical properties of the contaminant by describing the tissue–blood ratio of the contaminant in the stationary state. Additionally, the milk excretion model is the same as in Derks, that is, proportional to the amount of milk fat excreted CL_{Milk} [L/d]; likewise, the metabolism follows linear kinetics with rate $k_{met} = CL_{Liver}/P_{Liver}$ [1/d], where CL_{Liver} [1/d] is the liver clearance.

The parameters should all be taken from the literature, except for the partition coefficient they proposed, which can be calculated using the contaminant's log (K_{ow}) value if no further information is available. But as mentioned in the classical PBTK approach by Derks, such a method suffers from prediction problems for PCDD/Fs and PCBs. An alternative would be to predict partition coefficients with other methods (see e.g. Graham *et al.* (2011)[31] or Endo *et al.* (2013)[32]).

An even more general model that considers multiple trophic levels for several kinds of contaminants was developed by Hendriks *et al.* (2001)[39]. It was later adapted to cattle by Hendriks *et al.* (2007) to calculate the BTF of various contaminants into milk and beef[40]. For lactating cows, this latter model essentially boils down to a one-compartment model with multiple input and output sources (Fig. 9), yielding a differential equation of the form

$$\frac{dC_{Cow}(t)}{dt} = k_{in,n}C_{Feed} + k_{in,w}C_{Water} - (k_{out,n} + k_{out,w} + k_p + k_{met})C_{Cow}(t). \quad (44)$$

and the concentration in milk fat is thus given by

$$C_{Milk}(t) = C_{Cow}(t)\frac{V_{Cow}}{V_{Milk}}k_{Milk} \quad (45)$$

Here, $k_{in,n}$ and $k_{out,n}$ [1/d] are the input and output rates via feed, where $k_{out,n}$ includes the excretion with milk fat at rate k_{Milk} [1/d]; $k_{in,w}$ and $k_{out,w}$ [1/d] are the input and output rates via water (irrelevant for highly hydrophobic contaminants such as PCDD/Fs and PCBs). Additionally, elimination of the substance can happen via metabolism/transformation with rate constant k_{met}, and dilution of biomass (e.g. growth) with rate constant k_p. The concentration in food and water are given by C_{Feed}[ng/L] and C_{Water} [ng/L]. Finally, the volumes of the cow and its daily milk fat yield is given by V_{Cow} [L] and V_{Milk} [L/d], respectively.

One of the main focuses of Hendriks (2001) was to show how to calculate the rate constants, especially k_{in} and k_{out}[39]. For these, it was assumed that the contaminant moves in a path through lipid and water layers upon both entering and leaving the animal via feed or water, similarly to the approach by McLachlan (1994)[38]. From this, they derived formulas describing k_{in} and k_{out} only depending on the K_{ow} value of the contaminant and the weight of the animal. For the dilution of biomass constant k_p, they assume it also scales with the weight of the animal. Lastly, for the elimination via metabolism, the model has to be fitted using experimental data.

As an aside, we note that models related to Hendriks' have been developed for broader applications. For example, the model for transfer from feed into cow's milk is only one part of a larger model for PCDD/Fs and PCBs along the human food chain (e.g. ACC-Human)[41].

Calculating transfer parameters from toxicokinetic models

The compartment models described in this review can be used to calculate transfer parameters, such as congener-specific elimination half-lives and transfer rates mentioned in part I of the review chapter on Kinetic parameters to characterise the feed-to-milk transfer behaviour[6]. While we always recommend using a full model in risk analysis instead of transfer parameters, calculating them allows for easy comparison among congeners, among mathematically diverse models and against experimental data; it also provides measures of transfer that are more intuitive to communicate. To calculate transfer parameters, we assume that the model parameters are constant over time (i.e. compartment values, input vector, etc.). To illustrate the present discussion, we can rewrite all these models in standard linear algebraic notation, that is,

$$\frac{dA(t)}{dt} = MA(t) + I, \quad (46)$$

https://doi.org/10.1017/S0954422422000208 Published online by Cambridge University Press

Table 2. Formulas for calculating the transfer parameters discussed in part I of the review chapter Kinetic parameters to characterise the feed-to-milk transfer behaviour. Here $A_{.,ss}$[ng] and $f_{.,ss}$[Pa] are the steady-state amounts and fugacities respectively in the respective compartment for each model. Additional $V_.$ [L] is the volume of the respective compartment; CL_{Milk} [ng/d] is the amount of milk fat excreted each day; Dose [ng/d] or [mol/d] in the fugacity context is the amount of contaminant given to the animal each day; Feed [kg/d] is the amount feed given to cow each day; $C_{Milkfat}$ [unitless] is the milk fat concentration; $P_.$ [unitless] is the partition coefficient for respective compartment and blood; finally D_{Milk} [mol/(Pa·d)] is the milk transport coefficient of the fugacity models; $k_.$ [1/d] are the respective transition rates in Hendriks' model[40]

Model	TR	TF	BTF
Derks model with udder[27] (and MacLachlan[30])	$\frac{A_{Udder,ss}CL_{Milk}}{V_{Udder}Dose}\cdot 100\%$	$\frac{A_{Udder,ss}Feed}{V_{Udder}Dose}$	$\frac{A_{Udder,ss}C_{Milkfat}}{V_{Udder}Dose}$
Derks model without udder[27]	$\frac{A_{Blood,ss}P_{Udder}CL_{Milk}}{V_{Udder}Dose}\cdot 100\%$	$\frac{A_{Blood,ss}P_{Udder}Feed}{V_{Blood}Dose}$	$\frac{A_{Blood,ss}P_{Udder}C_{Milkfat}}{V_{Udder}Dose}$
Fugacity model[13]	$\frac{f_{Blood,ss}D_{Milk}}{Dose}\cdot 100\%$	$\frac{f_{Blood,ss}D_{Milk}Feed}{CL_{Milk}Dose}$	$\frac{f_{Blood,ss}D_{Milk}C_{Milkfat}}{Dose}$
Hendriks' multiple trophic model[40]	$\frac{k_{in,n}V_{Cow}k_{milk}\cdot 100\%}{(k_{out,w}+k_{out,n}+k_p+k_{met})Feed}$	$\frac{k_{in,n}k_{milk}}{(k_{out,w}+k_{out,n}+k_p+k_{met})CL_{milk}}$	$\frac{k_{in,n}V_{Cow}k_{milk}C_{Milkfat}}{(k_{out,w}+k_{out,n}+k_p+k_{met})CL_{Milk}Feed}$

where $A(t)$ is the time-dependent amount vector containing the amount of contaminant in each compartment at time t; M is the transition matrix containing in its elements the transition rates between the compartments and I is the input vector containing the amount added into each compartment from outside, that is, feed; these are the model parameters are assumed to be independent of time. For a more detailed description, see Supplementary Material Chapters 1–8.

Calculating TR, TF and BTF for multicompartment models

Given a multicompartment model with a constant invertible transfer matrix M and input vector I[8], we first need to calculate the steady-state solution of this system. This is accomplished by inserting both into the formula

$$A_{ss} = M^{-1}I \tag{47}$$

or in the case of fugacity models

$$f_{ss} = M^{-1}I \tag{48}$$

Here M^{-1} is the inverse of the transfer matrix M, which can be calculated with numerical methods. Then A_{ss} is the amount vector in steady state, that is, the quantity of contaminant in each compartment, and f_{ss} is the fugacity vector in steady state, respectively. In the case of the one compartment model by Hendriks *et al.* (2001)[39], the steady state $C_{Cow,ss}$ concentration can be directly calculated as

$$C_{Cow,ss} = \frac{k_{in,n}C_{Feed}}{k_{out,w}+k_{out,n}+k_p+k_{met}}. \tag{49}$$

Here we assume that there is no input via water into the system ($k_{in,w} = 0$), as we consider only the transfer from feed. The transfer parameters discussed in the chapter on kinetic parameters to characterise the feed-to-milk transfer behaviour from part I of this review[6] can now be calculated for each compartment model type presented here using the formulas in Table 2.

Calculating the elimination half-lives for multicompartment models

For a given n-compartment model, the half-lives can be also calculated from the n eigenvalues λ_i of the transition matrix M. For this, we can use numerical algorithms, as a symbolic evaluation becomes involved for transition matrices of models with more than two compartments. Knowing the eigenvalues, the half-lives are

$$\tau_i = \frac{\ln(2)}{-\lambda_i} \text{with } i \; in\{1,\ldots,n\}. \tag{50}$$

As already mentioned, there are usually more than two half-lives, but most of them are either too short to be relevant for risk assessment or are almost identical to each other. This effectively leaves us with only two of the τ_i's being truly different practical observable half-lives: the shorter one (the α half-life) at the start of the depuration and the longer one (β) at the end.

Conclusions

In this review, we examined a wide range of toxicokinetic models developed to predict the transfer of PCDD/Fs and PCBs from feed to milk. These models vary in complexity, ranging from black-box approaches to others that closely mimic cow physiology and fugacity models based on thermodynamic equations. An overview of the strengths and limitations of each approach is summarised in Table 1. Because transfer parameters such as TR, TF, BTF, and half-lives are important to understand and compare models and congeners, we have also provided a guide for extracting these parameters from each toxicokinetic model discussed in this review.

What is the ideal model for risk assessors to use for predicting PCDD/F and PCB transfer into milk as a consequence of oral exposure? An ideal model has been validated with multiple datasets[42] and can predict the complete congener-specific spectrum of substances in question. Furthermore, it should include proper physiological modeling to allow extrapolation according to a specific cow (herd) metabolic and health status, such as body weight, body fat, milk yield and milk fat yield. Unfortunately,

https://doi.org/10.1017/S0954422422000208 Published online by Cambridge University Press

we have to report that no model currently satisfies all these criteria simultaneously.

For the fugacity approach, non-steady-state validation has only been performed in the work of McLachlan (1992) for PCB-138, but only the elimination phase used for calibration could be accurately described[28]. The newer versions of the fugacity approach were only evaluated at a near-steady state[13,36]. While we currently cannot recommend these fugacity approaches for dynamic prediction of content in milk fat owing to the lack of validation, the approach can be used alternatively to approaches presented in the chapter on non-physiological approaches for calculating transfer parameters to predict the TR, TF or BTF as already shown by Rosenbaum (2009)[36].

The classic PBTK approach of Derks was applied and calibrated to data published by Derks *et al.* (1994) for TCDD[27] and by Hoogenboom *et al.* (2010) for a mixture (PCDD/F WHO_{2005} TEQ)[2], with both parametrisations showing good performance against their respective datasets. For this reason, we would currently recommend the use of these models for TCDD and PCDD/F WHO_{2005} TEQ, respectively, although they do not fulfil all criteria mentioned above. An implementation of the Hoogenboom *et al.* (2010) model[2] can be found in the RIVM/WFSR tool www.FeedFoodTransfer.nl. For other congeners, there are only theoretically parametrised approaches that have not yet been sufficiently validated[13,29,30,34,36]. We recommend caution when employing them and encourage the community to perform additional validation. It would be beneficial if the models presented here were to be further validated for all congeners using independent datasets to assess predictive accuracy. This is also true for the Derks (1994) and Hoogenboom (2010) models since the validation dataset was also used for calibration. In addition, it would be interesting to see how well these models can predict changes in the excretion of these congeners caused by differences in cow (herd) metabolic and health status. The question of upscaling simulations to reflect whole herds is also not trivial, which is never directly addressed. It was only indirectly addressed in Hendriks (2007) by taking dilution biomass as a parameter into the model[40]. This was also done in models, which deal with a much broader context, that are not discussed here such as ACC-Human[41].

Future model developers are well advised to follow the guidelines from Lautz *et al.*[43,44], which include basing them on generic and flexible model structures and incorporating tools to assess model performance. We encourage the community of modellers to pursue congener-specific, physiologically based models that can be extrapolated, used for herds, and have been developed and validated with a multiplicity of independent datasets.

Acknowledgements

We would like to thank Dr. Matthew Salewski for the technical and linguistic proofreading of this manuscript.

H.S. and P.F. acknowledge the support from the Maria Sibylla Merian Fellowship; the Fellowship had no role in the design, analysis or writing of this article. All authors received no specific grant from any funding agency, commercial or not-for-profit sectors.

There are no conflicts of interest.

Jan-Louis Moenning: literature search, modelling aspects, writing (original draft), figures

Torsten Krause: literature search, data compilation and analysis, writing (review and editing), figures

Julika Lamp: literature search, data gathering, introduction, animal health and physiology aspects, figures

Ronald Maul: conceptualisation, writing (review and editing)

Hans Schenkel: conceptualisation, literature search

Peter Fürst: conceptualisation, literature search

Robert Pieper: animal health and physiology aspects, conceptualisation, writing (review and editing)

Jorge Numata: supervision, conceptualisation, modelling aspects, writing (original draft, review and editing), figures

Supplementary material

To view supplementary material for this article, please visit https://doi.org/10.1017/S0954422422000208.

References

1. Brambilla G, Fochi I, Falce M, *et al.* (2008) PCDD and PCDF depletion in milk from dairy cows according to the herd metabolic scenario. *Chemosphere* **73**, S216–S219.
2. Hoogenboom R, Zeilmaker M, van Eijkeren J, *et al.* (2010) Kaolinic clay derived PCDD/Fs in the feed chain from a sorting process for potatoes. *Chemosphere* **78**, 99–105.
3. Piskorska-Pliszczynska J, Maszewski S, Mikolajczyk S, *et al.* (2017) Elimination of dioxins in milk by dairy cows after the long-term intake of contaminated sugar beet pellets. *Food Addit. Contam: Part A* **34**, 842–852.
4. Fürst P, Beck H & Theelen R (1992) Assessment of human intake of PCDDs and PCDFs from different environmental sources. *Toxic Subst J* **12**, 133–150.
5. Knutsen HK, Alexander J, Barregård L, *et al.* (2018) Risk for animal and human health related to the presence of dioxins and dioxin-like PCBs in feed and food. *EFSA J* **16**, e05333.
6. Krause T, Moenning J-L, Lamp J, *et al.* (2022) Transfer of polychlorinated dibenzo-*p*-dioxins and dibenzofurans (PCDD/Fs) and polychlorinated biphenyls (PCBs) from oral exposure into cow's milk – part I: state of knowledge and uncertainties. *Nutr Res Rev.*
7. Bonate PL (2011) *Pharmacokinetic-Pharmacodynamic Modeling and Simulation*, 2nd ed. Boston, MA: Springer.
8. Klevenhusen F, Sudekum KH, Breves G, *et al.* (2020) Predicting the transfer of contaminants in ruminants by models – potentials and challenges. *ALTEX* **38**, 398–418.
9. Numata J (2016) Toxikokinetische Modellierung als Erweiterung des klassischen Transfer-Versuchs. In *128 VDLUFA-Kongress, Kongressband 2016 Rostock: Vorträge zum Generalthema: Anforderungen an die Verwertung von Reststoffen in der Landwirtschaft*, Vol. 73. Speyer, Germany: VDLUFA.
10. Wiecek W, Quignot N, Amzal B, *et al.* (2019) *TKPlate: R Package Prototype for TK Models Graphical Interface.* Geneva, Switzerland: Zenodo.

https://doi.org/10.1017/S0954422422000208 Published online by Cambridge University Press

11. Siemen H, Schafft H, Mueller-Graf C, *et al.* (2017) Risk tools for ready-to-use modeling of PFAS transfer from contaminated feed into foods of animal origin. *Organohalogen Compd.* **79**, 512–515.
12. Fries GF (1972) Polychlorinated biphenyl residues in milk of environmentally and experimentally contaminated cows. *Environ Health Perspect* **1**, 55–59.
13. Tremolada P, Guazzoni N, Parolini M, *et al.* (2014) Predicting PCB concentrations in cow milk: validation of a fugacity model in high-mountain pasture conditions. *Sci Total Environ* **487**, 471–480.
14. Box GEP (1979) Robustness in the strategy of scientific model building. In *Robustness in Statistics*, pp. 201–236 [RL Launer and GN Wilkinson, editors]. Speyer, Germany: Academic Press.
15. MacLachlan DJ & Bhula R (2009) Transfer of lipid-soluble pesticides from contaminated feed to livestock, and residue management. *Anim Feed Sci Technol* **149**, 307–321.
16. Savvateeva D, Numata J, Pieper R, *et al.* (2020) Physiologically based toxicokinetic models and in silico predicted partition coefficients to estimate tetrachlorodibenzo-*p*-dioxin transfer from feed into growing pigs. *Arch Toxicol* **94**, 187–196.
17. Research Triangle Institute (RTI) (2005) *Methodology for Predicting Cattle Biotransfer Factors*. RTI International.
18. Fries GF, Marrow GS & Gordon CH (1973) Long-term studies of residue retention and excretion by cows fed a polychlorinated biphenyl (Aroclor 1254). *J Agric Food Chem* **21**, 117–121.
19. Toutain PL & Bousquet-Mélou A (2004) Plasma terminal half-life. *J Vet Pharmacol Ther* **27**, 427–439.
20. Connett P & Webster T (1987) An estimation of the relative human exposure to 2,3,7,8-TCDD emissions via inhalation and ingestion of cow's milk. *Chemosphere* **16**, 2079–2084.
21. Travis CC & Arms AD (1988) Bioconcentration of organics in beef, milk, and vegetation. *Environ Sci Technol* **22**, 271–274.
22. Birak P, Yurk J, Adeshina F, *et al.* (2001) Travis and Arms revisited: a second look at a widely used bioconcentration algorithm. *Toxicol Ind Health* **17**, 163–175.
23. Takaki K, Wade AJ & Collins CD (2015) Assessment and improvement of biotransfer models to cow's milk and beef used in exposure assessment tools for organic pollutants. *Chemosphere* **138**, 390–397.
24. Dowdy DL, McKone TE & Hsieh DPH (1996) Prediction of chemical biotransfer of organic chemicals from cattle diet into beef and milk using the molecular connectivity index. *Environ Sci Technol* **30**, 984–989.
25. Mackay D, Shiu W-Y & Lee SC (2006) *Handbook of Physical-Chemical Properties and Environmental Fate for Organic Chemicals*. Boca Raton: CRC Press.
26. Randic M (1975) Characterization of molecular branching. *J Am Chem Soc* **97**, 6609–6615.
27. Derks HJGM, Berende PLM, Olling M, *et al.* (1994) Pharmacokinetic modeling of polychlorinated dibenzo-p-dioxins (PCDDs) and furans (PCDFs) in cows. *Chemosphere* **28**, 711–715.
28. McLachlan MS (1992) Das Verhalten hydrophober chlororganischer Verbindungen in laktierenden Rindern, Fakultät für Biologie, Chemie und Geowissenschaften der Universität Bayreuth.
29. van Eijkeren JCH, Jager DT & Sips AJAM (1998) *Generic PBPK-Modelling of Lipophilic Contaminants in the Cow*. Bilthoven: National Institute of Public Health and the Environment.
30. MacLachlan DJ (2009) Influence of physiological status on residues of lipophilic xenobiotics in livestock. *Food Addit Contam: Part A* **26**, 692–712.
31. Graham H, Walker M, Jones O, *et al.* (2012) Comparison of in-vivo and in-silico methods used for prediction of tissue: plasma partition coefficients in rat. *J Pharm Pharmacol* **64**, 383–396.
32. Endo S, Brown TN & Goss KU (2013) General model for estimating partition coefficients to organisms and their tissues using the biological compositions and polyparameter linear free energy relationships. *Environ Sci Technol* **47**, 6630–6639.
33. Freijer JI, van Eijkeren JCH & Sips AJAM (1999) *Model for Estimating Initial Burden and Daily Absorption of Lipophylic Contaminants in Cattle*. Bilthoven: Rijksinstituut voor Volksgezondheid en Milieu.
34. Bogdal C, Züst S, Schmid P, *et al.* (2017) Dynamic transgenerational fate of polychlorinated biphenyls and dioxins/furans in lactating cows and their offspring. *Environ Sci Technol* **51**, 10536–10545.
35. Leung H-W, Paustenbach DJ, Murray FJ, *et al.* (1990) A physiological pharmacokinetic description of the tissue distribution and enzyme-inducing properties of 2,3,7,8-tetrachlorodibenzo-p-dioxin in the rat. *Toxicol Appl Pharmacol* **103**, 399–410.
36. Rosenbaum RK, McKone TE & Jolliet O (2009) CKow: a dynamic model for chemical transfer to meat and milk. *Environ Sci Technol* **43**, 8191–8198.
37. Parnis JM & Mackay D (2020) *Multimedia Environmental Models: The Fugacity Approach*. Boca Raton: CRC Press.
38. McLachlan MS (1994) Model of the fate of hydrophobic contaminants in cows. *Environ Sci Technol* **28**, 2407–2414.
39. Hendriks AJ, van der Linde A, Cornelissen G, *et al.* (2001) The power of size. 1. Rate constants and equilibrium ratios for accumulation of organic substances related to octanol-water partition ratio and species weight. *Environ Toxicol Chem* **20**, 1399–1420.
40. Hendriks AJ, Smítková H & Huijbregts MAJ (2007) A new twist on an old regression: transfer of chemicals to beef and milk in human and ecological risk assessment. *Chemosphere* **70**, 46–56.
41. Czub G & McLachlan MS (2004) A food chain model to predict the levels of lipophilic organic contaminants in humans. *Environ Toxicol Chem* **23**, 2356–2366.
42. Savvateeva D, Ohlhoff B, Hoogenboom RLAP, Pieper R & Numata J (2022 (in print)) Toxicokinetic modelling of the transfer of non-dioxin-like polychlorinated biphenyls (ndl-PCBs) from feed and soil into laying hens and their eggs. *J Agric Food Chem*.
43. Lautz LS, Oldenkamp R, Dorne JL, *et al.* (2019) Physiologically based kinetic models for farm animals: critical review of published models and future perspectives for their use in chemical risk assessment. *Toxicol In* **60**, 61–70.
44. Lautz LS (2020) Towards next generation risk assessment of chemicals: development and application of physiologically based kinetic models in farm animals. PhD., Radboud University Nijmegen.

https://doi.org/10.1017/S0954422422000208 Published online by Cambridge University Press

5.1.2 Paper 2

Moenning, J.-L., et al., Transfer and toxicokinetic modeling of non-dioxin-like polychlorinated biphenyls (ndl-PCBs) into accidentally exposed dairy cattle and their calves-A case report. Environmental Toxicology and Pharmacology, 2023. **99**: p. 104106.

Environmental Toxicology and Pharmacology 99 (2023) 104106

Contents lists available at ScienceDirect

Environmental Toxicology and Pharmacology

journal homepage: www.elsevier.com/locate/etap

Transfer and toxicokinetic modeling of non-dioxin-like polychlorinated biphenyls (ndl-PCBs) into accidentally exposed dairy cattle and their calves - A case report

Jan-Louis Moenning [1], Jorge Numata [2], Dorit Bloch, Anne Jahnke [3], Helmut A. Schafft [4], Markus Spolders [5], Anja Lüth [6], Monika Lahrssen-Wiederholt, Kirsten Schulz [*,7]

German Federal Institute for Risk Assessment, Berlin, Germany

ARTICLE INFO

Edited by Dr. M.D. Coleman

Keywords:
Excretion kinetics
Depuration
PCB congeners
PBTK model
Pharmacokinetics

ABSTRACT

Polychlorinated biphenyls (PCBs) are persistent environmental pollutants that accumulate in tissues of exposed animals and humans. This case report refers ton = 3 dairy cows accidentally exposed to non-dioxin-like PCBs (ndl-PCBs) of unknown origin on a German farm. At study start they had a cumulative total of 122-643 ng/g fat in milk and 105–591 ng/g fat in blood, consisting mainly of PCBs 138, 153, and 180. Two cows calved during the study and their calves were raised on their mothers' milk, resulting in cumulative exposure until slaughter. A physiologically based toxicokinetic model was developed to describe the fate of ndl-PCBs in the animals. The toxicokinetic behavior of ndl-PCBs was simulated in individual animals, including transfer of contaminants into calves via milk and placenta. Both the simulations and experimental data indicate that contamination via both routes is significant. In addition, the model was used to estimate kinetic parameters for risk assessment.

1. Introduction

Polychlorinated biphenyls (PCBs) are organohalogen compounds consisting of a biphenyl where hydrogens are substituted with several chlorine atoms (1–10 per molecule) to yield 209 congeners. They are classified as persistent organic pollutants (POPs), are anthropogenic and highly resistant to environmental degradation. The substances accumulate in environmental matrices, in biota and in humans (Schecter et al., 2006). PCBs have been used as lubricants, insulators, heat conductors and fire retardants; due to their elasticity, they were also widely used in varnishing. Since 2001, PCBs have been banned worldwide by the Stockholm convention. Nonetheless, as a consequence of their extensive use in the past, their dispersion by long-range atmospheric transport and their persistence, PCBs can still be ubiquitously found (Tremolada et al., 2014). Being lipophilic molecules, PCBs tend to accumulate in the adipose tissue of exposed animals. They are known to transfer from oral exposure into cow's milk (Krause et al., 2022). Among foods of animal origin, milk and milk products represent a main source of PCB exposure for humans because of their high consumption rate (EFSA, 2005). Some PCBs share properties with polychlorinated dibenzo-*p*-dioxins and polychlorinated dibenzofurans (PCDD/Fs). Because of their molecular conformation and toxicological similarity to PCDD/Fs,

Abbreviations: PBTK, Physiologically based toxicokinetic; PCB, Polychlorinated biphenyl; ndl-PCB, Non-dioxin-like PCB; dl-PCB, Dioxin-like PCB; PCDD/Fs, Polychlorinated dibenzo-p-dioxins and dibenzofurans; POPs, Persistent organic pollutants; LOQ, Limit of quantification; SF, Scaling factor; BTF, Bio transfer factor; LBTF, Lactation bio transfer factor; QSAR, Quantitative structure-activity relationship; BfR, German Federal Institute for Risk Assessment; Ct-profile, Concentration time-profile.

* Correspondence to: German Federal Institute for Risk Assessment, Max-Dohrn-Str. 8-10, 10589 Berlin, Germany.
E-mail address: kirsten.schulz@bfr.bund.de (K. Schulz).
[1] ORCiD 0000-0002-9457-7032
[2] ORCiD 0000-0002-0033-4436
[3] ORCiD 0000-0001-9304-7737
[4] ORCiD 0000-0001-9212-0074
[5] ORCiD 0000-0002-4405-1497
[6] ORCiD 0000-0002-4752-9345
[7] ORCiD 0000-0002-0090-761X

https://doi.org/10.1016/j.etap.2023.104106
Received 27 October 2022; Received in revised form 28 February 2023; Accepted 9 March 2023
Available online 11 March 2023

12 PCB congeners are referred to as dioxin-like PCBs (dl-PCBs). The remaining 197 PCBs have different toxicological properties and are therefore referred to as non-dioxin-like PCBs (ndl-PCBs). In this paper we will focus on ndl-PCBs. From an analytical point of view, detailed measurements of all ndl-PCBs are time-consuming and expensive. Thus, ndl-PCBs 28, 52, 101, 138, 153 and 180 are used as indicators for risk assessment (Ballschmiter and Zell, 1980). In monitoring studies it was found that these six indicator ndl-PCBs account for about 50% of the total ndl-PCBs in food samples and at least one of these six indicator ndl-PCBs was quantified in 68.4% of feed samples and 82.6% of food samples (EFSA, 2012, 2018). According to Regulation (EU) No. 1259/2011, the maximum level (mL) for the sum of the six indicator ndl-PCBs in milk is 40 ng/g fat. Until now, a human health risk assessment for all ndl-PCBs is not possible, due to a lack of data (WHO, 2016).

A frequent exposure pathway for cows is the ingestion of contaminated soil and pasture while grazing. In some cases, diffuse sources are assumed to be the cause for elevated contaminant levels. In others, the contamination can be traced back to wall paint or items of stable equipment (e.g. Bogdal et al., 2017). The elimination of ndl-PCBs from the animal‘s body occurs either slowly through metabolism via CYP2B, CYP2C and CYP3A enzymes (WHO, 2016) and, in lactating cows, mainly through transfer into and excretion with milk. Therefore, the time required to reduce the PCB concentration in milk from contaminated cows can be quite long after the exposure source is removed and cows are fed a (practically) uncontaminated diet (Rossi et al., 2010). The excretion via milk is also important for the suckling calf, since it becomes the main uptake route of contaminants for the growing animal (Krause et al., 2022). This is especially true for animals from extensive farming. Furthermore, PCBs can be transferred across the placental barrier (Lancz et al., 2015). Therefore, elevated PCB levels can be expected already in newborn calves if the mother cow has been exposed to PCBs.

The aim of this study was to monitor the absorption, metabolism, excretion and accumulation of the indicator ndl-PCBs in the animals' blood, milk and several tissues (adipose tissue, muscle, liver) following accidental exposure. We focused on the three higher chlorinated congeners PCBs 138, 153 and 180, for which enough samples were quantifiable. A physiologically based toxicokinetic (PBTK) model was developed to describe the distribution of ndl-PCBs in mother cow and calf as well as the transfer between them via placenta and consumed milk. The PBTK model is structurally based on Bogdal et al. (2017), where they similarly investigated a contamination incident with PCBs of mother cows and their calves. In contrast to Bogdal et al. (2017), the parameters derived here are almost all based on experimental data from the case study and not predominantly on theoretical predictions (quantitative structure-activity relationship, QSAR). Furthermore, the toxicokinetic model was used to assess whether ndl-PCB exposure persisted beyond the time point of the last bulk milk measurement, which took place 68 days before the cows arrived from the farm to our site. An implementation of this model in python and as an FSKX file can be found in the supplementary material.

2. Materials and methods

2.1. Animals

In April 2016, an ndl-PCB contamination case occurred on a small dairy farm with 75 cattle in northern Germany. To determine the cause of contamination, all relevant feed and soil were sampled. The results were below the maximum levels (MLs) or were unremarkable. An inspection of the farm by representatives of the authorities also provided no indications. The milking and milk cooling technology cannot be excluded as a source of contamination. It is possible that a leakage of cooling liquid led to contamination of the immediate environment. The events were not scrutable in their entirety, so that the cause of contamination remains unclear. The competent authority measured ndl-PCB concentrations in the milk of cows above the mL of Regulation (EU) No. 1259/2011 of 40 ng/g fat over several months (April to June). Three cows (crossbreds beef x dairy; between 450 and 527 kg body weight, in their 1st or 2 nd lactation) with the highest ndl-PCB concentrations in milk were subsequently transferred from the dairy farm to the research station of the German Federal Institute for Risk Assessment (BfR; our site) in September 2016 for monitoring. They were kept on our site until June 2017. The cows were kept in a free-stall barn with free access to feed and water. The cows were fed a (practically) uncontaminated hay and total mixed ration (TMR) with ndl-PCB concentrations of 0.26 and 0.47 μg/kg feed (at 88% dry matter), respectively. These values are well below the mL of 10 μg/kg for feedstuffs of plant origin (Reg. (EU) No. 277/2012). The TMR was composed of the following ingredients (in g/kg dry matter): 11.1 g straw, 11.1 g hay, 431.3 g maize silage, 16.6 g sugar beet pulp, 22.1 g soy meal, 38.7 g rapeseed meal and 16.6 g supplement feed. The cows were milked twice daily at 7 a.m. and 4 p.m., and milk output was measured for each cow. The amount of milk per cow was recorded in liters and related to the weight (kg) using a density of 1.02 kg/L. The density was taken from the Milk Quality Regulation valid at the time of data evaluation (German *Milch-Güteverordnung*).

Two cows were pregnant on arrival. In March 2017 two apparently healthy calves were born. After calving, calves and mother cows were kept on our site for another 84 days (calf 1) and 70 days (calf 2). The calves were kept separately, but within sight of their mothers. The calves were bottle-fed with their mother's milk. Daily milk intake was recorded.They were additionally fed with hay according to their needs. At the end of the study, all animals were slaughtered and samples were taken for analysis of fat and ndl-PCBs.

2.2. Blood, milk and tissue sampling

Blood samples (200 mL for adult cows, 100 mL for calves) for ndl-PCB analysis were taken by venupuncture at the start of the monitoring program, on three further dates ante partum (a.p.) and on days 0, 14, 28, 56 and 84 post partum (p.p.) for cows 1 and 2. There were six sampling dates for blood in the case of cow 3 (not pregnant). Blood ndl-PCB levels in the calves were determined on days 0 (prior to colostrum uptake), 14, 28, 56 and 84 (calf 1) or 70 (calf 2). The first two blood samples from the adult animals were centrifuged and the serum was used for PCB concentration analysis. Subsequently, whole blood was used for all further ndl-PCB concentration analyses of blood (for both, adult cows and calves). The serum and whole blood samples were frozen at − 18 °C until analysis. According to a statement of the commission "Human Biomonitoring" of the German Federal Environment Agency, the test matrices whole blood, plasma and serum are equally suitable (UBA, 2003).

Milk samples were analyzed for ndl-PCBs on the day of arrival, and from then on in two-week intervals until drying off and on days 0, 7, 14, 21, 28, 42, 56, 70 and 84 p.p. Morning and previous evening milk samples were bulked on each sampling day for a total amount of about 800 mL per bulked sample. In the case of cow 3 (not pregnant), milk samples were taken in two-week intervals during the entire monitoring period. Milk samples were stored at − 18 °C until analysis.

At the end of the monitoring program all cows and calves were slaughtered. Representative samples of muscle tissues (adult cows: brisket and round; calves: brisket and saddle), adipose tissue (all animals: kidney fat and caul fat, including subcutaneous fat for adult cows), liver tissue (all animals) and udder tissue (adult cows) were taken. All tissue samples were stored at − 18 °C until analysis.

2.3. Sample analysis

The ndl-PCB concentration in blood (PCB 28, 52, 101, 138, 153, 180 and sum of 6 ndl-PCB) was determined by Eurofins GfA Lab Service GmbH (Hamburg, Germany). The concentrations of ndl-PCB in milk, animal tissues, hay and TMR were analyzed by the National Reference

Laboratory (NRL) for halogenated persistent organic pollutants (POP) in food and feed (Berlin, Germany). Both laboratories are accredited according to DIN EN ISO/IEC 17025. The Limit of Quantification (LOQ) for dioxins and PCB fulfilled the requirements as laid down in the Regulation (EU) No 2017/644.

For blood, the measurements of the samples were performed by High Resolution Mass Spectrometry (HRMS) combined with gas Chromatographs (GC). The samples were previously prepared analytically using internal methods for liquid extraction and gravimetric fat extraction.

For milk, the defrosted samples (raw milk) were centrifuged (4 °C, 4000 rpm) for 30 min and the precipitated cream layer was separated from the whey in order to perform freeze drying of the cream. The dried cream, which contains the milk fat, was then homogenized with anhydrous sodium sulfate, sand and diatomaceous earth followed by a column extraction of the fat at room temperature using 250 mL of n-hexane/acetone 1:1. The extract was vacuum evaporated (Büchi, Germany) and the obtained fat was further dried at 70 °C. The extractable lipid content was determined gravimetrically. The sample purification and PCB extraction was performed with the MIURA GO-xHT system (MIURA CO.,Ltd., Japan) using four different columns (silica gel impregnated with silver nitrate, silica gel impregnated with sulfuric acid, activated carbon and alumina). The extracted fat (~3 g) was dissolved in 5 mL hexane, transferred to the first column and automatically eluted with 95 mL of hexane. The PCDD/Fs and non-ortho PCBs (fraction A) were trapped on the activated carbon column while the mono-ortho- and ndl-PCB (fraction B) were caught on the alumina column. Both columns were eluted with 2.2 mL toluene resulting in the two fractions. Fraction B was concentrated under a nitrogen stream to a final volume of 20 μL.

The sample preparation of the animal tissues combined freeze drying, homogenizing with anhydrous sodium sulfate, sand and diatomaceous earth if necessary, followed by a column extraction of the fat at room temperature using 250 mL of dichloromethane/cyclohexane 1:1. The sample amount used for the extraction of 2–4 g fat varied depending on the tissue and was between 6 and 45 g, based on fresh weight. The remaining sample preparation steps were the same as described for the raw milk, only for liver tissue an additional manual clean-up step with a silica gel impregnated with sulfuric acid column was performed before. The automatic purification was carried out with the MIURA GO-xHT system (MIURA Co. LTD, Japan).

The hay and TMR samples were homogenized, 10 g per sample was then mixed with diatomaceous earth and the extraction was performed by accelerated solvent extraction (ASE 350, Thermo Fisher Scientific, USA). The pressure was set to 10 Mpa and the temperature to 100 °C. Before the vacuum evaporation to near dryness by using a rotary evaporator (Büchi, Germany) 2 mL of nonane was added to the extract. The sample purification and PCB extraction was performed as described for the raw milk. The water content of the hay and TMR samples were determined gravimetrically by drying the samples at 105 °C.

The isotope labeled analogs of all quantified PCBs (Wellington Laboratories Inc.) were added before the extraction step. In addition a ^{13}C-labeled PCB recovery standard was added to the sample prior to the measurement. The measurements of the samples were performed by gas chromatography (GC) (Agilent Technologies, USA) and high-resolution mass spectrometry (HRMS) (DFS, Thermo Fisher Scientific, USA; resolution 10,000; injection of 1 μL). For the determination of the mono-ortho- and ndl-PCBs (fraction B), a HT8-PCB 60 m x 0.25 mm × 0.25 μm (SGE) column was used. For quality assurance, an internal reference material from a proficiency test and a blank sample were analyzed in the same way as the samples in each analytical series. All samples were measured twice.

2.4. Development of the PBTK model

The PBTK model presented here is based on the one developed by Bogdal et al. (2017) to describe the concentration time (Ct) profile of PCBs in calving cows and their calves over the course of two lactation cycles. That model is in turn based on the six-compartment model developed by Derks et al. (1994). The Derks model has been widely used in the literature to simulate the behavior of dioxins and PCBs in lactating cows, for both the mother cow and its calf (Moenning, 2022).

2.4.1. Notation

In the following, the index *i* denotes the compartment for which this variable is applicable, i.e., $i \epsilon \{rich, slow, liver, udder, adipose, blood\}$. Rich refers to richly perfused, slow refers to slowly perfused compartment. The index *j* refers to the animal to which this variable belongs, i.e., $j \epsilon \{M_1, M_2, M_3, C_1, C_2\}$, where M_k is a mother cow and C_k is its calf ($k \epsilon \{1, 2, 3\}$). *The index* ℓ describes the ndl-PCB congener (contaminant substance) for which this variable applies, i.e., $\ell \epsilon \{138, 153, 180\}$..

2.4.2. Model structure

The model (Fig. 1) consists of a blood compartment, which connects all compartments; a liver compartment, where the metabolism takes place; an udder compartment, where the contaminant is excreted via lactation; an adipose compartment, which acts as a storage for the contaminants; and two separate compartments accounting for the relevant rest of the cow's body, i.e. a richly perfused tissue representing the remaining inner organs of the cow and a slowly perfused compartment representing mainly the muscle tissue of the cow's but also what isn't included in the previous compartments.

The transfer of contaminants between compartments is governed by three factors: the blood fat flow into non-blood compartments $Q_{fat,i}$; the volume of the fat $V_{fat,i}$ in each compartment and the partition coefficient $P_{i,\ell}$, which describes the equilibrium tissue fat: blood fat ratio of the contaminant and reflects the system's physico-chemical properties. Additionally, it is assumed that PCBs are solely metabolized in the liver with rate constant $k_{met,\ell}$. The excretion via milk is assumed to be proportional to the amount of milk fat excreted; in other words, the concentration of the ndl-PCB in milk fat is assumed to be the same as the concentration in udder fat. It should be noted that only the fat fraction of each compartment (including the blood) was considered, because ndl-PCBs are highly lipophilic (log Kow>3) and therefore distribute strongly into fat.

The transfer of contaminants from mother cow to calf after calving occurs via milk. It is assumed that the transfer from the mother cow to the calf via the milk is incomplete, as the calf does not consume all the milk produced by the mother cow, and because the ndl-PCBs in the milk are not completely absorbed (F_{abs}) by the calf. Additionally, the calf already has a certain body burden at birth due to transfer via placenta. Hereby it is presumed that the calf is in equilibrium with the mother cow, i.e., the concentrations in the calf at calving are the same in each compartment as in the mother cow. Finally, it is assumed that there is no dietary exposure for either the mother cow or the calf during the monitoring period at our site (see measurements of hay and TMR fed at our site under the Section 2.1 Animals).

Combining the assumptions above, the amounts in each compartment of mother cow and calf can be described by the differential equations

$$\frac{dA_i}{dt} = -\left(\frac{Q_{fat,i,j}}{V_{fat,i,j}P_{i,\ell}} + k_{met,\ell}\mathbf{1}_{\{liver\}}(i)\right)A_i + \frac{Q_{fat,i,j}A_{blood}}{V_{fat,blood,j}} + F_{abs}\frac{S_{milkfat,j}A_{udder}}{V_{fat,udder,j}}\mathbf{1}_{\{udder\}}(i) \quad (1)$$

and

$$\frac{dA_{blood}}{dt} = \sum_i \frac{Q_{fat,i,j}A_i}{V_{fat,i,j}P_{i,\ell}} - \frac{Q_{fat,blood,j}A_{blood}}{V_{fat,blood,j}} \quad (2)$$

for i ≠ blood. Here A_i is the amount in each compartment; $S_{milkfat,j}$ is the amount of milk fat sucked each day (=0 for adult cows) and $\boldsymbol{I}_{\{liver\}}$ and $\boldsymbol{I}_{\{udder\}}$ are the indicator functions. This can be simplified to

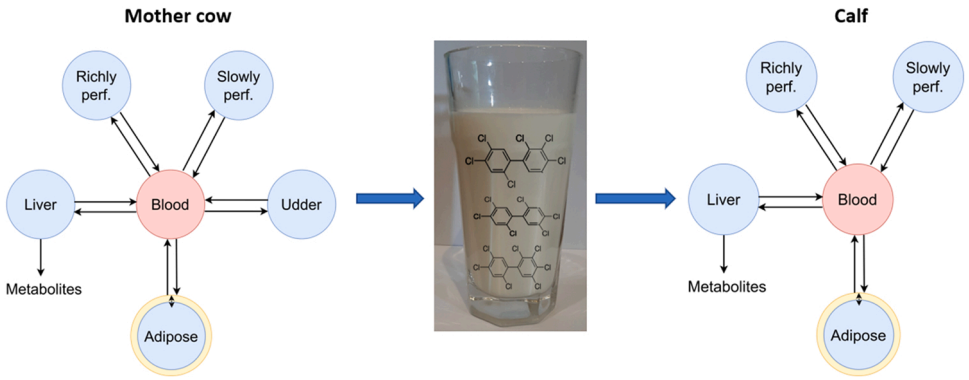

Fig. 1. Graphical illustration of the PBTK-Model describing the transfer of PCBs from mother cow to calf.

$$\frac{dA}{dt} = M_j A, \tag{3}$$

where M_j is a matrix induced by Eqs. (1) and (2) describing the kinetics of the respective animal without any input. Furthermore, it is possible to describe mother cow and calf at once, including the transfer of PCB from mother cow and calf via milk by instead using a matrix $M_{C_k+M_k}$, which describes both animals at once.

2.4.3. Parameterization

2.4.3.1. Compartment volumes. The adult cows' compartment "volumes" $V_{i,j}$ [kg] were derived by using the total body weight measurements of each cow $V_{Total,j}(t)$ and the data from Lin et al. (2020), which relates each compartment volume to the body weight of the animal, such that $V_{i,j}(t)=V_{Total,j}(t)\cdot f_{i,j}$. For calves, also the relative values reported in Lin et al. (2020) were used, except for the adipose compartment, which was assumed to be 0 at birth and its relative amount to increase linearly with age until reaching the levels report by Lin et al. (2020) at slaughter. The fat of each compartment $V_{fat,i,j}$ [kg] (except for blood) were calculated using the measured fat fraction $f_{fat,i,j}$[unitless] in representative tissues at the day of slaughter, i.e.

$$V_{fat,i,j}(t) = V_{i,j}(t)\cdot f_{fat,i,j} = V_{Total,j}(t)\cdot f_{i,j}\cdot f_{fat,i,j} \tag{4}$$

For the slowly perfused compartment, the average fat fraction from the measured muscle tissues (chest, back, top side) was used and for the adipose compartment the average fat fraction of the measured adipose tissues (caul fat, subcutaneous fat, kidney fat). The fat fraction of the liver and udder compartments were measured directly. Since for the richly perfused compartment no representative tissue was measured, a fat fraction of 5.8% was assumed (Bogdal et al., 2017). For calves, the fat fraction of the previously mentioned compartments was lowered by 20% at birth and assumed to increase linearly to the measured values. This was done to achieve realistic fat amounts in the newly born calves between 4% and 5% of BW (Blome et al., 2003; Driesen et al., 2022b; Diaz et al., 2001).

Contrary to the other compartments, the fat fraction in blood $f_{fat,blood,j}$[unitless] was measured at multiple time points and therefore estimated its fat fraction each day by using a piecewise linear function, which was then used to calculate the blood fat amount, i.e.,

$$V_{fat,blood,j}(t) = V_{blood,j}(t)\cdot f_{fat,blood,j}(t) = V_{Total,j}(t)\cdot f_{blood,j}\cdot f_{fat,blood,j}(t) \tag{5}$$

2.4.3.2. Blood fat flow rates. To estimate the blood fat flow rate $Q_{fat,i,j}$[L/d] into each compartment, we used the data published by Bodgal et al. (2017) (reproduced in Table 1), which describes the blood flow rate $Q_{i,j}$ [L/d] (full blood, fat and non-fat portions) into each compartment. For the mother cows, the blood flow rates for each compartment were set differently for the dry period and the lactation period, but otherwise assumed to be constant. An exception is the udder compartment, whose blood flow rate is considered to be proportional to the amount of milk excreted. Unlike Bogdal et al. (2017), it was assumed that the blood flow rate into the udder compartment is not 0 during the dry period, but rather similar to the volume adjusted blood flow rate of the slowly perfused tissue. To account for the fact that the adipose compartment is diffusion-limited, the blood flow rates from the adipose compartment were multiplied by 0.37 (Derks et al., 1994) From this, the blood fat flow rate into each compartment is

Table 1
Blood flow rates into each compartment during lactation and dry period of the cow. Data are mainly taken from Bogdal et al. (2017).

	Lactation period[L/d]	Dry period[L/d]
Liver	39600	19800
Adipose tissue	1221(= 0.37·3300)	1961(= 0.37·5300)
Richly perfused tissue	12400	13150
Slowly perfused tissue	17300	8650
Udder	400·(L milk produced)	$8650\frac{V_{Udder}}{V_{Slow}}$

$$Q_{fat,i,j}(t) = Q_{i,j}(t) f_{fat,blood,j}(t) \tag{6}$$

The blood fat flow rate into the blood compartment is simply the sum of all flow rates into the other compartments of the animal. For mother cows it is

$$Q_{fat,blood,M_k}(t) = Q_{fat,liver,M_k}(t) + Q_{fat,rich,M_k}(t) + Q_{fat,slow,M_k}(t) + Q_{fat,adipose,M_k}(t) + Q_{fat,udder,M_k}(t) \tag{7}$$

Regarding the calf, it was assumed that the blood flow rates into each compartment are in the same proportion to each other as in an average adult cow of 500 kg during its dry period. The blood flow for the calves is

$$Q_{fat,blood,C_k}(t) = Q_{fat,liver,C_k}(t) + Q_{fat,rich,C_k}(t) + Q_{fat,slow,C_k}(t) + Q_{fat,adipose,C_k}(t). \tag{8}$$

2.4.3.3. Metabolic rate. The metabolic rate constant $k_{met,\mathscr{C}}[1/d]$ in the liver was directly taken from Bodgal et al. (2017) (Table 2), who

Table 2
Metabolic rates and their corresponding metabolic half-lives for the three ndl-PCBs. Data are taken directly from Bogdal et al. (2017).

	$k_{met,\mathscr{C}}[1/d]$
PCB-138	$3.30\cdot10^{-3}$
PCB-153	$4.33\cdot10^{-3}$
PCB-180	$3.47\cdot10^{-3}$

presented the metabolic half-life $t_{1/2,\ell}[d]$ for these contaminants. The rate constants are then given by

$$k_{met,\ell} = -\frac{\ln(2)}{t_{1/2,\ell}} \tag{9}$$

Since the three higher chlorinated ndl-PCB congeners exhibit very long metabolic half-lives, i.e., high metabolic stability, the simulation will be only marginally affected by inclusion of metabolic rates.

2.4.3.4. Partition coefficients. To estimate all the partition coefficients $P_{i,\ell}$ [unitless], the partition coefficient for the richly perfused compartment $P_{rich,\ell}$ [unitless] was first derived based on Bodgal et al. (2017) where the authors used QSAR prediction methods. This was done because no data were available for richly perfused tissues in our case study. The derived $P_{rich,\ell}{}^{*}$[unitless] in Bodgal et al. (2017) describes the distribution between the complete compartment and full blood (full blood basis). To be used in our model, they must be transformed to blood fat basis and richly perfused fat basis, such that

$$P_{rich,\ell} = P_{\ell,rich}{}^{*}\frac{f_{fat,blood}}{f_{fat,rich}}, \tag{10}$$

where we assume again $f_{fat,rich} = 5.8\%$ as before. For blood, we assumed a fat fraction of the median across cow 1, cow 2, calf 1 and calf 2. Note that the choice of fat fraction in the richly perfused tissue does not have an influence on the overall model as it is shortened when multiplying $P_{rich,\ell}V_{fat,rich,j}$.

To calculate the other partition coefficients $P_{i,\ell}$[unitless] we presumed that the measured concentrations $C_{i,M_k,\ell}$ in the fat fraction of the adipose, slowly perfused and liver compartment of ndl-PCBs (same averaging as above for fat) are representative of distribution in these compartments in pseudo steady state of the mother cow, and that the concentrations $C_{i,C_k,\ell}$ in the fat fraction of adipose, slowly perfused and liver compartments of ndl-PCBs in calves are in equilibrium, i.e.,

$$P_{i,\ell,C_k} = \frac{C_{i,C_k,\ell}}{C_{blood,C_k,\ell}\left(t_{slaughter}\right)}. \tag{11}$$

To calculate the partition coefficients for the mother cow, a fitting approach was followed (Newville et al., 2016), where only the udder partition coefficient was fitted to the existing data and the remaining partition coefficients were derived from that. This can be done as under the pseudo steady state assumption the other partition coefficients are directly induced by the measurements in the remaining compartments at the day of slaughter, if the udder partition (and richly perfused) coefficient is given. More precisely, because pseudo steady state is assumed, it must hold true that

$$const \cdot A_{M_k}\left(t_{slaughter}\right) = d/dtA_{M_k}\left(t_{slaughter}\right) = M_{M_k}\cdot A_{M_k}\left(t_{slaughter}\right). \tag{12}$$

Thereby $const = \lambda_{\min}$ is the largest eigenvalue of M_{M_k}, i.e., the rate constant connected to the longest half induced by M_{M_k} and therefore $A_{M_k}(t_{slaughter})$ must live on the eigenvector space associated with the largest eigenvalue. Then $(P_{i,M_k,\ell})_{i\in\{slow,liver,adipose\}}$ is estimated via numerical methods so that $\lambda_{\min}A_{M_k} = M_{M_k}((P_{i,M_k,\ell})_{i\in\{slow,liver,adipose\}})A_{M_k}$ holds true for given P_{udder,M_k}, P_{rich,M_k} and the amounts A_{i,M_k}in the remaining compartment (slowly perfused, liver, adipose) at the day of slaughter, i.e.

$$A_{i,M_k} = V_{fat,i,M_k}\left(t_{slaughter}\right)\cdot C_{i,M_k,\ell}. \tag{13}$$

This method was performed only for cow 1 and 2, not for cow 3. For cow 3, almost all measured blood concentrations for PCBs were below the LOQ and therefore not valid. For evaluating the goodness of each udder partition coefficient in each step of the fit, the average over all of the individual compartment partition coefficients of mother cow and calf were taken to simulate the model. The starting vector was derived as described below. Then the results were compared to the data from the case study for the log values of blood and milk using the least square error simultaneously for cow 1 and 2.

2.4.3.5. Starting vector for ndl-PCB amounts in cow compartments. To begin the simulations, it is necessary to provide the starting vector at time t_{start,M_k} for the ndl-PCB amounts in each compartment of each mother cow. However, the total amount of ndl-PCBs in the cows and its compartmental distribution was not experimentally measured for t_{start,M_k}, so it needs to be inferred from the known data. To do this, it was presumed that the mother cows were in a pseudo steady state, which results in fixed, equilibrium proportions of ndl-PCB amounts between the compartments. Thus, the starting vector can be derived via varying only the total amount of contaminant in the animal and comparing the resulting blood and milk fat (⇔udder fat) concentrations to the measured data by minimizing the relative least square error of their log values.

With the data of the mother cow, it was possible to calculate the starting vector for the ndl-PCB amounts in the respective calf at the time of birth $t_{birth} = 0$(starting vector). For this purpose, the ndl-PCB amounts in the compartments of the mother cow until calving are simulated and used as starting amounts for the calf, i.e.

$$A_{i,C_k}(0) = A_{i,M_k}(0)\frac{V_{fat,i,C_k}}{V_{fat,i,M_k}}. \tag{14}$$

(for the richly perfused compartment, substitute V_{fat} by V).

2.4.3.6. Calf exposure. To calculate the total ndl-PCB exposure of the calf, two additional parameters were needed: the milk fat intake of the calf per day $S_{milkfat,C_k}$[kg/d], which was measured and transformed into a fitted linear interpolation function; and the absorption coefficient $F_{abs,\ell}$ for ndl-PCB, which was fitted using the blood measurements to derive the initial body burden of the calf and the measured contaminant concentration (linearly interpolated) in milk to derive the daily intake.

2.5. Transfer parameters

2.5.1. Transfer parameters & scaling factor

The concentrations of ndl-PCBs in milk can be used to estimate the extent of contamination of the calf that occurred via placental transfer. For this purpose, it was assumed that metabolism can be neglected (less than 1%) and that the calf compartments are in equilibrium at the day of slaughter. Furthermore, it was assumed that ndl-PCBs in the mother cow compartments are in equilibrium on the day of calving and that the first non-colustrum concentration of ndl-PCBs in milk fat is representative of the concentration of ndl-PCBs in udder fat at the end of the dry period. Thus, the concentrations of ndl-PCBs in each compartment of the mother cow immediately before calving can be calculated as

$$C_{i,M} = C_{Udder,M}\frac{P_i}{P_{Udder}} \tag{15}$$

Since the assumed ndl-PCB concentrations in each compartment fat of calf and mother cow are the same before birth on the day of calving, $C_{i,M}$ describes also the concentrations in the compartment fats of the calf right after birth. Moreover, the ratios between the concentrations in each compartment fat at equilibrium are unaffected by the volume of the compartment fat, i.e.,

$$\frac{C_{i,\cdot}}{C_{\check{i},\cdot}} = \frac{P_i}{P_{\check{i}}} = const \tag{16}$$

for compartments i and $\check{i}$.

Additionally, due to the mass balance equation

$$\sum_i C_i(t)V_{fat,i}(t) = const \tag{17}$$

it follows that

$$C_i(t_{slaughter}) = \frac{\sum_i C_{\swarrow i}(t_{birth}) V_{fat,\swarrow i}(t_{birth})}{\sum_i C_{\swarrow i}(t_{birth}) V_{fat,\swarrow i}(t_{slaughter})} C_i(t_{birth}) \tag{18}$$

Let

$$k := \frac{\sum_i C_{\swarrow i}(t_{birth}) V_{fat,\swarrow i}(t_{birth})}{\sum_i C_{\swarrow i}(t_{birth}) V_{fat,\swarrow i}(t_{slaughter})} \tag{19}$$

$$= \frac{\sum_i P_{\swarrow i} V_{fat,\swarrow i}(t_{birth})}{\sum_i P_{\swarrow i} V_{fat,\swarrow i}(t_{slaughter})} \tag{20}$$

Furthermore from (16) it follows

$$C_{i,C} = C_{Milkfat,M} \frac{P_i}{P_{Udder}} \kappa. \tag{21}$$

Therefore, for calculation of ndl-PCB concentrations in the respective compartment fats caused by the placental transfer, a scaling factor SF_i for the milk concentration can be derived

$$SF_i := \frac{C_{i,C}}{C_{Milkfat,M}} = \frac{P_i}{P_{Udder}} \kappa. \tag{22}$$

To be able to predict the contamination caused by transfer via milk the bio transfer factor (*BTF*) of ndl-PCB from mother's milk to the fat fraction of the calf compartments is calculated as follows:

$$BTF_{Milk-Calf,i} := \frac{ConcentrationInCompartmentFati}{AmountofContaminantInMilk} = \frac{C_i}{A_{Milk}}. \tag{23}$$

Assuming again that the amount of contaminant metabolized is negligible and that the calf's compartments are in equilibrium at the day of slaughter, then

$$BTF_{Milk-Calf,i} = F_{abs} P_i N(t_{slaughter}), \tag{24}$$

where N is the normalizing variable

$$N := \frac{1}{\sum_j P_j V_{j,C}(t_{slaughter})} \tag{25}$$

where we set $P_{blood} = 1$. Like $BTF_{Milk-Calf,i}$ the partition coefficients can also be used to calculate the bio transfer factor from absorbed contaminants by the mother cow into its individual compartment fats, i.e.,

$$BTF_{abs-Mother,i} := \frac{ConcentrationInComparmentfati}{AmountofContaminantAbsorbed}. \tag{26}$$

The $BTF_{abs-Mother,i}$ can be calculated as follows

$$BTF_{abs-Mother,i} = P_i N(t), \tag{27}$$

where N is like above the normalizing variable, i.e.,

$$N(t) = \frac{1}{\sum_i P_j V_{j,M}(t)} \tag{28}$$

It is important to note that $BTF_{abs-Mother,i}$ is related to the absorbed amount of contaminants into the compartments and not the amount in feed. Furthermore, the $BTF_{abs-Mother,i}$ can be also used to estimate the *BTF* from absorbed contaminants into the respective calf compartment via placenta by multiplying it with the before mentioned κ. For the mother cow in lactation, it is not possible to apply the *BTF* in the same sense as before because the ndl-PCBs do not accumulate constantly in the mother cow under constant contamination, but rather converge to a steady state. Therefore, we define the lactation biotransfer factor as

$$LBTF_{abs-Mother,i} := \frac{concentrationincompartmentfatiinss}{dailyamountabsorpt} \left[\mathrm{d} \Big/ \mathrm{kg} \right] \tag{29}$$

This $LBTF_{abs-Mother,i}$ still strongly depends on the amount of milk fat excreted daily. However, if the whole transition matrix M is given for a mother cow, i.e., all data is given, it can be calculated by

$$LBTF_{abs-Mother,i} = -M^{-1} I / V_{fat}, \tag{30}$$

where $I := (1,0,0,0,0,0)^T$, V_{fat} the vector containing the compartment fat volumes and I is meant in a component wise manner.

2.5.2. Half-lives

The decay of concentration of ndl-PCBs follows a multiexponential function and can therefore be described by half-lives, which roughly describe how long it takes to halve the concentration in milk. These half-lives can be computed by calculating the eigenvalues $\lambda_l (l \epsilon \{0,...,5\})$ of the transition matrix M_{M_k} of the mother cow and are then given by

$$t_{1/2,l} = \frac{\ln(2)}{\lambda_l}. \tag{31}$$

Therefore, the transition matrix M_{M_k} induces a total of six half-lives, but only the largest two, i.e., the α- and β-half-lives are influential enough to be relevant for risk assessment. As the matrix M_{M_k} is time dependent, also the half-lives are time dependent.

3. Results

3.1. Performance parameters of animals

Cow 1 and cow 2 were pregnant on arrival at our site. The average milk yield ante partum for the two cows was 10.7 and 12.2 kg/d with a mean milk fat yield of 0.39 and 0.55 kg/d. Until calving at our site (March 2017), the two animals had been in milk for 282 days (cow 1) and 379 days (cow 2), with a subsequent dry period of 76 and 90 days, respectively (starting 103 days after arrival at our site). Postpartum, the average milk yield increased to 18.7 and 24.8 kg/d; the milk fat yield was then 0.66 and 0.95 kg/d, respectively. Cow 3 was not pregnant and milked continuously for 184 days (in total: 314 DIM). The average milk yield was 9.7 kg/d (mean fat yield: 0.38 kg/d) during monitoring. The monitoring program of cow 3 was completed 214 days after arrival at our site.

Because there is no data on milk yield (and milk fat yield) for individual animals on the farm (before arrival at our site), it is assumed that the mother cows excreted twice as much milk as the cows described in Bogdal et al. (2017) at the same time in the lactation cycle. Fig. 2 represents the milk yield (assumed for the time on the farm and measured for the time at our site) of the three adult dairy cows.

Calves were born with a live weight of 42 kg (calf 1, female) and 42.5 kg (calf 2, male). When the monitoring was terminated, the live weight had increased to 147 kg and 136 kg, respectively (see Fig. 3a). The milk intake increased from 6 to 12 L/d during their lifetime as shown in Fig. 3b. For all cows, the fat fractions of each compartment are shown in Table 3.

3.2. ndl-PCB concentrations in milk, blood and tissues

The higher chlorinated indicator ndl-PCBs (congeners 138, 153, and 180) were dominant in all matrices studied. The lower chlorinated indicator ndl-PCBs (congeners 28, 52, 101) were below the limit of quantification (LOQ) in almost all samples and are considered negligible in the following evaluations. The results for descriptive statistics correspond to the lower bound approach.

Total levels of the six indicator ndl-PCBs in blood were 105, 591 and 126 ng/g fat in cows 1, 2 and 3 at the beginning of the monitoring. After parturition, cow 1 and 2 had blood levels of 20 and 136 ng/g fat. The concentrations continued to decrease to reach levels of 10 and 36 ng/g fat, when the study was terminated. In cow 3, the ndl-PCB concentration in the blood was no longer quantifiable from day 100 onwards (below LOQ).

Milk was highly contaminated in cow 2 (643 ng ndl-PCB/g milk fat at

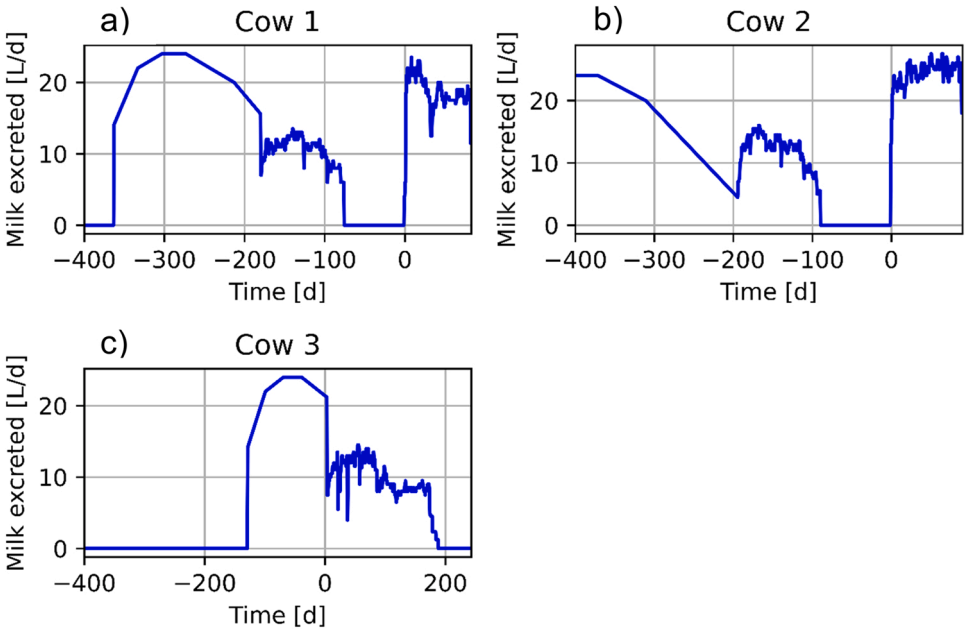

Fig. 2. Daily milk yields for the three adult cows. The time is relative to the birth of the calf at day 0 (for cows 1 and 2) and relative to the day of the arrival at our site (for the non-pregnant cow 3). The milk yields during their time at our site were directly measured and the milk yields before that were estimated using data from Bogdal et al. (2017).

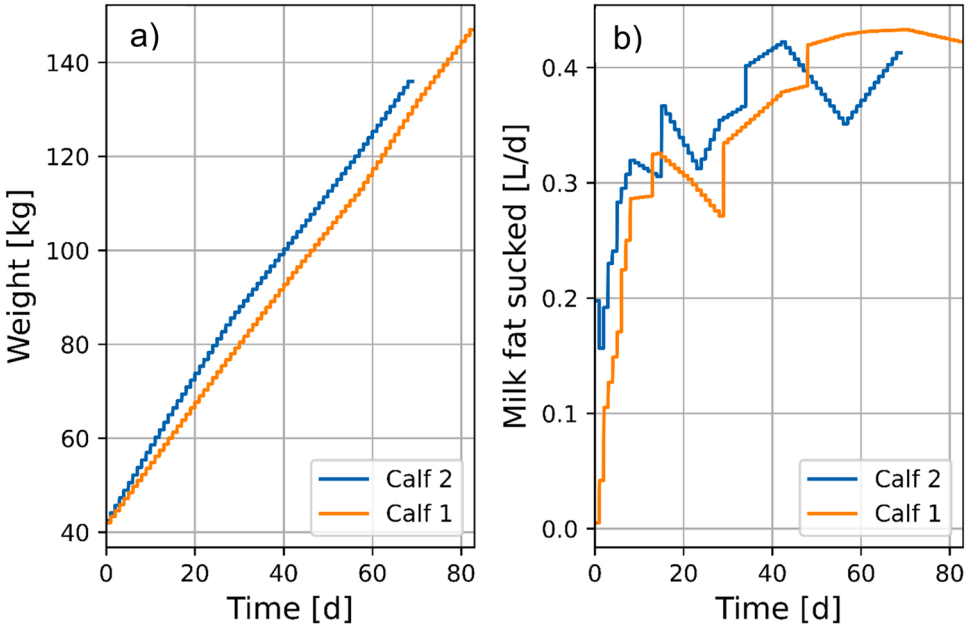

Fig. 3. Weight of the calves a) and amount of milk fat sucked per day b) during the study until their slaughter.

Table 3
Fat fraction $f_{i,j}$ [%] in each compartment i and for every animal j.

	$f_{slow,j}$	$f_{liver,j}$	$f_{adipose,j}$	$f_{udder,j}$	$f_{rich,j}$	$f_{blood,j}$
Cow 1	3.2	2.8	39.4	6.11	5.8[a]	0.24[b]
Cow 2	5.9	2.8	22.5	6.22	5.8[a]	0.19[b]
Cow 3	6.2	2.5	72.8	7.3	5.8[a]	0.22[b]
Calf 1	6.3	3.3	86.0	-	5.8[a]	0.24[b]
Calf 2	6.8	2.0	86.3	-	5.8[a]	0.22[b]

[a] literature values, since no representative tissue was measured
[b] average value for demonstrative purposes, whereas the model uses a dynamically changing value

initial sampling). Until drying off after 103 days levels decreased to 29% of the initial level with the steepest decline during the first six weeks. At parturition, milk contained 177 ng ndl-PCB/g milk fat with a further decrease to 10% of the initial level (66 ng/g) when the experiment was terminated. In cow 1, milk levels were 122 ng/g initially and 37 ng/g at parturition. The concentration time profile was similar to cow 2, with levels decreasing to equally 29% until drying off and a final level of 17 ng/g fat (14% of initial level). For cow 3, the initial level was 181 ng/g milk fat and levels decreased to 19 ng/g fat until day 97 with almost constant levels from then on.

The last known bulk milk sample (n = 27 dairy cows) was taken on the farm on June 22, 2016 and showed a concentration of 74.1 ng/g fat.

This result was used to narrow down the timing of the contamination incident - based on the PBTK model developed here.

At parturition, prior to colostrum uptake, the blood ndl-PCB level of calf 1 was 27.2 ng/g fat and of calf 2 107 ng/g fat. The concentration increases until the 28th day after birth. At the end of the study, the ndl-PCB concentrations in blood were 23.9 ng/g fat (calf 1) and 95.2 ng/g fat (calf 2). In calf 1, the daily exposure to ndl-PCB via milk reached its maximum on day 13 with 10 µg/d (milk intake of 9 L, containing 3.9% fat and 28 ng ndl-PCB/g fat). In calf 2, the same was true for day 15 and an ndl-PCB intake of 53 µg/d (milk intake of 11 L, containing 4.0% fat and 123 ng ndl-PCB/g fat). The cumulative intake of ndl-PCB via milk until slaughter was 0.7 mg for calf 1 and 2.9 mg for calf 2.

The ndl-PCB concentrations in the slowly perfused muscle tissues (brisket, round, saddle) and adipose tissues (kidney fat, caul fat, subcutaneous fat) were summarized by mean (± SE), as there were no significant differences between the subgroups ($P > 0.05$). The individual ndl-PCB concentrations per compartment (PCB 138, 153 and 180) are shown in Tables S1-S3.

3.3. Simulations

The simulation results of the PBTK model for the concentration time profile of PCB-138 in milk fat and blood fat of mother cow and calf are shown in Fig. 4 and Fig. 5 as an example. The simulation results of PCB-153 and PCB-180 can be found in the Supplementary Data (Figs. S1-S2), as the results are very similar to PCB-138. Furthermore, the derived partition coefficients between blood fat and tissue fat are shown in Table 4.

Comparing the measured and predicted concentration-time profiles of PCB-138 in the milk fat (Fig. 4a.)), there was a very good agreement for cow 1 and cow 2 but less so for cow 3. In contrast to milk fat, the predictions of the concentration-time profile of PCB 138 in blood fat for cow 1 and cow 2 were consistent with the measured data only in the second lactation period but deviate more for the first lactation and dry periods. In contrast to measured data, the model predicts an immediate decline in the ndl-PCB concentration of the blood fat directly after calving. Furthermore, does the model under predict the decline in ndl-

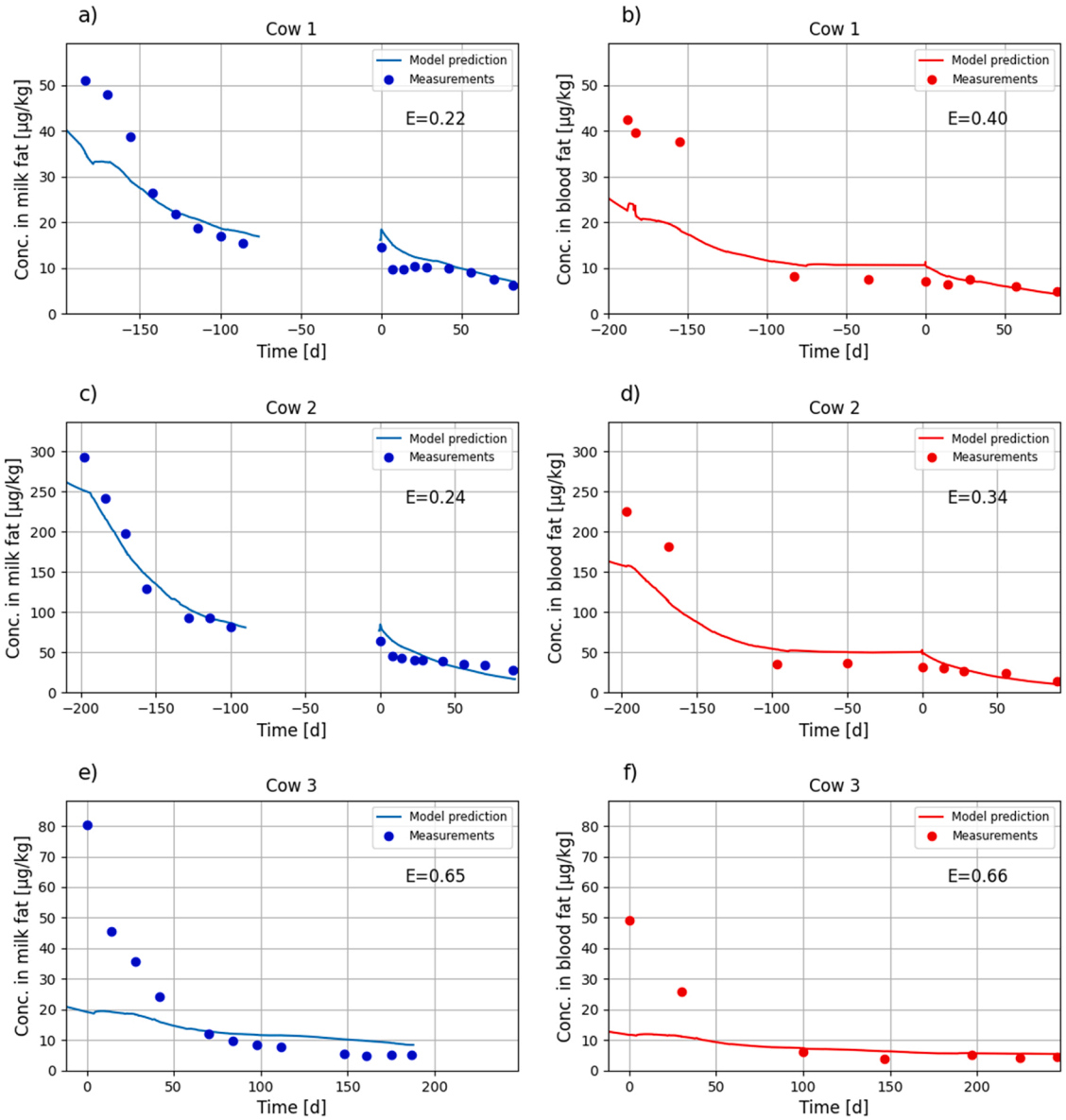

Fig. 4. Ct-profile of ndl-PCB-138 in milk fat (a,c,e) and blood fat (b,d,f) of the three cows derived from the model (solid line) and from experimental data (dots). Cow 1 and 2 were impregnated at our site. The time $t = 0$ represents calving. Cow 3 was not pregnant. Here, the time $t = 0$ characterizes the day of arrival and the associated start of monitoring. Model accuracy is described via the root mean square error E of the log-concentrations (basis e).

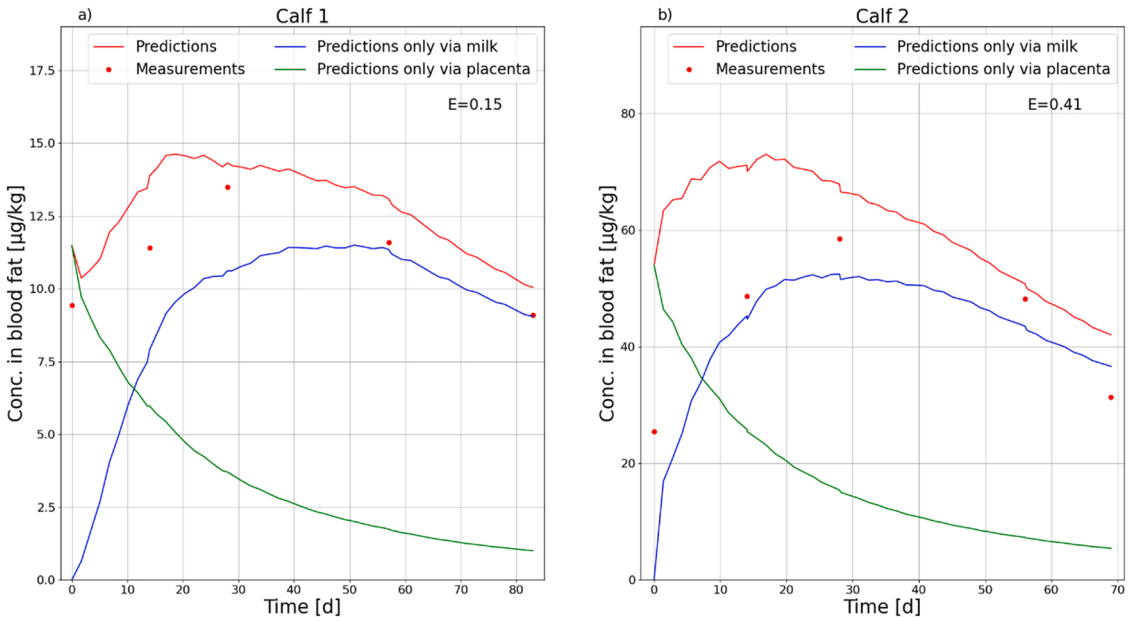

Fig. 5. Ct-profile of ndl-PCB-138 in blood fat for the Calf 1 (a) and Calf 2 (b) derived from the model (solid line) and from the experimental data (dots). The input amounts via placenta or milk fat are from the simulations of the mother cow shown in Fig. 4. In addition to the prediction of the total concentration (red line), the contributions from transfer via placenta (green line) and from consumed milk fat (blue line) are shown. Model accuracy is describe via the root mean square error E of the log-concentrations.

Table 4
Partition coefficients $P_{i,\mathcal{J}}$ [unitless] derived for each compartment, cow/calf and contaminant, as well as the fraction absorbed from milk F_{abs} [%] for each contaminant. These partition coefficients are with respect to the fat fraction in blood and the compartment fat.

	PCB-138	PCB-153	PCB-180
$P_{Liver,\mathcal{J}}$	7.53	4.68	3.97
$P_{Adipose,\mathcal{J}}$	2.18	2.04	1.94
$P_{Slow,\mathcal{J}}$	2.12	2.03	1.85
$P_{Rich,\mathcal{J}}$	0.55	0.59	0.71
$P_{Udder,\mathcal{J}}$	1.73	1.39	1.00
F_{abs}	85.0	84.3	95.2

PCB concentration in blood fat at the start of the simulation. The worst overall prediction is again observed for cow 3.

This poor performance in the case of cow 3 could indicate some physiological differences between this animal and the other two cows. In addition, this animal was found to have abnormal behavior, which is why this animal could not be inseminated either. However, no obvious health deficiencies were observed. For these reasons the data of cow 3 was mostly disregarded and not further evaluated.

Fig. 5 additionally shows the concentration time profile of PCB-138 in the blood fat for the calves of cow 1 and cow 2. For PCB-153 and PCB-180 see Figs. S3-S4. Good agreement is observed for most of the measured data points and the prediction. In addition to predicted concentrations in blood fat, contributions from prenatal transfer through the placenta or postnatal intake of milk fat are also presented. It is shown here that the contribution via placenta is significantly lower than the contribution via milk fat but still accounts 10–14% of the total concentration of each of the 3 ndl-PCBs. The predicted concentration of PCB-138 in the individual compartments of mother cow and calf are compared with the actual measured concentrations in Fig. 6, showing overall good agreement.

3.4. *Parameters relevant for risk assessment*

3.4.1. *Transfer parameters and scaling factors*

To enable the calculation of the ndl-PCB concentration in different tissues of the calf depending on the contamination of the mother's milk,

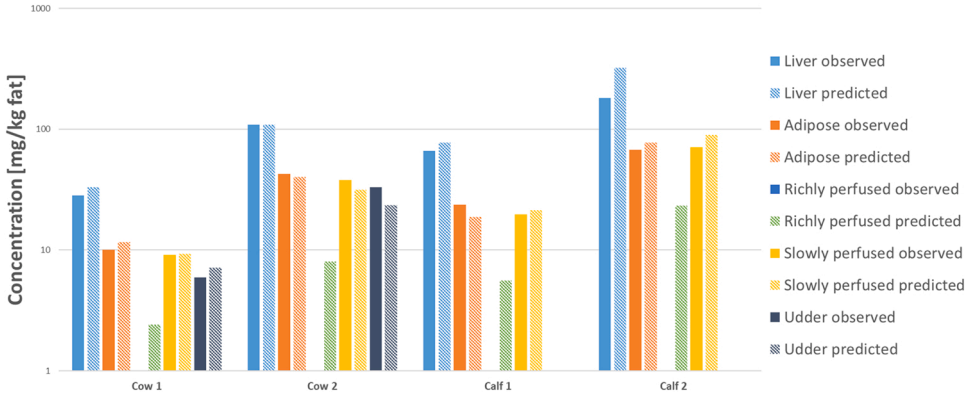

Fig. 6. Comparison of the predicted and measured concentrations of PCB-138 in all compartment's fats of the model at the of slaughter. * No measured data was available.

the SF_i and the $BTF_{Milk-Calf,i}$ were determined. They are listed in Table 5. For the calculation, it is assumed that the calf weighs 40 kg at birth; 150 kg at the day of slaughter; has a 0.2% blood fat fraction and average fat fractions of the calves. This results in a $\kappa = 0.098$, which almost equivalent to the ratio of fat in slowly perfused + adipose tissue at birth and slaughter. The parameters SF_i and $BTF_{Milk-Calf,i}$ are not directly comparable but the proportion between the compartments are very similar. In both cases, the highest contaminant concentration is found in liver fat, followed by adipose and the slowly perfused compartments, which show quite similar values for all three contaminants. Lowest concentrations are observed in the richly perfused and blood compartment. However, the values for the richly perfused compartment should be considered with caution, since they are only estimated via a QSAR method and not based on actual measured data.

To describe the distribution of contamination in the different compartments of the mother cow during dry and lactation period, the $BTF_{abs-Mother,i}$ and the $LBTF_{abs-Mother,i}$ for each compartment were calculated. For the calculations, a weight of 500 kg and a blood fat fraction of 0.2% are assumed for the mother cow. It is also supposed that the mother cow excretes 24 l milk per day with 3.5% fat during lactation. The results are shown in Table 6. Although again not directly comparable to each other or the parameters derived for the calves, the proportion between the compartments are quite similar for all these parameters. In contrast to the calves, the mother cow has an additional udder compartment with *BTF's* slightly above the *BTF*'s of blood.

3.4.2. Half-lives

To have a better understanding of the elimination process of these ndl-PCBs, their milk excretion half-lives were estimated (Table 7). The αhalf-life for each congener describes the initial fast elimination of the contaminant during which the non-adipose compartments are depleted at higher rate than the adipose compartments; likewise, the β half-life describes the latter and final phase of continuous elimination, in which all compartments are depleted at the same rate. It is assumed that the cows are at the height of lactation i.e., they yield 24 L/d with 3.5% fat. Furthermore, it is assumed again that both cows weigh 500 kg and have a blood fat fraction of 0.2%. The α half-lives are rather similar across all three ndl-PCBs ranging between 4.8 and 5.2 days. The β half-lives vary somewhat more across the PCBs with PCB-180 having the longest β half-life of 68 days and PCB-138 the shortest with 49 days.

4. Discussion

4.1. Model assumptions

For developing the herein described model, two main assumptions were made. First of all, the three ndl-PCBs are present only in the fat portion of any compartment and therefore the distribution into each compartment depends almost exclusively on the fat portions of each compartment. In the literature, this assumption is often found for PCBs and similarly highly lipophilic contaminants. Nevertheless, the partition coefficient is usually calculated with respect to the entire compartment rather than exclusively for the fat portion of the compartment. We choose the latter in order to be able to use the partition coefficients across all mother cows and their calves despite varying fat fractions across animals. In addition, we assumed that this also applies for the blood compartment, which has not been considered in other models in the literature (Derks et al., 1994; Hoogenboom et al., 2010; McLachlan, 1994). This hypothesis is further justified by the data showing that the concentration of ndl-PCBs related to blood fat of the mother cows and their calves are very similar shortly after calving, but concentrations related to whole blood are not, which is due to varying blood fat concentrations (Müller et al., 2019). This suggests that blood fat is a major factor affecting the PCB concentration in blood. Comparable ndl-PCB concentrations in the portion of the blood relevant for PCB, e.g., fat, of the mother cow and calf are to be expected, since it is known that the placenta is not a relevant permeation barrier for ndl-PCBs, and thus an unrestricted exchange between mother cow and calf can take place (Carreira et al., 2011). However, this is in contrast to the findings of Driesen et al. (2022), where a 1.5-fold increase in concentration of ndl-PCB in calf blood compared to mother cow blood was reported (Hirako, 2008). This might be caused by different blood fat compositions. Nevertheless, in Driesen et al. (2022) it is also reported that the concentrations of ndl-PCBs in body fat of mother cow and calf seem to be similar shortly after calving, supporting our general hypothesis that the concentration in each compartment with respect to fat are the same in mother cow and calf shortly after calving.

The second assumption in this model is that it is useful to divide the cow into liver, udder, richly perfused, slowly perfused, adipose and blood compartments. Especially the liver compartment and the slowly perfused, which mainly consists of muscle tissue, were chosen as they are edible and thus of major interest for risk assessment. Furthermore, this classification has also proven useful in other models (Derks et al., 1994). However, a comparison of the derived partition coefficients of slowly perfused tissue and adipose tissue (Table 4) shows that they are very similar and therefore if these compartments are close to equilibrium they will have very similar concentrations (on a fat basis), so there

Table 5
Parameters for estimating the concentration of ndl-PCBs in the fat of different compartments in calves given concentration in milk. For the calculation, it is assumed that the calf weighs 40 kg at birth and 150 kg at the day of slaughter and has a blood fat fraction of 0.2%.

	SF_i [unitless]			$BTF_{Milk-Calf,i}$ [1/kg]		
	PCB-138	PCB-153	PCB-180	PCB-138	PCB-153	PCB-180
Liver	0.387	0.300	0.345	0.191	0.126	0.128
Adipose	0.112	0.130	0.169	0.055	0.055	0.063
Slowly perfused	0.109	0.123	0.161	0.054	0.055	0.060
Richly perfused[a]	0.028	0.038	0.062	0.014	0.016	0.023
Blood	0.051	0.064	0.087	0.025	0.027	0.032

[a] No measured data for validation and calibration available.

Table 6
Parameters for estimating the concentration of ndl-PCBs in the compartment fats of the mother cows during dry and lactation period given the absorbed amount of contaminant. For the calculations, a weight of 500 kg and a blood fat fraction of 0.2% are assumed for the mother cow.

	$BTF_{abs-Mother,i}$ [1/kg]			$LBTF_{abs-Mother,i}$ [d/kg]		
	PCB-138	PCB-153	PCB-180	PCB-138	PCB-153	PCB-180
Liver	0.093	0.062	0.057	5.64	4.31	4.96
Adipose	0.027	0.027	0.027	1.61	1.85	2.41
Slowly perfused	0.026	0.027	0.026	1.57	1.84	2.29
Richly perfused[a]	0.007	0.008	0.010	0.41	0.54	0.88
Udder (=Milkfat)	0.021	0.018	0.014	1.19	1.19	1.19
Blood	0.012	0.013	0.014	0.74	0.91	1.24

[a] No measured data for validation and calibration available.

Table 7
α half-life andβ half-life of an average 500 kg mother cow, which has the average fat fraction of cow 1 and cow 2; blood fat fraction of 0.2% and yield 24 L/d milk with 3.5% fat.

	PCB-138	PCB-153	PCB-180
α – *half life*	5.2	5.0	4.8
β – *half life*	49	55	68

is no need to differentiate them in such a scenario. In contrast, the partition coefficient of the liver is much higher and that of the udder much lower than those of the aforementioned compartments and should therefore be considered separately. The high partition coefficient in liver was also already seen in Hoogenboom et al. (2021) and could be due to liver-specific sequestration mechanisms such as binding to liver proteins, likely in a fashion similar to dl-PCBs (EFSA, 2018) (or potentially active transport), which strongly influence its kinetic behavior. However, the very low partition coefficient in the udder must be viewed with caution as it is the only partition coefficient derived via fitting and therefore acts also as error correction so that this coefficient is probably also distorted from its physiological value. It must also be mentioned that similar models described in the literature (Hoogenboom et al., 2010) do not consider the udder compartment as separate due to its low volume and high blood flow rate (Van Eijkeren et al., 1998) during lactation. It is rather assumed that the contaminants are directly excreted from blood. The partition coefficient of the richly perfused tissue is solely based on QSAR methods and is not validated by experimental data (Bogdal et al., 2017).

4.2. Model accuracy and limitations

As mentioned above, the prediction of ndl-PCB concentration in the various compartments and milk are mostly in good agreement with experimental data of cows 1, 2 and their calves. The reason for the poor prediction of cow 3 is not understood, since the breeding and husbandry of the adult cows took place mostly outside our site and thus not under fully controlled conditions. One could suspect pathophysiological reasons, among others. Although, as already mentioned, the prediction of ndl-PCB concentrations in blood fat of the mother cow agrees reasonably well with the experimental data, there are some discrepancies in the period directly after calving. In contrast to the experimental data, a significant decrease in ndl-PCB concentration is predicted shortly after the birth of the calf compared to the ndl-PCB concentration pre calving. A possible explanation is the change of blood fat composition due to the change in metabolic state of the animal. It can be assumed that the physiological changes during the transition period influenced the blood fat composition. To compensate for the energy deficit after calving, deposited fat is mobilized, coming primarily from the subcutaneous adipose tissue. In addition, the concentrations in blood fat decrease notably faster than predicted shortly after arrival at our site, which could be explained by the change in diet upon arrival, which also presumably leads to changes in blood fat composition. However, to evaluate these effects further, a more frequent blood sampling under a more controlled environment would have been needed. In the present study, numerically higher ndl-PCB concentrations were detectable in subcutaneous adipose tissue (compared with caul and renal fat). This fact would explain why the decrease in ndl-PCB concentrations in the blood of the mother cows after calving was less than expected by modeling. Variations in blood fat fraction due to changes in the feeding management (restrictive on the farm versus ad libitum on our site) could also explain the notably high ndl-PCB concentrations in the blood fat of the cows shortly after arrival at BfR.

Despite the prominent nature of the blood fat compartment in this model, these inaccuracies in blood fat do not have a large impact on the overall model quality with respect to risk assessment. This is due to the fact that the volume of the fat fraction of the blood compartment is rather small compared to the other compartments and therefore the amount of ndl-PCBs present in blood fat is negligible compared to total amount in the cow. Furthermore, the cows compartments are most of the time close to equilibrium, i.e., the ratios of concentration between the individual compartments are close to the ratios of the individual partition coefficients due to the rather slow excretion/metabolization compared to the blood fat flow rate.

4.3. Conjecture about the time of contamination

To obtain clues on the course of contamination, the predicted ndl-PCB concentrations of the different diary cows were compared with the measurements in the bulk milk of dairy cows of the farm (coming from n = 27individuals mostly not sampled for this study). For this comparison, it was assumed that the milk fat fraction in the milk of different cows is always identical. Therefore, the increase in the concentration of ndl-PCB in bulk milk due to contamination of one animal is given by 1/n of the concentration in the milk fat of the contaminated animal. In addition, we also included a prediction of the ndl-PCB concentration in milk fat of cow 3. Due to the poor model prediction of this cow with the developed PBTK model, we instead estimated it by fitting the milk data from cow 3 to a simple exponential function. The results are summarized in Table 8.

Comparing the measured ndl-PCB concentration in the bulk milk with the sum of the predicted ndl-PCB concentration in milk of the three cows shows only a slight underprediction of the concentrations in the milk fat. This indicates strongly that the contamination of cows happened exclusively prior to the collecting of the milk as otherwise we would expect an overprediction (Fig. 7).

4.4. Transfer via placenta

Exposure of mammals to lipophilic compounds begins before birth through transfer from maternal blood to the fetus via the placenta (Koppe et al., 1992). After parturition, these compounds continue to be mobilized from maternal fat to be released into milk during lactation, reflecting the gradual depletion of maternal stores (Tuinstra et al., 1992). This is reflected in both predicted and experimental data (Fig. 5), where initial (t = 0) contamination with ndl-PCBs is already observed in the blood fat of the calf. The additional contamination of the calf via milk intake is also reflected in the predicted and experimental data, where a further increase in the amount of ndl-PCBs in the calf is observed. This shows that there is a significant transfer of ndl-PCBs from mother cow to calf, with the transfer via milk being the most relevant factor. At the same time, the transfer via placenta cannot be neglected and would become more important for cows fed with little or no mother's milk. In contrast to our findings, Driesen et al. (2022b) was reported a much lower relevance of the transfer via; however, in that study the calves were older and heavier (lipid mass of more than 60 kg) at slaughter, and the mother cows were continuously exposed even after birth, which increases the amount of contaminants transferred via milk fat relative to placenta even further.

5. Conclusion

The PBTK model presented in this work proved to be a robust tool to describe the fate of the most abundant ndl-PCBs 138, 153 and 180 in cows and their calves. In addition to predicting the distribution of the contaminant in different compartments and milk of the cow and her calf during lactation and the dry period, certain parameters relevant to risk assessment were calculated, such as the α half-life and β half-life, which ranged from 4.8 to 5.2 days and 49–68 days, respectively. In addition, parameters were derived to predict the concentration of these contaminants under near equilibrium or (pseudo) steady state conditions. The highest contaminant concentration was calculated for the fat of the liver compartment, followed by the adipose compartments and the slowly perfused compartments, which had roughly comparable concentrations. The PBTK model also allows the simulation of prenatal and postnatal transfer of the investigated ndl-PCBs, i.e., via placenta and via milk, respectively, from cow to calf. It could be shown that the amount of contaminants transferred to the calf via the placenta accounts for 10–14% of the total amount transferred in our setting.

In the literature several other PBTK models are reported describing the transfer of PCBs and similar highly lipophilic contaminants (e.g.

Table 8
Measured and predicted concentrations of ndl PCBs in milk. Concentrations in the bulk milk were measured, concentrations of ndl PCBs in the milk of cow 1 and 2 were predicted using the PBTK model. The contribution of cow 3 to ndl PCBs concentration found in the bulk milk was predicted via fitting the milk data to an exponential function.

	measured	prediction via PBTK model		exponential fitted	predicted
	Bulk milk	Milk cow 1	Milk cow 2	Milk cow 3	Sum cow 1–3
Day in model [d]	***(22.06.2016)***[a]	-252	-266	-68	
PCB-138 [µg/kg]	**30.92**	2.80	13.85	7.73	**24.40**
PCB-153 [µg/kg]	**32.61**	2.54	12.38	7.00	**21.92**
PCB-180 [µg/kg]	**9.98**	0.50	2.87	1.64	**5.01**

[a] date of milk sampling

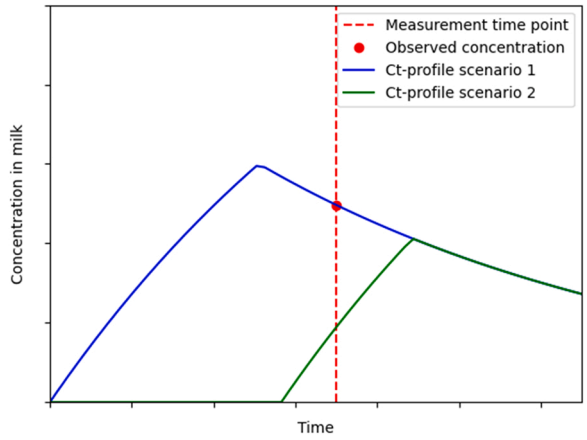

Fig. 7. Schematic depiction of the concentration time-profile (Ct-profile) in two different scenarios. Scenario 1 shows the Ct-profile if the assimilation phase ended before the measurement in bulk milk and scenario 2 shows the Ct-profile if the assimilation phase ended after the measurement in bulk milk.

dioxins) into cows milk and their compartments (see, e.g. Bogdal et al., 2017; Derks et al., 1994; McLachlan, 1994**).** Furthermore, an obviously effective placental transfer of PCBs from mother to fetus was also shown in other species, like in reindeer, where stillborn calves were examined (Suutari et al., 2011**).** With exception of Bogdal et al. (2017), whose predictions heavily rely on in silico methods, the herein investigated ndl-PCBs are often neglected. In contrast to the approach of Bogdal et al. (2017), our model is mainly based on actual measured concentrations in the respective compartment and is therefore able to provide a more accurate prediction of concentrations in all compartments including blood of the mother cow and its calf.

Therefore, our model will provide an excellent opportunity of assessing precise time-dependent toxicokinetic effects of environmental contaminants in cows and calves. In its current form, this model is best suited for describing the depuration of a pregnant cow and the contamination via placenta and milk fat of its calf during early life. However, this model also presents a good starting point for future developments describing the whole life cycle of a cow with not only depuration but also continuous exposure of the animals.

Ethical approval

All applicable international, national, and/or institutional guidelines for the care and use of animals were followed. All procedures on cows and calves (blood sampling and slaughtering) were approved and licensed by the Ethics Committee of the Federal State Berlin, Germany (Landesamt für Gesundheit und Soziales) with approval number G 0262/16.

Funding

This research did not receive any specific grant from funding agencies in the public, commercial, or not-for-profit sectors.

CRediT authorship contribution statement

Jan-Louis Moenning: Contribution: Methodology, Software, Formal analysis, Visualization, Writing – original draft. **Jorge Numata**: Contribution: Conceptualization, Methodology, Validation, Writing – review & editing. **Dorit Bloch**: Contribution: Writing – original draft. **Anne Jahnke**: Contribution Sample analysis and Quantification, Writing. **Helmut A. Schafft**: Contribution Conceptualization. **Markus Spolders**: Contribution Conceptualization, Veterinary Care and Control. **Anja Lüth**: Contribution Coordination of sample analysis, Writing. **Monika Lahrssen-Wiederholt**: Contribution, Conceptualization. **Kirsten Schulz**: Contribution, Investigation, Project administration, Data curation, Visualization, Writing – original draft.

Declaration of Competing Interest

The authors declare that they have no known competing financial interests or personal relationships that could have appeared to influence the work reported in this paper.

Data availability

Data will be made available on request.

Acknowledgment

We gratefully acknowledge our colleagues from the Unit Animal Husbandry, Aquaculture and Reference Materials of the German Federal Institute for Risk Assessment, for their great support in caring for the animals. We would also like to thank Karl-Heinz Südekum for helpful discussions on animal physiology.

Appendix A. Supporting information

Supplementary data associated with this article can be found in the online version at doi:10.1016/j.etap.2023.104106.

References

Ballschmiter, K., Zell, M., 1980. Analysis of polychlorinated biphenyls (PCB) by glass capillary gas chromatography. Fresenius' Zeitschrift analytische Chem. 302, 20–31.
Blome, R., et al., 2003. Growth, nutrient utilization, and body composition of dairy calves fed milk replacers containing different amounts of protein. J. Anim. Sci. 81, 1641–1655.
Bogdal, C., et al., 2017. Dynamic transgenerational fate of polychlorinated biphenyls and dioxins/furans in lactating cows and their offspring. Environ. Sci. Technol. 51, 10536–10545.
Carreira, S.C., et al., 2011. Studying placental transfer of highly purified non-dioxin-like PCBs in two models of the placental barrier. Placenta 32, 283–291.
Derks, H.J.G.M., et al., 1994. Pharmacokinetic modeling of polychlorinated dibenzo-p-dioxins (PCDDs) and furans (PCDFs) in cows. Chemosphere 28, 711–715.

Diaz, M., et al., 2001. Composition of growth of Holstein calves fed milk replacer from birth to 105-kilogram body weight. J. Dairy Sci. 84, 830–842.

Driesen, C., et al., 2022. Accumulation and decontamination kinetics of PCBs and PCDD/Fs from grass silage and soil in a transgenerational cow-calf setting. Chemosphere 296, 133951.

Driesen, C., et al., 2022b. Transgenerational mass balance and tissue distribution of PCBs and PCDD/Fs from grass silage and soil into cow-calf continuum. Chemosphere 307, 135745.

EFSA, E.F.S.A., 2005. Opinion of the Scientific Panel on contaminants in the food chain [CONTAM] related to the presence of non dioxin-like polychlorinated biphenyls (PCB) in feed and food. EFSA J. 3, 284.

EFSA, E.F.S.A., 2012. Update of the monitoring of levels of dioxins and PCBs in food and feed. EFSA J. *10*.

EFSA, E.F.S.A., 2018. Risk for animal and human health related to the presence of dioxins and dioxin-like PCBs in feed and food. Efsa J., e05333

EU. COMMISSION REGULATION (EU) No 1259/2011 of 2 December 2011 amending Regulation (EC) No 1881/2006 as regards maximum levels for dioxins, dioxins-like PCBs and non dioxin-like PCBs in foodstuffs. Official Journal of the European Union 2011, L 320/18.

EU. COMMISSION REGULATION (EU) No 277/2012 of March 2012 amending Annexes I and II to Directive 2002/32/EC of the European Parliament and the Council as regards maximum levels and action thresholds for dioxins and polychlorinated biphenyls. Official Journal of the European Union 2012, L 91/1.

EU. COMMISSION REGULATION (EU) No 2017/644 of 5 April 2017 laying down methods of sampling and analysis for the control of levels of dioxins, dioxin-like PCBs and non-dioxin-like PCBs in certain foodstuffs and repealing Regulation (EU) No 589/2014. Official Journal of the European Union 2017, L 92/9.

Hirako, M., 2008. Transfer and accumulation of persistent organochlorine compounds from bovine dams to newborn and suckling calves. J. Agric. Food Chem. 56, 6768–6774.

Hoogenboom, R., et al., 2010. Kaolinic clay derived PCDD/Fs in the feed chain from a sorting process for potatoes. Chemosphere 78, 99–105.

Hoogenboom, R.L.A.P., et al., 2021. High levels of dioxins and PCBs in meat, fat and livers of free ranging pigs, goats, sheep and cows from the island of Curaçao. Chemosphere 263, 128057.

Koppe, J.G., Olie, K., Van Wijnen, J., 1992. Placental transport of dioxins from mother to fetus. Dev. Pharmacol. Ther. 18, 9–13.

Krause, T., et al., 2022. Transfer of polychlorinated dibenzo-p-dioxins and dibenzofurans (PCDD/Fs) and polychlorinated biphenyls (PCBs) from oral exposure into cow's milk-part i: state of knowledge and uncertainties. Nutr. Res. Rev. 1–53.

Lancz, K., et al., 2015. Ratio of cord to maternal serum PCB concentrations in relation to their congener-specific physicochemical properties. International journal of hygiene and environmental health, Band 218, 91–98.

Lin, Z., et al., 2020. Physiological parameter values for physiologically based pharmacokinetic models in food-producing animals. Part I: cattle and swine. J. Vet. Pharmacol. Ther. 43, 385–420.

McLachlan, M.S., 1994. Model of the fate of hydrophobic contaminants in cows. Environ. Sci. Technol. 28, 2407–2414.

Moenning, J.L., et al., 2022. Transfer of polychlorinated dibenzo-p-dioxins and dibenzofurans (PCDD/Fs) and polychlorinated biphenyls (PCBs) from oral exposure into cow's milk - part II: toxicokinetic predictive models for risk assessment. Nutr. Res. Rev. 1–14.

Müller, M.H.B., et al., 2019. Prenatal exposure to persistent organic pollutants in Northern Tanzania and their distribution between breast milk, maternal blood, placenta and cord blood. Environ. Res. 170, 433–442.

Newville, M., et al., 2016. LMFIT: non-linear least-square minimization and curve-fitting for Python. Astrophys. Source Code Libr.

Rossi, F., et al., 2010. Monitoring of the declining trend of Polychlorobifenyls concentration in milk of contaminated dairy cows. Ital. J. Anim. Sci. 9, e18.

Schecter, A., et al., 2006. Dioxins: an overview. Environ. Res. 101, 419–428.

Suutari, A., et al., 2011. Polychlorinated dibenzo-p-dioxins (PCDDs), dibenzofurans (PCDFs), polychlorinated biphenyls (PCBs), and polybrominated diphenyl ethers (PBDEs) in Finnish semi-domesticated reindeer (Rangifer tarandus tarandus L.). Environ. Int. 37, 335–341.

Tremolada, P., et al., 2014. Predicting PCB concentrations in cow milk: validation of a fugacity model in high-mountain pasture conditions. Sci. Total Environ. 487, 471–480.

Tuinstra, L.T., et al., 1992. Excretion of polychlorinated dibenzo-p-dioxins and-furans in milk of cows fed on dioxins in the dry period. J. Agric. Food Chem. 40, 1772–1776.

UBA (Umweltbundesamt; German Environment Agency), 2003. Aktualisierung der Referenzwerte für PCB-138, -153, -180 im Vollblut sowie Referenzwerte für HCB, β-HCH und DDE im Vollblut [Update of reference values for PCB-138, -153, -180 in whole blood and reference values for HCB, β-HCH and DDE in whole blood]. Bundesgesundheitsblatt - Gesundheitsforsch - Gesundheitsschutz 2/2003.DOI 10.1007/s00103–002-0545–6.

Van Eijkeren, J.C.H., Jager, D.T. & Sips, A.J.A.M., 1998. Generic PBPK-modelling of lipophilic contaminants in the cow.

WHO, World Health Organisation, 2016. Safety evaluation of certain food additives and contaminants, supplement 1: non-dioxin-like polychlorinated biphenyls, prepared by the eightieth meeting of the Joint FAO/WHO Expert Committee on Food Additives (ſ˚JECFA)ſ˚. WHO Food Additive Series: 71-S1.

Environmental Toxicology and Pharmacology 103 (2023) 104274

Contents lists available at ScienceDirect

Environmental Toxicology and Pharmacology

journal homepage: www.elsevier.com/locate/etap

Erratum or Corrigendum

Corrigendum to "Transfer and toxicokinetic modeling of non-dioxin-like polychlorinated biphenyls (ndl-PCBs) into accidentally exposed dairy cattle and their calves – A case report" Environ. Toxicol. Pharmacol. 99 (2023) 104106

Jan-Louis Moenning, Jorge Numata, Dorit Bloch, Anne Jahnke, Helmut A. Schafft, Markus Spolders, Anja Lüth, Monika Lahrssen-Wiederholt, Kirsten Schulz *

German Federal Institute for Risk Assessment, Berlin, Germany

The authors regret a mistake to the readers of the article " Transfer and toxicokinetic modeling of non-dioxin-like polychlorinated biphenyls (ndl-PCBs) into accidentally exposed dairy cattle and their calves - A case report " (DOI: https://10.1016/j.etap.2023.104106) and provide the following correction:

Eqs. (1)–(3) as well as the paragraph in between, should read as detailed below, while this has no impact on the included computer code or the results of the paper:

$$\frac{dA_{i,j}}{dt} = -\left(\frac{Q_{fat,i,j}}{V_{fat,i,j}P_{i,\not}} + k_{met,\not}\mathbf{1}_{\{liver\}}(i) + \frac{CL_{milkfat,j}}{V_{fat,udder,j}}\mathbf{1}_{\{udder\}}(i)\right)A_{i,j} + \frac{Q_{fat,i,j}A_{blood,j}}{V_{fat,blood,j}} + F_{abs}\frac{S_{milkfat,j}A_{udder,M_k}}{V_{fat,udder,M_k}}\mathbf{1}_{\{liver\}}(i) \quad (1)$$

and

$$\frac{dA_{blood,j}}{dt} = \sum_i \frac{Q_{fat,i,j}A_{i,j}}{V_{fat,i,j}P_{i,\not}} - \frac{Q_{fat,blood,j}A_{blood,j}}{V_{fat,blood,j}} \quad (2)$$

for i ≠ blood. Here $A_{i,j}$ is the amount in each compartment; $CL_{milkfat,j}$ is the amount of milk fat excreted each day; $S_{milkfat,j}$ is the amount of milk fat sucked each day (=0 for adult cows) and $\boldsymbol{I}_{\{liver\}}$ and $\boldsymbol{I}_{\{udder\}}$ are the indicator functions. This can be simplified to

$$\frac{dA_j}{dt} = M_j A_j, \quad (3)$$

DOI of original article: https://doi.org/10.1016/j.etap.2023.104106.

* Corresponding author.
E-mail address: kirsten.schulz@bfr.bund.de (K. Schulz).

https://doi.org/10.1016/j.etap.2023.104274

Available online 19 September 2023

5.1.3 Paper 3

Moenning, J.-L., et al., Toxicokinetic modeling of the transfer of polychlorinated biphenyls (PCBs) and polychlorinated dibenzo-p-dioxins and dibenzofurans (PCDD/Fs) into milk of high-yielding cows during negative and positive energy balance. Computational Toxicology, 2023: p. 100290

Computational Toxicology 28 (2023) 100290

Contents lists available at ScienceDirect

Computational Toxicology

journal homepage: www.sciencedirect.com/journal/computational-toxicology

Toxicokinetic modeling of the transfer of polychlorinated biphenyls (PCBs) and polychlorinated dibenzo-*p*-dioxins and dibenzofurans (PCDD/Fs) into milk of high-yielding cows during negative and positive energy balance

Jan-Louis Moenning [a], Julika Lamp [b], Karin Knappstein [b], Joachim Molkentin [b], Andreas Susenbeth [c], Karl-Heinz Schwind [d], Sven Dänicke [e], Peter Fürst [f], Hans Schenkel [g], Robert Pieper [a], Torsten Krause [b], Jorge Numata [a,*]

[a] *Department Safety in the Food Chain, German Federal Institute for Risk Assessment (BfR), Max-Dohrn-Straße 8-10, 10589 Berlin, Germany*
[b] *Department of Safety and Quality of Milk and Fish Products, Max Rubner-Institut (MRI), Hermann-Weigmann-Str. 1, 24103 Kiel, Germany*
[c] *Institute of Animal Nutrition and Physiology, Kiel University (CAU), 24118 Kiel, Germany*
[d] *Department of Quality and Safety of Meat, Max Rubner-Institut (MRI), E.-C.-Baumann-Str. 20, 95326 Kulmbach, Germany*
[e] *Institute of Animal Nutrition, German Federal Research Institute for Animal Health, Friedrich-Loeffler-Institut (FLI), Bundesallee 37, 38116 Braunschweig, Germany*
[f] *Chemical and Veterinary Analytical Institute Münsterland-Emscher-Lippe (CVUA-MEL), Joseph-König-Straße 40, 48147 Münster, Germany*
[g] *Department of Animal Nutrition, University of Hohenheim, Emil-Wolff-Str. 10, 70599 Stuttgart, Germany*

ARTICLE INFO

Keywords:
Food safety
Feed safety
Toxicokinetics
Carry-over
Bos taurus

ABSTRACT

A toxicokinetic modeling approach was used to study the transfer of 7 polychlorinated dibenzo-*p*-dioxins (PCDDs), 10 dibenzofurans (PCDFs), 12 dioxin-like polychlorinated biphenyls (dl-PCB) and 3 non-dioxin like (ndl) PCBs in dairy cows. The model describes the concentration–time profile of each congener in milk and blood of high-yielding dairy cows. It was parametrized using an in-house transfer study with 3 cows exposed to a defined synthetic congener mixture for two dosing periods, as well as 3 control cows to account for background exposure. The first dosing was administered during negative energy balance (NEB) after calving, and the second during positive energy balance (PEB) in late lactation. Results include extrapolated steady-state transfer rates and elimination half-lives, many of which have never been reported before. Transfer rates (*TRs*) were significantly higher during the NEB by a median of 27%, likely due to an increase in non-milk elimination during PEB. The difference draws attention to the influence of the metabolic state of food-producing animals in risk assessment. Comparison of the *TRs* derived here with those reported in the literature showed that they were, in median, 43% higher in the NEB phase and 16% higher in the PEB phase probably because we report *TRs* in steady-state unlike most literature sources.

1. Introduction

Polychlorinated dibenzo-*p*-dioxins (PCDDs) and dibenzofurans (PCDFs) (collectively and colloquially referred to as "dioxins") as well as polychlorinated biphenyls (PCBs) are lipophilic environmental contaminants that accumulate along the food chain. Some dioxins have minor natural sources, but these substances are formed nowadays mostly as byproducts of human activity [1,2]. In contrast, most PCBs were intentionally mass-produced in the past and persist in the environment to this day [3]. The most important source of human exposure to these chemicals are foods of animal origin, chiefly dairy products, eggs, meat and fish [4]. In the last decades, several studies have been

Abbreviations: BMRT, blood mean residence time; GC, gas chromatograph; GIT, gastro-intestinal tract; HpCDD, heptachlorodibenzo-*p*-dioxin; HpCDF, heptachlorodibenzofuran; HRMS, high resolution mass spectrometer; HxCDD, hexachlorodibenzo-*p*-dioxin; HxCDF, hexachlorodibenzofuran; LOQ, limit of quantification; NEB, negative energy balance; OCDD, octachlorodibenzo-*p*-dioxin; OCDF, octachlorodibenzofuran; PBTK, physiological based toxickinetic; PCBs, polychlorinated biphenyls; PCDD/Fs, polychlorinated dibenzo-*p*-dioxins and dibenzofurans; PCDDs, polychlorinated dibenzo-*p*-dioxins; PCDFs, polychlorinated dibenzofurans; PEB, positive energy balance; PeCDF, pentachlorodibenzofuran; TCDD, tetrachlorodibenzo-*p*-dioxin; TCDF, tetrachlorodibenzofuran; TEQ, toxic equivalency; *TR*, transfer rate; *TT*, transition time; T_{ss}, time until steady-state (90%); WHO, World Health Organization; dl, dioxin-like; ndl, non-dioxin-like.

* Corresponding author.
E-mail address: jorge.numata@bfr.bund.de (J. Numata).

https://doi.org/10.1016/j.comtox.2023.100290
Received 11 August 2023; Received in revised form 7 November 2023; Accepted 12 November 2023
Available online 14 November 2023

published describing the transfer of PCDD/Fs and PCBs from feed into cows' milk, where parameters such as the transfer factor and half-lives were estimated [5,6]. These parameters are often based on feeding studies or use predictive modeling techniques. Transfer parameters derived explicitly for high-yielding cows [7] remain the exception, with the most recent studies focused on low to medium yielding cows [8–10]. Furthermore, the transfer of some toxicologically relevant congeners has not yet been quantified. The elimination kinetics for 1,2,3,7,8-PeCDF and some PCBs such as 77, 81, 114 and 123 have not yet been reported. It also remains unclear whether the metabolic status of the cow has an influence on the transfer of these contaminants, and if transfer parameters derived from older studies are still valid for high-yielding dairy cow breeds [5]. This work aims to address most of these knowledge gaps.

The balance between catabolic and anabolic processes has a direct impact on body fat reserves, which are the main compartment for the storage of lipophilic xenobiotics. This is particularly true for high-performing dairy cows, which display a markedly negative energy balance (NEB) because the supplies needed for increasing milk production in the first weeks after calving cannot be replenished fast enough from feed intake [11]. During NEB, a cow mobilizes body fat reserves for milk fat production, reducing the size of the body fat compartment, where lipophilic xenobiotics are stored. This would theoretically create or increase a concentration gradient for lipophilic compounds between blood and body fat, allowing more PCDD/Fs and PCBs to be released into the blood, ultimately increasing the elimination rates until the cow regains a positive energy balance (PEB).

The present work aims to describe the transfer kinetics of various PCDD/F and PCB congeners from oral exposure into milk using toxicokinetic modeling [12]) in both the NEB and PEB phases. A toxicokinetic model performs predictive estimations of the transfer based on mathematical equations that reflect the fate (absorption, distribution, metabolism and excretion) of the congeners and the physiological processes in the cow. The model was calibrated separately for the NEB and PEB phases using data from an in-house controlled transfer study conducted from 2016 to 2018 [13]. In the study, 5 German Holstein cows were exposed to a mixture of PCDD/Fs and PCBs for two 28-day dosing periods, the first during the post-calving NEB and the second during the late lactation PEB. Due to health issues, data from only 3 cows could be further evaluated. The model was then used to calculate several transfer parameters, such as transfer rates and biphasic elimination half-lives, including the elusive α half-lives in NEB and PEB. Using statistical techniques, differences in transfer parameters between NEB and PEB phases of lactation were tested for significance. The model presented here formally belongs to the class of PBTK models (Table 1 of ref [12]) and can also be extended by others to provide a more dynamic view of contamination incidents by accounting for dynamic effects such as different milk fat yields over time or general non-steady-state conditions [14,15].

2. Materials and methods

2.1. Ethics approval statement

The animal study was approved by the Ministry of Energy, Agriculture, the Environment, Nature, and Digitalization of Schleswig-Holstein, Germany (reference number V241-37856/2017; 102–8/16).

2.2. Animal study

To evaluate the transfer of PCDD/Fs and PCBs from feed into milk fat, a controlled feeding study was conducted with 9 healthy lactating German Holstein cows, black and white, in their second pregnancy. The animals were divided into 1 experimental group originally consisting of 5 animals and 1 control group consisting of 4 animals. The experimental group was dosed daily with capsules containing a known mixture of PCDD/Fs and PCBs during the first 28 days of lactation and later again for 28 consecutive days during the PEB phase of lactation (Tables 2, S1 and S2 of Krause et al. [13] for the daily dose). Throughout the study, all animals were fed with practically uncontaminated feed that was monitored for its PCDD/F and PCB content. All quantifiable amounts in the feed were considered in modeling. During the course of this study, one of the experimental cows and one of the control cows died and were therefore not included in this evaluation. In addition, one cow in the experimental group exhibited subclinical symptoms and was also excluded from this evaluation. Detailed discussion of these symptoms can be found in Krause et al. section "PCDD/Fs and PCBs in feces and exclusion of cow 3425" [13]. This left 3 experimental animals (labeled 3426, 3438 and 3448) and 3 control animals (labels not relevant, as the data were grouped) for this evaluation. The experimental setup and an analysis of the experimental data are described in more detail in a related publication [13]. To further refine the transfer kinetics, blood samples were analyzed and this previously unpublished data were used for toxicokinetic modeling.

Table 1
Interpretation of the derived parameters from the model.

Parameter name, different for each congener and phase (NEB, PEB)	Interpretation
Transfer rate (*TR*)	After a finite oral exposure of the animal, the *TR* describes the relative amount of the substance that is excreted with milk over an assumed infinite period of time. Or: Upon continuous exposure at constant daily dose, the *TR* describes the relative amount of the substance excreted daily with milk after the steady-state has been reached.
Time until steady-state (90 %) (T_{ss})	Under continuous exposure at constant daily dose, T_{ss} is the time required to reach 90 % of the steady-state concentration in daily milk.
α- and *β*-half-lives	A half-life is the time it takes for the substance concentration in the milk to be halved. The depuration phase begins when the exposure ends. The initial depuration is fast and characterized by an α-half-life. Later the depuration becomes slower and is characterized by a β-half-life.
Transition time (*TT*)	The depuration phase begins when the exposure is ended. The *TT* is the time from the beginning of depuration until the dominant half-life changes from α to β.
Blood mean residence time (*BMRT*)	The average time a molecule spends in the blood compartment after being absorbed from the gastrointestinal tract.

2.3. Sampling, chemical analytics and quality assurance

For milk and feed, sampling and analysis of 17 PCDD/Fs, 12 dl-PCBs and 6 ndl-PCBs were described in detail in ref. [13]; for blood, they are described below. The performance of the analytical setup was checked by analysis of certified milk powder containing PCDD/Fs (BCR-607) and PCBs (BCR-450). Blanks and daily calibration checks were performed for additional quality assurance. The recoveries of the isotope-labeled congeners added to milk fat, blood and feed were within the limits of EPA Method 1613B [16] for PCDD/Fs and EPA Method 1668C [17] for PCBs. The congener-specific limit of quantification (LOQ, Table S1) for all three matrices was calculated using a signal-to-noise ratio of 3:1 [18].

Of the 6 ndl-PCBs, only data for the 3 higher chlorinated congeners (PCB-138, PCB-153 and PCB-180) were used for further evaluation due to fluctuating background contamination of PCB-28, PCB-52 and PCB-101 observed in the milk fat of the control group.

Blood samples (200 mL) were collected from the jugular vein of the animals and mixed with 8 mL of an 0.1 mol/L

ethylenediaminetetraacetic acid solution (Titriplex III, Merck, Darmstadt). Samples for PCDD/F and PCB analysis were collected every other day during the first week of the dosing and depuration phases and then every third day for the next three weeks. During the later stages of the depuration phase, blood samples were collected in parallel with the milk samples once a week and then every other week. Samples were frozen and stored at −20 °C until analysis.

For the analysis of PCDD/Fs and PCBs in whole blood, a liquid–liquid extraction method was adapted. Briefly, after defrosting, the sample was transferred to a 1 L glass bottle and mixed with PCDD/F and PCB extraction standards (Cambridge Isotopes Laboratories, Inc., Andover, USA). 60 mL of a saturated ammonium sulphate (Emsure, Merck, Darmstadt, Germany) solution and 240 mL ethanol (SupraSolv, Merck, Darmstadt, Germany) and n-hexane (Picograde, LGC Standards, Teddington, England) in a 1:4 ratio were added to the blood sample and shaken for 40 min. The organic phase was separated and the remaining blood was extracted three times with 100 mL n-hexane including a washing step with 200 mL demineralized water. The organic phases were combined over sodium sulphate (Emprove, Merck, Darmstadt, Germany), filtered and concentrated first on a rotary evaporator and finally at 40 °C in an oven overnight. Subsequent sample cleanup on a DexTech (LCTech GmbH, Obertaufkirchen, Germany) and residue analysis with a MAT 95 (Finnigan MAT, Bremen, Germany) GC-HRMS are described in the related publication [13]. While the chosen blood extraction method allows the handling of larger samples, it is insufficient for the extraction of phospholipids [19] and thus inadequate for the quantification of the full fat content. Therefore, PCDD/F and PCB concentrations in blood are expressed on a whole blood basis.

2.4. Toxicokinetic modelling

A three-compartment model was used to describe the toxicokinetic behavior of PCDD/F and PCB congeners in cows. The model consists of a central Blood compartment (Fig. 1), which is directly connected to two turnover compartments: a Slow turnover compartment, tantamount to adipose tissue, and a Fast turnover compartment, which represents the rest of the body, where the congeners are presumably bound to proteins or intracellular fat. The Blood compartment is in constant exchange with these compartments, albeit at different rates. After partial absorption from the gastrointestinal tract (GIT), the congeners enter the systemic circulation (in actuality via the liver or the lymphatic system). The congener-dependent absorption process is simplified in this model using multiplicative constants, while distinguishing between absorption from the capsule dose $F_{i,Dose}$ and absorption from feed $F_{i,Feed}$.

Throughout this work, the index i stands for the congener, j stands the individual animal and k stands for the compartment. If a parameter has no index i and/or j, it is not dependent on the congener and/or individual. Most parameters are fitted independently for each phase, differentiated where needed by a minus sign in NEB (-) and a plus sign in PEB (+).

Transition rates between the Slow and Fast compartments depend mainly on the Blood flow rate into a specific compartment Q_k, the compartment volume V_k (and $V_{j,Blood}$), and the partition coefficient $P_{i,k}$ describing the thermodynamic equilibrium concentration in the respective compartment relative to the concentration in blood. Furthermore, it is assumed that the transition rate into the Slow turnover compartment is diffusion-limited, which is in contrast to the blood flow-limited transfer rate into the Fast turnover compartment [20]. To account for this, the blood flow rate into the Slow turnover compartment is reduced by a congener-dependent diffusion factor $D_i < 1$.

Explicit excretion is considered to occur only from the Blood compartment into milk fat, depending on the milk fat yield $CL_{j,Milk}(t)$ and the congener-specific partition coefficient $P_{i,Milk}$. Any metabolic elimination and/or non-milk excretion is implicitly accounted for by the absorption coefficients $F_{i,Dose}$ and $F_{i,Feed}$; this was done because it is impossible to distinguish between unabsorbed and non-milk eliminated congeners from the available data. In summary, the amount of congener $A_{i,j}(t) = (A_{i,j,Blood}(t), A_{i,j,Slow}(t), A_{i,j,Fast}(t))^T$ in each compartment of the model at a time t can be described by the differential equation

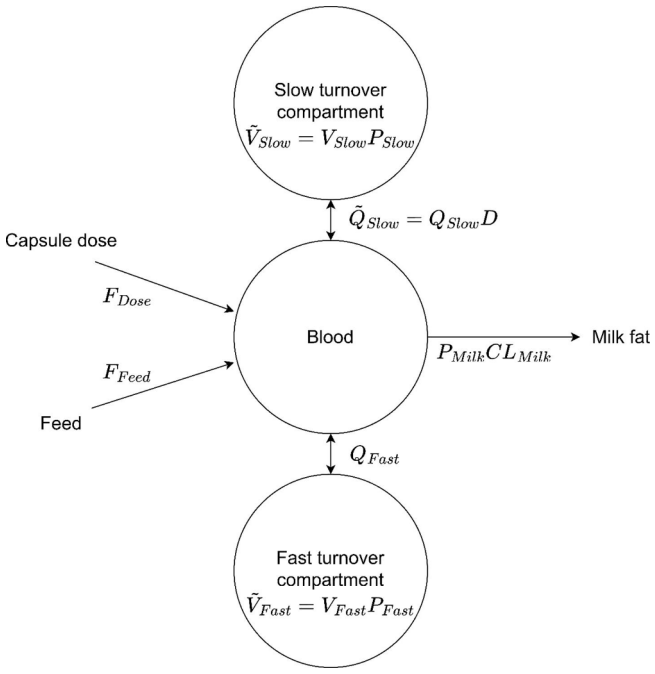

Fig. 1. Schema of the three-compartment model. Here, Q_{Slow} and Q_{Fast} [L/d] are the blood flows into the respective compartments; V_{Slow} and V_{Fast} [L] are the volumes of the respective compartments; P_{Slow}, P_{Fast} and P_{Milk} [unitless] are the partition coefficients of the respective compartments and milk; $CL_{Milkfat}$ [L/d] is the milk fat yield per day; D_i [unitless] is the factor induced due to the diffusion-limited nature of the Slow turnover compartment ; F_{Feed} and F_{Dose} [unitless] are the absorbed fractions from feed and capsule dose, respectively, into the blood. Here, the congener index i and the animal individual index j have been suppressed for readability, but a model exists for each congener and some parameters, such as the compartment size V, are individual-dependent.

$$\dot{A}_{i,j}(t) = M_{i,j}(t)A_{i,j}(t) + I_{i,j}(t) \tag{1}$$

where $M_{i,j}(t)$ is the transition matrix given by

$$M_{i,j}(t) = \begin{pmatrix} -\frac{Q_{Fast} + Q_{Slow}D_i + CL_{j,Milk}(t)P_{i,Milk}}{V_{j,blood}} & \frac{Q_{Slow}D_i}{V_{Slow}P_{i,Slow}} & \frac{Q_{Fast}}{V_{Fast}P_{i,Fast}} \\ \frac{Q_{Slow}D_i}{V_{j,blood}} & -\frac{Q_{Slow}D_i}{V_{Slow}P_{i,Slow}} & 0 \\ \frac{Q_{Fast}}{V_{j,blood}} & 0 & -\frac{Q_{Fast}}{V_{Fast}P_{i,Fast}} \end{pmatrix} \tag{2}$$

and I is the input vector given by

$$I_{i,j}(t) = \left(Dose_{i,j}(t)F_{i,Dose} + Feed_{i,j}(t)F_{i,Feed}, 0, 0\right) \tag{3}$$

To reduce the number of model parameters, the partition coefficients and volumes of the Slow and Fast turnover compartments were not fitted separately, but the relative capacity (relative to blood) of both compartments was estimated, i.e. $\widehat{V}_{i,Slow} := V_{Slow}P_{i,Slow}$ and $\widehat{V}_{i,Fast} := V_{Fast}P_{i,Fast}$ as they only appear in this arrangement in (1). Instead of separately deriving the blood flow rate into the Slow turnover compartment Q_{slow} and the factor D, only the effective blood flow rate $\widehat{Q}_{i,Slow} := Q_{Slow}D_i$ was used as a parameter. Besides these, only the values for the blood flow rate Q_{Fast} into the Fast turnover compartment and the blood volume $V_{j,Blood}$ have to be approximated.

Since a two-compartment model is considered sufficient to describe the transfer accurately in a quantitative sense for each of the congeners studied [21], it is expected that the Blood and Fast turnover compartments are in equilibrium almost immediately. Therefore, the blood flow rate was assumed to be equal to the total cardiac output of a dairy cow [22], i.e. $V_{j,Total}$· 164 L/kg/d, where $V_{Total,j}$ is the average weight of the individual animal in kg. The blood is assumed to be 4.35 wt% of the total body mass of each cow [22], i.e. $V_{j,Blood} = V_{j,Total}$· 0.0435. These last two physiological parameters are independent of the metabolic state (identical for NEB and PEB phases).

2.5. Model parametrization

The remaining model parameters are assumed to depend on the metabolic state of the animal and are therefore estimated or optimized separately for the NEB (-) and for the PEB (+) phases. The first parameter estimated is the milk fat/whole blood partition coefficients $P^{-}_{i,milk}$ for NEB and $P^{+}_{i,milk}$ for PEB. It was estimated as the median ratio of congener concentrations in milk fat and in blood when measured on the same day. This was done for all 3 control and 3 experimental cows considered.

To derive the remaining parameters, a fitting approach was used in which the absorption coefficient from feed is fitted separately for each set of parameter values to be evaluated. To evaluate a given set of parameters $\mathscr{P}_i$=($\widehat{V}^{-}_{i,Fat}$, $\widehat{V}^{-}_{i,Rest}$, $\widehat{Q}^{-}_{i,Fat}$, $F^{-}_{i,Dose}$, $\widehat{V}^{+}_{i,Fat}$, $\widehat{V}^{+}_{i,Rest}$, $\widehat{Q}^{+}_{i,Fat}$, $F^{+}_{i,Dose}$), the optimal parameters related to the exposure from feed $\mathscr{T}_{i,j}$=($A_{0,i,j}$, $F^{-}_{i,Feed}$, $F^{+}_{i,Feed}$) (given $\mathscr{P}_i$) were first determined by fitting them to the data of the control cows (since those cows received no exposure from dose capsules). $A_{0,i,j}$ is the starting vector describing the burden of each compartment at the beginning of lactation, assuming that the cows are in a steady-state, i.e., there exists a $\kappa_i \geq 0$ so that $A_{0,i,j} = M_{i,j}(0)^{-1}(\kappa_i, 0, 0)^T$and therefore only κ_i needs to be fitted instead of the initial burden of each compartment $A_{0,i,j}$. If the control animals had on average not more than 2 data points of milk fat concentration above the LOQ during NEB or PEB, then $\kappa_i = 0$, $F^{-}_{i,Feed} = 0$ or $F^{+}_{i,Feed} = 0$, respectively. Finally, all parameters together (including the starting vector) were used to evaluate the viability of the parameter set values $\mathscr{P}_i$ given the measured data of only the experimental cows. For both procedures (fitting of $\mathscr{P}_i$ and $\mathscr{T}_{i,j}$), the weighted natural logarithmic error was used due to the exponential nature of the data, i.e.

$$E_i = \sqrt{\frac{\sum_j \sum_l W_{t_{i,j,l},i,j}\left(ln(p_{t_{i,j,l},i}) - ln(x_{t_{i,j,l},i})\right)^2}{\sum_j \sum_l W_{t_{i,j,l},i,j}}} \tag{4}$$

where $p_{t_{i,j,l},i}$, $x_{t_{i,j,l},i}$ are the model prediction and measured data respectively at time $t_{i,j,l}$ in milk of all measurements of all experimental cows. Since the measurement times were not equispaced, it is necessary to compensate for the unequal distribution of information available around each measurement time; this is done by $W_{t_{i,j,l},i}$, which performs a weighting of the data at time $t_{i,j,l}$ and was derived from a kernel density estimation of the measurement times, i.e.

$$W_{t_{i,j,l},i,j} = \frac{1}{\mathscr{K}_{i,j}(t_{i,j,l})} \tag{5}$$

where $\mathscr{K}_{i,j}$ is kernel density function, which is estimated via the standard Gaussian Kernel $\mathscr{K}_G$

$$\mathscr{K}_{i,j}(t) = \frac{1}{n_{i,j}h_{i,j}}\sum_{l=1}^{n_{i,j}} \mathscr{K}_G\left(\frac{t - t_{i,j,l}}{h_{i,j}}\right). \tag{6}$$

Here $n_{i,j}$ is the number of chromatographically quantifiable samples and $h_{i,j}$ is the window width. The window width was set to

$$h_{i,j} = 0.9min\left\{\left(interquartilerangeoft_{i,j,l}\right)/1.34, standarddeviationoft_{i,j,l}\right\}n_{i,j}^{-1/5} \tag{7}$$

as proposed by Silverman 1986 [23]. The window width was calculated separately for each animal.

In addition, data below LOQ was also accounted for by setting the error to 0 if both measurement and prediction were below LOQ. Otherwise, if the data prediction was above LOQ and the measurement was below LOQ, the measured data point was replaced by the LOQ value.

The differential evolution algorithm implemented in Python 3.8 was used to find the optimal parameters [24]. Thus, we obtain two separate toxicokinetic models for NEB and PEB fitted on the entire dataset that can be compared for differences using statistical techniques.

2.6. Estimation of transfer parameters

Although it is generally recommended to use the full model to simulate an exposure event and its consequences for the milk, it is still useful to estimate transfer parameters such as the transfer rate (*TR*) and half-lives (defined in Table 1) that characterize the kinetic properties of the congeners and to compare the results with other studies. To derive these parameters, a static environment is assumed: 1) A fixed milk fat yield for each phase (average milk fat yield, i.e. 1.81 kg/d in the NEB phase and 1.56 kg/d in the PEB phase). 2) A body weight of 675 kg, averaged over all 3 experimental cows across NEB and PEB, and only used to derive the not strongly fluctuating blood volume. The mathematical details of the calculation of the parameters in Table 1 can be found in the Supplementary Material Section on “Estimation of transfer parameters”.

2.7. Statistics

Based on the hypothesis delineated in the introduction that the redistribution of lipids should cause an alteration in the kinetic behavior of the congeners between the NEB and PEB phases, it follows that all congeners should be similarly affected. Therefore, a statistical test for each transfer parameter (except milk fat/blood partition coefficient P_{Milk}, as described below) was performed simultaneously for all 32 modeled congeners. For the analysis, the Wilcoxon signed-rank test [25] was selected and applied to the log values of the cow-specific parameter determined by the delete-one jackknife samples for all congeners simultaneously.

For the delete-one jackknife samples, the respective transfer parameters for all 3 possible subsets of 2 experimental cows were determined and used to estimate the transfer parameter for the individual animal. A more detailed description can be found in the Supplementary Material section “Wilcoxon test on Jackknife samples”.

If the Wilcoxon test showed a significant difference ($p < 0.05$) for the transfer parameter tested between NEB and PEB phases, a post-hoc test was performed to see if such difference could also be seen on a congener-specific level. To test this, the paired samples dependent *t*-test [26] was used, which was self-implemented in a Python 3.8 script [27]. This was done because the variance for the difference between NEB and PEB phase was not calculated directly, but was rather derived using the delete-one jackknife method [28,29], i.e. the parameters for all 3 possible subsets of 2 experimental cows were derived and used to calculate the variance.

The delete-one jackknife method was also used to derive the confidence intervals. Unlike all other parameters, for the elimination half-lives their inversed values were used instead for all statistical tests as in general the harmonic mean is recommended for half-lives [30,31].

In order to test for a significant difference in the milk fat/blood partition coefficient P_{Milk} between NEB and PEB phase, the Mann-Witney *U* test [32] was used instead of the *t*-test, as there were some notable

outliers in these data The before described Wilcoxon test could not be used for it as it requires pairing of the samples, which can be done here. It should be noted that with a sample size of 3, this approach assumes a normal distribution of the parameters, which cannot be reliably verified with such a small sample size.

2.8. Qualitative criteria for model performance

To indicate how well the model describes the concentration–time profile in milk fat and blood, the model performance for each congener was visually assessed according to the qualitative criteria in Table 2. In general, the milk scores are more important, as they help to determine the reliability of the transfer parameters derived here. Roughly, a score of 4 or 5 means that the transfer parameters are quite reliable; a score of 3 means that only some of the transfer derived parameters are reliable; and a score of 1 or 2 means that the *TR* is at best a rough estimate.

3. Results and discussion

3.1. Milk Fat/Whole blood partition coefficients

The partition coefficient $P_{Milk,i} := \frac{concentrationinmilkfat}{concentrationinblood}$ for each congener was estimated as delineated in the model parametrization and a statistical analysis plotted in Fig. 2. For most congeners (21 out of 32), these partition coefficients were significantly higher in the NEB phase than in the PEB phase ($P^{-}_{Milk} > P^{+}_{Milk}$), by a median of 17 % (NEB/PEB = 117 % as a median of all congeners); the opposite was not found to be significant for any of the congeners. This justifies the use of separate partition coefficients for the NEB and PEB phases. The reasons for these differences could be many, such as changes in blood fat composition and concentration during lactation [33] or changes in milk fat composition due to higher rates of de novo fat synthesis in the later stages of lactation [34].

3.2. Simulation results

Two separate toxicokinetic models for NEB and PEB were optimized using the method described under model parametrization. A simulation was performed with these models using the exposure estimated from measurements of the feed and the capsule dose for all PCDD/F and dl-PCB congeners and plotted as the toxic equivalency (TEQ)-weighted sum of all measured and predicted concentrations in milk fat and whole blood (Fig. 3). As expected, the congener concentration–time profile in milk fat and whole blood shows an accumulation phase in which the congener content increases during dosing. When the exposure from the dosing capsules is removed, a depuration phase follows in which the content decreases again. Furthermore, although the TEQ-weighted sum is the result of the kinetic behavior of several congeners, each with its own biexponential behavior, a TEQ biexponential behavior can still be observed in both the accumulation and depuration phases. This is due to the fact that the TEQ-weighted sum in milk fat and blood is mainly controlled by 2,3,7,8-TCDD, 1,2,3,7,8-PeCDD and PCB-126 (due to their high contribution to the TEQ-weighted sum and their high *TR*); these three congeners have rather similar kinetics (Figure S8, S9, S34). The simulation results for each congener are plotted in Figures S8-S39. The model performance for each congener is summarized in Table 3 separately per congener, phase, milk and blood. Most of the congeners have a good performance in describing the concentration–time profiles in milk fat (score 4 or 5 for 25 (NEB)/25 (PEB) out of 32). Furthermore, for the remaining congeners the model was still reasonable (score 3 for 6 (NEB)/6 (PEB) out of 32) except for OCDD, although in all these cases the β-phase elimination could not be described satisfactorily.

For blood, the prediction quality was generally lower. Only 12 (NEB)/16 (PEB) out of 32 congeners had a score of 4 or 5. For 11 (NEB)/7 (PEB) of the 32 congeners the model was still reasonable because either almost no data points were above the LOQ during β-elimination or the start of the assimilation phase described by the model was too sharp compared to the observed data. The latter could be explained by the changes in partitioning during each phase, already described across phases in section "Milk Fat/Whole Blood Partition Coefficients", since in this model the concentrations in whole blood are simply derived by dividing the concentration in milk fat by a constant $P^{\bullet}_{Milk,i}$. For most of the remaining congeners, only noise could be observed in the data, since the amount dosed was presumably too low to elevate the blood concentration above the background levels. Furthermore, looking at the predicted concentration of PCBs in the control cows, it is noticeable that the concentration in blood is often underpredicted compared to the concentration in milk fat, which are well predicted. The reason for this could be the ubiquitous presence of PCBs, causing additional contamination of the samples, but this could not be confirmed by the concentrations present in the analytical blanks. Another explanation could be a dose-dependent transfer of these congeners from blood to milk fat, but this seems unlikely because some congeners (e.g., PCB-157) had similar concentrations in experimental cows but did not show large discrepancies between milk fat and blood prediction accuracies. Therefore, the underlying reasons for this observation are unfortunately not fully understood.

Table 2
Qualitative criteria for describing the model performance in milk fat and blood.

Score	Meaning
5	The measured and simulated data are in good agreement with a clear absorption and depuration period with a clearly visible α and β phase.
4	The measured data have a higher degree of uncertainty, but an absorption and depuration period with distinct α and β phases is still present and are well reproduced by the simulated data.
3	Most measured and simulated values are in good agreement, but certain phases are either not well reproduced or have no clear observable pattern.
2	The measured data do not show a pronounced exponential biphasic behavior, but the simulated data are in limited agreement with the measured data.
1	The simulation and the measured data are in poor agreement.

3.3. Transfer rates (TRs)

The steady-state transfer rates (*TR*s) derived from this model are shown in Figure S1 and Table S5. Comparing the derived *TR*s for the NEB and PEB phases across all congeners reveals that there is a statistically highly significant difference between *TR*s of the two phases ($p < 10^{-8}$) of 27 % in median. Furthermore, for 7 out of the 32 congeners statistically analyzed, this difference is also significant at the congener-specific level. The *TR*s differ widely between congeners due to their different physicochemical properties.

The steady-state transfer rate in the present model is identical to the absorption coefficient, which in turn accounts for the true absorption in the gastro-intestinal tract (GIT) and additionally for any possible non-milk elimination mechanisms (metabolism and/or non-milk excretion). Therefore, the observed difference in *TR*s between the two phases may be due to these two processes. One possibility is that the amount of congeners absorbed by the cow from the feed is higher in the NEB phase than in the PEB phase; another is that the extent of some non-milk elimination of congeners is lower in the NEB phase than in the PEB phase.

With regard to changes in GIT absorption, there is some evidence for a reduced capacity of the intestine to produce chylomicrons and, thus, probably a reduced ability to absorb fat in the early stages of lactation (NEB phase) [35]). However, this would also imply a reduced absorption of lipophilic PCDD/Fs and PCBs during the NEB, which is at odds with the observed elevated *TR*s for the NEB phase. Therefore, such changes in lipid absorption alone are not sufficient to explain the lower *TR*s during PEB compared to NEB. A possible non-milk elimination pathway is the phase 1 metabolism of PCBs [36,37] depending on the chlorination

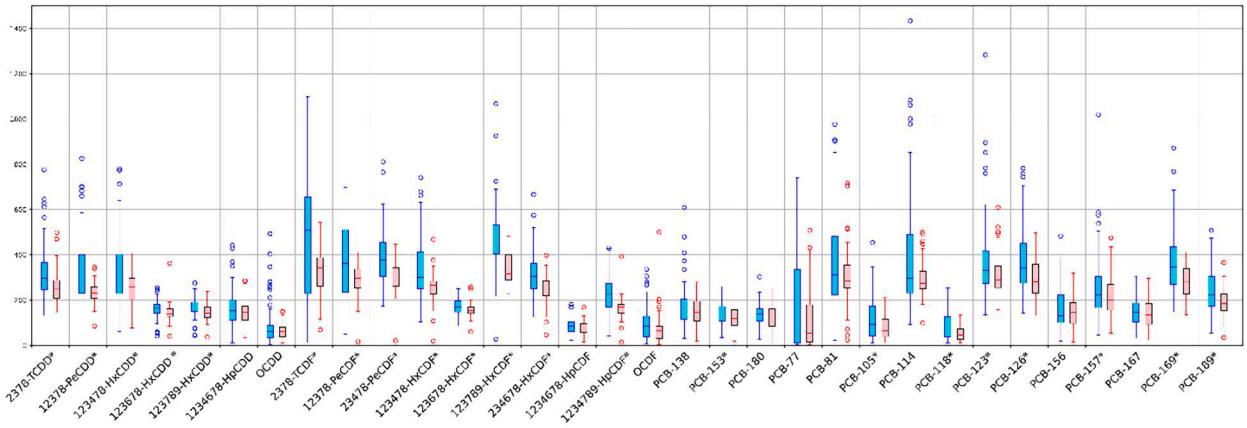

Fig. 2. Boxplots of the Milk Fat/Whole Blood partition coefficients P_{Milk} in the NEB (cyan) and PEB (red) phase. Boxes are defined as the interquartile range (IQR) between 25th percentile (Q1) and 75th percentile (Q3) of the data according to the standard method. The line in the box represents the median. Whiskers include data within 1.5 times of IQR below Q1 and above Q3. *marks congeners with a statistically significant difference ($p < 0.05$) between both phases. (For interpretation of the references to color in this figure legend, the reader is referred to the web version of this article.)

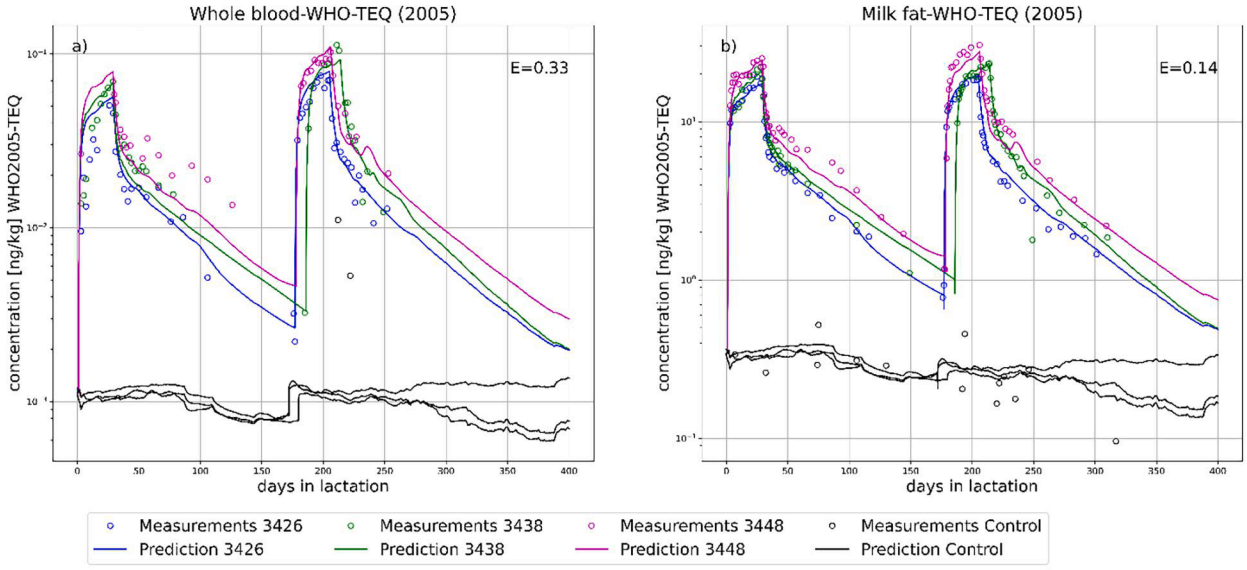

Fig. 3. Concentration-time profiles of the TEQ (toxic equivalency)-weighted sum of all investigated PCDD/Fs and dl-PCBs in whole blood and in milk fat of the 3 control cows (black, all individuals) and the 3 experimental cows considered (differentiated by color for each individual animal 3426, 3438 and 3448). The plot is in logarithmic scale. The dots represent the measured data and the lines the model predictions, which are the TEQ-weighted sum of the model results for the individual congeners. E describes the weighted log (basis e) error of equation (4) for the respective data set.

pattern [38,39]; certain PCDD/Fs are also known to be susceptible to metabolism [40–46]. Rumen microorganisms are unlikely to play a significant role in the metabolic degradation of PCDD/Fs and PCBs, as inferred from *in vitro* fermentation experiments [38]. Another possible non-milk elimination pathway is excretion via sebum, as has been observed for PCBs in the hair coat of dairy cows [47]. The partition between GIT and blood could lead to fecal excretion of congeners from blood [48].

Thus, higher *TR*s in milk could indeed be explained by a lower non-milk elimination. This in turn could be caused by either by a lower elimination rate in the respective organ (e.g., reduced metabolic activity in the liver) or by a generally lower concentration in the excretory organs during the NEB phase. The latter scenario is supported by the observation that blood mean residence times (*BMRT*s) were significantly ($p < 10^{-12}$) different, with NEB phase being 15 % lower than the PEB phase in median. On a congener-specific level, significant differences were observed for 4 of 32 congeners (Figure S2, Table S6).

In addition, the steady-state *TR*s reported here tended to be higher than *TR*s of other studies (by 43 % and 16 % in median during NEB and PEB phase respectively). One reason for this is likely that most animals of previous studies had lower milk fat yields [5] compared to this study, which presumably reduces the amount excreted via the milk pathway.

The assimilation phases in most previous studies were substantially shorter than the here predicted time until 90 % of steady-state is reached [5] (T_{ss}) shown in Figure S3 and Table S7, implying that the parameters derived from those studies are not in steady-state. As the *TR*s reported in those studies were often not extrapolated to steady-state conditions, they are likely to report lower values. This could also explain the lower median *TR*s in the literature summarized by Krause et al. [5] and even the lower *TR*s derived directly from our data [13] (the here reported values are 49 % and 38 % higher in median during NEB and PEB phase respectively). Hao et al. 2023 reported results implying much shorter T_{ss} for some congeners (<21 days), which is not in line with our data [50]. More studies, such as McLachlan and Richter (1998) [46] and Hoogenboom et al. (2015) [49], support our longer T_{ss} values. Finally, a comparison of the T_{ss} predicted shows low significance for a difference

Table 3
Scores given to models according to Table 2 describing concentration time profile in blood and milk fat for each congener in the respective phase.

	Score Milk		Score Blood	
Name	**NEB**	**PEB**	**NEB**	**PEB**
2,3,7,8-TCDD	5	5	4	5
1,2,3,7,8-PeCDD	5	5	4	5
1,2,3,4,7,8-HxCDD	5	5	4	4
1,2,3,6,7,8-HxCDD	5	5	4	4
1,2,3,7,8,9-HxCDD	5	5	5	5
1,2,3,4,6,7,8-HpCDD	5	5	3	3
OCDD	2	2	1	1
2,3,7,8-TCDF	4	3	3	3
1,2,3,7,8-PeCDF	5	5	3	3
2,3,4,7,8-PeCDF	5	5	4	4
1,2,3,4,7,8-HxCDF	5	5	4	4
1,2,3,6,7,8-HxCDF	5	5	4	4
1,2,3,7,8,9-HxCDF	4	3	3	3
2,3,4,6,7,8-HxCDF	5	5	4	4
1,2,3,4,6,7,8-HpCDF	4	4	3	3
1,2,3,4,7,8,9-HpCDF	5	5	3	3
OCDF	3	3	1	1
PCB-138	4	4	1	1
PCB-153	3	4	1	1
PCB-180	3	3	1	1
PCB-77	3	3	1	1
PCB-81	5	5	3	4
PCB-105	3	3	1	1
PCB-114	5	5	3	4
PCB-118	3	4	1	1
PCB-123	5	5	5	5
PCB-126	5	5	4	5
PCB-156	5	5	1	1
PCB-157	5	5	3	4
PCB-167	4	5	3	3
PCB-169	5	5	4	5
PCB-189	5	5	3	4

between the NEB and PEB phases between across all congeners ($p < 0.05$), with only 4 out of 32 being significant at a congener-specific level. In median, the NEB phase T_{ss} is 34 % longer than in PEB.

3.4. Distribution in steady-state

The distribution of the congeners in the three compartments during steady-state is shown in Figure S4 and Table S8. As expected for most congeners according to the model, the majority of each substance is found in the Slow turnover compartment (tantamount to adipose tissue), accounting in median for 85 % in NEB and 82 % in the PEB phase of the total burden. Furthermore, there is a significant difference observable across all congeners ($p < 10^{-3}$) that a larger fraction of the substance is stored in the Slow turnover compartment $(A_{slow}/A_{total})_{steady\text{-}state}$ during the NEB phase than during the PEB phase (in median 3 %). However, this was not significant for any congener on a congener-specific level. In general, the decrease during the PEB phase could be due to the fact that the adipose tissue, although rapidly decreasing at the beginning of lactation, was comparatively larger than at the beginning of the second dosing period [51].

Most of the remaining substance is distributed to the Fast turnover compartment, i.e., approximately 15 % and 18 % in median of the total burden in the NEB and PEB phases, respectively. Blood accounts for only 0.1 % and 0.3 %, in median, of the total body burden in NEB and PEB phase, respectively. This low relevance of the storage capacity of blood on the one hand explains the overall short *BMRT*s in Figure S2 and on the other hand illustrates the reason for the need of a third compartment (Fast turnover), as the Blood compartment alon could not produce noticeable α-half-lives (next section).

3.5. Elimination half-lives

By exposing the cows to a synthetic mixture, the elimination half-lives of several congeners could be observed that have not been reported before in literature [5], probably due to low exposure. For several congeners, α-half-lives for the quick depuration phase and for all PCDD/Fs and all dl-PCBs β-half-lives for the slower depuration phase were estimated. The Wilcoxon test comparing the α-half-lives of both phases over all congeners shows that the α-half-life is not significantly ($p = 0.06$) different between both phases (Figure S5, Table S9). The median α-half-life of NEB and PEB phase was 1.77 days.

Comparison of the β-half-lives between the two phases (Figure S6, Table S10) using the Wilcoxon test shows a marginally significant difference ($p < 0.04$) between the two phases and 2 out of 32 congeners show significance at a congener-specific level. The median β-half-life of NEB phase is 19 % longer than that of the PEB phase, with a median NEB β-half-life of 53.5 days and a median NEB phase β-half-life of 46.5 days. Looking at the specific results for each congener in Figure S5, a pattern emerges with some congeners having unreasonably long β-half-lives in at least one of the two phases, namely 1,2,3,4,6,7,8-HpCDF, OCDF, PCB-153, PCB-77 and PCB-105; these congeners also except for 1,2,3,4,6,7,8-HpCDF have low scores for the β-depuration phase (Table 3). This overestimation of the β-half-life leads to an unreasonably long T_{ss} (Figure S3) and presumably overestimated *TR*s (Figure S1) for these congeners. In general, for all congeners rated with 3 or less for milk fat performance in Table 3, the β-half-life could not be reliably predicted (see Section Simulation results), therefore causing also a less reliable estimation of *TR*, T_{ss}, *BMRT* and distribution in steady-state for the such congeners. Some of the β-half-lives presented here are much shorter than those presented in the literature, especially for the PCBs. However, because the scores for most of these congeners are high, we are confident that our values better represent the kinetics in high-yielding cows.

3.6. Transition times (TTs)

Comparing the *TT*s of NEB and PEB phase across all congeners (Figure S7, Table S11) yields a low statistically significant difference ($p < 0.02$) between NEB and PEB phase and only 1 out of 32 congeners showed a significance at a congener-specific level. In median, the *TT*s, where 16 % shorter in NEB phase than in PEB phase with the NEB phase having *TT*s of 9.14 days and PEB phase 8.21 days.

4. Conclusions

For almost all congeners studied here, the model developed is the first one to describe their kinetics in dairy cows milk under dynamic conditions [12] and to allow a distinction between the NEB and PEB phases. Thanks to this approach, it was possible for the first time to derive transfer parameters specific to the NEB and PEB phases including some α-half-lives hitherto unreported in the literature. The comparison of these parameters across all congeners showed that steady-state *TR*, *BMRT* and the fraction of the substance stored in the Slow turnover compartment $(A_{Slow}/A_{total})_{steady\text{-}state}$ differed with a highly significance ($p < 10^{-3}$ or better) between the NEB and PEB phases using statistical tests across all congeners. These differences were however only occasionally significant at the individual congener level. Remarkable is the difference for the all-important transfer rate (*TR*), which is lower in the PEB phase, presumably because of an increased non-milk elimination of the substances. Furthermore, T_{ss}, β-half-lives and *TT*s also differed between NEB and PEB phase but with lower significance. It was also observed that the time to reach 90 % of the steady-state is quite long for most congeners and exceeds the exposure time used in several studies, pointing to a problem in the experimental design of those studies [5]. Taken at face value, *TR*s from the past may lead to an underestimation of the amount transferred to milk after long exposure scenarios. In general, it is strongly recommended to employ simulations using toxicokinetic

models rather than simple multiplicative parameters to predict concentrations in milk after a specific exposure scenario, since simulations can be adapted to the specific exposure situation. In this study, the model was separately parameterized for the NEB and PEB phases. An effect of the energy balance on the transfer of lipophilic contaminants in dairy cows has been discussed before [52–55], modeled in the literature [56] and suspected from observation [57–61], but had not until now been statistically validated. The present study shows that the energy balance indeed has an effect on transfer kinetics, which implies that the metabolic state of the animals should be taken into account for risk assessment in pertinent situations. Further research is needed to prove the causality and causal mechanisms of our findings and to develop more detailed and mechanistic, dynamic models, as the changes in metabolic state of the animal are not instantaneous processes (as modeled here), but rather of a continuous nature.

Author contributions

The manuscript was written through contributions of all authors. All authors have given approval to the final version of the manuscript.

Funding sources

This research was funded with the core budgets of the Max Rubner-Institut and the German Federal Institute for Risk Assessment.

Declaration of Competing Interest

The authors declare that they have no known competing financial interests or personal relationships that could have appeared to influence the work reported in this paper.

Data availability

Data will be made available on request.

Appendix A. Supplementary data

Supplementary data to this article can be found online at https://doi.org/10.1016/j.comtox.2023.100290.

References

[1] M. Dopico, A. Gomez, Review of the current state and main sources of dioxins around the world, J Air Waste Manag Assoc 65 (9) (2015) 1033–1049, https://doi.org/10.1080/10962247.2015.1058869.
[2] R.A. Hites, Dioxins: an overview and history, Environ Sci Technol 45 (1) (2011) 16–20, https://doi.org/10.1021/es1013664.
[3] K. Breivik, A. Sweetman, J.M. Pacyna, K.C. Jones, Towards a global historical emission inventory for selected PCB congeners–a mass balance approach 3, An Update. *Sci Total Environ* 377 (2–3) (2007) 296–307, https://doi.org/10.1016/j.scitotenv.2007.02.026.
[4] H.K. Knutsen, J. Alexander, L. Barregård, M. Bignami, B. Brüschweiler, S. Ceccatelli, B. Cottrill, M. Dinovi, L. Edler, B. Grasl-Kraupp, et al., Risk for animal and human health related to the presence of dioxins and dioxin-like PCBs in feed and food, EFSA J. 16 (11) (2018), https://doi.org/10.2903/j.efsa.2018.5333.
[5] T. Krause, J.-L. Moenning, J. Lamp, R. Maul, H. Schenkel, P. Fürst, R. Pieper, J. Numata, Transfer of polychlorinated dibenzo-p-dioxins and dibenzofurans (PCDD/Fs) and polychlorinated biphenyls (PCBs) from oral exposure into cow's milk – Part I: state of knowledge and uncertainties, Nutr. Res. Rev. (2022) 1–23, https://doi.org/10.1017/S0954422422000178.
[6] F. Amutova, M. Delannoy, A. Baubekova, G. Konuspayeva, S. Jurjanz, Transfer of persistent organic pollutants in food of animal origin - Meta-analysis of published data, Chemosphere 262 (2021), https://doi.org/10.1016/j.chemosphere.2020.128351.
[7] R.L.A.P. Hoogenboom, A. Klop, R. Herbes, J.C.H. van Eijkeren, M.J. Zeilmaker, A. M. van Vuuren, W.A. Traag, Carry-over of polychlorinated dibenzo-p-dioxins and dibenzofurans (PCDD/Fs) and polychlorinated biphenyls (PCBs) in dairy cows fed smoke contaminated maize silage or sugar beet pulp, Chemosphere 137 (2015) 214–220, https://doi.org/10.1016/j.chemosphere.2015.07.040.
[8] J. Piskorska-Pliszczynska, S. Maszewski, S. Mikolajczyk, M. Pajurek, P. Strucinski, M. Olszowy, Elimination of dioxins in milk by dairy cows after the long-term intake of contaminated sugar beet pellets, Food Additives & Contaminants: Part A 34 (5) (2017) 842–852, https://doi.org/10.1080/19440049.2017.1300943.
[9] V. Lorenzi, B. Angelone, E. Ferretti, A. Galli, M. Tonoli, M. Donati, F. Fusi, G. Zanardi, S. Ghidini, L. Bertocchi, PCDD/Fs, dl-PCBs, and ndl-PCBs in dairy cows: Carryover in milk from a controlled feeding study, Journal of Agricultural and Food Chemistry 68 (7) (2020) 2201–2213, https://doi.org/10.1021/acs.jafc.9b08180.
[10] C. Driesen, S. Lerch, R. Siegenthaler, P. Silacci, H.D. Hess, B. Nowack, M. Zennegg, Accumulation and decontamination kinetics of PCBs and PCDD/Fs from grass silage and soil in a transgenerational cow-calf setting, Chemosphere 296 (2022), https://doi.org/10.1016/j.chemosphere.2022.133951.
[11] C. Weber, C. Hametner, A. Tuchscherer, B. Losand, E. Kanitz, W. Otten, S.P. Singh, R.M. Bruckmaier, F. Becker, W. Kanitz, H.M. Hammon, Variation in fat mobilization during early lactation differently affects feed intake, body condition, and lipid and glucose metabolism in high-yielding dairy cows, J. Dairy Sci. 96 (1) (2013) 165–180, https://doi.org/10.3168/jds.2012-5574.
[12] J.-L. Moenning, T. Krause, J. Lamp, R. Maul, H. Schenkel, P. Fürst, R. Pieper, J. Numata, Transfer of polychlorinated dibenzo-p-dioxins and dibenzofurans (PCDD/Fs) and polychlorinated biphenyls (PCBs) from oral exposure into cow's milk – part II: toxicokinetic predictive models for risk assessment, Nutr. Res. Rev. (2022) 1–14, https://doi.org/10.1017/S0954422422000208 From Cambridge University Press Cambridge Core.
[13] Krause, T.; Lamp, J.; Knappstein, K.; Walte, H.-G.; Moenning, J.-L.; Molkentin, J.; Ober, F.; Susenbeth, A.; Westreicher-Kristen, E.; Schwind, K.-H.; et al. Experimental Study on the Transfer of Polychlorinated Biphenyls (PCBs) and Polychlorinated Dibenzo-p-dioxins and Dibenzofurans (PCDD/Fs) into Milk of High-Yielding Cows during Negative and Positive Energy Balance. *Journal of Agricultural and Food Chemistry* **2023 (accepted)**.
[14] C. Driesen, M. Zennegg, M. Rothacher, S. Dubois, U. Wyss, B. Nowack, S. Lerch, Transgenerational mass balance and tissue distribution of PCBs and PCDD/Fs from grass silage and soil into cow-calf continuum, Chemosphere 307 (2022), 135745, https://doi.org/10.1016/j.chemosphere.2022.135745.
[15] J.-L. Moenning, J. Numata, D. Bloch, A. Jahnke, H.A. Schafft, M. Spolders, A. Lüth, M. Lahrssen-Wiederholt, K. Schulz, Transfer and toxicokinetic modeling of non-dioxin-like polychlorinated biphenyls (ndl-PCBs) into accidentally exposed dairy cattle and their calves - a case report, Environ. Toxicol. Pharmacol. 99 (2023), https://doi.org/10.1016/j.etap.2023.104106.
[16] Telliard, W. A. Method 1613B - Tetra- through Octa-Chlorinated Dioxins and Furans by Isotope Dilution HRGC/HRMS; Washington, D.C., 1994.
[17] U.S. Environmental Protection Agency. Method 1668C - Chlorinated Biphenyl Congeners in Water, Soil, Sediment, Biosolids, and Tissue by HRGC/HRMS; Washington, DC, 2010.
[18] P. Robouch, J. Stroka, J. Haedrich, A. Schaechtele, T. Wenzl, Guidance document on the estimation of LOD and LOQ for measurements in the field of contaminants in feed and food, in: European Commission; Joint Research Centre, Publications Office of the European Union, 2016, https://doi.org/10.2787/8931.
[19] J.J. Ryan, P. Mills, Lipid extraction from blood and biological samples and concentrations of dioxin-like compounds, Chemosphere 34 (5–7) (1997) 999–1009, https://doi.org/10.1016/S0045-6535(97)00402-5.
[20] H.J.G.M. Derks, P.L.M. Berende, M. Olling, H. Everts, A.K.D. Liem, A.P.J.M. de Jong, Pharmacokinetic modeling of polychlorinated dibenzo-p-dioxins (PCDDs) and furans (PCDFs) in cows, Chemosphere 28 (4) (1994) 711–715, https://doi.org/10.1016/0045-6535(94)90222-4.
[21] P. Tremolada, N. Guazzoni, M. Parolini, B. Rossaro, M.M. Bignazzi, A. Binelli, Predicting PCB concentrations in cow milk: validation of a fugacity model in high-mountain pasture conditions, Sci. Total Environ. 487 (2014) 471–480, https://doi.org/10.1016/j.scitotenv.2014.04.042.
[22] Z. Lin, M. Li, Y.-S. Wang, L.A. Tell, R.E. Baynes, J.L. Davis, T.W. Vickroy, J. E. Riviere, Physiological parameter values for physiologically based pharmacokinetic models in food-producing animals. Part I: Cattle and swine, J. Vet. Pharmacol. Ther. 43 (5) (2020) 385–420, https://doi.org/10.1111/jvp.12861.
[23] B.W. Silverman, Density estimation for statistics and data analysis, Springer, 1986.
[24] *LMFIT: Non-Linear Least-Square Minimization and Curve-Fitting for Python (1.0.2)*; Zenodo: 2021. 10.5281/zenodo.4516651 (accessed 07.02.2021).
[25] F. Wilcoxon, Individual Comparisons by Ranking Methods, Biometrics 1 (6) (1945) 80–83, https://doi.org/10.2307/3001968 (acccessed 2022/07/07/).JSTOR.
[26] Student., The Probable Error of a Mean, Biometrika 6 (1) (1908) 1–25, https://doi.org/10.2307/2331554, acccessed 2022/07/07/).JSTOR.
[27] *Python 3.8.8*; Python Software Foundation: 2021. www.python.org (accessed 19.02.2021).
[28] J.W. Tukey, Bias and confidence in not quite large samples, Ann. Math. Stat. 29 (2) (1958) 614–623, https://doi.org/10.1214/aoms/1177706647.
[29] M.H. Quenouille, Notes on the Bias in Estimation, Biometrika 43 (3–4) (1956) 353–360, https://doi.org/10.1093/biomet/43.3-4.353 (acccessed 7/7/2022).
[30] F.C. Lam, C.T. Hung, D.G. Perrier, Estimation of Variance for Harmonic Mean Half-Lives, J Pharm Sci 74 (2) (1985) 229–231, https://doi.org/10.1002/jps.2600740229.
[31] M.N. Martinez, M.J. Bartholomew, What Does It "Mean"? A Review of Interpreting and Calculating Different Types of Means and Standard Deviations, Pharmaceutics 9 (2) (2017), https://doi.org/10.3390/pharmaceutics9020014.
[32] Mann, H. B.; Whitney, D. R. On a Test of Whether one of Two Random Variables is Stochastically Larger than the Other. *The Annals of Mathematical Statistics* **1947**, *18* (1), 50-60, 11. DOI: 10.1214/aoms/1177730491.
[33] Q.C.D. Van, E. Knapp, J.L. Hornick, I. Dufrasne, Influence of Days in Milk and Parity on Milk and Blood Fatty Acid Concentrations, Blood Metabolites and

Hormones in Early Lactation Holstein Cows, Animals-Basel 10 (11) (2020), https://doi.org/10.3390/ani10112081.
[34] R. Khiaosa-ard, M.T. Kleefisch, Q. Zebeli, F. Klevenhusen, Milk fatty acid composition reflects metabolic adaptation of early lactation cows fed hay rich in water-soluble carbohydrates with or without concentrates, Anim. Feed Sci. Technol. (2020) 264, https://doi.org/10.1016/j.anifeedsci.2020.114470.
[35] M. Bionaz, E. Vargas-Bello-Perez, S. Busato, Advances in fatty acids nutrition in dairy cows: from gut to cells and effects on performance, J Anim Sci Biotechno 11 (1) (2020).
[36] A.M. Gardner, H.F. Righter, J.A.G. Roach, Excretion of hydroxylated polychlorinated biphenyl metabolites in cows' milk, J. Assoc. Off. Anal. Chem. 59 (2) (1976) 273–277, https://doi.org/10.1093/jaoac/59.2.273.
[37] S. Safe, N. Platonow, O. Hutzinger, Metabolism of chlorobiphenyls in the goat and cow, J. Agric. Food Chem. 23 (2) (1975) 259–261, https://doi.org/10.1021/jf60198a053.
[38] G.O. Thomas, A.J. Sweetman, K.C. Jones, Metabolism and body-burden of PCBs in lactating dairy cows, Chemosphere 39 (9) (1999) 1533–1544, https://doi.org/10.1016/S0045-6535(99)00050-8.
[39] M.S. McLachlan, Mass balance of polychlorinated biphenyls and other organochlorine compounds in a lactating cow, J. Agric. Food Chem. 41 (3) (1993) 474–480, https://doi.org/10.1021/jf00027a024.
[40] D. Firestone, M. Clower, A.P. Borsetti, R.H. Teske, P.E. Long, Polychlorodibenzo-p-dioxin and pentachlorophenol residues in milk and blood of cows fed technical pentachlorophenol, J. Agric. Food Chem. 27 (6) (1979) 1171–1177, https://doi.org/10.1021/jf60226a075.
[41] M.S. McLachlan, H. Thoma, M. Reissinger, O. Hutzinger, PCDD/F in an agricultural food chain Part 1: PCDD/F mass balance of a lactating cow, Chemosphere 20 (7–9) (1990) 1013–1020, https://doi.org/10.1016/0045-6535(90)90214-E.
[42] K. Welsch-Pausch, M.S. McLachlan, Fate of airborne polychlorinated dibenzo-p-dioxins and dibenzofurans in an agricultural ecosystem, Environ. Pollut. 102 (1) (1998) 129–137, https://doi.org/10.1016/S0269-7491(98)00071-2.
[43] G.F. Fries, D.J. Paustenbach, D.B. Mather, W.J. Luksemburg, A congener specific evaluation of transfer of chlorinated dibenzo-p-dioxins and dibenzofurans to milk of cows following ingestion of pentachlorophenol-treated wood, Environ. Sci. Technol. 33 (8) (1999) 1165–1170, https://doi.org/10.1021/es981153d.
[44] G.F. Fries, D.J. Paustenbach, W.J. Luksemburg, Complete mass balance of dietary polychlorinated dibenzo-p-dioxins and dibenzofurans in dairy cattle and characterization of the apparent synthesis of hepta- and octachlorodioxins, J. Agric. Food Chem. 50 (15) (2002) 4226–4231, https://doi.org/10.1021/jf020037y.
[45] M. Olling, H.J.G.M. Derks, P.L.M. Berende, A.K.D. Liem, A.P.J.M. de Jong, Toxicokinetics of eight 13C-labelled polychlorinated dibenzo-p-dioxins and -furans in lactating cows, Chemosphere 23 (8–10) (1991) 1377–1385, https://doi.org/10.1016/0045-6535(91)90162-7.
[46] M. McLachlan, W. Richter, Uptake and transfer of PCDD/Fs by cattle fed naturally contaminated feedstuffs and feed contaminated as a result of sewage sludge application. 1. Lactating cows, J. Agric. Food Chem. 46 (3) (1998) 1166–1172, https://doi.org/10.1021/jf970922u.
[47] Klein, U.; Drochner, W.; Forschner, E.; Johannes, B. PCB-Konzentrationen in Haaren, Blut, Geweben und Ausscheidungen chronisch belasteter Milchkühe, Mastbullen und Kälber. 1. Mitteilung: Verlauf und Beziehung der Konzentration einiger hochchlorierter Biphenyle in Haaren, Milch und Gewebenbei belasteten Ammenkühen und konventionell gehaltenen Milchrindern. *Deutsche Tierärztliche Wochenschrift* **1992**, *99*, 242-248.
[48] B.C. Kelly, F.A. Gobas, M.S. McLachlan, Intestinal absorption and biomagnification of organic contaminants in fish, wildlife, and humans, Environ Toxicol Chem 23 (10) (2004) 2324–2336, https://doi.org/10.1897/03-545 From NLM Medline.
[49] R. Hoogenboom, W. Traag, A. Fernandes, M. Rose, European developments following incidents with dioxins and PCBs in the food and feed chain, Food Control 50 (2015) 670–683, https://doi.org/10.1016/j.foodcont.2014.10.010.
[50] Y.F. Hao, C. Wang, P. Wang, J. Cheng, H. Xian, M. Liu, Z.W. Li, J. Ma, Y.M. Li, R. Q. Yang, et al., Kinetics of PCDD/Fs from feed to cow milk and its implications for food safety, Sci. Total Environ. (2023) 874, https://doi.org/10.1016/j.scitotenv.2023.162477.
[51] U.J. Schröder, R. Staufenbiel, Invited Review: Methods to Determine Body Fat Reserves in the Dairy Cow with Special Regard to Ultrasonographic Measurement of Backfat Thickness, J. Dairy Sci. 89 (1) (2006) 1–14, https://doi.org/10.3168/jds.S0022-0302(06)72064-1.
[52] F. Rossi, T. Bertuzzi, A. Vitali, A. Rubini, F. Masoero, M. Morlacchini, G. Piva, Monitoring of the declining trend of Polychlorobifenyls concentration in milk of contaminated dairy cows, Ital. J. Anim. Sci. 9 (1) (2010) 88–92, https://doi.org/10.4081/ijas.2010.e18.
[53] G. Rychen, S. Jurjanz, H. Toussaint, C. Feidt, Dairy ruminant exposure to persistent organic pollutants and excretion to milk, Animal 2 (2008) 312–323, https://doi.org/10.1017/S1751731107001139.
[54] G. Rychen, S. Jurjanz, A. Fournier, H. Toussaint, C. Feidt, Exposure of ruminants to persistent organic pollutants and potential of decontamination, Environ. Sci. Pollut. Res. 21 (10) (2014) 6440–6447, https://doi.org/10.1007/s11356-013-1882-8.
[55] M.S. McLachlan, Model of the fate of hydrophobic contaminants in cows, Environ. Sci. Technol. 28 (13) (1994) 2407–2414, https://doi.org/10.1021/es00062a028.
[56] D.J. MacLachlan, Influence of physiological status on residues of lipophilic xenobiotics in livestock, Food Additives & Contaminants: Part A 26 (5) (2009) 692–712, https://doi.org/10.1080/02652030802669170.
[57] T. Jilg, W. Mueller, H. Hagenmaier, O. Paepke, Carry-over of polychlorinated dibenzodioxins (PCDD) and dibenzofurans (PCDF) from feed into the milk of the dairy cow, Agribiol. Res. 45 (1992) 303–310.
[58] G.O. Thomas, A.J. Sweetman, K.C. Jones, Input-output balance of polychlorinated biphenyls in a long-term study of lactating dairy cows, Environ. Sci. Technol. 33 (1) (1999) 104–112, https://doi.org/10.1021/es980322r.
[59] L.B. Willett, T.T.Y. Liu, Effects of thyroprotein on excretion of polychlorinated biphenyls by lactating cows, J. Dairy Sci. 65 (1) (1982) 72–80, https://doi.org/10.3168/jds.S0022-0302(82)82155-3.
[60] G. Brambilla, I. Fochi, M. Falce, S.P.D. Filippis, A. Ubaldi, A. di Domenico, PCDD and PCDF depletion in milk from dairy cows according to the herd metabolic scenario, Chemosphere 73 (1, Supplement), S216–S219 (2008), https://doi.org/10.1016/j.chemosphere.2007.11.071.
[61] G.F. Fries, Polychlorinated biphenyl residues in milk of environmentally and experimentally contaminated cows, Environ. Health Perspect. 1 (1972) 55–59, https://doi.org/10.1289/ehp.720155.

5.2 Modelling of ndl-PCBs in fattening pigs

5.2.1 Paper 4

Moenning, J.-L., et al., Toxicokinetic modelling of the transfer of non-dioxin like polychlorinated biphenyls from feed into edible tissues of pigs. Science of The Total Environment, 2023: p. 164539

Science of the Total Environment 892 (2023) 164539

Contents lists available at ScienceDirect

Science of the Total Environment

journal homepage: www.elsevier.com/locate/scitotenv

Toxicokinetic modelling of the transfer of non-dioxin like polychlorinated biphenyls from feed into edible tissues of pigs

Jan-Louis Moenning, Britta Ohlhoff, Mariko Yamamoto, Anke Jährmann, Anne Jahnke, Anja Lüth, Robert Pieper, Jorge Numata *

German Federal Institute for Risk Assessment (BfR), Department Safety in the Food Chain, Berlin, Germany

HIGHLIGHTS

- Elimination speed of 6 ndl-PCBs decreases with time due to increased fat fraction.
- Elimination classified: fast (PCB-28), intermediate (52, 101), slow (138, 153, 180).
- Transfer rates of 10 % (fast), 35–39 % (intermediate) and 71–77 % (slow) identified

GRAPHICAL ABSTRACT

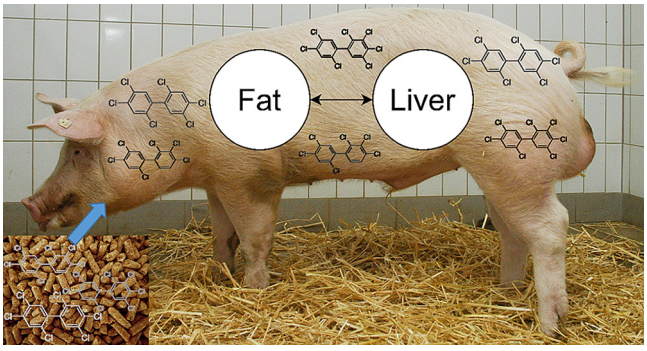

ARTICLE INFO

Editor: Jay Gan

Keywords:
PBTK
Pharmacokinetics
Food safety
Sus scrofa domesticus

ABSTRACT

Non-dioxin-like polychlorinated biphenyls (ndl-PCBs) are persistent environmental pollutants that accumulate in the tissues of exposed animals and humans. Contaminated feed can lead to ndl-PCB contaminated food of animal origin; such foods are the main route of human exposure. Therefore, predicting ndl-PCB transfer from feed into animal products is important for human health risk assessment. Here, we developed a physiologically based toxicokinetic model describing the transfer of PCBs-28, 52, 101, 138, 153 and 180 from contaminated feed into the liver and fat of fattening pigs. The model is based on a feeding study with fattening pigs (PIC hybrids) that were temporarily fed contaminated feed containing known concentrations of ndl-PCBs. Animals were slaughtered at different ages, and ndl-PCB concentrations in muscle fat and liver were determined. The model accounts for animal growth and excretion via the liver. Based on their elimination speed and half-lives, they can be categorized into fast (PCB-28), intermediate (PCBs 52 and 101) and slow (PCBs 138, 153 and 180). Using a simulation with realistic growth and feeding patterns, the following transfer rates were found: 10 % (for fast), 35–39 % (intermediate) and 71–77 % (slow eliminated congeners). Using the models, the highest level of 3.8 μg/kg dry matter (DM) was calculated for any sum of ndl-PCBs in pig feed to ensure that the current maximum levels in pork meat and liver (40 ng/g fat) are not be exceeded. The model is included in the Supplementary Material.

1. Introduction

Polychlorinated biphenyls (PCBs) are a group of 209 congeners of organohalogenated substances that differ in the number (1–10 per molecule) and position of the chlorine atoms on the biphenyl rings. They are related to polychlorinated dibenzo-*p*-dioxins and furans (PCDD/Fs or

* Corresponding author at: German Federal Institute for Risk Assessment, Max-Dohrn-Str. 8-10, 10589 Berlin, Germany.
E-mail address: jorge.numata@bfr.bund.de (J. Numata).

http://dx.doi.org/10.1016/j.scitotenv.2023.164539
Received 10 March 2023; Received in revised form 23 May 2023; Accepted 27 May 2023
Available online 1 June 2023

colloquially "dioxins"). But unlike dioxins, PCBs were intentionally manufactured and used for various historical applications, mainly as non-burning and viscous fluids with low conductivity in transformers and hydraulic oils (Robertson and Ludewig, 2011). Despite their worldwide ban, PCBs are still formed as unwanted by-products of chemical reactions (Tremolada et al., 2014). Like dioxins, PCBs are lipophilic, chemically and thermally stable (persistent) and accumulate in the tissues of humans and animals. Some PCB congeners show a molecular conformation and binding similar to dioxins that is also associated with a comparable toxicological profile, leading to their designation as dioxin-like PCBs (dl-PCBs). The rest of the PCB congeners differ in their toxicological profile and are referred to as non-dioxin-like PCBs (ndl-PCBs). The ndl-PCBs show e.g. liver and thyroid toxicity for single congeners in animal models (Viluksela et al., 2012). To reduce the analytical complexity, ndl-PCBs are often reported as the sum of six indicator congeners (Σ_6 PCBs 28, 52, 101, 138, 153 and 180). These six ndl-PCBs account for around 50 % of the total ndl-PCBs in food samples, and at least one of them was found in 68.4 % of feed and 82.6 % of food samples (EFSA, 2012) Due to their persistent and bioaccumulative properties, PCBs may enter the food chain via various routes, including animal feed. Therefore, legislation in the EU (Commission, 2006; Commission, 2011; EU, 2013) and elsewhere has fixed maximum levels (MLs) for PCBs in food. For ndl-PCBs, the MLs were not derived based on toxicological considerations, but according to the ALARA (As Low As Reasonable Achievable) principle; the same applies to the MLs in complete feed according to Regulation (EU) No. 277/2012 (Union, 2012). Importantly, the transfer of ndl-PCB from feed to foods of animal origin was not explicitly taken into account, as the regulation on feed explicitly mentions. Therefore, it cannot be excluded that feed that is safe under feed law (does not exceed feed MLs) could result in food that is not fit for human consumption due exceeding food MLs.

In the autumn of 2018, ndl-PCBs were detected in individual samples of poultry meat and eggs in Germany at concentrations exceeding the ML for food. The putative cause was identified as the chipping of (PCB-containing) paint in the loading cells of a feed company (BMEL, 2018). In the course of the incident, feed for fattening poultry was obtained that did not exceed the ML for feed, but apparently caused an exceedance of ndl-PCB MLs in chicken meat. This feed was used to perform feeding studies where the animals received a diet with a known ndl-PCB content, leading to experimental transfer results and toxicokinetic models for the transfer of ndl-PCBs in fattening chickens (Ohlhoff et al., 2021), laying hens (Ohlhoff et al., 2022; Savvateeva et al., 2022) and, in the present manuscript, in fattening pigs. The pigs were temporarily fed with the aforementioned ndl-PCB contaminated feed and then slaughtered at different ages. Liver and meat were subsequently analyzed for their ndl-PCB content. The derived data was used for the development of a physiologically based toxicokinetic (PBTK) model describing the transfer of ndl-PCB from feed into liver and adipose tissue of pigs.

The use of PBTK models in risk assessment offers several advantages over the traditional use of transfer parameters such as half-lives or transfer rates. One key advantage is their ability to extrapolate to a wide range of scenarios not originally covered by experiments, including longer or shorter exposure times. This reduces the need for additional in vivo and in vitro studies. Additionally, PBTK models provide a more accurate description of the kinetic behavior of the contaminants under study that cannot always be captured by static transfer parameters. For example, half-lives always assume exponential depuration, but this is not always the case. Furthermore, PBTK models can help to derive parameters that better describe the relevant situation for risk assessment than static parameters. Thus, it is not surprising that a wide variety of PBTK models have been developed for various substances and in different farm animals (Adolphs et al., 2013; Krishnan and Peyret, 2009; Lautz et al., 2020; Moenning et al., 2023; Moenning et al., 2022; Savvateeva et al., 2020; Taverne et al., n.d.). Although PBTK models are available for the transfer of ndl-PCBs in a variety of farm animals, no PBTK model has yet been developed specifically for pigs. The purpose of the newly developed PBTK model is to predict the concentrations of 6 ndl-PCBs in the fat and liver of pigs during their fattening phase under different exposure scenarios. In addition, the PBTK model can be used to determine the highest levels in the feed that will prevent the maximum levels (ML) in the liver and fat from being exceeded.

For the sake of transparency and reusability, the model described here is included in the Supplementary Material in both in the Food Safety Knowledge Exchange .fskx and in the Python .py formats.

2. Materials and methods (including safety information)

2.1. Ethics approval statement

All experimental procedures involving animals were registered at the Regional Office for Health and Social Affairs Berlin (LAGeSo) in Berlin, Germany under StN004/20 and T0070/20.

2.2. Animal husbandry, study design, and experimental diets

A total of $n = 15$ male neutered pigs (PIC Hybrid), aged 8 weeks with BW of 26.2 ± 2.7 kg (mean ± std.dev.), were kept in four groups (3, 3, 3, 6) in pens (8.0 m^2 per pen) with concrete floor littered with straw. Room temperature was maintained at 21 ± 3 °C. Animals were fed twice daily at 8:30 am and 4:00 pm with equal amounts of control and experimental rations designed to meet the energy and nutrient requirements of growing pigs. Water was provided ad libitum. During an adaptation period of 7 days, pigs of all three groups received a commercial complete compound feed (based on wheat grain, corn grain, soybean meal, rapeseed meal, vegetable oil and a vitamin and mineral supplement as main ingredients; control diet). Subsequently, groups A and B each consisted of 3 animals receiving a mashed diet contaminated with ndl-PCBs from the above-mentioned contamination event (PCB diet) for 21 days. At the end of this sub-period, the animals of group A were slaughtered (by stunning followed by exsanguination) approximately 3 h after the morning meal to determine the ndl-PCB content in meat and liver. The animals of group B were then returned to the control diet for 60 days. Group C, consisting of 3 animals, received the control diet until 7 days before the end of the experimental period and was then switched to the PCB diet. At the end of the experimental period of 81 days, all remaining animals were slaughtered, and samples of meat and liver were analyzed. The control group consisted of 6 animals that received the control diet throughout the entire period. At the beginning and at the end of the experimental period, 3 animals of the control group were slaughtered to assess the background ndl-PCB level in meat and liver. Concentrations of ndl-PCB congeners in the control diet, the PCB diet and the litter are given in Table 1.

Over the entire course of the experiment, feed intake W_S^i was determined for each group daily. Body weight (BW) was recorded weekly for each animal and used in aggregated form (Fig. S3). Health status including behavior, appearance and fecal consistency was recorded daily.

2.3. Analyses of samples

Analyses of ndl-PCBs in feed, litter, meat and liver samples were conducted by the German National Reference Laboratory (NRL) for Halogenated Persistent Organic Pollutants (POPs) in Feed and Food located at the German Federal Institute for Risk Assessment (Berlin, Germany). The analysis of feed, litter and meat is similar to that described by Ohlhoff et al. (2021). The NRL is accredited according to DIN EN ISO/IEC 17025.

The feed and litter were homogenized; 10 g per sample were mixed with diatomaceous earth and the PCB extraction was performed by accelerated solvent extraction (ASE 350, Thermo Fisher Scientific, USA) using toluene in the first cycle and toluene/ethanol 9:1 in the second and third cycles (pressure 10 MPa, temperature 100 °C). Prior to vacuum evaporation to near dryness by using a rotary evaporator (Büchi, Germany), 2 mL of nonane were added. The sample purification was performed with the MIURA GO-xHT system (MIURA CO., Ltd., Japan) using four different columns (i.e. silica gel impregnated with silver nitrate, silica gel impregnated with sulfuric acid, activated carbon and alumina). The extracts were

Table 1
Concentration of the sum of 6 indicator ndl-PCB congeners (Σ_6) and individual concentration C_S^i of each indicator ndl-PCB i (μg/kg; 88 % dry matter (DM))[a] in experimental diets and littering material. The expanded uncertainty of the measurements is 37.4 %.

C_S^i	Σ_6	PCB 28	PCB 52	PCB 101	PCB 138	PCB 153	PCB 180
Control diet	0.06	0.01	0.01	0.01	0.01	0.01	0.01
PCB diet	11.67	0.36	0.98	1.78	2.71	3.23	2.61
Litter	1.08	0.03	0.07	0.20	0.27	0.35	0.15

[a] Expanded uncertainty of the measurement is 37.7 %.

dissolved in 5 mL hexane, transferred to the first column and automatically eluted with 95 mL of hexane. The ndl-PCBs (fraction B) were caught in the alumina column. This column was eluted with 2.2 mL toluene and then concentrated under a nitrogen stream to a final volume of 20 μL.

The dry matter content of the feed and litter were determined gravimetrically by drying the samples at 105 °C. The PCB concentrations were reported at 88 % dry matter content. Liver and muscle tissue were freeze dried and homogenized. For fat extraction, the sample weight was selected so that 2–3 g of fat were extracted. Subsequently, only sodium sulfate was added. The free-flowing powder was placed in a glass column and the fat was extracted with a mixture of cyclohexane/dichloromethane (1,1). The subsequent clean-up of the samples was performed fully automatically with the MIURA GO-xHT system (MIURA CO., Ltd., Japan). The isotope-labeled analogues of all quantified PCBs were added before the extraction step. In addition, a 13C-labelled PCB recovery standard was added to the sample prior the measurement.

Samples were analyzed by gas chromatography (GC) (Agilent Technologies, USA) and high-resolution mass spectrometry (HRMS) (DFS, Thermo Fisher Scientific, USA; resolution 10,000; injection of 1 μL). For the determination of the ndl-PCBs, a HT8-PCB 60 m × 0.25 mm × 0.25 μm (SGE Analytical Science Europe Ltd) column was used. For quality assurance, an internal reference material from a proficiency test and a blank sample were analyzed in the same way as the samples in each analytical series. The expanded uncertainty (Eppe et al., 2017) for liver and meat were 12.3 % and for feed and litter 37.4 %.

2.4. Physiologically based toxicokinetic (PBTK) modelling

A compartmental model was developed to describe the transfer of each indicator ndl-PCB congener i from the feed into the tissues of the pig (Fig. 1). The model consists of two compartments: 1) a liver compartment, where the congener is eliminated (metabolized); and 2) a fat compartment (representing the body lipid fraction), where the contaminants are stored. Other excretion pathways, such as urinary and respiratory, are considered negligible due to the physicochemical properties (high K_{ow} and K_{oa}) of these compounds. For these two compartments, it is assumed that each congener concentration is instantly in equilibrium, i.e. the concentrations among the compartments can be calculated using a partition coefficient $P_{FL}^i > 0$ [unitless] such that

$$C_F^i(t) = C_L^i(t)\, P_{FL}^i \tag{1}$$

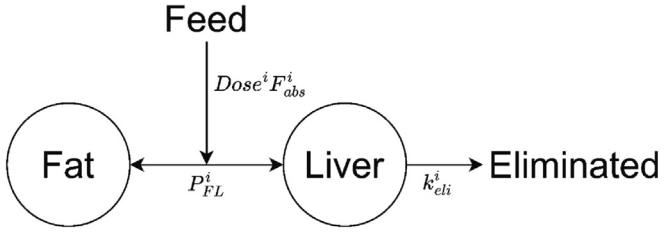

Fig. 1. Schema of the compartmental model for the pigs. Here, the $Dose^i$ represents the ndl-PCB congener amount in feed and F_{abs}^i is the fraction of congener i absorbed from the gastrointestinal tract (GIT). P_{FL}^i is the partition coefficient between the fat and liver compartments.

Here $C_F^i(t)$ [μg/kg] is the congener concentration in the fat compartment (fat basis) and $C_L^i(t)$ [μg/kg] in the liver compartment (wet weight, ww basis) at time t [d]. Therefore, it has a behavior tantamount to a one compartment model. This strategy was chosen because no experimental data were available shortly after the onset of assimilation and depuration, which would have been necessary to observe and describe the distribution phase. An advantage of this approach is that this model requires no blood-specific data or assumptions (e.g. blood flow rates, blood volumes or diffusion velocities). However, a major drawback is that such a model does not reproduce the biexponential behavior typical of PCBs (Moenning et al., 2022; Ohlhoff et al., 2021; Savvateeva et al., 2020) (assuming constant physiological parameters).

The next assumption is that the elimination of the congeners occurs exclusively in the liver of the pigs with a first-order elimination rate constant k_{eli}^i [1/d]. The total congener amount in the body A_T^i [μg] can thus be described by

$$\dot{A_T^i} = -k_{eli}^i C_L^i V_L + I^i \tag{2}$$

$$= -k_{eli}^i A_L^i + I^i \tag{3}$$

where V_L [kg] is the volume of the liver; A_L^i [μg] is the amount of congener in the liver and I^i [μg] is the congener input function. The input into the pig consists of the total amount of congener in daily feed (*Dose*) multiplied by the fraction of congener absorbed from the gastrointestinal tract (GIT) F_{abs}^i [unitless], i.e.,

$$I^i(t) := F_{abs}^i Dose^i(t) \tag{4}$$

where $Dose^i(t) = C_S^i(t) W_S^i(t)$ [μg] or the multiplication of congener concentration C_S^i [μg/kg] and daily amount of feed W_S^i [kg]. Combining Eqs. (1) and (3) results in a differential equation of the form

$$\dot{A_T^i} = \frac{-A_T^i k_{eli}^i}{1 + \frac{V_F}{V_L} P_{FL}^i} + I^i \tag{5}$$

where V_F [kg] fat volume. In Adolphs et al. (2013) Section 2.2, it was proposed that the fat ratio of pigs can be estimated by a linear function of time, i.e.

$$V_F(t) := V_T(t) r_F t \tag{6}$$

where r_F [d^{-1}] is the fat gain rate constant and V_T [kg] is the total animal weight. Furthermore, it is assumed that the liver grows linearly with respect to the total weight of the animal, i.e.

$$V_L(t) := V_T(t) r_L + a_L \tag{7}$$

where r_L [unitless] is the liver growth rate and a_L [kg] the intersecting point with the y axis.

2.5. Parametrization

The experimental data used for parametrization included measurements of the concentration of each of the 6 congeners in liver as well as meat (muscle in fat basis). It was assumed that the muscle fat concentration is representative for the complete body fat. The total body weight of the

animals was measured weekly, and $V_T(t)$ is estimated by a stepwise linear function connecting those measured data points. In addition, post-slaughter liver weights were recorded and used to estimate r_L and a_L (Eq. (7)) via the linear regression function in Excel 2016. Both the concentration of each congener in the feed C_S^i and the weekly total amount of feed fed to all animals were recorded, and the $Dose^i$ (t) function for each animal was estimated from these data using a step function assuming that each animal consumed the amount of feed. The parameters k_{eli}^i, P_{FL}^i and F_{abs}^i were fitted using the Levenberg-Marquardt algorithm (implemented in Python 3.8.8 (Newville, 2021)) by minimizing the log square error

$$E = \sqrt{\frac{\Sigma_k(\log_{10}(p_k) - \log_{10}(x_k))^2}{N}} \tag{8}$$

of the model predictions p_k of the measured liver and muscle fat x_k concentration, where N is the number of samples. Some fitting domains were set quite permissively to ensure that they contain the optimal values; that is the case of the parameter to k_{eli}^i with [0,30] d^{-1} and P_{FL}^i with [0,100]. For F_{abs}^i, the fitting domain was set to [0, 100] % for mass conservation. The fitting of k_{eli}^i, P_{FL}^i and F_{abs}^i was done separately for each congener. In addition, the fat gain rate r_F was also fitted using differential evolution (implemented in Python 3.8.8 (Newville, 2021)) minimizing the log square error of the model prediction Eq. (8) to the measured liver and muscle fat concentration for all six congeners at once estimating the same r_F for all congeners. At each fitting step, the model parameters k_{eli}^i, P_{FL}^i and F_{abs}^i for each of the six congeners were optimized as described above. This was done because literature values for fat content based on their age or weight vary considerably (GfE, 2006; Kasper et al., 2021; Kouba et al., 1999; Pfeiffer et al., 1984) and corresponding experimental data were not recorded. The fitting domain was set quite permissively at [0.01, 5] %/d. Due to constraints in computational resources, the Levenberg-Marquardt algorithm (which formally optimizes towards a local minimum near the starting values) was used instead of differential evolution (which formally is a global optimization independent of starting values) at each step of the inner fit for the parameter k_{eli}^i, P_{FL}^i and F_{abs}^i. It was sporadically tested whether the fitting results for these parameters were independent of the chosen starting values.

2.6. Sensitivity analysis

Since r_F could only be derived indirectly by fitting to experimental data not including body fat measurements, the uncertainty with respect to this parameter is quite large. To understand the impact of this uncertainty, a sensitivity analysis was performed to study the influence of r_F on the 3 subsequently fitted parameter k_{eli}^i, P_{FL}^i and F_{abs}^i. In addition, a sensitivity analysis was performed on the other parameters to understand their influence on the overall model performance. In all cases, the respective parameters were varied by up to ±50 % in increments of 10 %.

2.7. Transfer parameters

Both the transfer factor (TF) and the transfer rate (TR) describe the retention in the animal after continued exposure to the congeners. The TF describes the concentration in the animal at a given the concentration in feed, i.e.

$$TF_j^i := \lim_{t\to\infty} \frac{C_j^i(t)}{C_S^i} \text{ [unitless]}, \tag{9}$$

where $j \in \{F, L\}$ and C_S is the constant concentration of the congener in feed. In contrast, the TR describes the relative amount of a congener given with feed that is retained in the animal's body, i.e.

$$TR^i := \lim_{t\to\infty} \frac{A_T^i(t)}{\int_0^t Dose^i(\check{t})d\check{t}} \text{ [unitless]}, \tag{10}$$

where $Dose^i$ is the function describing the daily congener amount in feed. The TR has also been called assimilation efficiency by other authors (Jondreville et al., 2017). For this work, the TR is only calculated with respect to the total amount of the congener A_T^i, as V_F grows quadratically and V_L only linearly; therefore, due to Eq. (1) the relative amount in liver always converges to 0. To calculate these parameters, it is assumed that the PCB concentration in the feed is constant and that the daily feed intake and total body weight grow linearly according to the regression of the experimental data. Under these conditions, shown in the Supplementary Material, the function for both the TF_j^i and the TR^i converge above 0. In addition, it should be noted that for both transfer parameters the contamination does not have to start at $t = 0$ but rather can begin at any time and the functions would still converge to the same limit.

Here it should be noted that both the TFs and TR are defined as limits, which are presumably never reached. This by calculating the time dependent transfer factor.

$$\widetilde{TF_j^i}(t) := \frac{C_j^i(t)}{C_S^i} \text{ [unitless]} \tag{11}$$

and transfer rate.

$$\widetilde{TR^i}(t) := \frac{A_{Total}^i(t)}{\int_0^t Dose^i(\check{t})d\check{t}} \text{ [unitless]} \tag{12}$$

assuming that the contamination started at day 60 and continued until slaughter at day 150. This roughly describes the scenario that the feed at a fattening farm is contaminated with a constant concentration of the respective congener.

Another common parameter in risk analysis is the half-life ($\tau_{1/2}^i$), which assumes an exponential concentration-time profile (Ct-profile) during the depuration phase, and describes the time until half of the contaminant concentration is eliminated. However, there is no such exponential Ct-profile during depuration phase in our model, since the body mass V_F grows quadratically and the liver mass V_L only linearly. This behavior, on the one hand, reduces the relative amount of the congener in the liver, resulting in a reduction in the overall rate of elimination of the congener; on the other hand, it causes mass dilution, diminishing the concentration of the contaminant in the tissues without reducing the absolute amount. However, because most risk assessors are familiar with the concept of half-life, we use the algorithm developed for calculating half-life to represent the variable speed of concentration elimination at each time point. Therefore, first the negative slope of the logarithmic depuration Ct-profile needs to be calculated at each time point, i.e.

$$\overline{k}_j^i(t) = -\ln\left(\dot{C}_j^i(t)\right) = -\frac{\dot{C}_j^i}{C_j^i}(t) \tag{13}$$

$\overline{k}_j^i$ [1/d] describe the relative concentration diminished per day and is derived via numerical approximation. Due to Eq. (1) $C_F^i \propto C_j^i$ for $j \in \{T, L\}$ and therefore the concentration of all compartments decreases at the same rate, i.e.

$$\overline{k}_F^i(t) = \overline{k}_L^i(t) = \overline{k}_T^i(t) =: \overline{k}^i(t) \tag{14}$$

To derive a half-life like parameter $\tau_{1/2}^i$ [d] this is inserted into

$$\tau_{1/2}^i(t) = \frac{\ln(2)}{\overline{k}^i(t)} \tag{15}$$

Note that $\tau_{1/2}^i$ is not a constant, but changes depending on the time point. All the here used parameters are summarized in Table 2.

Table 2
List of parameters and variables that are used for modelling, together with their names, units, sources and values if the values are constant across all animals and congeners.

Name	Interpretation	Value	Unit	Source
C_L	Concentration in liver		μg/kg	Measured and modelled
C_F	Concentration in liver		μg/kg	Measured and modelled
C_S	Concentration in feed		μg/kg	Measured
W_S	Amount of feed		kg	Measured
A_T	Amount of congener in pig		μg	Modelled
A_L	Amount of congener in liver		μg	Modelled
A_F	Amount of congener in fat		μg	Modelled
$Dose^i$	Daily amount of congener i ingested	$C_S W_S$	μg/d	Measured or linear regression
F^i_{abs}	Fraction absorbed from feed		%	Fitted
P^i_{FL}	Fat-Liver partition coefficient		Unitless	Fitted
k^i_{eli}	Liver elimination rate		d^{-1}	Fitted
I^i	Effective input into the pig	$Dose^i F^i_{abs}$	d^{-1}	Measured or linear regression
V_L	Liver wet weight	$V_T r_L + a_L$	kg	Linear regression
r_L	Growth rate liver relative to bodyweight	0.015	unitless	Linear regression
a_L	Intersection x axis liver weight	0.24	kg	Linear regression
V_F	Weight of total body fat	$V_T r_F t$	kg	Fitting
r_F	Fat gain rate	0.11	%/d	Fitting
V_T	Total bodyweight of the pig		kg	Measured or linear regression
TF^i_F	Transfer factor into fat		Unitless	Modelled
TF^i_L	Transfer factor into liver		Unitless	Modelled
TR^i	Transfer rate into pig		Unitless	Modelled
$\tilde{TF}^i_F$	Time-dependent transfer factor liver		Unitless	Modelled
$\tilde{TF}^i_F$	Time-dependent transfer factor fat		Unitless	Modelled
$\tilde{TR}^i$	Time-dependent transfer rate		Unitless	Modelled
k^i	Time-dependent concentration elimination rate		d^{-1}	Modelled
$\tau^i_{1/2}$	Time-dependent half-life		d	Modelled

3. Results and discussion

3.1. Simulation results

The ndl-PCB concentration in the control animals was substantially lower than in the supplemented groups, with <0.170 ng/kg fat basis in muscle and <0.012 ng/kg (wet weight) for the sum of six ndl-PCBs (Table 3). Therefore, the background contamination is assumed to be irrelevant. The simulated Ct-profiles for all six ndl-PCBs in liver and fat of all supplemented animals, as well as their experimental data, are depicted in Fig. 2. In general, the simulation describes the measured data for liver and fat quite well. In all cases the fat concentrations are better described than the liver concentration, which on the one hand is due to the fact that the liver measurements show a higher variance and on the other hand this could be also due to the fact that the fat Ct-profile can be better described by one compartment model than the liver Ct-profile. For each congener, the Ct-profile in liver and in fat is identical except for the scaling factor P^i_{FL} according to Eq. (1).

The course of the Ct-profile of all congeners (Fig. 2) is predominantly increasing during the assimilation phase, followed by a monotonous decrease during the elimination phase. In the assimilation phase, a periodic non-continuous change in the slope can be observed ("hump-shape"), which is caused by the stepwise increase in the total amount of feed. The strongest effects were observed for PCB 28 (Fig. 2a and b), the congener with highest elimination rate (Table 4). In fact, the hump-shaped profile in the assimilation phase is directly related to the high rate of elimination in the liver (i.e. shorter half-life) causing a fast decline in the accumulation speed (lower second derivative) during the assimilation phase, which is reflected as a disparity between the slopes before and after each increase in feed.

3.2. Derived parameters

3.2.1. Fat gain rate r_F

The recorded data included the measurements of the total body weight but not of the body lipid mass, so that this latter important physiological variable had to be inferred using fitting of Eq. (6) using data other than the body fat itself; the optimized fat gain rate r_F obtained by the fitting method is 0.110 %/d, which leads to a fat content of 11.0 % at the age of 100 days and a rough body weight of 60 kg, respectively. This is relatively low with respect to data of other published studies (GfE, 2006; Kasper et al., 2021; Kouba et al., 1999; Pfeiffer et al., 1984). One factor contributing to this low estimate is the consideration of total body weight rather than empty body weight as in most of the other studies, which would reduce the total body weight by approximately 6 % (GfE, 2006). In addition, many of the studies were conducted several decades ago (e.g. in 1984 (Pfeiffer et al., 1984)), when pigs had much higher fat content (GfE, 2006; Kouba et al., 1999; Pfeiffer et al., 1984). There has been a trend in commercial livestock breeding to reduce the fat content to meet today's market demands (Knap and Rauw, 2008).

A technical explanation for the estimated low fat content can also be provided by the type of fat sample taken. Congeners were analyzed in muscle fat, and then considered representative of all fat deposits of the animal. However, Delannoy et al. (2014) and Hoogenboom et al. (2021) showed that the concentration of most ndl-PCBs tends to be lower in muscle fat than in adipose fat. Interestingly, this would imply that either the actual absorption coefficient should be higher than estimated (Table 4) as this would imply that the "true" body burden is even higher than predicted, or that the total fat amount in the animal is even lower than already estimated as this result in less diluted (i.e. higher concentration) congeners in fat. However,

Table 3
Average concentration on the day of slaughter of the six ndl-PCBs in the liver and muscle fat tissue of the control animals ($n = 6$).

	PCB-28	PCB-52	PCB-101	PCB-138	PCB-153	PCB-180
Liver [μg/kg] (wet weight)	1.12×10^{-3}	3.40×10^{-3}	3.12×10^{-3}	1.11×10^{-2}	6.17×10^{-3}	3.64×10^{-3}
Muscle [μg/kg] (fat basis)	2.19×10^{-2}	4.25×10^{-2}	4.81×10^{-2}	1.68×10^{-1}	1.28×10^{-3}	9.11×10^{-2}

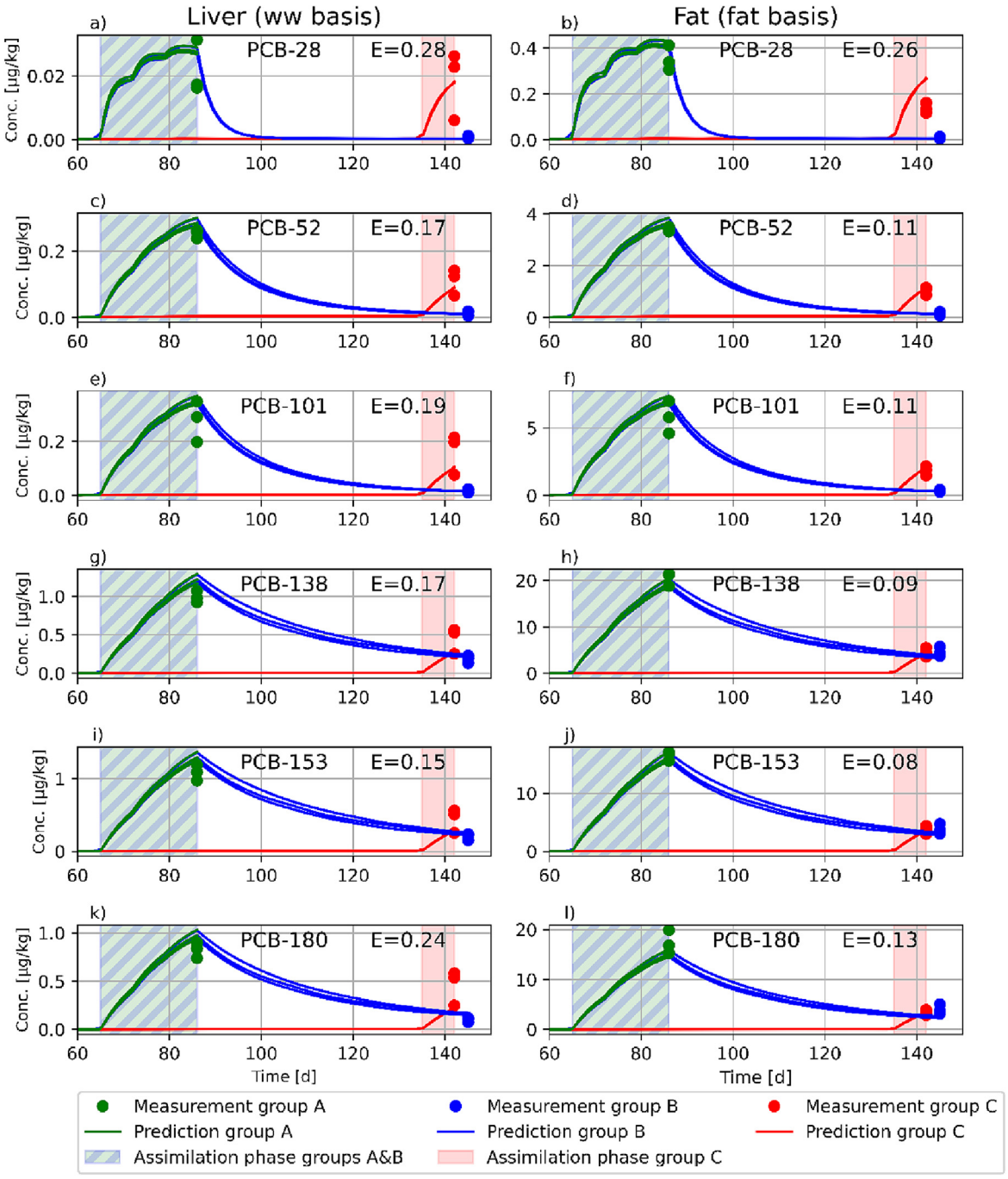

Fig. 2. Concentration-time profiles in liver (ww) and fat of PCB-28 (a and b); PCB-52 (c and d); PCB-101 (e and f); PCB-138 (g and h); PCB-153 (i and j) and PCB-180 (k and l) predicted by the model (lines) for each individual animal. This is compared to the measured concentration of each congener in each animal (dots). Here E denotes the log square error of Eq. (8) for only the measurement points of the respective compartment.

Table 4
Optimized congener-specific toxicokinetic model parameters.

	F^i_{abs} [%]	P^i_{FL} [unitless]	k^i_{eli} [1/d]
PCB-28	91.8	14.8	20.5
PCB-52	95.7	12.8	3.54
PCB-101	93.4	20.0	4.68
PCB-138	100	15.8	0.708
PCB-153	100	12.5	0.543
PCB-180	100	15.5	0.916

since the calculated absorption rate of 3 of the 6 congeners is already 100 %, it is unlikely that the absorption rate was underestimated. Consequently, this would indicate an even lower actual fat content in the animals.

3.2.2. Congener-specific toxicokinetic model parameters

Congener-specific parameters, namely the absorption coefficient F^i_{abs}, the partition coefficient P^i_{FL} and the liver elimination rate k^i_{eli} are summarized in Table 4.

The absorption coefficients F^i_{abs} are very high for all congeners, ranging from 91.8 % for PCB-28 to 100 % for PCBs-138, 153 and 180. That means that for all congeners under study, the absorption from the GIT is nearly

Table 5
Congener-specific limit *TF*s and *TR* for the average pig from this study. These values are valid only for a long continuous exposure. It is recommended to use the full PBTK model for the specific exposure length in question (especially if it is shorter than around 90 days) instead of resorting to these *TF* and *TR*.

	TF_F^i [unitless], fat basis	TF_L^i [unitless], ww basis	TR^i [%]
PCB-28	1.21	0.0817	9.57
PCB-52	4.57	0.357	34.6
PCB-101	4.98	0.249	38.5
PCB-138	10.6	0.668	76.6
PCB-153	10.6	0.850	77.2
PCB-180	9.82	0.634	71.2

complete. A possible overestimation of the fat content as an artificial cause for the high absorption coefficients can be excluded with high confidence, since the calculated fat contents in the study described here are already lower than in many other studies. In addition, it should be noted that F_{abs}^i may depend on the type of feed contamination, which in our case was by paint particles. This means that other types of feed contamination, e.g. via PCB contaminated oils, could result in different F_{abs}^i values. However, once F_{abs}^i has been adjusted, the model should be able to handle other types of feed contamination or even other types of oral exposure scenarios such as soil. Furthermore, it should be noted that although F_{abs}^i may differ between such scenarios, the difference is unlikely to be too drastic, as can be seen in Savvateeva et al. (2022), where rather similar F_{abs}^i are derived for soil and feed in laying hens. Finally, due to the fact that the F_{abs}^i predicted here are already close to 100 %, using these values for different oral exposure scenarios is likely to be an upper bound.

The partition coefficient between fat and liver P_{FL}^i range from 12.5 for PCB-153 to 20.0 for PCB-101 must be interpreted taking into account a fat fraction of 5 % (Savvateeva et al., 2020) in liver. In this light, it is clear that PCB concentration tends to be higher in the liver than in fat when the same fat basis is used (i.e. $P_{FL}^i < 20$), in line with the findings of Hoogenboom et al. (2021).

The last congener-specific parameter determined is the liver elimination rate k_{eli}^i, which shows the highest variability among the here derived parameters. The six ndl-PCBs can be categorized into 3 liver elimination velocity categories: PCB-28 is the fastest eliminated congener with $k_{eli}^i = 20.5\ d^{-1}$; PCB-52 and PCB-101 have intermediate liver elimination rates with $k_{eli}^i = 3.54$ and $4.68\ d^{-1}$, respectively; and finally PCB-138, PCB-153 and PCB-180, which are relatively slowly eliminated from the liver with k_{eli}^i ranging from 0.543 to $0.916\ d^{-1}$. In general, the lower chlorinated ndl-PCBs are found to be eliminated faster than the higher chlorinated congeners. However, this isn't always the case, as PCB-28 in chickens (Ohlhoff et al., 2021) and ring droves (Drouillard and Norstrom, 2003) is eliminated more slowly than the other 5 ndl-PCBs. The elimination velocity of PCB-28 in rats appears to be more similar to that of PCBs 52 and 101 (EFSA, 2005), suggesting that a fast elimination of PCB-28 is characteristic of pigs. It can be concluded that the difference in kinetic behavior of the congeners is controlled primarily by the elimination rate k_{eli}^i, since the differences in F_{abs}^i and P_{FL}^i are minor.

3.3. Sensitivity analysis

From the sensitivity analysis (data shown in the Supplementary Material), it is evident that the choice of r_F has a notable impact on all three parameters. However, the changes in these parameters are not too dramatic, i.e., with no ratio $>>1$ or $<<-1$ with respect to r_F. Furthermore, the decrease in performance when deviating from the optimal r_F is quite noticeable. Therefore, the here derived parameters are reasonably trustworthy despite the uncertainty with respect to r_F.

3.4. Transfer parameters

The limit transfer parameters are summarized in Table 5. The proportions between transfer factor into fat TF_F^i in fat basis and the transfer factor into liver TF_L^i in wet weight (ww) basis are given by P_{FL}^i (see Table 4). The TF_F^i ranges from 1.21 for PCB-28 to 10.6 for PCB-153. The lowest TF_L^i is obtained again for PCB-28 with and the highest TF_L^i is again for PCB-153 with 0.850. The same is true for the transfer rate (TR^i); again PCB-28 has the lowest TR^i at 9.57 % and PCB-153 has the highest TR at 77.2 %.

To show the actual relevance in practice of these limit parameters the convergence of the time dependent transfer parameters are shown in Fig. 3. For both $\tilde{TF}_j^i$ it can be seen that they converge from below against

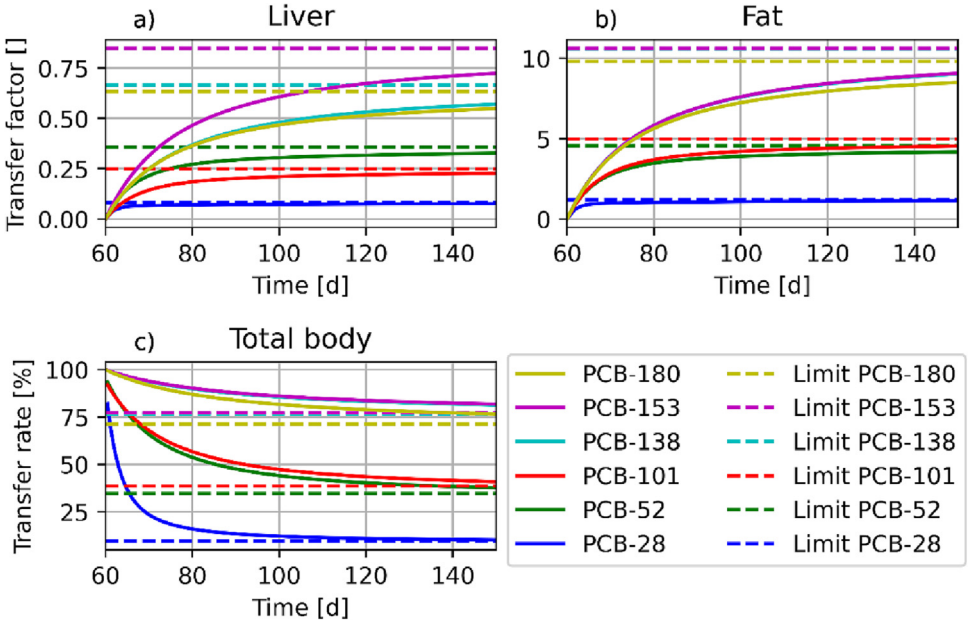

Fig. 3. Exemplary prediction of the simulated $\tilde{TF}_j^i$ (a, b) and $\tilde{TR}^i$ (c) converging to their respective limit TF_L^i and TR^i. The $\tilde{TF}_L^i$ and $\tilde{TR}^i$ for PCB-153 and PCB-138 are very similar and can therefore only be barley seen. Here it is assumed that the contamination of feed starts at day 60 and has the same concentration of the respective congener until the day of slaughter at day 150.

their limit (i.e. $TF_j^i > \tilde{TF}_j^i(t)$ for all t) reaching >85 % of the limits value at day 150. Whereas the $\tilde{TR}^i$ converges from above (i.e. $TR^i < \tilde{TR}^i(t)$ for all t) starting from the respective F_{abs}^i value and reaching <110 % of the limits value at day 150.

3.5. Highest level in feed so as not to exceed the maximum level in food

What is the highest level in feed that is compatible with the current maximum levels in meat (40 ng ndl-PCB/g fat)[6] and liver (3 ng/g fresh weight)[7]? To answer this question, one can use the transfer factors (Table 5) and choose the worst-case scenario (PCB-153). The result is that the levels in feed over a period of 90 days or more should not exceed 3.8 μg/kg feed 88 % dry matter for the sum of indicator ndl-PCBs so as not to exceed the maximum levels in neither meat (muscle fat) nor the liver. This highest level is protective for any congener mixture of the six indicator ndl-PCBs. The calculated highest level of 3.8 μg/kg for pigs is similar to that calculated for fattening chickens (3.9 μg/kg for a 56-day fattening period) (Ohlhoff et al., 2021) and laying hens (2.4 μg/kg) (Savvateeva et al., 2022) and at the same time lower than the ML in feed of 10 μg/kg (Union, 2012). In this sense, there is a potential risk for feed under the current ML to lead to pig products above the ML, as the EU regulation itself mentions (Union, 2012).

3.6. Half-lives

The dynamic half-life-like parameters $\tau_{1/2}^i$ for all tested ndl-PCBs from day 60 to day 150 are shown in Fig. 4. Similarly to the liver elimination (see Section 3.2.2), also the total elimination $\tau_{1/2}^i$ can be categorized into fast (PCB-28), intermediate (PCB-52 and PCB-101) and slow (PCB-138, PCB-153 and PCB-180). All half-lives grow asymptotically and linearly, as they are controlled by the liver (which is assumed to grow linearly as opposed to the fat, which is assumed to grow quadratically). Over the time period shown, the half-lives for all 6 congeners increase by >3 times the baseline on day 60.

4. Monoexponential model behavior

As mentioned above, a major drawback of the model developed here is that it acts more like a one compartment model and cannot describe the typical biexponential behavior observed for PCBs, but only monoexponential behavior. This will have a particular impact on the predictions of liver concentrations, as the liver is typically part of the central compartment in which absorption, metabolism and excretion happens, and therefore has a more pronounced biexponential behavior. Because of this, we expect larger prediction errors in liver concentrations, especially shortly after the onset of the depuration or assimilation phases. In contrast, the fat compartment is the peripheral compartment for lipophilic contaminants and is the root cause of the longer second half-life; it therefore does not display a very pronounced biexponential behavior, so that we expect smaller prediction errors for fat concentrations at all times using the model proposed here. This expectation is grounded on a mathematical proof in the Supplementary Section “Relevance of the biexponetial behavior in the peripheral compartment”. Furthermore, in the results from Ohlhoff et al. (2021), it can be seen that the depuration in the fat compartment is effectively monoexponetial.

5. Conclusion

The PBTK model presented in this work is able to describe the contamination events of the studied indicator ndl-PCB congeners under different contamination scenarios. Besides predicting the concentration-time profiles in liver and fat of fattening pigs, the PBTK model also allows the derivation of various parameters such as transfer factors and transfer rates. Furthermore, the model allows a rough characterization of the toxicokinetic behavior in the pig body from assimilation to elimination. The model results show that all six ndl-PCBs under study are almost completely absorbed (F_{abs}^i > 91.8 %) from the GIT of fattening pigs. Furthermore, it is concluded that the main differentiating factor between the kinetics of the individual congeners are their elimination rates in the liver, which can be categorized into fast (PCB-28), intermediate (PCB-52 and PCB-101) and slow (PCB-138, PCB-153 and PCB-180). In this sense, the elimination rates in pigs obey the general expectation that lower chlorinated congeners (PCB-28, 52 and 101) should be metabolized more rapidly than higher-chlorinated ones (PCB-138, PCB-153 and PCB-180). A deviation from this expectation was observed in fattening chickens and laying hens (Savvateeva et al., 2022), where PCB-28 unexpectedly was part of the slowly eliminated group of congeners. In addition to elimination via liver, also dilution via weight gain is responsible for the reduction of ndl-PCB concentrations in pigs after assimilation; at the same time, the growth of the pigs also causes the total elimination rate of the animal to decrease over time, as the fat compartment grows faster than the liver compartment. A limiting factor in this study

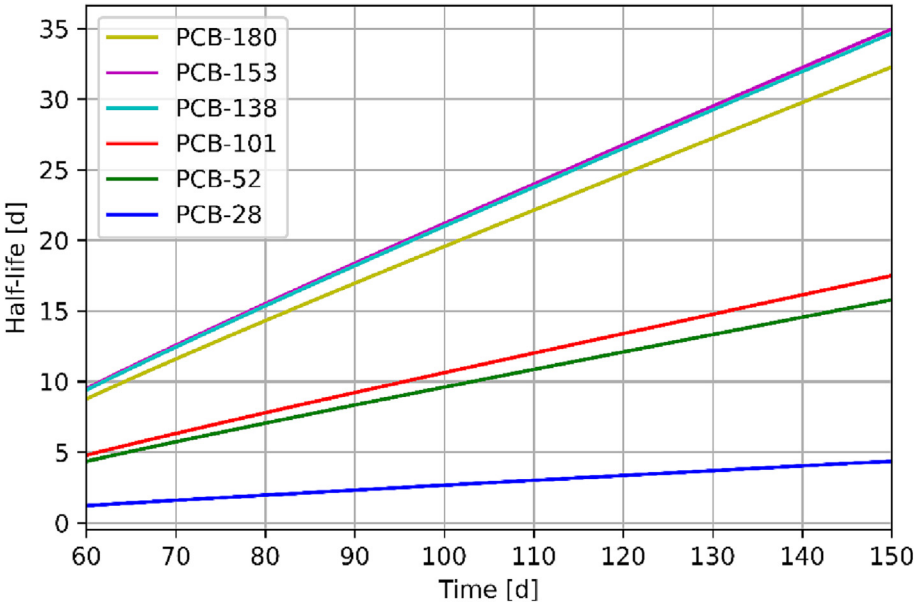

Fig. 4. Congener-specific time dependency of the dynamic half-life like parameters $\tau_{1/2}^i$.

was the lack of recorded fat content of the pigs, forcing us to derive it indirectly via fitting methods. Therefore, it is advisable in similar studies with lipophilic substances to use methods to quantify body fat (e.g. with non-invasive methods) to reduce the uncertainty of the model. Furthermore, future studies should also include at least one measurement a few days after the start of the depuration phase to be able to observe and describe the typical biexponential behavior of ndl-PCBs using a two compartment model without the equilibrium assumption used here. The PBTK model derived here can nevertheless be used in risk assessment and was used here to derive various parameters, such as transfer factors, transfer rates and half-lives under realistic feeding conditions.

Abbreviations

BfR	German Federal Institute for Risk Assessment, Berlin, Germany
BW	body weight
Ct-profile	concentration-time profile
DM	dry matter
GIT	gastrointestinal tract
K_{oa}	Octanol-air partition coefficient
K_{ow}	Octanol-water partition coefficient
ML	maximum level
ndl	non-dioxin-like
PBTK	physiologically-based toxicokinetic
PCDD/F	Polychlorinated dibenzo-*p*-dioxins (PCDDs) and polychlorinated dibenzofurans (PCDFs)
PCB	polychlorinated biphenyl
PCB 28	2,4,4′-trichlorobiphenyl
PCB 52	2,5,2′,5′-tetrachlorobiphenyl
PCB 101	2,4,5,2′,5′-pentachlorobiphenyl
PCB 138	2,2′,3,4,4′,5′-hexachlorobiphenyl
PCB 153	2,2′,4,4′,5,5′-hexachlorobiphenyl
PCB 180	2,2′,3,4,4′,5,5′-heptachlorobiphenyl
ww	wet weight

Funding sources

The study was funded by the German Federal Institute for Risk Assessment (grant BfR-SiN-08-1322-760).

Data availability

Data will be made available on request.

Declaration of competing interest

The authors declare that they have no known competing financial interests or personal relationships that could have appeared to influence the work reported in this paper.

Acknowledgment

We would like to thank Andreas Susenbeth for helpful discussions on the growth of fattening pigs.

Appendix A. Supplementary data

Supplementary data to this article can be found online at https://doi.org/10.1016/j.scitotenv.2023.164539.

References

Adolphs, J., Kleinjung, F., Numata, J., Mielke, H., Abraham, K., Schafft, H., et al., 2013. A probabilistic model for the carry-over of PCDD/fs from feed to growing pigs. Chemosphere 93, 474–479.

BMEL. Information zu PCB in Futtermitteln. 2023, 2018.

Commission E, 2006. Commission regulation (EC) no 1881/2006 of 19 December 2006 setting maximum levels for certain contaminants in foodstuffs. Off. J. Eur. Union 364, 5–24.

Commission E, 2011. Commission regulation (EU) no 1259/2011 of 2 December 2011 amending regulation (EC) no 1881/2006 as regards maximum levels for dioxins, dioxin-like PCBs and non dioxin-like PCBs in foodstuffs. Off. J. Eur. Union 320, 18–23.

Delannoy, M., Rychen, G., Fournier, A., Jondreville, C., Feidt, C., 2014. Effects of condensed organic matter on PCBs bioavailability in juvenile swine, an animal model for young children. Chemosphere 104, 105–112.

Drouillard, K., Norstrom, R., 2003. The influence of diet properties and feeding rates on PCB toxicokinetics in the ring dove. Arch. Environ. Contam. Toxicol. 44, 0097–0106.

EFSA, 2005. Opinion of the scientific panel on contaminants in the food chain [CONTAM] related to the presence of non dioxin-like polychlorinated biphenyls (PCB) in feed and food. EFSA J. 3, 284.

EFSA, 2012. Update of the monitoring of levels of dioxins and PCBs in food and feed. EFSA J. 10, 2832.

Eppe, G., Schaechtele, A., Haedrich, J., Fernandes, A., 2017. Guidance Document on Measurement Uncertainty for Laboratories Performing PCDD/F and PCB Analysis Using Isotope Dilution Mass Spectrometry.

EU, 2013. Commission Regulation (EU) No. 1067/2013 of 30 October 2013 amending Regulation (EC) No. 1881/2006 as regards maximum levels of the contaminants dioxins, dioxin-like PCBs and non-dioxin-like PCBs in liver of terrestrial animals. Off. J. Eur. Union L 289/56-L 289/57.

GfE, 2006. Empfehlungen zur Energie-und Nährstoffversorgung von Schweinen. DLG Germany.

Hoogenboom, R.L., Ten Dam, G., van Leeuwen, S.P., van Egmond, H., Nicolina, J., Dwarkasing, A.J., 2021. High levels of dioxins and PCBs in meat, fat and livers of free ranging pigs, goats, sheep and cows from the island of Curaçao. Chemosphere 263, 128057.

Jondreville, C., Cariou, R., Méda, B., Dominguez-Romero, E., Omer, E., Dervilly-Pinel, G., et al., 2017. Accumulation of α-hexabromocyclododecane (α-HBCDD) in tissues of fast- and slow-growing broilers (Gallus domesticus). Chemosphere 178, 424–431.

Kasper, C., Schlegel, P., Ruiz-Ascacibar, I., Stoll, P., Bee, G., 2021. Accuracy of predicting chemical body composition of growing pigs using dual-energy X-ray absorptiometry. Animal 15, 100307.

Knap, P., Rauw, W., 2008. Selection for High Production in Pigs. Resource Allocation Theory Applied to Farm Animal Production. CABI Wallingford UK, pp. 210–229.

Kouba, M., Bonneau, M., Noblet, J., 1999. Relative development of subcutaneous, intermuscular, and kidney fat in growing pigs with different body compositions. J. Anim. Sci. 77, 622–629.

Krishnan, K., Peyret, T., 2009. Physiologically based toxicokinetic (PBTK) modeling in ecotoxicology. Ecotoxicol. Model. 145–175.

Lautz, L., Hoeks, S., Oldenkamp, R., Hendriks, A., Dorne, J., Ragas, A., 2020. Generic physiologically based kinetic modelling for farm animals: part II. Predicting tissue concentrations of chemicals in swine, cattle, and sheep. Toxicol. Lett. 318, 50–56.

Moenning, J.L., Krause, T., Lamp, J., Maul, R., Schenkel, H., Fürst, P., et al., 2022. Transfer of polychlorinated dibenzo-p-dioxins and dibenzofurans (PCDD/fs) and polychlorinated biphenyls (PCBs) from oral exposure into cow's milk - part II: toxicokinetic predictive models for risk assessment. Nutr. Res. Rev. 1–14.

Moenning, J.-L., Numata, J., Bloch, D., Jahnke, A., Schafft, H.A., Spolders, M., et al., 2023. Transfer and toxicokinetic modeling of non-dioxin-like polychlorinated biphenyls (ndl-PCBs) into accidentally exposed dairy cattle and their calves-a case report. Environ. Toxicol. Pharmacol. 99, 104106.

Newville M., Otten R., Nelson A., Ingargiola A., Stensitzki T., Allan D. et al. 2021. lmfit/lmfit-py 1.0.2 (1.0.2). Zenodo. https://doi.org/10.5281/zenodo.4516651.

Ohlhoff, B., Savvateeva, D., Bernsmann, T., Spolders, M., Jahnke, A., Lüth, A., et al., 2021. Unraveling congener-specific transfer of non-dioxin-like polychlorinated biphenyls (ndl-PCBs) from feed into chicken meat. Environ. Sci. Technol. 55, 11080–11090.

Ohlhoff, B., Savvateeva, D., Leisner, J., Hartmann, F., Südekum, K.-H., Bernsmann, T., et al., 2022. Transfer of non-dioxin-like polychlorinated biphenyls (ndl-PCBs) from feed and soil into hen eggs. J. Agric. Food Chem. 70, 8955–8962.

Pfeiffer H, Lengerken Gv, Gebhardt Gn, Bergmann M, Liebert F, Pahle T. Wachstum und Schlachtkörperqualität bei landwirtschaftlichen Nutztieren–Schweine. 1984.

Robertson LW, Ludewig G. Polychlorinated Biphenyl (PCB) carcinogenicity with special emphasis on airborne PCBs. Gefahrstoffe, Reinhaltung der Luft= Air quality control/ Herausgeber, BIA und KRdL im VDI und DIN 2011; 71: 25.

Savvateeva, D., Numata, J., Pieper, R., Schafft, H., Lahrssen-Wiederholt, M., Bulik, S., 2020. Physiologically based toxicokinetic models and in silico predicted partition coefficients to estimate tetrachlorodibenzo-p-dioxin transfer from feed into growing pigs. Arch. Toxicol. 94, 187–196.

Savvateeva, D., Ohlhoff, B., Hoogenboom, R.L., Pieper, R., Numata, J., 2022. Toxicokinetic modeling of the transfer of non-dioxin-like polychlorinated biphenyls (ndl-PCBs) from feed and soil into laying hens and their eggs. J. Agric. Food Chem. 70, 13754–13764.

Taverne F, Meijer B, Heederik D, Mouton J, Kramer N. Physiologically-based pharmacokinetic modelling. Exposure of food-producing animals to antimicrobials: 144.

Tremolada, P., Guazzoni, N., Parolini, M., Rossaro, B., Bignazzi, M.M., Binelli, A., 2014. Predicting PCB concentrations in cow milk: validation of a fugacity model in high-mountain pasture conditions. Sci. Total Environ. 487, 471–480.

Union E, 2012. Commission regulation (EU) no 277/2012 of 28 march 2012 amending annexes I and II to directive 2002/32/EC of the European Parliament and of the council as regards maximum levels and action thresholds for dioxins and polychlorinated biphenyls. Off J Eur Communities L 91, 1–7.

Viluksela, M., van der Ven, L., Schrenk, D., Lilienthal, H., Andersson, P.L., Halldin, K., et al., 2012. Biological and toxicological effects of non-dioxin-like PCBs. Acta Vet. Scand. 54, 1–2 BioMed Central.

5.3 Modelling of quinolizidine alkaloids (QAs) in dairy cows

5.3.1 Paper 5

Engel, A.M., et al., Investigations on the transfer of quinolizidine alkaloids from Lupinus angustifolius into the milk of dairy cows. Journal of Agricultural and Food Chemistry, 2022. **70**(37): p. 11749-11758.

JOURNAL OF AGRICULTURAL AND FOOD CHEMISTRY

pubs.acs.org/JAFC Article

Investigations on the Transfer of Quinolizidine Alkaloids from *Lupinus angustifolius* into the Milk of Dairy Cows

Anna Maria Engel, Fenja Klevenhusen, Jan-Louis Moenning, Jorge Numata, Carola Fischer-Tenhagen, Benjamin Sachse, Bernd Schäfer, Hildburg Fry, Oliver Kappenstein, and Robert Pieper*

Cite This: *J. Agric. Food Chem.* 2022, 70, 11749−11758 Read Online

ACCESS | Metrics & More | Article Recommendations | Supporting Information

ABSTRACT: Lupin varieties with a low content of quinolizidine alkaloids (QAs) like blue sweet lupin (BSL) have long been used as a protein source for dairy cows. A health concern for humans may arise from the transfer of acute toxic QAs from feed into cow's milk. This study is the first to quantify the transfer of QAs from BSL into cow's milk with experimental and modeling methods. Four lactating dairy cows were subjected to two 7 day feeding periods with 1 and 2 kg/d BSL, respectively, each followed by a depuration period. BSL contained 1774 mg/kg dry matter total QAs. Individual milk samples were taken twice daily and QA contents in feed and milk determined with liquid chromatography−tandem mass spectrometry. Transfer of QAs into the milk was already seen with the administration of 1 kg/d BSL, with differences in transfer rates (TRs) between individual QAs. A toxicokinetic model was derived to quantify and predict QA feed-to-food transfer. For the four most prominent QAs, our model shows an α-half-life of around 0.27 d. TRs were obtained for six QAs and were between 0.13 (sparteine) and 3.74% (multiflorine). A toxicological assessment of milk containing QAs as measured in this study indicated a potential health concern.

KEYWORDS: *carry-over, secondary plant metabolites, plant alkaloids, cattle, lupins*

INTRODUCTION

Lupins have a long tradition as a protein source in animal nutrition because of their high crude protein (CP) content (up to 40% in dry matter, DM), and they are further gaining importance in Europe, especially in organic animal husbandry. While several secondary plant metabolites in lupins have been shown to have beneficial effects (e.g., antidiabetic or antioxidant activity),[1] some alkaloids are known to have detrimental effects on human and animal health. The latter is the case for quinolizidine alkaloids (QAs), which constitute the main secondary plant metabolites occurring in lupins, offering protection against insects and herbivores.[2] To date, more than 300 lupine species are known, with varying QA contents. Depending on their alkaloid content, lupins are commonly classified into bitter lupins (with a total QA content of up to 8% in DM) and sweet lupins with a low alkaloid content.[3] This low alkaloid content should not exceed 0.05% in DM (500 mg/kg DM) in agricultural practice, while levels <0.02% in DM (<200 mg/kg DM) are recommended by health authorities for lupin seeds used for food production.[4−7]

The synthesis of QAs occurs mainly in the leaves, but they are distributed via the phloem into other parts of the plant including the seeds, causing a bitter taste as a protection against herbivores.[8] More than 170 QAs have been identified among lupin species, with lupanine, 13α-hydroxylupanine, and sparteine being the most abundant ones.[9] Depending on their chemical structure, QAs can be chemically divided into, for example, sparteine and its derivatives, lupanine and its derivatives, angustifoline and its derivatives, multiflorine and its derivatives, lupinine, and anagyrine(Figure 1).

The QAs exert their toxicity by inhibiting acetylcholine receptors and voltage-dependent ion channels in the central nervous system, on motor endplates and the peripheral autonomic nervous system, where the individual QAs appear to have different levels of toxicity.[10] Common acute toxic exposure symptoms in humans and mammals include respiratory depression, vomiting, and tachycardia.[10,11] Some QAs, such as anagyrine, also show teratogenic properties and have been associated with congenital skeletal malformations (crooked calf disease) in calves.[12] Thus, to minimize the risk of QA intoxication in livestock animals, only sweet lupins are listed as feed for livestock species in the catalogue of feed materials.[13]

However, mutations, cross-breeding, or recombination can result in descendants with higher QA contents despite their original classification as sweet lupins.[14,15]

Most of the toxicological data originate from research on lupanine and sparteine, the latter compound was used as a pharmaceutical in the past.[10] The European Food Safety Authority (EFSA) stated that "anticholinergic effects and changes in cardiac electric conductivity" are the relevant endpoints for risk assessment. A dose of 0.16 mg sparteine/kg bodyweight (bw) was identified as the 'lowest single oral effective dose' in humans for such acute effects, while no

Received: April 12, 2022
Revised: August 2, 2022
Accepted: August 16, 2022
Published: September 6, 2022

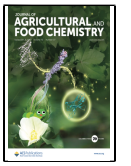

https://doi.org/10.1021/acs.jafc.2c02517
J. Agric. Food Chem. 2022, 70, 11749−11758

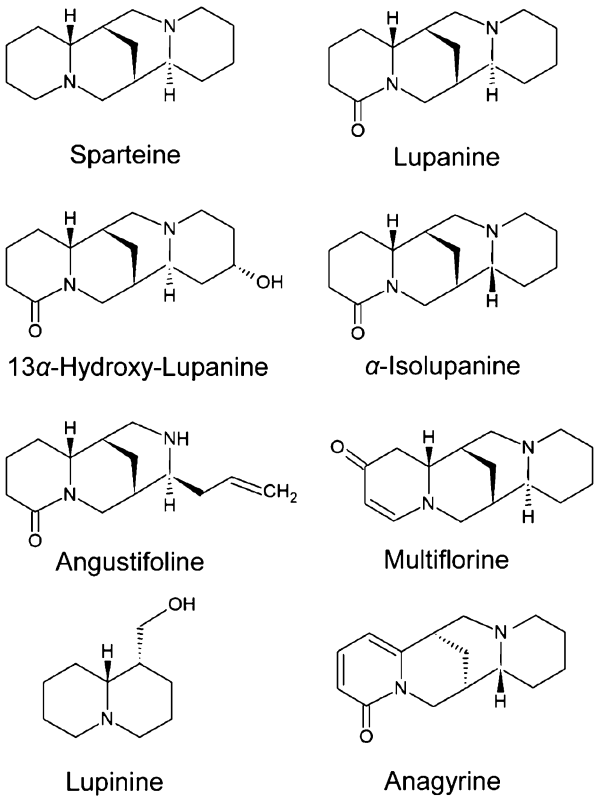

Figure 1. Chemical structures of selected QAs.

reference point could be identified for risks potentially resulting from chronic exposure. Due to similar modes of action of QAs, the EFSA assumed dose additivity for all derivatives. Furthermore, due to the limited overall data basis and the associated uncertainties, no health-based guidance value could be derived. Therefore, the EFSA applied the margin of exposure (MoE) approach for a preliminary risk characterization using the dose of 0.16 mg sparteine/kg bw as an appropriate reference point. The authority concluded that an MoE >1 would not indicate a health concern. However, the assessment revealed the possibility of exposures for some consumer groups, resulting in MoE values <1, indicating a potential risk for these consumers. Additionally, the EFSA stated that there is indirect evidence of a possible transfer of QAs from feed into milk, due to the QAs' weak basic nature, which makes milk a possible additional exposure source.[10] However, until now, there has only been one published case report of possible QA intoxication in a human infant after its mother drank goat milk in early pregnancy.[16] Lambs from the same goats showed skeletal deformations as described for crooked calf disease, indicating QA intoxication.[17] In the present study, we tested the hypothesis that QAs from lupin in the diet of dairy cows are transferred into cow's milk. We determined the profiles of six QAs in milk and quantified the TRs of the four most prominent QAs from lupin seeds into the milk of four lactating dairy cows fed with increasing amounts of QA-containing sweet lupin seeds. We conducted a toxicological assessment in order to evaluate the potential risk resulting from the sole exposure to QAs via milk containing QA levels as measured in the present study.

MATERIALS AND METHODS

Ethics Approval Statement. All experimental procedures involving animals were approved by the local authority (Regional Office for Health and Social Affairs, Berlin—LAGESO, Germany) under registration number StN010/19.

Animals, Housing, and Sampling. Four Holstein-Friesian dairy cows (3 primiparous, 1 multiparous, 58 ± 11 days in milk) with an average milk yield of 30.4 ± 4.12 kg/day were housed in one group in an open barn stable with free access to water. During the experiment, which lasted 46 days in total, cows were milked twice daily at 6.00 a.m. and 4.30 p.m. in a tandem milking parlor (Lemmer Fullwood). Milk samples were taken during each milking and stored at −20 °C until being analyzed for QA contents.

Lupin Seeds and Diets. Lupin seeds (whole grain, untoasted, *Lupinus angustifolius* var. *Boregine* [blue sweet lupine, BSL]) harvested in Brandenburg, Germany, approximately 52°6′ N 12°7′ E, in August 2019 were milled in a common hammer mill (Siemens) to pass a screen of 3 mm, divided into four subsamples of 25 kg each and stored in a container under dry, cool, and dark conditions prior to use. Forages, beet pulp, and minerals were offered as a partial mixed ration (27.7% grass silage, 29.5% maize silage, 6.0% straw, 30.1% hay, 6.0% beet pulp, and 0.61% minerals) *ad libitum* in feeding troughs. A concentrate mixture was provided in separate feeding troughs, transponder-controlled one for each cow, to meet the energy requirements for a milk yield of 25 kg/d energy-corrected milk (Table 1).

Table 1. Composition of Experimental Diets

	experimental diets[a]		
	BSL-free	BSL-1	BSL-2
ingredients (g/kg DM)			
concentrate mixture	569.6	569.6	569.6
rapeseed meal	430.4	289.6	140.8
BSL	0	140.8	289.6
chemical composition (g/kg DM)			
CP	288	275	262
crude ash	69.6	63.7	57.4
NDF[b]	274	271	267

[a]Blue sweet lupin seeds (BSL), BSL-free, blue sweet lupin-free feeding; BSL-1, blue sweet lupin seeds 1 kg; BSL-2, blue sweet lupin seeds 2 kg. [b]Neutral Detergent Fiber (NDF).

The feeding trial, carried out in July to September 2020, started with a 7-day adaptation period without lupin seed meal [BSL-free (AP)]. Afterward, 1 kg of rapeseed meal was replaced by 1 kg of BSL for 7 days (BSL-1). Therefore, a corresponding mixture of rapeseed meal, BSL, and dairy concentrate was prepared and offered in two equal portions daily at 7 a.m. after the morning milking and 2 p.m. before the evening milking to ensure total uptake. The period was followed by a 10-day depuration period [BSL-free (DP1)], without BSL in the diet. Afterward, 2 kg of rapeseed meal was replaced by 2 kg of BSL (BSL-2). Therefore, again a corresponding mixture of rapeseed meal and BSL was prepared and fed twice daily for 7 days, which was followed again by a 10-day depuration period [BSL-free (DP2)].

Analysis of Feed Ingredients. Feed components were analyzed for DM, crude ash, CP, and neutral detergent fiber (NDF) according to VDLUFA (Association of German Agricultural Analytic and Research Institutes) standard methods.[18−20]

Analysis of Milk Ingredients. Milk yield was recorded daily. Milk samples were taken twice daily during each milking and stored at −20 °C for analysis of QAs. In regular intervals, milk samples were taken for proximate analysis of milk protein, fat, and lactose according to § 64 L01.00-78 of the German Food and Feed Code (LFGB), and milk urea according to directive 1.13 of the German Association for Performance and Quality Testing e.V. (DLQ).[21,22]

https://doi.org/10.1021/acs.jafc.2c02517
J. Agric. Food Chem. 2022, 70, 11749−11758

Solvents and Chemicals. All organic solvents used in this work were of at least analytical grade. Solvents used for liquid chromatography−tandem mass spectrometry (LC−MS/MS) analysis were of LC−MS grade.

Analytical Standards. For identification and quantification, the following analytical standards were used: (+)-13α-hydroxylupanine (purity 97%, TRC), (+)-lupanine perchlorate (purity 97%, TRC), (+)-α-iso-lupanine perchlorate (purity 97%, TRC), (−)-angustifoline (purity 97%, CfmOT), (−)-lupinine (purity 96%, Sigma-Aldrich), multiflorine (purity 99%, CfmOT), and (−)-sparteine-sulfate·5 H_2O (purity, 98%; Targetmol), respectively.

QAs in BSL and Milk. For determination of the QAs in ground BSL, representative samples of about 100 g each were collected (samples from four storage containers of 25 kg). Subsequently, the samples were ground with an Ultra Centrifugal Mill passing a sieve of 1 mm. QA analyses were performed at the National Reference Laboratory (NRL) for Feed Additives at the German Federal Institute for Risk Assessment (BfR). Samples were analyzed for nine QAs (anagyrine, cytisine, angustifoline, 13α-hydroxylupanine, isolupanine, lupanine, lupinine, multiflorine, and sparteine), which were also used to calculate the sum of the QAs. Analysis and quantification of all samples was done using high-performance liquid-chromatography−tandem mass spectrometry with electrospray ionization in positive ion mode (LC-ESI-MS/MS; API 6500 Sciex). Each measurement was performed in duplicate.

Two in-house validated sample preparation methods were utilized, one for solid (feed) and the other for liquid matrices (milk). Briefly, BSL or milk samples were mixed and the QAs were extracted with an acidified acetonitrile/water solution. For this purpose, 5 g of BSL was extracted with 5 mL of extraction solution (0.1% formic acid, acetonitrile/water, 50:50, v/v) or 2 mL of milk was extracted with 25 mL of extraction solution (0.1% formic acid, acetonitrile/water, 90:10, v/v). After 15 min extraction time in an overhead-shaker, the samples were frozen (−80 °C) to precipitate proteins. After thawing, samples were centrifuged (4000 × g) for 5 min to separate precipitated proteins from the solution.

For milk samples, additionally a degreasing step of the supernatant was included by using n-hexane. The n-hexane layer was discarded.

The sample extracts must be diluted with ultrapure water and injection solution. The dilution factor depends on the concentration of the analytes in the respective sample and must be within the concentration range of the standard curve used. The concentration ranges of the standard curves are between 0.5 mg/kg and 5.5 mg/kg for BSL and between 34 and 370 μg/kg for milk samples. After centrifugation (4000 × g for 5 min), the final supernatant was decanted into a 2 mL crimp vial for injection into the LC-ESI-/MS−MS. Measurement results were evaluated with the software Analyst 1.6.

For identification (examples of chromatograms are given in Figures S1−S5 in the Supporting Information pages S1−S4), a retention time window of ±0.1 min around the expected retention time of the corresponding QA was set. Furthermore, the QAs were identified by using two multiple reaction monitoring (MRM) transitions (at least 1 precursor and 2 product ions detected) and calculating the relative ion ratio between both MRM transitions according to regulation (EU) 2021/808.[23] Quantification was performed by preparing a matrix-matched external calibration curve using the analytical standards mentioned before. Briefly, the obtained validation parameters of both methods (milk and BSL) are summarized here for the assessment of the transfer study.

For the analysis of QA in BSL, the recovery was determined by analyzing soybean meal fortified at two different QA concentrations 5 mg/kg and 50 mg/kg (n = 6), respectively. The recoveries for all determined QAs ranged between 80 and 110%. The coefficient of variation (CV) as measure for the repeatability of the applied methods was below 10%. The inter-laboratory reproducibility determined by analyzing samples on different days, by different operators, and with different LC−MS/MS instruments was below 10%.

For the BSL, the limit of detection (LOD) ranged between 0.01 mg/kg (lupanine) and 0.36 mg/kg (multiflorine), and the limit of quantitation (LOQ) ranged between 0.03 mg/kg (lupanine) and 1.19 mg/kg (multiflorine).

For the analysis of milk, the recovery was determined by analyzing milk samples fortified at two different QA concentrations 6 and 60 μg/kg (n = 6), respectively. The mean recovery for the determined QAs ranged between 85 and 105%. The CV as measure for the repeatability is below 10%. The inter-laboratory reproducibility determined by analyzing samples on different days, by different operators, and with different LC−MS/MS instruments was below 8%. For milk, the LOD ranged between 0.02 μg/kg (13α-hydroxylupanine) and 0.41 μg/kg (multiflorine), and the LOQ ranged between 0.06 μg/kg (13α-hydroxylupanine) and 1.36 μg/kg (multiflorine).

Statistical Analysis. Statistical analyses were carried out using the MIXED procedure of SAS (version 9.4, 2016, SAS Institute Inc., Cary, NC, USA). Days and periods were included as fixed effects in the model for milk yield, fat, protein, urea, and lactose concentration. Measurements taken on the same cow but at different times were considered as repeated measures. Multiple comparisons among periods were evaluated by Tukey's post hoc test. A p-value of <0.05 was considered as indicative for significant difference between periods.

Toxicokinetic Modeling of QA Transfer into the Milk. To derive transfer parameters relevant for risk assessment and to allow the prediction of the transfer of QAs from feed into cow's milk, a mathematical model was developed based on the data, specifically a 3-compartment physiologically based toxicokinetic (PBTK) model (Figure 2 and eqs 1 and 2). The model was fitted for the four most prevalent QAs, for which enough data were available: lupanine, 13α-hydroxylupanine, isolupanine, and angustifoline.

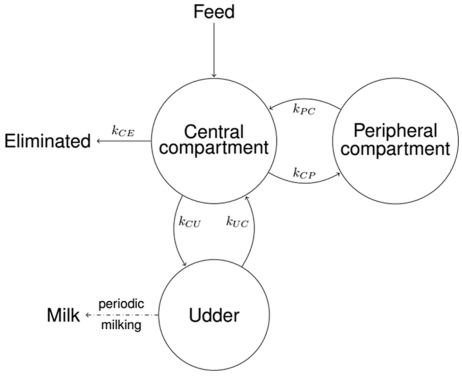

Figure 2. Schema of the 3-compartment model of QA toxicokinetics in dairy cows. The central compartment represents the entry point for QAs into the cow and the output site for elimination (grouping unabsorbed as well as putatively metabolized and/or excreted QAs). The peripheral compartment acts as a small storage. The udder compartment is where the milk is produced, stored, and periodically emptied at milking events (together with the QAs contained). The parameter k_{ij} represents the transition rate from compartment i to compartment j for the compartments: i,j = C, Central; P, Peripheral; U, Udder; and E, Elimination.

The PBTK model in Figure 2 was compared to other similar models (with different arrangements of compartments) using the Bayesian information criterion (BIC), where the chosen model performed best (data not shown). The chosen model consists of 3 compartments. The first one is the central compartment, the entry point for QAs with feed into the cow, as well as the place where QAs are eliminated. These elimination groups together unabsorbed as well as putatively metabolized and/or excreted QAs. The central compartment represents both blood plasma and a biological component (e.g., groups of cells, proteins, or lipids) that is in rapid equilibrium with plasma regarding QAs. The second compartment is the peripheral compartment, which acts as a small storage for QAs; it is a biological component that more slowly exchanges QAs with the central compartment. The third and last is the udder compartment,

https://doi.org/10.1021/acs.jafc.2c02517
J. Agric. Food Chem. 2022, 70, 11749−11758

Table 2. Milk Yield and Milk Composition of the Cows[a]

	experimental periods[b]						
	BSL-free (AP1)	BSL-1	BSL-free (DP1)	BSL-2	BSL-free (DP2)	SEM	*p*-value period
milk yield (kg)	31.6[c]	31.4[c,d]	30.3[c,d,e]	29.9[d,e]	29.1[e]	1.04	0.002
fat (%)	3.85[c,d]	4.13[c]	3.91[c,d]	3.50[d]	3.77[c,d]	0.23	0.039
protein (%)	3.01	2.90	2.85	2.86	2.96	0.07	0.144
lactose (%)	4.83	4.84	4.84	4.81	4.66	0.08	0.136
urea (mg/L)	668	626	632	675	520	62.1	0.128

[a]SEM, standard error of the mean. [b]BSL-free (AP1), Adaptation period, blue sweet lupin-free feeding; BSL-1, experimental period 1, blue sweet lupin seeds 1 kg; BSL-free (DP1), depuration period 1, blue sweet lupin-free feeding; BSL-2, experimental period 2, blue sweet lupin seeds 2 kg; BSL-free (DP2), depuration period 2, blue sweet lupin-free feeding. [c]Means in the same row with different letters differ significantly. [d]Means in the same row with different letters differ significantly. [e]Means in the same row with different letters differ significantly.

which can also exchange QAs with the central compartment, while producing and storing milk and, critically, excreting QAs with that milk at periodic milking events. Since only milk data were available, the exact biological nature of all the components of each compartment could not be established, which does not undermine the predictive ability of the model. The PBTK model (Figure 2) is described by the following differential equations between milking events

$$\dot{A}(t) = \mathbf{M}A(t) + I(t) \tag{1}$$

where $A(t)=(A_C(t), A_U(t), A_P(t))^T$ is the amount vector containing the amount of the respective compartment at time t; $I(t)$ is the input vector at time t; and $\mathbf{M}$ is the transition matrix given by

$$\mathbf{M} = \begin{pmatrix} -(k_{CP} + k_{CU} + k_{CE}) & k_{UC} & k_{PC} \\ k_{CU} & -k_{UC} & 0 \\ k_{CP} & 0 & -k_{PC} \end{pmatrix} \tag{2}$$

here the model parameter k_{ij} represents the transition rate from compartment i to compartment j for the following compartments: i,j = C, Central; i,j = P, Peripheral; i,j = U Udder; and i,j = E, Eliminated (conceptually lumping any metabolization and excretion). Here, the complete emptying of the udder compartment occurs twice daily during the periodic morning and evening milking events.

A peripheral compartment was included based on the shape of the data from the depuration period (Figure S6, Days 14−17 and 31−34), where a biphasic behavior (two half-lives) was apparent. A very dominant short α-half-life, reflecting elimination of QAs from the central compartment, and a second less prevalent longer β-half-life, reflecting elimination of QAs from the peripheral compartment, were identified. The model mechanics assume complete and uniform absorption of QAs into the central compartment distributed uniformly across 5 h after feeding; this does not imply that the effective physiological absorption is 100%; the effective absorption from feed and bioavailability for milk excretion is included via the interplay of rate constant k_{ij}. The last piece of the model is the implementation of the periodic emptying of the udder at each milking time, which is performed algorithmically as detailed in the Supporting Information Section Complete Toxicokinetic Model.

An optimization approach was used to obtain model parameter k_{ij} by minimizing the log squared error for the best fit.[24] In addition, the tails of the depuration (10 days after start of feeding for each feeding period) was weighted with only 25% in order not to overvalue the more irrelevant β-phase of elimination. Data below LOQ or LOD were also considered for the fit by interpreting them as an interval in which the true values lie, so that the error function does not penalize values within that interval. A permutation test was applied to check the hypothesis of a dose-dependent transfer into the milk.[25] Confidence intervals were derived using the delete-two jackknife method.[26] In addition, the optimized model for each QA was used to estimate transfer parameters: the α- and β-half-lives of the respective elimination phases as well as the steady-state TR from feed to milk, defined as

$$\mathrm{TR} = \frac{\text{amount in milk[ng/d]}}{\text{amount in feed[ng/d]}} 100\% \tag{3}$$

Lastly, the relative transition amount (RTA) was determined for each QA. RTA is helpful to understand at what point there is a transition from the α- to the β-elimination phase. Specifically, RTA tells us at what amount in milk (as a percentage of steady state or maximum) the slope of the depuration is better approximated by the β-half-life rather than the α-half-life. A more detailed description of the derivation of transfer parameters can be found in the Supporting Information Sections 2.1−2.3.

Assessment of Consumer Exposure to QAs Using the EFSA RACE Tool. The EFSA Rapid Assessment of Contaminant Exposure (RACE) software tool was used to estimate the exposure to QAs resulting from milk consumption, considering the determined QA levels.[27] With the help of food consumption information from the EFSA Comprehensive European Food Consumption Database, RACE provides an estimate of acute and chronic exposure from single foods. These values can then be compared with relevant toxicological reference points. For the assessment, maximum QA levels in milk during the exposure phases were used. As in the EFSA opinion on QAs, risk characterization was performed by applying the MoE approach using the dose of 0.16 mg sparteine/kg bw as reference point.

RESULTS AND DISCUSSION

Feed Intake and Milk Yield. Throughout the experiment, the whole concentrate proportion was ingested, indicating no obvious adverse effect of BSL on concentrate intake. The forage mixture was provided *ad libitum*, and individual intake was not recorded. Milk yield slightly declined over the course of the experiment from 31.6 ± 4.7 kg/d to 29.1 ± 4.5 kg/d ($p < 0.001$) (Table 2).

The period had a significant effect on the fat content in milk ($p = 0.039$), with highest contents found in BSL-1 with 4.13% and lowest contents in BSL-2 with 3.5%. Contents of protein, lactose, and urea in milk did not differ between periods ($p > 0.05$). The lactation stage of the individual cows and external influences, such as the outside temperature, which exceeded 25 °C throughout the present experiment, can have an impact on the performance parameters like milk production.[28] Additionally, other authors previously reported decreases in milk yield due to the feeding of lupin seeds in comparison to feeding rapeseed meal- or soybean meal-based concentrates, which might be related to the lower CP content in lupin seeds (Table 1).[29−31] In addition to a generally lower CP content in lupin seeds, the CP of unprocessed lupin seeds is known to be extensively degraded in the rumen, causing a reduction in amino acid flux to the duodenum.[30,32] Joch suggested that decreases in milk yield may be due to the lower methionine content of lupin protein, although the addition of ruminally

https://doi.org/10.1021/acs.jafc.2c02517
J. Agric. Food Chem. 2022, 70, 11749−11758

protected methionine did not increase the milk yield in that study.[31]

Milk fat represents the most variable component in milk and can be influenced by nutritional as well as physiological aspects.[33] Froidmont showed increased levels of milk fat after protein replacement of soybean meal with lupin and attributed increased milk fat to the higher fiber content in lupin seeds, with a concomitant increase in acetate liberation in the rumen as a precursor for milk fat.[34] This was not observed in the present study and may depend on other dietary effects and lactation stage of the cows. A reduced milk fat content due to the feeding of lupin seeds has also been observed by others.[35,36]

QAs in BSL and Transfer into the Milk. The sum of determined QAs in the present BSL ranged between 0.17 and 0.19% in DM and was higher than the commonly reported <0.05% for "sweet" lupins.[4] Higher levels of QAs in *L. angustifolius* have been reported before and are most likely due to abiotic influences, cross mutation, and backcrossing with wild varieties. Higher outdoor temperatures or lower soil pH values during the growing season can also lead to higher levels of QAs in sweet lupins.[37,38]

The literature reports the main alkaloids for *L. angustifolius*: lupanine, 13α-hydroxylupanine, isolupanine, angustifoline, 13-angeloyloxylupanine, and 13-tigloyloxylupanine.[39,40] We found a slightly different set in the present study, where levels of 13α-hydroxylupanine, lupanine, angustifoline, and isolupanine in BSL were higher than levels of multiflorine and sparteine, resulting in high intakes of 13α-hydroxylupanine and lupanine (Table 3). The intake of total QAs was 1774 mg/d during the BSL-1 feeding period and 3549 mg/d during the BSL-2 feeding period (Table 3).

Table 3. Intake of QAs with BSL in mg/d

	experimental diets[b]	
QA intake with BSL (mg/d)	BSL-1 kg	BSL-2 kg
total[a]	1774	3549
angustifoline	223	446
13α-hydroxylupanine	702	1404
isolupanine	129	257
lupanine	715	1430
multiflorine	2.45	4.89
sparteine	3.03	6.06

[a]QAs as analyzed in BSL. [b]Blue sweet lupine (BSL), BSL-1, blue sweet lupin seeds 1 kg/d; BSL-2, blue sweet lupin seeds 2 kg/d.

Toxicity of QAs has been more thoroughly studied for sparteine and lupanine in humans and rats, while effects of other QAs have not yet been systematically investigated.[10,12,41,42] In rat studies, a lower toxicity was observed for lupanine and 13α-hydroxylupanine than for sparteine.[42,43] Until now, there are only few studies evaluating the toxicity of QAs in cattle. For instance, cattle showed reduced voluntary feed intake when intact lupin seeds were fed in contrast to lupin seeds that were previously detoxified by boiling and soaking in water.[44] However, QA intake with *Lupinus albus* used in that study was considerably higher than that in the present one, reaching estimated levels of 60 g/d of lupanine and 21 g/d 13α-hydroxylupanine with *L. albus*. Increased levels of QAs therefore appear to result in decreased appetite, confirming observations made by others.[30,45] No negative effects on animal health were seen in the present study with intakes of 1.27−2.54 mg lupanine/kg bw and 1.24−2.49 mg 13α-hydroxylupanine/kg bw. However, other studies with cattle observed symptoms like reduced general condition, frothing at the mouth, and protrusion of the nictating membrane with higher total QA intake levels of 57.6 g QAs/kg bw.[46] Severe toxic effects of QA in cattle have been described only for the teratogenic QA anagyrine.[47−49] During critical times of gestation, the ingestion of several lupin species by pregnant cattle has been associated with the so-called crooked calf syndrome.[12,50,51] Anagyrine has been identified as a main causative QA, but anagyrine was not detected in BSL used in the present study.[50,51] So far, possible intoxication of calves by anagyrine or other QA in milk has not been reported, but according to the present results, this has to be taken into consideration.

There are currently no maximum levels of QAs for animal or human nutrition in the EU. Nevertheless, gathering knowledge concerning the transfer of QAs from feed to animal food is vital. Although animals showed no adverse health effects in the present study, it was demonstrated that with the administration of only 1 kg sweet lupin seeds, a transfer of QAs into the milk occurs, resulting in a total QA concentration of 2.81 mg/kg milk. Although the quantities of QAs excreted via milk differed slightly between the cows, the QA excretion pattern was similar (Figure 3).

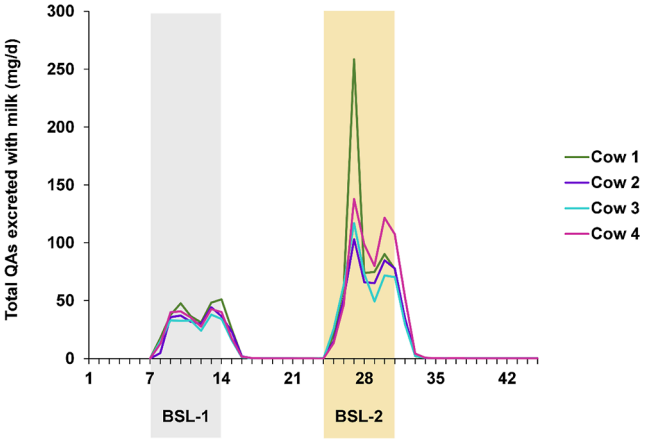

Figure 3. Total QAs excreted with milk daily. Shaded are the feeding periods BSL−1 (blue sweet lupin seeds 1 kg/d) and BSL−2 (blue sweet lupin seeds 2 kg). Unshaded are periods with no QA feeding: the adaptation periods before BSL-1 as well as the depuration periods following BSL-1 and BSL-2.

The concentrations of individual QAs quantified in morning and evening milk during steady state are shown in Figure 4.

As in BSL, 13α-hydroxylupanine and lupanine were found to be the most abundant QA in milk. Despite of average contents in BSL of 3.03 mg/kg, concentrations in milk of sparteine were near or below the LOQ of <0.10 μg/kg milk.

Concentrations of multiflorine, angustifoline, and especially lupanine were noticeably higher in the evening milk than in the morning milk (Figure 4). This effect was also reflected in the higher TRs of multiflorine, angustifoline, and lupanine for evening milk (Table 4). In the evening, cows were fed with lupin seeds 2 h before milking, while in the morning, cows were milked before feeding. It follows that QAs both from morning feeding and in part from evening feeding were excreted in the evening milk, while in the morning milk, only

https://doi.org/10.1021/acs.jafc.2c02517
J. Agric. Food Chem. 2022, 70, 11749−11758

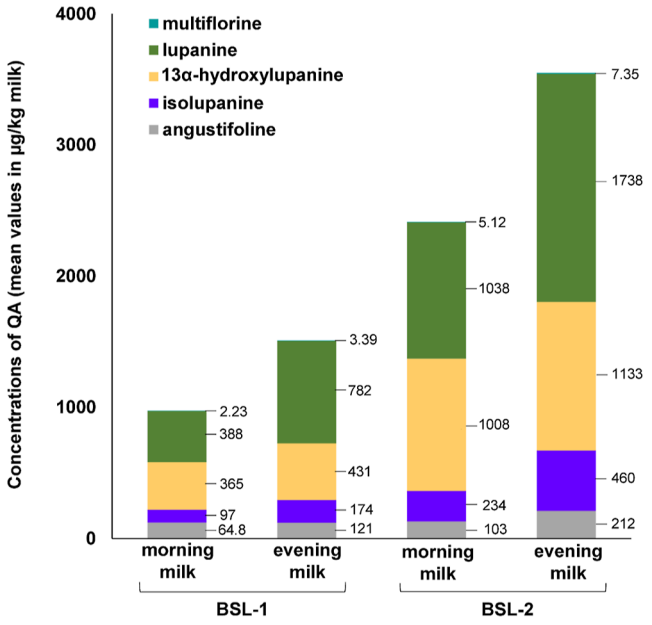

Figure 4. QA contents in morning and evening milk during BSL-1 and BSL-2 feeding (mean values in steady state in μg/kg). Feeding periods, BSL−1 (blue sweet lupin seeds 1 kg/d) and BSL−2 (blue sweet lupin seeds 2 kg/d).

Table 4. Estimated TRs of QAs from Feed into Milk, which is made up out of morning + evening Milk

	mean [%] = (morning + evening)	95% confidence interval [%]
13α-hydroxylupanine	1.74 (0.95 + 0.79)	1.34−2.16
lupanine	2.31 (0.96 + 1.35)	1.85−2.77
isolupanine	2.92 (1.21 + 1.71)	2.57−3.35
angustifoline	1.05 (0.43 + 0.62)	0.93−1.18
multiflorine[a]	3.74 (1.79 + 1.95)	
sparteine[a]	0.13 (0.06 + 0.06)	

[a]Marks the QAs for which no model was developed but nevertheless a rough approximation of the TRs from the data was made.

the remainder was found. Interestingly and in contrast to the other QAs, the TR of 13α-hydroxylupanine was higher in the morning than in the evening milk (Table 4). An explanatory hypothesis is the possible biotransformation of QAs in the cow. So far, metabolism of individual QAs has been investigated only in rats, pigs, rabbits, and humans.[10,52,53] Studies in rats showed that sparteine was oxidized to lupanine, which was found in the urine of orally dosed rats in vivo (suspected microsomal metabolization), while lupanine was found to be presumably transformed to a hydroxyl derivative through a yet unknown pathway.[10,54] Until now, there exists no information regarding the possible metabolization of lupanine into 13α-hydroxylupanine in cows. However, conversion could explain its higher values in the morning milk.

It is known that ruminants can render certain plant toxins harmless via microbial metabolization in the rumen. However, an in vitro rumen fermentation study conducted in our department (data not shown) did not find ruminal degradation of lupanine, which confirms the previous results of Aguiar.[55] Accordingly, metabolization of QAs in the liver might be the cause for the observed differences in QA excretion, but further research is needed in this regard. Other metabolites were not investigated with the current analytical method, therefore, an occurrence of possible metabolites in milk cannot be excluded.

Toxicokinetic Modeling and TRs for QAs. As a first step, the hypothesis of dose-dependent QA transfer into milk[24] was tested. A permutation test was applied to verify whether the experimental data allow rejection of the hypothesis. With the exception of angustifoline, the permutation test provided no indication of a non-linear dose-dependent TR for the QAs studied. The apparent non-linearity for angustifoline was neglected because it can be attributed to the small sample size. Therefore, all QAs were fitted to the 3-compartment PBTK model (eqs 1 and 2, Figure 2) using the data for all cows and all experimental periods (both doses BSL-1 and BSL-2) simultaneously to obtain the optimized model parameters (Table S4). Results of the PBTK model for QA excretion via milk are shown in Figure 5.

In Figure 5, QA excretion from morning and evening milk was lumped together as daily excretion (total bar for model and dots for experiment). During the first BSL feeding period (BSL-1), the concentration profiles of QAs could be adequately predicted. Concerning the second feeding period (BSL-2), the model was only able to reproduce the average behavior, as the measured QA contents in milk displayed higher variability. In particular, the model was unable to reproduce the apparent peak (Figure 5, day 27) in the analyzed QA contents in milk at the beginning of BSL-2 feeding, which might indicate more complex underlying kinetics. Since the PBTK model could nevertheless reproduce the average behavior, it was used to calculate transfer parameters, namely TRs (Table 4) and milk excretion α- and β-half-lives (Tables S1, S2).

All four investigated QAs showed fast and dominant milk excretion α-half-lives of around 0.27 d (Table S1), which are similar to the literature plasma half-lives for lupanine of 0.29 and 0.23 d in cows.[48,49] In contrast, the half-life of lupanine in beef cattle reported in another study was 0.48 d with a mean residence time of 50−61 h, equivalent to half-lives of 1.44 and 1.76 d, respectively, in a 1-compartment setting.[49,56,57] Those values are considerably higher than the derived values of the present study (Table S1), suggesting that there are differences in the kinetic behavior of lupanine between different breeds or production purposes and may be attributable to the lack of excretion with milk.[49]

The shape of the data profile from the depuration period (Figure S6, days 14−17 and 31−34) shows a biphasic behavior (two half-lives). The chosen model (Figure 2) reproduces this behavior; from it, β-half-lives of 2.48−5.18 d for the four QAs were estimated (Table S2). The intake of QAs from sources other than measured feed can be excluded. Additionally, the QA analysis showed values above the LOQ in the depuration periods contrary to the adaptation period. This suggests that small amounts of QAs remained in the peripheral compartment after exposure, resulting in an extended β-half-life during the depuration period. But how relevant are these β-half-lives for risk analysis? The answer comes from the postulated parameter RTA (eq S17, Table S3) that quantifies the relative importance of the α- and β-half-lives. RTA indicates when the system moves from the α-phase to the β-phase of depuration. The RTAs found for QAs (Table S3) range from 0.11 to 0.33% of the steady state amounts, which means that more than 99.67% of the depuration occurs in the α-phase. Therefore, the β-phase of depuration is practically irrelevant, provided it happens at amounts that are toxicologically of no concern.

https://doi.org/10.1021/acs.jafc.2c02517
J. Agric. Food Chem. 2022, 70, 11749−11758

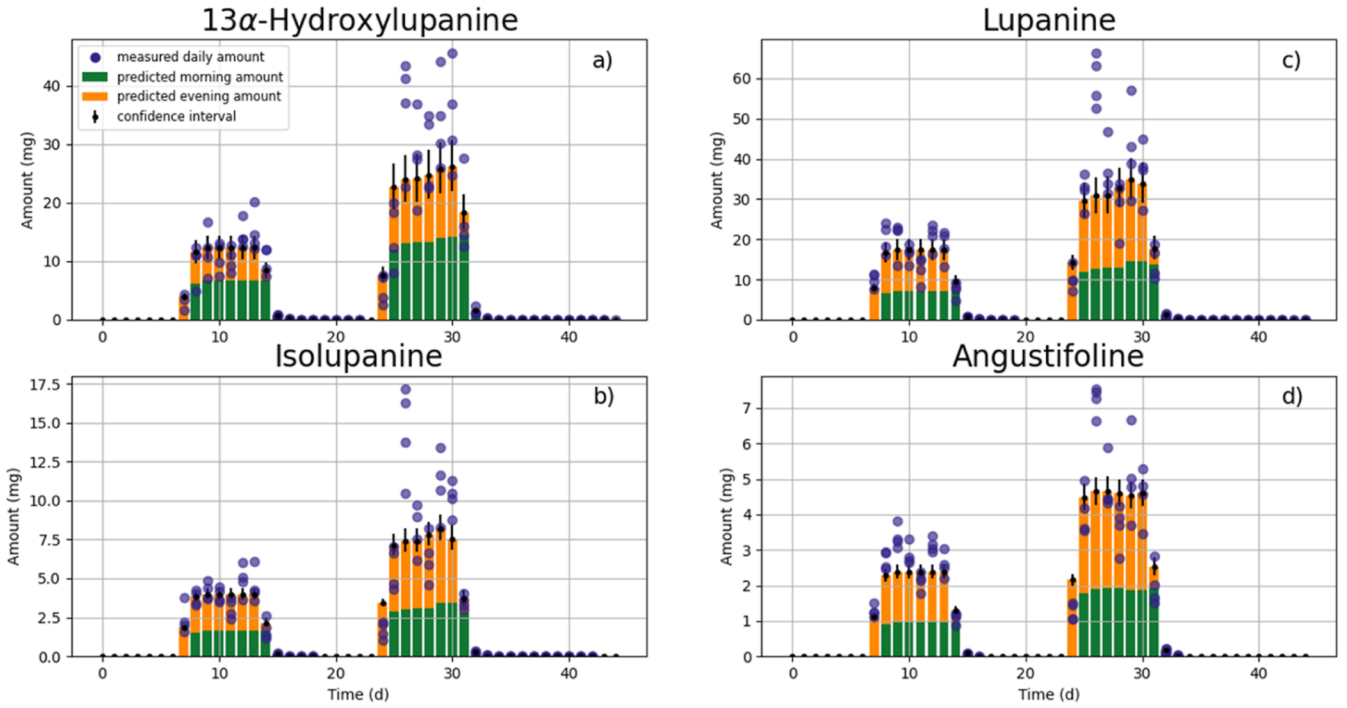

Figure 5. Daily amounts excreted via milk for four QAs. Bars denote the toxicokinetic model results plotted together with their confidence intervals across animals (divided into morning—yellow—and evening excretion—green). Blue dots represent the daily amount excreted obtained from the feeding experiment.

Combined with knowledge of a very short α-half-life (Table S1), we conclude that in most cases, it is possible to rely on a simple multiplicative TR calculation. The TRs into morning + evening milk of individual modeled QAs (Table 4) range from 1.05% for angustifoline to 2.92% for isolupanine. Furthermore, although the data did not allow the development of a PBTK model for sparteine, its TR can be roughly estimated directly from the data by averaging

$$\mathrm{TR} = \frac{\text{Daily excretion}}{\text{Daily feed}} \tag{4}$$

for all days in apparent steady state with measurements above LOQ, resulting in a TR of 0.12%. The same method for multiflorine yields a TR of 3.74%. These results may partly be explained by the fact that, so far, it cannot be ruled out that individual QAs are metabolized to other QAs, resulting in higher TR for individual QA. Although the use of simple multiplicative calculations using TR should suffice for most cases of risk analysis, the full predictive toxicokinetic model code is included as part of the Supporting Information as it can help understanding how these contaminants are transported into the milk.

Assessment of Consumer Exposure to QAs Using the EFSA RACE Tool. A preliminary estimation of the dietary acute exposure by using the EFSA RACE tool showed that the sole consumption of milk containing QAs at a level as measured in the present study might result in intakes above 0.16 mg/kg bw for high milk consumers.[8] This, in turn, means that the corresponding MoE is <1, reflecting an exposure in the effect level and consequently a health concern (Table 5).

Already in BSL-1, MoEs <1 were measured for all population groups. Additionally, in BSL-2, maximum levels in milk also represent an exposure in the effect level for all population groups.

Table 5. Comparison of the Exposure of High (P95) Milk Consumers to the Lowest Single Oral Effective Dose for QA[a]

population group	high consumer (P95)	
	QA content in cow's milk (μg/kg)	
	BSL-1	BSL-2
	max	max
	19607.3	90186.5
	comparison of exposure to toxicological reference point expressed as MoE	
infants	**0.04**	**0.01**
toddlers	**0.11**	**0.02**
other children	**0.18**	**0.04**
adolescents	**0.41**	**0.09**
adults	**0.72**	**0.16**
elderly	**0.93**	**0.20**
very elderly	**0.96**	**0.21**
pregnant woman	**0.77**	**0.17**
lactating woman	**0.92**	**0.20**

[a]The EFSA Rapid Assessment of Contaminant Exposure (RACE) tool was used for calculation of different exposure scenarios. Maximum QA in the milk during BSL-1 and BSL-2 of the feeding experiment and a lowest single oral effective dose of 0.16 mg sparteine/kg bw/d were taken as a basis. Bold numbers: exceedance of MoE 1.

The calculated MoE values refer only to the sole consumption of raw milk containing QA levels as measured in the present study. Therefore, it cannot be excluded that dilution, processing of milk, as well as the production of dairy products may have consequences for the content of QA and, consequently, for the exposure level and the resulting MoE values.

https://doi.org/10.1021/acs.jafc.2c02517
J. Agric. Food Chem. 2022, 70, 11749−11758

However, QA contents and QA profiles differ considerably between lupin breeds and even within the same variety. The different excretion patterns of individual QAs also show that further investigations are necessary to understand the metabolism of QAs within dairy cows. In conclusion, the present study proves the transfer of QAs from BSL into milk of dairy cows already at low inclusion levels of lupin seeds in the ruminant diet.

■ ASSOCIATED CONTENT

Supporting Information

The Supporting Information is available free of charge at https://pubs.acs.org/doi/10.1021/acs.jafc.2c02517.

LC−MS/MS chromatograms; overlay LC−MS/MS chromatogram of the quantifier MRM transitions of nine QAs in a standard solution with a concentration of 2.5 ng/mL each; overlay LC−MS/MS chromatogram of the quantifier MRM transitions of five QAs analyzed in lupin seeds (whole grain, untoasted) used for feeding; overlay LC−MS/MS chromatogram of the quantifier MRM transitions of nine QAs in a matrix matched calibration by utilizing cow milk (dilution 1:20) fortified at a level of 2.5 ng/mL; overlay LC−MS/MS chromatogram of the quantifier MRM transitions of four QAs analyzed in a cow milk sample (dilution 1:20); overlay LC−MS/MS chromatogram of the quantifier MRM transitions of four QAs analyzed in a cow milk sample (dilution 1:200); parameters for risk assessment (TRs, half-lives, and RTA); α-Half-lives; β-half-lives; RTA relative transition amount; complete toxicokinetic model; optimized model parameters; logarithmic plot to show biphasic behavior during depuration and computer code for running the predictive toxicokinetic model including instructions (PDF)

■ AUTHOR INFORMATION

Corresponding Author

Robert Pieper − *German Federal Institute for Risk Assessment, Department Safety in the Food Chain, Berlin 10589, Germany;* orcid.org/0000-0002-0292-1482; Email: Robert.Pieper@bfr.bund.de

Authors

Anna Maria Engel − *German Federal Institute for Risk Assessment, Department Safety in the Food Chain, Berlin 10589, Germany;* orcid.org/0000-0002-6552-0723

Fenja Klevenhusen − *German Federal Institute for Risk Assessment, Department Safety in the Food Chain, Berlin 10589, Germany;* orcid.org/0000-0001-6015-5459

Jan-Louis Moenning − *German Federal Institute for Risk Assessment, Department Safety in the Food Chain, Berlin 10589, Germany*

Jorge Numata − *German Federal Institute for Risk Assessment, Department Safety in the Food Chain, Berlin 10589, Germany;* orcid.org/0000-0002-0033-4436

Carola Fischer-Tenhagen − *German Federal Institute for Risk Assessment, Department Experimental Toxicology and ZEBET, Berlin 12277, Germany*

Benjamin Sachse − *German Federal Institute for Risk Assessment, Department Food Safety, Berlin 10589, Germany;* orcid.org/0000-0001-7486-4045

Bernd Schäfer − *German Federal Institute for Risk Assessment, Department Food Safety, Berlin 10589, Germany*

Hildburg Fry − *German Federal Institute for Risk Assessment, Department Safety in the Food Chain, Berlin 10589, Germany*

Oliver Kappenstein − *German Federal Institute for Risk Assessment, Department Safety in the Food Chain, Berlin 10589, Germany*

Complete contact information is available at: https://pubs.acs.org/10.1021/acs.jafc.2c02517

Funding

The study was funded by the German Federal Institute for Risk Assessment grant BfR-SiN-1322−789.

Notes

The authors declare no competing financial interest.

■ ACKNOWLEDGMENTS

The authors would like to thank the animal care staff of the German Federal Institute for Risk Assessment for assistance during the feeding experiment. The support of Mandy Schwieters from the National Reference Laboratory (NRL) for Feed Additives of the BfR is highly appreciated.

■ ABBREVIATIONS USED

AP, adaptation period; BIC, Bayesian information criterion; BfR, German Federal Institute for Risk Assessment; BSL, blue sweet lupin; DLQ, German Association for Performance and Quality Testing e.V.; DM, dry matter; DP, depuration period; EFSA, European Food Safety Authority; LC/MS−MS, high-performance liquid-chromatography−tandem mass spectrometry; LFGB, German Food and Feed Code; LOQ, limit of quantification; MoE, margin of exposure; MRM, multiple reaction monitoring; NDF, neutral detergent fiber; NRL, national reference laboratory; PBTK, physiologically based toxicokinetic model; QAs, quinolizidine alkaloids; TR, transfer rate; VDLUFA, Association of German Agricultural Analytic and Research Institutes

■ REFERENCES

(1) Mazumder, K.; Biswas, B.; Kerr, P. G.; Blanchard, C.; Nabila, A.; Golder, M.; Aziz, M. G.; Farahnaky, A. Comparative assessment of nutritional, thermal, rheological and functional properties of nine Australian lupin cultivars. *Sci. Rep.* **2021**, *11*, 2151.

(2) Wink, M. Chemical Defense of Leguminosae. Are Quinolizidine Alkaloids part of the antimicrobial defense system of lupins? *Z. Naturforsch.* **1984**, *39*, 548−552.

(3) Gresta, F.; Wink, M.; Prins, U.; Abberton, M.; Capraro, J.; Scarafoni, A.; Hill, G. Lupins in European Cropping Systems. *Legumes in Cropping Systems*; CAB International, 2017; pp 88−108. DOI: 10.1079/9781780644981.0088

(4) Von Baer, D.; Perez, I. Quality standard propositions for commercial grain of white lupin (Lupinus albus). *Proceeding of the 6th International Lupin Conference*; Temuco-Pucon: Chile, 1991; pp 158−167.

(5) Board of Food Standards Australia New Zealand. Schedule 19 − Maximum Levels of Contaminants and Natural Toxicants − Food Standards (Proposal P1025 − Code Revision) Variation − Australia New Zealand Food Standards Code − Amendment No. 154, Rev. 01/2016, last revised June 2021. https://www.legislation.gov.au/Details/F2021C00628 (accessed Jan 19, 2022).

(6) ACNFP. *Report on Seeds from Narrow Leafed Lupin. Appendix IX*; MAFF Publications: London, GB. 1996, p 107.

(7) EU Commission (Direction Générale de la. 1998. Avis du 17 mars 1998 du Conseil supérieur d'hygiène publique de France (section de l'alimentation et de la nutrition) relatif à l'emploi de farine de lupin en alimentation humaine. *Bulletin Officiel*; EU, 1998. n 98/27.

(8) Wink, M.; Hartmann, T.; Witte, L.; Rheinheimer, J. Interrelationship between Quinolizidine Alkaloid Producing Legumes and Infesting Insects: Exploitation of the Alkaloid- Containing Phloem Sap of Cytisus scoparius by the Broom Aphid Aphis cytisorum. *Z. Naturforsch.* **1982**, *37*, 1081−1086.

(9) Boschin, G.; Resta, D. C. Alkaloids Derived from Lysine: Quinolizidine (a Focus on Lupin Alkaloids). In *Natural Products*; Ramawat, K. G., Mérillon, J. M.; Springer: Berlin, Heidelberg, 2013; pp 381−403.

(10) Schrenk, D.; Schrenk, L.; Bodin, J. K.; Chipman, J.; del Mazo, B.; Grasl-Kraupp, C.; Hogstrand, L. R.; Hoogenboom, J. C.; Leblanc, C. S.; Nebbia, E.; EFSA Panel on Contaminants in the Food Chain; et al. Scientific opinion on the risks for animal and human health related to the presence of quinolizidine alkaloids in feed and food, in particular in lupins and lupin-derived products. *EFSA J.* **2019**, *17*, 5860.

(11) Yovo, K.; Huguet, F.; Pothier, J.; Durand, M.; Breteau, M.; Narcisse, G. Comparative Pharmacological Study of Sparteine and its Ketonic Derivative Lupanine from Seeds ofLupinus albus. *Planta Med.* **1984**, *50*, 420−424.

(12) Keeler, R. F. Lupin alkaloids from teratogenic and non-teratogenic lupins. III. Identification of anagyrine as the probable teratogen by feeding trials. *J. Toxicol. Environ. Health* **1976**, *1*, 887−898.

(13) Commission Regulation (EU) *No 1017/2017 of 15 June 2017 Amending Regulation (EU) No 68/2013 on the Catalogue of Feed Materials*; Off J Eur Union, 2017. L 159/48.

(14) Wink, M. Quinolizidine and Pyrrolizidine Alkaloid Chemical Ecology - a Mini-Review on their similarities and differences. *J. Chem. Ecol.* **2019**, *45*, 109−115.

(15) Böhme, A.; Dietze, M.; Gefrom, A.; Priepke, A.; Schachler, B.; Struck, C.; Wehling, P. *Lupinen - Anbau und Verwertung*; Publisher: Universität Rostock, Agrar- und Umweltwissenschaftliche Fakultät - Phytomedizin: Gesellschaft zur Förderung der Lupine (G.F.L.), 2016.

(16) Ortega, J. A.; Lazerson, A. Anagyrine-induced red cell aplasia, vascular anomaly, and skeletal dysplasia. *J. Pediatr.* **1987**, *111*, 87−89.

(17) Shupe, JL.; Binns, W.; James, LF.; Keeler, R. F. A congenital deformity in calves induced by the maternal consumption of lupin. *Aust. J. Agric. Res.* **1968**, *19*, 335−340.

(18) VDLUFA (Association of German Agricultural Analytic and Research Institutes). 3.1 Bestimmung von Feuchtigkeit. In: VDLUFA. *Method Book Volume III of VDLUFA: The Chemical Analysis of Feedstuffs*; VDLUFA-Verlag: Darmstadt, 1976.

(19) VDLUFA (Association of German Agricultural Analytic and Research Institutes). 4.1.1 Bestimmung von Rohprotein. In: VDLUFA. *Method Book Volume 3 of VDLUFA: The Chemical Analysis of Feedstuffs*; VDLUFA-Verlag: Darmstadt, 1993.

(20) VDLUFA (Association of German Agricultural Analytic and Research Institutes). 6.5.1 Bestimmung der Neutral-Detergenzien-Faser nach Amylasebehandlung (aNDF) sowie nach Amylasebehandlung und Veraschung (aNDFom). In: VDLUFA; *Method Book Volume 3 of VDLUFA: The Chemical Analysis of Feedstuffs*; VDLUFA-Verlag: Darmstadt, 2012.

(21) Lebensmittel- und Futtermittelgesetzbuch (LFGB) as amended by the announcement of September 15, 2021 (BGBl. I S. 4253) established by Article 7 of the Law of 27 in September 2021 (BGBl. I S. 4530).

(22) DLQ. *DLQ Directive 1.13 on DLQ Reference Method for the Determination of Urea Content in Milk Continuous Flow Analysis*; Deutscher Verband für Leistungs- und Qualitätsprüfung e. V.; 2013.

(23) EU Commission Regulation (EU) *No 2021/808 of March 2021 Amending Regulation (EC) No 657/2007 and No 179/98 on the Performance of Analytical Methods for Residues of Pharmacologically Active Substances Used in Food-Producing Animals and on the Interpretation of Results as Well as on the Methods to Be Used for Sampling and Repealing*; Off J Eur Union, 2021. L 180/84.

(24) LMFIT. *Non-Linear Least-Square Minimization and Curve-Fitting for Python (0.8.0)*; Newville, M., Stensitzki, T., Allen, D. B.; Ingargiola, A.; Zenodo, 2014.

(25) Collingridge, D. S. A Primer on Quantitized Data Analysis and Permutation Testing. *J. Mix. Methods Res.* **2012**, *7*, 81−97.

(26) Shao, J. Consistency of jackknife variance estimators jun. *Statistics* **1991**, *22*, 49−57.

(27) EFSA, European Food Safety Agency. *Risk Evaluation of Chemical Contaminants in Food in the Context of RASFF Notifications: Rapid Assessment of Contaminant Exposure Tool (RACE)*; EFSA Supporting publication, 2019: EN-1625. 2019.

(28) West, J. W.; Mullinix, B. G.; Bernard, J. K. Effects of Hot, Humid Weather on Milk Temperature, Dry Matter Intake, and Milk yield of lactating dairy cows. *J. Dairy Sci.* **2003**, *86*, 232−242.

(29) Boguhn, J.; Kluth, H.; Bulang, M.; Engelhard, T.; Spilke, J.; Rodehutscord, M. Effects of using thermally treated lupins instead of soybean meal and rapeseed meal in total mixed rations onin vitromicrobial yield and performance of dairy cows. *J. Anim. Physiol. Anim. Nutr.* **2008**, *92*, 694−704.

(30) Guillaume, B.; Otterby, D. E.; Linn, J. G.; Stern, M. D.; Johnson, D. G. Comparison of Sweet White Lupin Seeds with Soybean Meal as a Protein Supplement for Lactating Dairy Cows. *J. Dairy Sci.* **1987**, *70*, 2339−2348.

(31) Joch, M.; Kudrna, V. Partial replacement of soybean meal by white lupine seeds in the diet of dairy cows. *Asian-Australas. J. Anim. Sci.* **2020**, *33*, 957−964.

(32) Benchaar, C.; Moncoulon, R.; Bayourthe, C.; Vernay, M. Effects of a supply of raw or extruded white lupin seeds on protein digestion and amino acid absorption in dairy cows. *J. Anim. Sci.* **1994**, *72*, 492−501.

(33) Bauman, D. E.; Griinari, J. M. Regulation and nutritional manipulation of milk fat: low-fat milk syndrome. *Livest. Prod. Sci.* **2001**, *70*, 15−29.

(34) Froidmont, E.; Bartiaux-Thill, N. Suitability of lupin and pea seeds as a substitute for soybean meal in high-producing dairy cow feed. *Anim. Res.* **2004**, *53*, 475−487.

(35) Kuoppala, K.; Jaakkola, S.; Garry, B.; Ahvenjärvi, S.; Rinne, M. Effects of faba bean, blue lupin and rapeseed meal supplementation on nitrogen digestion and utilization of dairy cows fed grass silage-based diets. *Animal* **2021**, *15*, 100300.

(36) Mendowski, S.; Chapoutot, P.; Chesneau, G.; Ferlay, A.; Enjalbert, F.; Cantalapiedra-Hijar, G.; Germain, A.; Nozière, P. Effects of replacing soybean meal with raw or extruded blends containing faba bean or lupin seeds on nitrogen metabolism and performance of dairy cows. *J. Dairy Sci.* **2019**, *102*, 5130−5147.

(37) Jansen, G.; Jürgens, H. U.; Ordon, F. Effects of Temperature on the Alkaloid Content of Seeds of Lupinus angustifolius Cultivars. *J. Agron. Crop Sci.* **2009**, *195*, 172.

(38) Jansen, G.; Jürgens, H.-U.; Schliephake, E.; Ordon, F. Effect of the Soil pH on the Alkaloid Content ofLupinus angustifolius. *Int. J. Agron.* **2012**, *2012*, 1−5.

(39) Wink, M.; Meißner, C.; Witte, L. Patterns of quinolizidine alkaloids in 56 species of the genus Lupinus. *Phytochemistry* **1995**, *38*, 139−153.

(40) Boschin, G.; Annicchiarico, P.; Resta, D.; D'Agostina, A.; Arnoldi, A. Quinolizidine alkaloids in seeds of lupin genotypes of different origins. *J. Agric. Food Chem.* **2008**, *56*, 3657−3663.

(41) Robbins, M. C.; Petterson, D. S.; Brantom, P. G. A 90-Day Feeding Study of the Alkaloids of Lupinus angustifolius in the Rat. *Food Chem. Toxicol.* **1996**, *34*, 679−686.

(42) Pothier, J.; Cheav, S.-L.; Galand, N.; Dormeau, C.; Viel, C. A Comparative Study of the Effects of Sparteine, Lupanine and Lupin Extract on the Central Nervous System of the Mouse. *J. Pharm. Pharmacol.* **2011**, *50*, 949−954.

(43) Petterson, D. S.; Ellis, Z. L.; Harris, D. J.; Spadek, Z. E. Acute toxicity of the major alkaloids of cultivated Lupinus angustifolius seed to rats. *J. Appl. Toxicol.* **1987**, *7*, 51−53.

(44) Mukisira, E. A.; Phillip, L. E.; Mitaru, B. N. The effect of feeding diets containing intact or partially detoxified lupin on voluntary intake and milk production by Friesian dairy cows. *Anim. Sci.* **1995**, *60*, 169−175.
(45) Johnson, J. C.; Miller, J. D.; Bedell, D. M. Tifwhite-78 Lupine Seed as a Feedstuff for Cattle. *J. Dairy Sci.* **1986**, *69*, 142−147.
(46) Gardner, D. R.; Panter, K. E. Comparison of blood plasma alkaloid levels in cattle, sheep and goats fed Lupinus caudatus. *J. Nat. Toxins* **1993**, *2*, 1.
(47) Kennelly, E. J.; Flynn, T. J.; Mazzola, E. P.; Roach, J. A.; McCloud, T. G.; Danford, D. E.; Betz, J. M. Detecting potential teratogenic alkaloids from blue cohosh rhizomes using an in vitro rat embryo culture. *J. Nat. Prod.* **1999**, *62*, 1385−1389.
(48) Green, B. T.; Lee, S. T.; Welch, K. D.; Gardner, D. R.; Stegelmeier, B. L.; Davis, T. Z. The serum concentrations of lupine alkaloids in orally-dosed Holstein cattle. *Res. Vet. Sci.* **2015a**, *100*, 239−244.
(49) Green, B. T.; Panter, K. E.; Lee, S. T.; Welch, K. D.; Pfister, J. A.; Gardner, D. R.; Stegelmeier, T. Z.; Davis, T. Z. Differences between Angus and Holstein cattle in the Lupinus leucophyllus induced inhibition of fetal activity. *Toxicon* **2015b**, *106*, 1−6.
(50) Panter, K. E.; Welch, K. D.; Gardner, D. R.; Green, B. T. Poisonous plants: effects on embryo and fetal development. *Birth Defects Res., Part C* **2013a**, *99*, 223−234.
(51) Panter, K. E.; Gay, C. C.; Clinesmith, R.; Platt, T. E. Management practices to reduce lupine-induced crooked calf syndrome in the Northwest. *Rangelands* **2013b**, *35*, 12−16.
(52) Jurima, M.; Inaba, T.; Kalow, W. Sparteine oxidation by the human liver: absence of inhibition by mephenytoin. *Clin. Pharmacol. Ther.* **1984**, *35*, 426−428.
(53) Ebner, T.; Meese, C. O.; Eichelbaum, M. Mechanism of cytochrome P450 2D6-catalyzed sparteine metabolism in humans. *Mol. Pharmacol.* **1995**, *48*, 1078−1086.
(54) Chaudhuri, A.; Keller, W. J. New mammalian metabolites of sparteine. *Life Sci.* **1990**, *47*, 319−325.
(55) Aguiar, R.; Wink, M. Do Naïve Ruminants Degrade Alkaloids in the Rumen? *J. Chem. Ecol.* **2005**, *31*, 761−787.
(56) Gay, C. C.; Panter, E. P.; Mealey, K. L.; Gay, J. M.; Hjartarson, S. W.; Tibary, E. S.; Motteram, T.; Wierenga, L. F.; James, L. F. Comparison of plasma disposition of alkaloids after lupine challenge in cattle that had given birth to calves with lupine-induced arthrogryposis or clinically normal calves. *Am. J. Vet. Res.* **2004**, *65*, 1580−1583.
(57) Veng-Pedersen, P. Mean Time Parameters in Pharmacokinetics. *Clin. Pharmacokinet.* **1989**, *17*, 424−440.

https://doi.org/10.1021/acs.jafc.2c02517
J. Agric. Food Chem. 2022, 70, 11749−11758

6 Summary & discussion

6.1 Transfer of dioxins and PCBs in dairy cows

At first, a literature review was conducted summarizing the published papers describing the transfer of dioxins and PCBs from feed into cow's milk. The results of this review were published in two papers, one paper primarily focused on transfer parameters, such as half-lives derived via feeding studies and transfer rates [108], and the second publication, which is part of this cumulative work, focuses on mathematical models that describe the transfer from oral exposure into cow's milk.

The models discussed within "Transfer of polychlorinated dibenzo- p-dioxins and dibenzofurans (PCDD/Fs) and polychlorinated biphenyls (PCBs) from oral exposure into cow's milk - part II: toxicokinetic predictive models for risk assessment" (PUB 1) [109] can be broadly classified into five categories: non-compartmental models, one-compartment models, two-compartment models, PBTK models, and fugacity models.

The non-compartmental models examined aim to derive specific transfer parameters, namely transfer rate (*TR*), transfer factor (*TF*), or bio-transfer factor (*BTF*). These parameters are closely interconnected, as they involve multiplying a value with the amount or concentration of the contaminant in feed to determine the corresponding amount or concentration in milk or milk fat. Specifically, they are defined as follows:

Transfer Rate

$$TR[\%] := \frac{DailyExcretionViaMilk\left[\frac{ng}{d}\right]}{DailyIntakeViaFeed\left[\frac{ng}{d}\right]} 100\%, \tag{56}$$

Transfer Factor

$$TF[\quad] := \frac{ConcentrationInMilkFat\left[\frac{ng}{kg}\right]}{ConcentrationInFeed\left[\frac{ng}{kg}\right]}, \tag{57}$$

Biotransfer Factor

$$BTF\left[\frac{d}{kg}\right] := \frac{ConcentrationInMilk\left[\frac{ng}{kg}\right]}{DailyIntake\left[\frac{ng}{d}\right]}. \tag{58}$$

Note that these transfer parameters are interconvertible given the amounts of feed, milk yield and milk fat yield. The non-compartmental models discussed predict these parameters by fitting a curve e.g., a linear function, to some chemical parameter and the corresponding transfer parameter. While these models can be often implemented with already existing data, they generally provide only a rough approximation and may suffer from significant prediction errors for certain congeners. Furthermore, they completely lack the capability to dynamically

predict concentration-time profiles under different feeding scenarios. Hence, these non-compartmental models are not of major interest for this work and instead the focus lies primarily on the compartmental models.

The concepts of simple one- and two-compartment models, with their respective mono- and bi- exponential behaviour, have commonly been employed for direct data analysis. In this approach, the experimental concentration data is fitted to a mono or bi-exponential curve:

$$C(t) = C_0 e^{\lambda_0 t} \tag{59}$$

or

$$C(t) = C_0 e^{\lambda_0 t} + C_1 e^{\lambda_1 t} \tag{60}$$

with $C_0, C_1 > 0$ and $\lambda_0, \lambda_1 < 0$ for concentration $C(t)$ at time t. However, the resulting parameters do not involve any specific physiological process of the cow and are therefore mostly descriptive in nature. Furthermore, without additional data, this information can only be used to predict the depuration phase of the contaminant. Only a few single compartment models and no two-compartment models were published in the literature, where the model parameters represented specific physiological processes such as metabolism [110]. A major advantage of these models is their simplicity, allowing for easy integration into more complex models that encompass multiple trophic levels beyond just the cow itself.

Indeed, most of the reported physiological models for PCBs or dioxins in cows contain more than two compartments. In general, they are based on two different modelling approaches, a classical PBTK approach by Derks [111] and a fugacity approach by McLachlan [112]. In the classical PBTK approach by Derks, the cow is divided into six compartments: liver, udder, richly perfused, slowly perfused and blood. Blood is the central compartment that connects all the others. The rate of transfer between blood and other compartments depends on the congener concentration $C_i = \frac{A_i}{V_i}$, the relative affinity of the congener for that tissue described by the partition coefficient P_i and the blood flow rate Q_i into that compartment. Elimination occurs in the liver by metabolization and in the udder by lactation. In addition, the congeners are absorbed from the GIT via first pass directly into the liver. All this can be described by the following differential equations

$$\frac{dA_i}{dt} = -\left(\frac{Q_i}{V_i P_i} + k_{met}\mathbf{1}_{\{liver\}}(i) + \frac{CL_{milkfat}}{V_{udder}}\mathbf{1}_{\{udder\}}(i)\right)A_i + \frac{Q_i A_{blood}}{V_{blood}} \tag{61}$$

and

$$\frac{dA_{blood}}{dt} = \sum_i \frac{Q_i A_i}{V_i P_{i,}} - \frac{Q_{blood} A_{blood}}{V_{blood}}, \tag{62}$$

where i represents the respective non-blood compartment; F_{abs} is the proportion of congener that gets absorbed from the GIT; and $S_{milkfat}$ is the daily milk fat yield excreted. Furthermore, it is assumed that the transport into the fat compartment is diffusion limited; therefore, the blood flow rate into the fat compartment is reduced by a factor $\mathrm{D} < 1$. This model was used

multiple times with only minor changes to the general structure i.e., the udder compartment was sometimes removed and excretion via milk fat happens instead directly from the blood.

In contrast, the McLachlan fugacity approach offers a different perspective [112]. This approach divides the model into three compartments: the digestive tract, fat, and blood, with blood serving as the connecting compartment between the other two. The key feature of this approach is the utilization of fugacity to describe the transfer of contaminants between compartments.

In the fugacity conceptual framework, each compartment possesses its own contaminant pressure determined by the concentration in the compartment and the fugacity capacity in that compartment. The contaminant traverse water and lipid layers to equalize the pressures among the compartments. The ingestion of contaminants occurs in the digestive tract, where excretion can also take place. Furthermore, the blood compartment serves as the site for elimination of contaminants, either through metabolism or excretion via milk fat. Throughout these processes, the pressure within the respective compartment increases or decreases accordingly. It is interesting to note that unlike the Derks approach [111], the fugacity approach is not influenced by the blood flow rate at any point. Therefore, it is assumed that the toxicokinetic of contaminants are primarily governed by their diffusion-limited behaviour, which is somewhat reasonable considering the long half-lives compared to the fast blood flow. A mathematical description for this without any equilibrium assumptions is given by

$$\frac{df_{Dig}}{dt} = \frac{D_{Grass}f_{Grass} + D_{Feed}f_{Feed} + D_{Soil}f_{Soil} + D_{Blood-Dig}f_{Blood} - (D_{Exc} + D_{Dig-Met})f_{Dig}}{V_{Dig}Z_{Dig}} \quad (63)$$

$$\frac{df_{Blood}}{dt} = \frac{D_{Blood-Dig}(f_{Dig} - f_{Blood}) + D_{Blood-Fat}(f_{Fat} - f_{Blood}) - (D_{Milk} + D_{Blood-Meta})f_{Blood}}{V_{Blood}Z_{Blood}} \quad (64)$$

$$\frac{df_{Fat}}{dt} = \frac{D_{Blood}(f_{Blood} - f_{Fat})}{V_{Fat}Z_{Fat}}. \quad (65)$$

Here f_i are the fugacities in the respective compartment; D_{i-j} or D_k are the transport coefficients; V_i are the volumes of the compartments; Z_i are the fugacity capacities, where $C_i = Z_i f_i$ [88].

Despite the considerable effort that has gone into the development and parameterisation of these models, it is important to note that their validation has been limited. Only for the classical PBTK approach, specifically for TCDD [111] and a specific dioxin mixture [113], is there a degree of satisfactory validation where sufficient results have been obtained. However, in both cases the evaluation was carried out on the same data set that was used to derive some

of the model parameters by fitting. On the other hand, parametrisation of other models often relies on in silico methods and is typically evaluated using very limited experimental data sets (e.g. [68]) or only under steady-state conditions (e.g. [114]).

Therefore, there is still a need for the development of fully parametrized PBTK models describing the transfer from feed into dairy cows', which should be validated on sufficient data in a non-steady state setting. This is the contribution from this cumulative work consisting of two published papers PUB 2 [115] and 3 [116] published as part of the work presented here.

The publication "Transfer and toxicokinetic modelling of non-dioxin-like polychlorinated biphenyls (ndl-PCBs) into accidentally exposed dairy cattle and their calves - A case report" (PUB 2) [115] presents a case study on lactating mother cows and their calves contaminated with ndl-PCBs. Here, a contamination incident at a farm was investigated, where the source of contamination was unknown. The cows were taken over for further investigation at the research farm of the BfR. At the BfR site, where further analysis was to be carried out, two of the cows were successfully impregnated and, following the end of their initial lactation and a dry period, they gave birth to two healthy calves, initiating a new lactation period. All five animals involved in the study (two calves and three adult cows) were slaughtered 70-80 days later and samples from various tissues were taken. Throughout the study, samples of milk from the lactating cows and blood from all animals, including the calves, were collected. All samples were subsequently analysed for ndl-PCBs and lipid content. The derived data was then used to develop a model describing the distribution of the contaminant in the mother cow and the subsequent transfer via milk and placenta into the calves. This was done by adapting the mother cow and calf model developed by Bogdal et al. (2022) [68] to the present case. In this model, Derks' classic PBTK approach was used and appropriately adapted to describe both the adult cow and the calf, where the calf is simply a scaled-down version of the mother cow without an udder compartment [111]. The transfer of congeners from the mother cow to the calf occurs instantaneously at birth through the placenta and continuously through the suckling of contaminated mother's milk. For this adaptation, as far as possible, the model parameters required were derived directly from the data of the represented study, as the use of the model parameters from the original model by Bogdal did not lead to satisfactory results. In particular, most of the partition coefficients P_i were derived from actual congener concentration measurements in the respective tissues and not from in silico predictions as in Bogdal's paper [68]. However, the derivation of these parameters in this case study presented some unique challenges because, unlike most feeding studies, the original exposure of the animal was unknown. Consequently, the initial body burden of the cows upon arrival at our site was also unknown and had to be estimated. This was successfully done by fitting the resulting predictions of congener concentration in milk fat and blood fat and assuming that the adult cows were in a pseudo steady state upon arrival and on the day of slaughter as described in section 4.1 "Analytical solution of first-order TK models". Another interesting aspect of this study was that the observation period included two different lactation periods with different milk fat yields and a dry period in between. This made the traditional approaches to estimating half-lives, such as fitting the data to an exponential function (eq. 1

and 2), inappropriate for this data set. This further highlights the appeal of the PBTK modelling approach for such data sets. The final fully parametrised model was able to describe the concentration in milk fat and blood fat for two out of three adult cows well during their monitoring period. However, for unknown reason one adult cow, which could not be impregnated, could not be described well by this model.

The model was subsequently used to derive some unique biotransfer factor-like parameters, which can be used in risk analysis to describe the distribution of congeners in different tissues of adult cows, where a distinction was made between cows during lactating and dry period. However, it was not possible to derive transfer parameters from the feed into a tissue or milk fat, as no information was available on the transfer of the congeners from oral exposure into the cow. Nevertheless, half-lives for the individual congeners could be derived from this model.

In addition, as stated already above, the calves were assumed to be simply scaled-down versions of the adult cows, so the model parameters were also used for the parametrisation of the model describing the individual congeners in the calves. Notably, a key aspect of the calves was their continuous growth during the monitoring period, resulting in substantial alterations in their physiological parameter over time. This growth had a progressive dilution effect on the congeners over time, thereby influencing the overall TK behaviour. The resulting model for the calves was able to describe the exposure via milk fat and placenta of these calves quite well, whereby only the absorption coefficient from milk fat was fitted to the data from the calves. Subsequently, the model was used to derive several parameters describing the transfer from milk fat or placenta to the tissues of the growing calf. Thereby it was also possible to distinguish between transfer by the placenta and the transfer of via milk fat through suckling. Interestingly, it was found that only 10-14% of the contamination on the day of slaughter was due to placental contamination. However, it should be kept in mind that placental transfer may in most cases is the most relevant aspect, as in practice calves are not usually raised with their mother's milk, but with milk exchanger, which eliminates the route of exposure via mother's milk.

The PBTK modelling described in “Toxicokinetic modelling of the transfer of polychlorinated biphenyls (PCBs), polychlorinated dibenzo-p-dioxins and dibenzofurans (PCDD/Fs) into milk of high-yielding cows during negative and positive energy balance” (PUB 3) [116] deals with the modelling of a feeding study for dioxins and PCBs in lactating cows. The aim of this study was to derive a PBTK model as well as several transfer parameters for theses congeners, with an emphasis on the novel question of the influence of energetic status on the transfer from feed to milk. High milk yielding cows (N=5) were dosed with a mixture of 17 dioxins, 12 dl-PCBs, and 6 ndl-PCBs twice for 28 consecutive days each time. The dosing periods occurred at the beginning of their lactation during the negative energy balance (NEB) phase and in the middle of the lactation (starting at around 170-180 days) during the positive energy balance (PEB) phase. In addition, four control animals were present, which were not dosed during their lactation. During the entire study, among other experimental evaluations, blood and milk samples were taken. At the end of the study, all animals involved were slaughtered and

samples taken from various tissues. All samples collected were analysed for their content of the 35 dosed congeners. The modelling approach is two-tiered; the first model (part of this cumulative work) focuses on a model based on the blood and milk samples; the second, more complex model, will also utilize tissue sample results (work in progress, not part of this cumulative dissertation). The daily milk fat content was measured. The blood fat concentration was unfortunately not measured. During the study, one experimental and control cow died untimely; after the end of the study, another experimental cow was found to show subclinical symptoms of a sub-acute ruminal acidosis (SARA). Therefore, it was decided to exclude these cows from the data analysis, using the remaining three dosed and three control animals. In addition, strong and variable background contamination of samples was apparent for three ndl-PCBs (28, 52, 101), hindering any further analyses for these congeners. To analyse the data of the remaining 32 congeners, a PBTK model was designed consisting of a blood compartment connected to two storage compartments: a slow turnover and a fast turnover compartment. Two simplifying assumptions were used: 1) absorbed congeners flow directly from the gastrointestinal tract into the blood compartment; 2) excretion via milk occurs directly from the blood compartment. Both of these assumptions can be justified in terms of the congeners' long milk excretion half-lives (days) compared to the shorter time scale of GIT absorption and milk fat excretion. Most parameters describing this PBTK model were derived via fitting methods, and not from physiological data. Only the volume of the blood compartment; the blood flow rate into the fast turnover compartment, which was set equal to the total cardiac output of the animal; and the milk fat excretion rate were based on measured physiological data. Distinct sets of the fitted model parameters were derived for the NEB and for the PEB phases. This was done because the primary objective of this modelling approach was to closely describe the milk data while maintaining simplicity, allowing us to derive transfer parameters based on the underlying data without incorporating too many physiological assumptions.

The fitting algorithm used for deriving these parameters takes the LOQ data into account using the method described in chapter 4.5.1 "Dealing with censored data". Furthermore, the fitting algorithm also took into account that the measurement timepoints were not equally distributed over the course of the study by weighting the residuals according to an approximated density of measurement points. Although the modelling approach often reflects the measured data closely, it also has some disadvantages. On the one hand, purely fitted parameters without clear physiological correlates are challenging to adapt to cows with slightly different physiology. On the other hand, the parameters of the model change abruptly at the transition from the NEB to the PEB phase, whereas in reality this transition occurs smoothly throughout the lactation period.

Nevertheless, the developed model was able to describe the concentration-time (ct) profile in milk fat quite well for most of the congeners. The ct-profile in blood was also well described for some of the congeners but was generally worse than in milk fat. Unfortunately, the measurement results for many congeners in the blood were hampered by background

contamination ("strong noise"), so that they could not always be adequately described by the model.

Despite the challenges mentioned above, the present model is well suited for deriving several parameters describing the transfer of the congeners into milk fat. This includes fundamental parameters, such as transfer rate in steady state and half-lives, which for some congeners had never been reported in the literature. But it also includes parameters that have rarely been discussed in the literature before, such as the time until steady state (90%) describing the time it takes before 90% steady state concentrations in milk are reached assuming constant dosing. Another example is the transition time, which describes the time it takes to transition from the α phase to the β phase of depuration.

The comparison between the derived parameters in NEB and PEB phase was done in two steps. First, it was investigated whether there is a general statistically significant difference in the parameters across all contaminants evaluated simultaneously using the Wilcoxon test due to the prevalence of outliers. If this was the case, the contaminants were then checked individually for the observed difference using the t-test as Wilcoxon test for a sample size of three would always accept the H_0 hypothesis independent of sample distribution.

This approach was followed because of the small sample size (N=3) and because any changes in TK behaviour are presumably due to lipid redistribution, which should affect all congeners in a similar manner. However, the risk of this approach is that individual animal specific effects will have a strong impact on the results. Transfer rates were significantly different, with higher transfer rates at NEB phase (median of 43%) than at PEB phase (median of 32%). This may be due to a higher non-milk excretion during the PEB phase, which is supported by the fact that the mean blood residence time during the PEB phase is significantly higher than during the NEB phase i.e., the contaminant has more time to be eliminated by other means. A comparison of the transfer rates derived here with values published in the literature are summarized in the above-mentioned review „Transfer of polychlorinated dibenzo- p-dioxins and dibenzofurans (PCDD/Fs) and polychlorinated biphenyls (PCBs) from oral exposure into cow's milk - Part I: state of knowledge and uncertainties" [108] shows that the values derived here are clearly higher. This is almost certainly due to the fact that the values found in the literature are often not derived at steady state, as it takes a long time for most congeners to approach it, and often no extrapolation of the data to steady state has been attempted. This is supported by the fact that the non-steady transfer rates (days 21-28), also derived from the same data used here, are comparable to those reported in the literature [117].

Beside *TR*, significant differences could also be found for the β-half-life (median of 54 d in NEB and 47 d in PEB); the time until steady state (90%) (median of 129 d in NEB and 94 d in PEB); and the transition time (median of 9.1 d in NEB and 8.2 d in PEB). However, these significances were at much lower level than the ones found for *TR*. For the α-half-life (median of 1.8 d across NEB and PEB), no significant difference between NEB and PEB was found.

The analysis of the data also provided clues about the fate of the contaminants in the cow's body. It indicated that congeners are mainly distributed into the slow turnover compartments,

in median 85% during NEB phase and 82% during PEB phase. This challenges the notion that the slow turnover compartment consists solely of adipose tissue, as the lipid mass in adipose tissue alone does not account for close to 80% of the total body lipid fraction. Additionally, the partition coefficient into the fat of the adipose tissue is not significantly higher than that into the fat of other tissues like muscle, as demonstrated in the previous PUB 2 [115]. Moreover, the study reveals that the reduced blood flow volume coefficients into the slow turnover compartment are considerably lower than those derived in the Derks model [111]. During the NEB phase, the median coefficient is only 338 kg/d, and during the PEB phase, it is 194 kg/d compared to the 33% of total blood flow in Derks model [111]. This suggests that in complex models, such as the ones from Derks, more than just the adipose compartment should be considered diffusion limited [111]. Furthermore, it implies that the blood flow rate into these compartments is nearly irrelevant, which is in agreement with the assumptions made in MacLachlan-type fugacity models. Nevertheless, a significant proportion of congeners still reside in the fast turnover compartment, indicating the presence of tissues that rapidly exchange contaminants with the blood and therefore could be blood-flow limited. Potential candidates for such compartments include the udder, liver, and intestine, as they are known to exhibit rapid lipid exchange with the blood. There is evidence that the udder is the most important compartment for rapid turnover. This is supported by the fact that dioxins and PCBs do not show significant biphasic behaviour in rodents, which lack a large fat excretory organ [114, 118, 119]. Further data are needed to provide an authoritative answer on this question.

In conclusion, this work has yielded a well-parametrized model based on experimental measurements for the most relevant dioxins and PCBs. This model enables future risk assessors and risk managers to reliably predict ct-profiles in milk fat and blood. There is potential for more complex models, for instance models that predict transfer into edible tissues, and that incorporate more metabolic parameters. Future models may dynamically describe changes in animal physiology in response to variations in energy balance, rather than in a binary fashion, as in the current model. Future models should take into account that most tissues exchange these contaminants with the blood very slowly. Additionally, the current model as well as a future models should be evaluated using independent datasets, not used for parameter derivation, to better assess the predictive capabilities.

6.2 Modelling of ndl-PCBs in fattening pigs

Besides cow's milk, beef and veal, other animal fat sources in the human diet are important potential exposure pathways for lipophilic contaminants. This is the case of pork, which also contains significant amounts of fat. Hence, it is important to understand the transfer of dioxins and PCBs into pork. Pigs are monogastric animals, in contrast to the multiple stomachs of ruminants, and have a very different metabolism. Presently, to my knowledge there are only two published models that describe the transfer of 2,3,7,8-TCDD [73] and 1,2,3,4,7,8-HxCDD [120] into the meat of fattening pigs, but no model for other congeners. To address this

knowledge gap, a feeding study was conducted at the BfR using fattening pigs and ndl-PCB contaminated feed. The findings from this study were utilized to develop a PBTK model for these contaminants in fattening pigs. The results were published in the paper "Toxicokinetic modelling of the transfer of non-dioxin like polychlorinated biphenyls from feed into edible tissues of pigs" (PUB 4) [121]. In this feeding study, two groups (A and B) of fattening pigs were fed contaminated diets for 21 consecutive days at the beginning of their fattening period, when they were 65 days old and another group (C) was fed contaminated diets for seven consecutive days at the end of their fattening period, when they were 135 days old. Groups A and C were slaughtered at the end of their exposure period and group B was fed with uncontaminated feed after the exposure period for another 60 days before slaughter, i.e., group B had a depuration phase. After slaughter, liver and muscle fat samples were collected and analysed for their ndl-PCB content. This data was then used to derive a compartment model. Due to the limited number of data points available, some compromises had to be made in the model design. Firstly, the model consists of only two compartments, i.e., a liver compartment, where the contaminants are metabolized, and a fat compartment, which represents all the lipids of the animal. Secondly, the exchange between the two compartments is instantaneous, which means that the model behaves more like a one-compartment model with time-dependent elimination rates, and therefore cannot describe the biexponential behaviour typical for PCBs, but only a monoexponential behaviour. This was done because no data points were available shortly after the start of the depuration phase, i.e., during the α phase of depuration. In addition, a mathematically based argument could be derived that the fat compartment should be reasonably well described by a monoexponential decay. Even though this model design acts more like a one compartment model, it still does not induce a strictly monoexponential decay because the pigs are constantly growing, causing a dilution effect and a constant change in the volume ratio between fat and liver, which also changes the body clearance rate over time. Such a dilution affect could already be observed in the suckling calve discussed above (PUB 2) [121]. Interestingly, this made it impractical to derive parameters such as Transfer Rate *TR*, Transfer Factor *TF* (in steady state) and half-lives in the traditional sense assuming constant physiology and feeding. Therefore, the definition of *TR*, *TF* for this study was broadened, not requiring constant physiology and feeding. They can be calculated as follows

$$TF_j \coloneqq \lim_{t\to\infty} \widetilde{TF}_j(t) \coloneqq \lim_{t\to\infty} \frac{C_j(t)}{C_S} \tag{66}$$

and

$$TR \coloneqq \lim_{t\to\infty} \widetilde{TR}\,(t) \coloneqq \lim_{t\to\infty} \frac{A_T(t)}{\int_0^t Dose(\check{t})d\check{t}}, \tag{67}$$

where j represents the respective compartment (liver, fat or total); $C_j(t)$ are the concentrations in the respective compartments; C_S the concentration in feed, $A_T(t)$ the total body burden; and $Dose(t)$ is the daily dose at time t. This is more realistic, as feed intake increases with increasing

body weight. With this definition under realistic feeding conditions, it was shown that $\widetilde{TR}$and $\widetilde{TF_j}$ converge and therefore *TR*, TF_j could be calculated and presenting the first proper quantification of the transfer of theses ndl-PCBs in growing pigs. The *TR* varied between 9.57% for PCB-28 and 77.2% for PCB-153, the TF_{liver} ranged from 0.0817 for PCB-28 to 0.850 for PCB-153 and the TF_{fat} from 1.21 for PCB-28 to 10.6 for PCB-153. For half-lives, however, no good equivalent could be found, and they can only be reported as a time-dependent variable, which also presents the first time that this has been quantified for fattening pigs. However, a comparison of the half-lives during the fattening period of pigs with the constant values for dairy cows derived in the above-mentioned studies (PUB 2 and PUB 3) [115, 116] shows that pigs tend to be more efficient than dairy cows in eliminating (or diluting) these ndl-PCBs resulting in time dependent half-lives always ≤35 d, even though these fattening pigs did not lactate, which is the dominant elimination pathway in dairy cows. Furthermore, the elimination speed of PCB-28 in fattening pigs is much faster compared to the other five ndl-PCBs, in contrast to other species (rats or birds). This highlights once more the species-dependent differences in the toxicokinetic behaviour, in this case in the elimination of ndl-PCBs.

6.3 Modelling of quinolizidine alkaloids (QAs) in dairy cows

Obviously, the toxicokinetic behaviour of contaminants does not only depend on the species investigated, but also on the properties of the substance in question.

Therefore, different undesirable substances may require completely different model approach than dioxins or PCBs in the same species. This indeed is the case for QAs and was taken into account in the publication “Investigations on the Transfer of Quinolizidine Alkaloids (QAs) from Lupinus angustifolius into the Milk of Dairy Cows” (PUB 5) [122], where the transfer of QAs from lupin feed into cow’s milk is investigated. The study published in the paper is based on a controlled feeding study with lupin. For this evaluation, four dairy cows were feed for seven consecutive days with 1 kg/d lupin followed by a 10-day depuration phase. Thereafter, they were again feed for seven consecutive days with lupins but this time with 2 kg/d, which was then followed again by a 10-day depuration phase. Daily samples were collected throughout the study from the morning and evening milk, as well as the lupin feed, which were analysed for their content of different QAs. When analysing the data, four of the analysed QAs were quantifiable during depuration phase, allowing development of a toxicokinetic model for describing the transfer of these four QAs from feed into milk. The model consists of three compartments: a central compartment where the contaminant enters the system and becomes eliminated; a peripheral compartment, which acts as a small storage compartment; and an udder compartment, which is instantaneously emptied at milking events. This model structure is primarily based on the observed ct-profile in the measurements, as little knowledge was available about the kinetics of QAs in the animals. Therefore, the central and peripheral compartments cannot be directly ascribed to specific tissues of the animal. Hereby two design decisions have been made. Firstly, a peripheral

compartment was added, which was motivated by the observation that QA milk concentrations exhibited in a logarithmic scale a biphasic behaviour during the depuration phase with two distinct half-lives, i.e., an initial rapid decline, followed by a significantly slower decline. This suggested the presence of a second half-life induced by the peripheral compartment. Secondly, the model departed from previous approaches by representing milk excretion not as a continuous process, but rather as an instantaneous emptying of an udder compartment. This modification was necessary due to the considerably shorter half-lives (<<1 day) of QAs, which necessitated a more detailed portrayal of the milking process to account for changes that occur throughout the day. As a result of this, instead of a continuous ct-profile, the model predicts the concentration at discrete time points, i.e., morning and evening milking time. It is also important to note that this introduction of the udder compartment does not induce a third half-life in milk, as the milking event can be described by multiplying the current state with a matrix of rank two. The resulting PBTK model was able to describe the concentration measured in milk well; therefore, the model was also able to describe the differences observed in morning and evening milk. Using this model, it was possible to derive several transfer parameters such as α-half-lives ranging from 0.26 d lupanine to 0.28 d hydroxylupanine, β-half-lives ranging from 2.48 d isolupanine to 5.18 d Angustifoline and even transfer rates ranging from 1.05 % for angustifoline to 2.92 % for isolupanine.The β-half-lives and transfer rates in cows are reported here for the first time. However, it was also deduced that the observed β-half-lives occur at such low concentrations that they presumably irrelevant for practical purposes.

Even though two dosing regimens were used, they only differed by a factor of two. This made it difficult to conclusively determine whether or not the transfer of QAs into milk is dose-dependent. The differences in dose were not large enough given the high variability of the data and the small sample size of only four animals. The current model thus assumes dose-independence.

7 Future perspective

The PBTK models developed in this thesis provide a valuable tool for risk assessment to reduce and understand the human exposure to dioxins, PCBs and QAs. This has been achieved by creating fully parameterised non-steady state models, which can describe the transfer of contaminant from feed into food given wide range of contamination scenarios. Nevertheless, there is still an ongoing necessity to optimise the models that describe contaminant transfer in order to facilitate continuous improvement of risk assessment.

To achieve this, an important next step is to extend the dioxin and PCB model for high yielding dairy cows to a more physiologically based whole body PBTK model by incorporating more measurements of specific tissues and faeces from the animals [116, 117]. The resulting model should take into account physiological changes such as the depletion and replenishment of adipose tissue during lactation and be able to describe the differences found in the NEB and PEB phases solely based on physiological changes of the animals. If successful, the knowledge

gained, such as the presumed diffusion-limited nature of most tissues, could also be used to update the mother-calf model [115] and improve its predictability. With regard to QAs there are several unanswered questions about the fate of QAs in the body of the cow, which could have significant impact on the prediction [122]. Thus, future studies should focus on the β-half-life, which may indicative for distribution into deeper compartments representing certain tissues or organs. Furthermore, it should be investigated whether QAs are subject to processes such as enterohepatic circulation, as evidenced by cyclic behaviour observed in ct-profiles of milk [123]. As the assessment of the dose dependence of QAs was very limited due to insufficient dose difference, further studies are also required to address this issue. The knowledge gained from all these studies should be integrated into the modelling in order to transition from the current predominately data driven modelling approach to a more physiologically-based model. This should improve the ability of the model to extrapolate to different scenarios that are not covered by any experimental setting.

In general, all models developed here should be validated on an independent data set [109]. In this respect, it would be interesting to investigate whether the implementation of a physiological trait in the models represents the effect of that trait well [115, 116, 121]. For example, it could be investigated whether the implementation of milk fat yield allows extrapolation from high yielding dairy cows to low yielding dairy cows by simply changing the milk fat yield in the model.

However, as the development of PBTK models is usually based on animal testing, it should be investigated whether the required parameters could also be derived using in vitro or in silico methods [86]. A combination of in vitro, in silico and in vivo methods to derive parameters for future PBTK models would result in a significant reduction in the number of animal tests. This approach would facilitate more rapid risk assessment, even for contaminants with limited or no animal data, while also reducing animal suffering.

8 Abbreviations

AhR	aryl hydrocarbon receptor
ALARA	as low as reasonable achievable
BTF	bio-transfer factor
ct	concentration-time
CYP	cytochrome P-450
DDT	dichlorodiphenyltrichloroethane
dl	dioxin-like
GIT	gastrointestinal tract
IARC	International Agency for Research on Cancer
LOD	limit of detection
LOQ	limit of quantification
MRT	mean residence time
ndl	non-dioxin-like
NEB	negative energy balance
PBK	physiologically-based pharmacokinetic and physiologically-based toxicokinetic
PBTK	physiologically-based toxicokinetic
PCBs	polychlorinated biphenyls
PCDDs	polychlorinated dibenzo-p-dioxins
PCDFs	polychlorinated dibenzofurans
PEB	positive energy balance
PFAS	poly- and perfluoroalkyl substances
POPs	persistent organic pollutants
QAs	quinolizidine alkaloids
QSAR	quantitative/qualitative structure activity relationship
TCDD	2,3,7,8-tetrachlorodibenzo-*p*-dioxin
TEF	toxic equivalency factor
TEQ	toxic equivalency
TF	transfer factor
TK	toxicokinetic
TR	transfer rate
TWI	tolerable weekly intake

9 References

1. Yu, M.-H. and H. Tsunoda, *Environmental toxicology: biological and health effects of pollutants*. 2004: crc press.
2. Vallero, D.A., *Environmental contaminants: assessment and control*. 2010: Elsevier.
3. Canada, G.o. *Environmental Contaminants*. 2019; Available from: https://www.canada.ca/en/health-canada/services/food-nutrition/food-safety/chemical-contaminants/environmental-contaminants.html.
4. UN, *STOCKHOLM CONVENTION ON PERSISTENT ORGANIC POLLUTANTS (POPS).* 2001.
5. Jones, K.C. and P. De Voogt, *Persistent organic pollutants (POPs): state of the science.* Environmental pollution, 1999. **100**(1-3): p. 209-221.
6. Buccini, J., *The development of a global treaty on persistent organic pollutants (POPs).* Persistent organic pollutants, 2003: p. 13-30.
7. Chain, E.P.o.C.i.t.F., et al., *Scientific opinion on the risks for animal and human health related to the presence of quinolizidine alkaloids in feed and food, in particular in lupins and lupin-derived products.* EFSA Journal, 2019. **17**(11): p. e05860.
8. Rappe, C., *Analysis of polychlorinated dioxins and furans.* Environmental science & technology, 1984. **18**(3): p. 78A-90A.
9. Frumkin, H., *Agent Orange and cancer: an overview for clinicians.* CA: a cancer journal for clinicians, 2003. **53**(4): p. 245-255.
10. Safe, S., *Limitations of the toxic equivalency factor approach for risk assessment of TCDD and related compounds.* Teratogenesis, carcinogenesis, and mutagenesis, 1997. **17**(4-5): p. 285-304.
11. Van den Berg, M., et al., *The 2005 World Health Organization reevaluation of human and mammalian toxic equivalency factors for dioxins and dioxin-like compounds.* Toxicological sciences, 2006. **93**(2): p. 223-241.
12. Broman, D., et al., *Occurrence and dynamics of polychlorinated dibenzo-p-dioxins and dibenzofurans and polycyclic aromatic hydrocarbons in the mixed surface layer of remote coastal and offshore waters of the Baltic.* Environmental science & technology, 1991. **25**(11): p. 1850-1864.
13. Terzaghi, E., et al., *New data set of polychlorinated Dibenzo-p-dioxin and Dibenzofuran half-lives: natural attenuation and rhizoremediation using several common plant species in a weathered contaminated soil.* Environmental Science & Technology, 2020. **54**(16): p. 10000-10011.
14. Dopico, M. and A. Gómez, *Review of the current state and main sources of dioxins around the world.* Journal of the Air & Waste Management Association, 2015. **65**(9): p. 1033-1049.
15. Olie, K., P. Vermeulen, and O. Hutzinger, *Chlorodibenzo-p-dioxins and chlorodibenzofurans are trace components of fly ash and flue gas of some municipal incinerators in the Netherlands.* Chemosphere, 1977. **6**(8): p. 455-459.
16. BMUV. *Dioxine und PCB*. 2023; Available from: https://www.bmuv.de/themen/gesundheit-chemikalien/gesundheit/lebensmittelsicherheit/verbraucherschutz/uebersicht-ueber-dioxine-und-pcbs/dioxine-und-pcb#c15637.
17. Hites, R.A., *Dioxins: an overview and history.* Environmental science & technology, 2011. **45**(1): p. 16-20.
18. Karpf, R. and A. Wiedl, *Significance of and Challenges for Flue Gas Treatment Systems in Waste Incineration.*
19. Quaß, U., M. Fermann, and G. Bröker, *The European dioxin air emission inventory project—final results.* Chemosphere, 2004. **54**(9): p. 1319-1327.
20. Mills Iii, S.A., D.I. Thal, and J. Barney, *A summary of the 209 PCB congener nomenclature.* Chemosphere, 2007. **68**(9): p. 1603-1612.
21. Megson, D., et al., *Evaluation of the effectiveness of different indicator PCBs to estimating total PCB concentrations in environmental investigations.* Chemosphere, 2019. **237**: p. 124429.

22. Terzaghi, E., et al., *Rhizoremediation half-lives of PCBs: Role of congener composition, organic carbon forms, bioavailability, microbial activity, plant species and soil conditions, on the prediction of fate and persistence in soil.* Science of the Total Environment, 2018. **612**: p. 544-560.
23. Flasbarth, J., *Talk on PCB-Management: erledigte und unerledigte Hausaufgaben.* 2013.
24. ATSDR, *Toxicological Profile for Polychlorinated Biphenyls (PCBs).* 2014.
25. INTER, I., *Guidelines for the identification of PCBs and materials containing PCBS.* 1999.
26. Breivik, K., et al., *Towards a global historical emission inventory for selected PCB congeners—a mass balance approach: 3. An update.* Science of the Total Environment, 2007. **377**(2-3): p. 296-307.
27. Afghan, B. and A.S. Chau, *Analysis of trace organics in the aquatic environment*. 1989: CRC press.
28. Jartun, M., et al., *Painted surfaces–Important sources of polychlorinated biphenyls (PCBs) contamination to the urban and marine environment.* Environmental Pollution, 2009. **157**(1): p. 295-302.
29. Interdependent Task Force on PCBs. *Polychlorinated Biphenyls and the Environment*. 1972; Available from: https://nepis.epa.gov.
30. Jones, K., et al., *Evidence for a decline of PCBs and PAHs in rural vegetation and air in the United Kingdom.* Nature, 1992. **356**(6365): p. 137-140.
31. Hannah, T.J., D. Megson, and C.D. Sandau, *A review of the mechanisms of by-product PCB formation in pigments, dyes and paints.* Science of the Total Environment, 2022. **852**: p. 158529.
32. Safe, S., et al., *PCBs: structure–function relationships and mechanism of action.* Environmental health perspectives, 1985. **60**: p. 47-56.
33. Safe, S.H., *Comparative toxicology and mechanism of action of polychlorinated dibenzo-p-dioxins and dibenzofurans.* Annual review of pharmacology and toxicology, 1986. **26**(1): p. 371-399.
34. Sorg, O., *AhR signalling and dioxin toxicity.* Toxicology letters, 2014. **230**(2): p. 225-233.
35. Carpenter, D.O., *Polychlorinated biphenyls (PCBs): routes of exposure and effects on human health.* Reviews on environmental health, 2006. **21**(1): p. 1-24.
36. Nebert, D.W., *Aryl hydrocarbon receptor (AHR):"pioneer member" of the basic-helix/loop/helix per-Arnt-sim (bHLH/PAS) family of "sensors" of foreign and endogenous signals.* Progress in lipid research, 2017. **67**: p. 38-57.
37. Rothhammer, V. and F.J. Quintana, *The aryl hydrocarbon receptor: an environmental sensor integrating immune responses in health and disease.* Nature Reviews Immunology, 2019. **19**(3): p. 184-197.
38. Riaz, F., F. Pan, and P. Wei, *Aryl hydrocarbon receptor: The master regulator of immune responses in allergic diseases.* Frontiers in Immunology, 2022. **13**.
39. Vogel, C.F., et al., *The aryl hydrocarbon receptor as a target of environmental stressors–Implications for pollution mediated stress and inflammatory responses.* Redox biology, 2020. **34**: p. 101530.
40. Poland, A.P., et al., *Genetic expression of aryl hydrocarbon hydroxylase activity: induction of monooxygenase activities and cytochrome P1-450 formation by 2, 3, 7, 8-tetrachlorodibenzo-p-dioxin in mice genetically "nonresponsive" to other aromatic hydrocarbons.* Journal of Biological Chemistry, 1974. **249**(17): p. 5599-5606.
41. Murray, I.A., A.D. Patterson, and G.H. Perdew, *Aryl hydrocarbon receptor ligands in cancer: friend and foe.* Nature Reviews Cancer, 2014. **14**(12): p. 801-814.
42. Marinković, N., et al., *Dioxins and human toxicity.* Arhiv za higijenu rada i toksikologiju, 2010. **61**(4): p. 445-452.
43. Pelclová, D., et al., *Adverse health effects in humans exposed to 2, 3, 7, 8-tetrachlorodibenzo-p-dioxin (TCDD).* Reviews on environmental health, 2006. **21**(2): p. 119-138.
44. IARC, I.A.f.R.o.C., *Polychlorinated dibenzo-para-dioxins and polychlorinated dibenzofurans.* IARC monographs on the evaluation of carcinogenic risks to humans, 1997. **69**.

45. EFSA, P.o.C.i.t.F.C., et al., *Risk for animal and human health related to the presence of dioxins and dioxin-like PCBs in feed and food.* Efsa Journal, 2018. **16**(11): p. e05333.
46. EFSA, *Dioxins and related PCBs: tolerable intake level updated.* 2018.
47. Sorg, O., et al., *2, 3, 7, 8-tetrachlorodibenzo-p-dioxin (TCDD) poisoning in Victor Yushchenko: identification and measurement of TCDD metabolites.* The Lancet, 2009. **374**(9696): p. 1179-1185.
48. Centemeri, L., *The Seveso disaster legacy*. 2010, Ohio University Press & Swallow Press.
49. Aoki, Y., *Polychlorinated biphenyls, polychloronated dibenzo-p-dioxins, and polychlorinated dibenzofurans as endocrine disrupters—what we have learned from Yusho disease.* Environmental research, 2001. **86**(1): p. 2-11.
50. Fromme, H., et al., *PCBs, PCDD/Fs, and PBDEs in blood samples of a rural population in South Germany.* International Journal of Hygiene and Environmental Health, 2015. **218**(1): p. 41-46.
51. Henry, T.R. and M.J. DeVito, *Non-dioxin-like PCBs: effects and consideration in ecological risk assessment*. 2003: Ecological Risk Assessment Support Center, Office of Research and ….
52. EFSA, *Opinion of the Scientific Panel on contaminants in the food chain [CONTAM] related to the presence of non dioxin-like polychlorinated biphenyls (PCB) in feed and food.* EFSA Journal, 2005. **3**(11): p. 284.
53. Agudo, A., et al., *Polychlorinated biphenyls and polybrominated biphenyls*. 2016: IARC Press.
54. Commission, E., *Commission Regulation (EU) 2023/915 of 25 April 2023 on maximum levels for certain contaminants in food and repealing Regulation (EC) No 1881/2006.* Off. J. Eur. Union, 2023. **119**: p. 103-157.
55. Joob, B. and V. Wiwanitkit, *Inhalation exposure to dioxins air pollutant generated by dead body incineration at buddhist temple: Cancer risk estimation.* Indian Journal of Medical and Paediatric Oncology, 2019. **40**(S 01): p. S23-S24.
56. Eitzer, B.D. and R.A. Hites, *Vapor pressures of chlorinated dioxins and dibenzofurans.* Environmental science & technology, 1988. **22**(11): p. 1362-1364.
57. Mukerjee, D., *Health impact of polychlorinated dibenzo-p-dioxins: a critical review.* Journal of the Air & Waste Management Association, 1998. **48**(2): p. 157-165.
58. Banks, Y.B. and L.S. Birnbaum, *Absorption of 2, 3, 7, 8-tetrachlorodibenzo-p-dioxin (TCDD) after low dose dermal exposure.* Toxicology and applied pharmacology, 1991. **107**(2): p. 302-310.
59. WHO, W.H.O., *Exposure to dioxins and dioxin-like substances: a major public health concern.* Geneve: WHO, 2010.
60. Schlummer, M., G.A. Moser, and M.S. McLachlan, *Digestive tract absorption of PCDD/Fs, PCBs, and HCB in humans: mass balances and mechanistic considerations.* Toxicology and applied pharmacology, 1998. **152**(1): p. 128-137.
61. Ogura, I., *Half-life of each dioxin and PCB congener in the human body.* 2004.
62. Grimm, F.A., et al., *Metabolism and metabolites of polychlorinated biphenyls.* Critical reviews in toxicology, 2015. **45**(3): p. 245-272.
63. Abraham, K., et al., *Intake, fecal excretion, and body burden of polychlorinated dibenzo-p-dioxins and dibenzofurans in breast-fed and formula-fed infants.* Pediatric Research, 1996. **40**(5): p. 671-679.
64. Kedderis, L.B., et al., *Disposition of 2, 3, 7, 8-tetrabromodibenzo-p-dioxin and 2, 3, 7, 8-tetrachlorodibenzo-p-dioxin in the rat: Biliary excretion and induction of cytochromes CYP1A1 and CYP1A2.* Toxicology and applied pharmacology, 1991. **111**(1): p. 163-172.
65. Schecter, A., et al., *Decrease in milk and blood dioxin levels over two years in a mother nursing twins: estimates of decreased maternal and increased infant dioxin body burden from nursing.* Chemosphere, 1996. **32**(3): p. 543-549.
66. Yang, J., et al., *PCDDs, PCDFs, and PCBs concentrations in breast milk from two areas in Korea: body burden of mothers and implications for feeding infants.* Chemosphere, 2002. **46**(3): p. 419-428.
67. Rose, M., et al., *Transfer and uptake of polychlorinated dibenzo-p-dioxins and furans (PCDD/Fs) and polychlorinated biphenyls (PCBs) into meat and organs of indoor and outdoor reared pigs.* Food Additives & Contaminants: Part A, 2012. **29**(3): p. 431-448.

68. Bogdal, C., et al., *Dynamic transgenerational fate of polychlorinated biphenyls and dioxins/furans in lactating cows and their offspring.* Environmental Science & Technology, 2017. **51**(18): p. 10536-10545.
69. Thomas, G.O., A.J. Sweetman, and K.C. Jones, *Metabolism and body-burden of PCBs in lactating dairy cows.* Chemosphere, 1999. **39**(9): p. 1533-1544.
70. Lakshmanan, M., et al., *Studies on the mechanism of absorption and distribution of 2, 3, 7, 8-tetrachlorodibenzo-p-dioxin in the rat.* Journal of Pharmacology and Experimental Therapeutics, 1986. **239**(3): p. 673-677.
71. Savvateeva, D., et al., *Toxicokinetic modeling of the transfer of non-dioxin-like polychlorinated biphenyls (ndl-PCBs) from feed and soil into laying hens and their eggs.* Journal of Agricultural and Food Chemistry, 2022. **70**(42): p. 13754-13764.
72. Dobson, H., et al., *The high-producing dairy cow and its reproductive performance.* Reproduction in domestic animals, 2007. **42**: p. 17-23.
73. Savvateeva, D., et al., *Physiologically based toxicokinetic models and in silico predicted partition coefficients to estimate tetrachlorodibenzo-p-dioxin transfer from feed into growing pigs.* Archives of Toxicology, 2020. **94**(1): p. 187-196.
74. Ohlhoff, B., et al., *Unraveling Congener-Specific Transfer of Non-Dioxin-Like Polychlorinated Biphenyls (ndl-PCBs) from Feed into Chicken Meat.* Environmental Science & Technology, 2021. **55**(16): p. 11080-11090.
75. Cely-Veloza, W., M.J. Kato, and E. Coy-Barrera, *Quinolizidine-Type Alkaloids: Chemodiversity, Occurrence, and Bioactivity.* ACS omega, 2023. **8**(31): p. 27862-27893.
76. Bunsupa, S., M. Yamazaki, and K. Saito, *Quinolizidine alkaloid biosynthesis: recent advances and future prospects.* Frontiers in plant science, 2012. **3**: p. 239.
77. Wink, M. and L. Witte, *Quinolizidine alkaloids as nitrogen source for lupin seedlings and cell cultures.* Zeitschrift für Naturforschung C, 1985. **40**(11-12): p. 767-775.
78. Gresta, F., et al., *Lupins in European cropping systems*, in *Legumes in cropping systems*. 2017, CABI Wallingford UK. p. 88-108.
79. Von Baer, D. and I. Perez. *Quality standard propositions for commercial grain of white lupin (Lupinus albus)*. in *Proceedings of the 6th international lupin conference Temuco, International lupin association, Chile*. 1991.
80. Green, B.T., et al., *The serum concentrations of lupine alkaloids in orally-dosed Holstein cattle.* Research in Veterinary Science, 2015. **100**: p. 239-244.
81. Green, B.T., et al., *Differences between Angus and Holstein cattle in the Lupinus leucophyllus induced inhibition of fetal activity.* Toxicon, 2015. **106**: p. 1-6.
82. Gay, C.C., et al., *Comparison of plasma disposition of alkaloids after lupine challenge in cattle that had given birth to calves with lupine-induced arthrogryposis or clinically normal calves.* American journal of veterinary research, 2004. **65**(11): p. 1580-1583.
83. Krishnan, K. and T. Peyret, *Physiologically based toxicokinetic (PBTK) modeling in ecotoxicology.* Ecotoxicology modeling, 2009: p. 145-175.
84. Teorell, T., *Kinetics of distribution of substances administered to the body, I: The extravascular modes of administration.* Archives internationales de pharmacodynamie et de therapie, 1937. **57**: p. 205-225.
85. Andersen, M.E., *Toxicokinetic modeling and its applications in chemical risk assessment.* Toxicology letters, 2003. **138**(1-2): p. 9-27.
86. Graham, H., et al., *Comparison of in-vivo and in-silico methods used for prediction of tissue: plasma partition coefficients in rat.* Journal of Pharmacy and Pharmacology, 2012. **64**(3): p. 383-396.
87. Upton, R.N., D.J. Foster, and A.Y. Abuhelwa, *An introduction to physiologically-based pharmacokinetic models.* Pediatric Anesthesia, 2016. **26**(11): p. 1036-1046.
88. Tremolada, P., et al., *Predicting PCB concentrations in cow milk: validation of a fugacity model in high-mountain pasture conditions.* Science of the total environment, 2014. **487**: p. 471-480.
89. Robinson, R.C., *An introduction to dynamical systems: continuous and discrete*. Vol. 19. 2012: American Mathematical Soc.

90. Bullo, F., *Lectures on network systems*. 1.6 ed. 2022: Kindle Direct Publishing Seattle, DC, USA.
91. Anderson, D.H., *Compartmental modeling and tracer kinetics*. Vol. 50. 2013: Springer Science & Business Media.
92. Schrag, M. and K. Regal, *Pharmacokinetics and toxicokinetics*, in *A Comprehensive Guide to Toxicology in Nonclinical Drug Development*. 2013, Elsevier. p. 69-106.
93. Srinivasan, B., *A guide to the Michaelis–Menten equation: steady state and beyond.* The FEBS journal, 2022. **289**(20): p. 6086-6098.
94. Biswas, B., et al., *A discussion on Euler method: A review.* Electronic Journal of Mathematical Analysis and Applications, 2013. **1**(2): p. 2090-2792.
95. Butcher, J.C., *Numerical methods for ordinary differential equations*. 2016: John Wiley & Sons.
96. Albicker, J., *The Gauß-Newton Method and its Implementation in the Optimization Library Oppy*. 2022.
97. Gavin, H.P., *The Levenberg-Marquardt algorithm for nonlinear least squares curve-fitting problems.* Department of civil and environmental engineering, Duke University, 2019. **19**.
98. Jianchao, Y. and C.T. Chern. *Comparison of Newton-Gauss with Levenberg-Marquardt algorithm for space resection*. in *22nd asian conference on remote sensing*. 2001.
99. Häußler, W., *A local convergence analysis for the Gauss-Newton and Levenberg-Morrison-Marquardt Algorithms.* Computing (Wien. Print), 1983. **31**(3): p. 231-244.
100. Georgioudakis, M. and V. Plevris, *A comparative study of differential evolution variants in constrained structural optimization.* Frontiers in Built Environment, 2020. **6**: p. 102.
101. Pellicanò, F., et al., *A population approach for the estimation of methylmercury ToxicoKinetics in red mullets.* Toxicology and Applied Pharmacology, 2021. **428**: p. 115679.
102. Garay, A.M., et al., *Linear censored regression models with scale mixtures of normal distributions.* Statistical Papers, 2017. **58**: p. 247-278.
103. Oyeyemi, G., *Comparison of bootstrap and jackknife methods of re-sampling in estimating population parameters.* Global Journal of Pure and Applied Sciences, 2008. **14**(2): p. 217-220.
104. Student, *The probable error of a mean.* Biometrika, 1908. **6**(1): p. 1-25.
105. Welch, B.L., *The generalization of 'STUDENT'S'problem when several different population varlances are involved.* Biometrika, 1947. **34**(1-2): p. 28-35.
106. Wilcoxon, F., *Individual comparisons by ranking methods*, in *Breakthroughs in Statistics: Methodology and Distribution*. 1992, Springer. p. 196-202.
107. Mann, H.B. and D.R. Whitney, *On a test of whether one of two random variables is stochastically larger than the other.* The annals of mathematical statistics, 1947: p. 50-60.
108. Krause, T., et al., *Transfer of Polychlorinated Dibenzo-p-dioxins and Dibenzofurans (PCDD/Fs) and Polychlorinated Biphenyls (PCBs) from Oral Exposure into Cow's Milk-Part I: State of Knowledge and Uncertainties.* Nutrition research reviews, 2022: p. 1-53.
109. Moenning, J.-L., et al., *Transfer of polychlorinated dibenzo-p-dioxins and dibenzofurans (PCDD/Fs) and polychlorinated biphenyls (PCBs) from oral exposure into cow's milk – part II: toxicokinetic predictive models for risk assessment.* Nutrition Research Reviews, 2023. **36**(2): p. 484-497.
110. Hendriks, A.J., H. Smítková, and M.A. Huijbregts, *A new twist on an old regression: Transfer of chemicals to beef and milk in human and ecological risk assessment.* Chemosphere, 2007. **70**(1): p. 46-56.
111. Derks, H., et al., *Pharmacokinetic modeling of polychlorinated dibenzo-p-dioxins (PCDDs) and furans (PCDFs) in cows.* Chemosphere, 1994. **28**(4): p. 711-715.
112. McLachlan, M.S., *Model of the fate of hydrophobic contaminants in cows.* Environmental science & technology, 1994. **28**(13): p. 2407-2414.
113. Hoogenboom, R., et al., *Kaolinic clay derived PCDD/Fs in the feed chain from a sorting process for potatoes.* Chemosphere, 2010. **78**(2): p. 99-105.
114. Rosenbaum, R.K., T.E. McKone, and O. Jolliet, *CKow: a dynamic model for chemical transfer to meat and milk.* Environmental science & technology, 2009. **43**(21): p. 8191-8198.

115. Moenning, J.-L., et al., *Transfer and toxicokinetic modeling of non-dioxin-like polychlorinated biphenyls (ndl-PCBs) into accidentally exposed dairy cattle and their calves-A case report.* Environmental Toxicology and Pharmacology, 2023. **99**: p. 104106.
116. Moenning, J.-L., et al., *Toxicokinetic modeling of the transfer of polychlorinated biphenyls (PCBs) and polychlorinated dibenzo-p-dioxins and dibenzofurans (PCDD/Fs) into milk of high-yielding cows during negative and positive energy balance.* Computational Toxicology, 2023: p. 100290.
117. Krause, T., et al., *Experimental Study on the Transfer of Polychlorinated Biphenyls (PCBs) and Polychlorinated Dibenzo-p-dioxins and Dibenzofurans (PCDD/Fs) into Milk of High-Yielding Cows during Negative and Positive Energy Balance.* Journal of Agricultural and Food Chemistry, 2023. **71**(36): p. 13495-13507.
118. Birnbaum, L.S., *Distribution and excretion of 2, 3, 7, 8-tetrachlorodibenzo-p-dioxin in congenic strains of mice which differ at the Ah locus.* Drug metabolism and disposition, 1986. **14**(1): p. 34-40.
119. Rose, J., et al., *The fate of 2, 3, 7, 8-tetrachlorodibenzo-p-dioxin following single and repeated oral doses to the rat.* Toxicology and applied pharmacology, 1976. **36**(2): p. 209-226.
120. Adolphs, J., et al., *A probabilistic model for the carry-over of PCDD/Fs from feed to growing pigs.* Chemosphere, 2013. **93**(3): p. 474-479.
121. Moenning, J.-L., et al., *Toxicokinetic modelling of the transfer of non-dioxin like polychlorinated biphenyls from feed into edible tissues of pigs.* Science of The Total Environment, 2023: p. 164539.
122. Engel, A.M., et al., *Investigations on the transfer of quinolizidine alkaloids from Lupinus angustifolius into the milk of dairy cows.* Journal of Agricultural and Food Chemistry, 2022. **70**(37): p. 11749-11758.
123. Okour, M. and R.C. Brundage, *Modeling enterohepatic circulation.* Current Pharmacology Reports, 2017. **3**: p. 301-313.

Supplementary Material

Paper 1

Moenning, J.-L., et al., Transfer of polychlorinated dibenzo-p-dioxins and dibenzofurans (PCDD/Fs) and polychlorinated biphenyls (PCBs) from oral exposure into cow's milk – part II: toxicokinetic predictive models for risk assessment. Nutrition Research Reviews, 2023. 36(2): p. 484-497.

Supplementary Material
Transfer of Polychlorinated Dibenzo-p-dioxins and Dibenzofurans (PCDD/Fs) and Polychlorinated Biphenyls (PCBs) from Oral Exposure into Cow's Milk - Part II: Toxicokinetic Predictive Models for Risk Assessment

Authors

Jan-Louis Moenning[1] ORCiD 0000-0002-9457-7032
Torsten Krause[2] ORCiD 0000-0002-2080-7843
Julika Lamp[2] ORCiD 0000-0001-6412-4123
Ronald Maul[2] ORCiD none
Hans Schenkel[3] ORCiD 0000-0002-6278-0810
Peter Fürst[4] ORCiD none
Robert Pieper[1] ORCiD 0000-0002-0292-1482
Jorge Numata[*,1], ORCiD 0000-0002-0033-4436

[1] German Federal Institute for Risk Assessment (BfR), Department Safety in the Food Chain, Max-Dohrn-Straße 8-10, 10589, Berlin, Germany
[2] Max Rubner-Institut, Department of Safety and Quality of Milk and Fish, Hermann-Weigmann-Straße 1, 24103, Kiel, Germany
[3] Department of Animal Nutrition, University of Hohenheim, Emil-Wolff-Str. 10, 70599 Stuttgart, Germany
[4] Chemical and Veterinary Analytical Institute Münsterland-Emscher-Lippe (CVUA-MEL), Joseph-König-Straße 40, 48147 Münster, Germany
[*] Corresponding author: jorge.numata@bfr.bund.de, +49-30-184120

Chapter S-1: 2-compartment model

The matrix form of this model is given by

$$\frac{d}{dt}A(t) = MA(t) + I, \tag{S1}$$

with transition matrix M given by

$$\begin{pmatrix} -k_{Cent-Fat} - k_{Milk} & k_{Fat-Cent} \\ k_{Cent-Fat} & -k_{Fat-Cent} \end{pmatrix} \tag{S2}$$

and the input vector

$$I = \begin{pmatrix} F_{abs}Dose \\ 0 \end{pmatrix} \tag{S3}$$

for the given quantity vector

$$A(t) = \begin{pmatrix} A_{Cent}(t) \\ A_{Fat}(t) \end{pmatrix}. \tag{S4}$$

Chapter S-2: The original model by Derks

The matrix form of this model is given by

$$\frac{d}{dt}A(t) = MA(t) + I \tag{S5}$$

with transition matrix M given by

$$\begin{pmatrix} -\frac{F_Q Q_{Fat}+\sum_i Q_i}{V_{blood}} & \frac{F_Q Q_{Fat}}{V_{blood}} & \frac{Q_{Liver}}{V_{blood}} & \frac{Q_{Rich}}{V_{blood}} & \frac{Q_{Slow}}{V_{blood}} & \frac{Q_{Rich}}{V_{blood}} & \frac{Q_{Udder}}{V_{blood}} \\ \frac{F_Q Q_{Fat}}{V_{Fat} P_{Fat}} & -\frac{F_Q Q_{Fat}}{V_{Fat} P_{Fat}} & 0 & 0 & 0 & 0 & 0 \\ \frac{Q_{Liver}}{V_{Liver} P_{Liver}} & 0 & -\frac{Q_{Liver}}{V_{Liver} P_{Liver}} - k_{met} & 0 & 0 & 0 & 0 \\ \frac{Q_{Rich}}{V_{Rich} P_{Rich}} & 0 & 0 & -\frac{Q_{Rich}}{V_{Rich} P_{Rich}} & 0 & 0 & 0 \\ \frac{Q_{Slow}}{V_{Slow} P_{Slow}} & 0 & 0 & 0 & -\frac{Q_{Slow}}{V_{Slow} P_{Slow}} & 0 & 0 \\ \frac{Q_{Udder}}{V_{Udder} P_{Udder}} & 0 & 0 & 0 & 0 & -\frac{Q_{Udder}}{V_{Udder} P_{Udder}} & -\frac{CL_M}{V_{Udder}} \end{pmatrix} \tag{S6}$$

and the input vector

$$I = \begin{pmatrix} 0 \\ 0 \\ F_{abs} Dose \\ 0 \\ 0 \\ 0 \end{pmatrix} \tag{S7}$$

for the given state, or "quantity", vector

$$A(t) = \begin{pmatrix} A_{Blood}(t) \\ A_{Fat}(t) \\ A_{Liver}(t) \\ A_{Rich}(t) \\ A_{Slow}(t) \\ A_{Udder}(t) \end{pmatrix}. \tag{S8}$$

Chapter S-3: Derks model without udder compartment

The matrix form of this model is given by

$$\frac{d}{dt}A(t) = MA(t) + I \tag{S9}$$

with transition matrix M given by

$$\begin{pmatrix} -\frac{F_Q Q_{Fat}+\sum_i Q_i}{V_{Blood}} - CL_{Milk}P_{Milk} & \frac{F_Q Q_{Fat}}{V_{Fat}P_{Fat}} & \frac{Q_{Liver}}{V_{Liver}P_{Liver}} & \frac{Q_{Rich}}{V_{Rich}P_{Rich}} & \frac{Q_{Slow}}{V_{Slow}P_{Slow}} \\ \frac{F_Q Q_{Fat}}{V_{blood}} & -\frac{F_Q Q_{Fat}}{V_{Fat}P_{Fat}} & 0 & 0 & \\ \frac{Q_{Liver}}{V_{blood}} & 0 & -\frac{Q_{Liver}}{V_{Liver}P_{Liver}} - k_{met} & 0 & 0 \\ \frac{Q_{Rich}}{V_{blood}} & 0 & 0 & -\frac{Q_{Rich}}{V_{Rich}P_{Rich}} & 0 \\ \frac{Q_{Slow}}{V_{blood}} & 0 & 0 & 0 & -\frac{Q_{Slow}}{V_{Slow}P_{Slow}} \end{pmatrix} \tag{S10}$$

and the input vector

$$I = \begin{pmatrix} 0 \\ 0 \\ F_{abs}Dose \\ 0 \\ 0 \end{pmatrix} \tag{S11}$$

for the given quantity vector

$$A(t) = \begin{pmatrix} A_{Blood}(t) \\ A_{Fat}(t) \\ A_{Liver}(t) \\ A_{Rich}(t) \\ A_{Slow}(t) \end{pmatrix}. \tag{S12}$$

Chapter S-4: The original fugacity model by McLachlan

As this model only contains a single differential equation it can be reformulated into the form

$$\frac{d}{dt}(f_{Fat}(t)V_{Fat}Z_{Fat}) = Mf_{Fat}(t) + I. \tag{S13}$$

Here

$$M = \left(1 - \frac{D_{Dig-Blood}Dose}{D_{Blood}D_{Dig}}\right)^{-1} \frac{D_{Blood-Fat}^2}{D_{Blood}} - D_{Blood-Fat}, \tag{S14}$$

$$I = \left(1 - \frac{D_{Dig-Blood}Dose}{D_{Blood}D_{Dig}}\right)^{-1} \left(\frac{D_{Dig-Blood}D_{Blood-Fat}Dose}{D_{Blood}D_{Dig}}\right). \tag{S15}$$

with

$$D_{Blood} := D_{Dig-Blood} + D_{Milk} + D_{Blood-Fat} + D_{Blood-Meta}, \tag{S16}$$

$$D_{Dig} := D_{Dig-Blood} + D_{Exc} + D_{Dig-Meta}. \tag{S17}$$

The other two fugacities can then be calculated by

$$f_{Blood} = \left(1 - \frac{D_{Dig-Blood}Dose}{D_{Blood}D_{Dig}}\right)^{-1} \left(\frac{D_{Blood-Fat}f_{Fat}}{D_{Blood}} + \frac{D_{Dig-Blood}Dose}{D_{Blood}D_{Dig}}\right) \tag{S18}$$

$$f_{Dig} = \frac{Dose + f_{Blood}D_{Blood-Dig}}{D_{Dig}} \tag{S19}$$

Chapter S-5: The fugacity model by Binelli

The matrix form of this model is given by

$$\frac{d}{dt}f(t) = Mf(t) + I \tag{S20}$$

with transition matrix M given by

$$\begin{pmatrix} -\frac{D_{Exc}+D_{Dig-Meta}}{V_{Dig}Z_{Dig}} & \frac{D_{Blood-Dig}}{V_{Dig}Z_{Dig}} & 0 \\ \frac{D_Blood-Dig}{V_{Blood}Z_{Blood}} & -\frac{D_{Blood-Dig}+D_{Blood-fat}+D_{Milk}+D_{Blood-Meta}}{V_{Blood}Z_{Blood}} & \frac{D_{Blood-Fat}}{V_{Blood}Z_{Blood}} \\ 0 & \frac{D_{Blood-Fat}}{V_{Fat}Z_{Fat}} & -\frac{D_{Blood-Fat}}{V_{Fat}Z_{Fat}} \end{pmatrix} \tag{S21}$$

and the input vector

$$I = \begin{pmatrix} \frac{D_{Grass}f_{Grass}+D_{Conc}f_{Conc}+D_{Soil}f_{Soil}}{V_{Dig}Z_{Dig}} \\ 0 \\ 0 \end{pmatrix} \tag{S22}$$

for the given quantity vector

$$f(t) = \begin{pmatrix} f_{Dig}(t) \\ f_{Blood}(t) \\ f_{Fat}(t) \end{pmatrix}. \tag{S23}$$

Chapter S-6: MacLachlans PBPK model

The matrix form of this model is given by

$$\frac{d}{dt}A(t) = MA(t) + I \tag{S24}$$

with transition matrix M given by

$$
\begin{pmatrix}
-\frac{FQQ_{Fat}+\sum_i Q_i}{V_{Blood}} & \frac{FQQ_{Fat}}{V_{Fat}P_{Fat}} & \frac{Q_{Liver}}{V_{Liver}P_{Liver}} & \frac{Q_{Muscle}}{V_{Muscle}P_{Muscle}} & \frac{Q_{kidney}}{V_{kidney}P_{Kidney}} & \frac{Q_{Rest}}{V_{Rest}P_{Rest}} & \frac{Q_{Udder}}{V_{Udder}P_{Udder}} & 0 \\
\frac{FQQ_{Fat}}{V_{Blood}} & -\frac{FQQ_{Fat}}{V_{Fat}P_{Fat}} & 0 & 0 & 0 & 0 & 0 & 0 \\
\frac{Q_{Liver}}{V_{Blood}} & 0 & -\frac{Q_{Liver}}{V_{Liver}P_{Liver}} - \frac{k_{met}}{P_{Liver}} & 0 & 0 & 0 & 0 & 0 \\
\frac{Q_{Muscle}}{V_{Blood}} & 0 & 0 & -\frac{Q_{Muscle}}{V_{Muscle}P_{Muscle}} & 0 & 0 & 0 & 0 \\
\frac{Q_{Kidney}}{V_{Blood}} & 0 & 0 & 0 & -\frac{Q_{Kidney}}{V_{Kidney}P_{Kidney}} & 0 & 0 & 0 \\
\frac{Q_{Rest}}{V_{Rest}} & 0 & 0 & 0 & 0 & -\frac{Q_{Rest}}{V_{Rest}P_{Rest}} & 0 & 0 \\
\frac{Q_{Rich}}{V_{Udder}} & 0 & 0 & 0 & 0 & 0 & -\frac{Q_{Udder}}{V_{Udder}P_{Udder}} - \frac{CL_M P_{Udder}}{V_{Udder}} & 0 \\
0 & 0 & 0 & 0 & 0 & 0 & 0 & -k_a
\end{pmatrix}
\tag{S25}
$$

and the input vector

$$I = \begin{pmatrix} 0 \\ 0 \\ 0 \\ 0 \\ 0 \\ 0 \\ 0 \\ Dose \end{pmatrix} \tag{S26}$$

for given quanitiy vector

$$A(t) = \begin{pmatrix} A_{Blood}(t) \\ A_{Fat}(t) \\ A_{Liver}(t) \\ A_{Muscle}(t) \\ A_{Kidney}(t) \\ A_{Rest}(t) \\ A_{Udder}(t) \\ A_{Rumen}(t) \end{pmatrix}. \tag{S27}$$

Chapter S-7: Solving the linear differential equations

A stable linear differential equation of the form

$$\frac{d}{dt}A(t) = MA(t) + I \tag{S28}$$

with a n-dimensional matrix M (stability $\Rightarrow$ M is invertible) and constant vector I has a unique solution, which is given by

$$A(t) = x^* + e^{Mt}(x_0 - x^*) \tag{S29}$$

with

$$x^* = -M^{-1}I \tag{S30}$$

and x_0 being the starting condition. Additionally, it holds true that

$$A(t) \overset{t\to\infty}{\to} x^*, \tag{S31}$$

which means that x^* is the steady state of our system.
Note that the stability condition for the equation (S28) is met if and only if the real parts of all eigenvalues of M are all negative. Intuitively, this means that if the input vector $I \equiv 0$ then for any given starting contamination the systems total contamination would converge to 0 over time, which is always given for our systems due to the constant excretion via milk fat, i.e. for all here presented models the differential equation (S28) is stable.
During the depuration phase our system can be described by the following differential equation

$$\frac{d}{dt}A_D(t) = MA_D(t) \tag{S32}$$

and it's solution is given by

$$A_D(t) = e^{Mt}x_{0,D}, \tag{S33}$$

where $x_{0,D}$ is starting vector of the depuration phase. Note here that we do not need the stability assumption from above for this solution to be valid.

For deriving a more explicit formula using either equation (S29) or equation (S33), the most difficult part to write down explicitly is the exponential e^{Mt}. This can be simplified if M is diagonalizable, i.e., there exists an invertible matrix S such that

$$M = SDS^{-1} \tag{S34}$$

with D being diagonal matrix containing the eigenvalues of M on it's diagonal. Then

$$e^{Mt} = Se^{Dt}S^{-1} = \sum_{i=1}^{n} C_i e^{\lambda_i t}, \tag{S35}$$

where C_i are constant matrices and λ_i are the eigenvalues of M, which means that the exponential rate constants are given by the eigenvalues of M. The eigenvalues λ_i can be quite efficiently computed via numerical methods.
Note that the diagonalization condition is met if all eigenvalues of M are unique, i.e. we have n different eigenvalues.

Paper 2

Moenning, J.-L., et al., Transfer and toxicokinetic modeling of non-dioxin-like polychlorinated biphenyls (ndl-PCBs) into accidentally exposed dairy cattle and their calves-A case report. Environmental Toxicology and Pharmacology, 2023. **99**: p. 104106.

Supplementary Material

Transfer and toxicokinetic modeling of non-dioxin-like polychlorinated biphenyls (ndl-PCBs) into accidentally exposed dairy cattle and their calves - a case report

Jan-Louis Moenning[1] ORCiD 0000-0002-9457-7032 Contribution: Methodology, Software, Formal analysis, Visualization, Writing - Original Draft

Jorge Numata[1] ORCiD 0000-0002-0033-4436 Contribution: Conceptualization, Methodology Validation, Writing - Review & Editing

Dorit Bloch[1] Contribution: Writing - Original Draft

Anne Jahnke[1] ORCiD 0000-0001-9304-7737, Contribution: Sample analysis and Quantification, Writing

Helmut A. Schafft[1] ORCiD 0000-0001-9212-0074, Contribution: Conceptualization

Markus Spolders[1] ORCiD 0000-0002-4405-1497, Contribution: Conceptualization, Veterinary Care and Control

Anja Lüth ORCiD[1] 0000-0002-4752-9345, Contribution: Coordination of sample analysis, Writing

Monika Lahrssen-Wiederholt[1] Contribution: Conceptualization

Kirsten Schulz[1] ORCiD 0000-0002-0090-761X Contribution: Investigation, Project administration, Data Curation, Visualization, Writing - Original Draft

[1] *German Federal Institute for Risk Assessment, Berlin, Germany*

Correspondence to: Kirsten Schulz, German Federal Institute for Risk Assessment, Max-Dohrn-Str. 8-10, 10589 Berlin, Germany, email: kirsten.schulz@bfr.bund.de

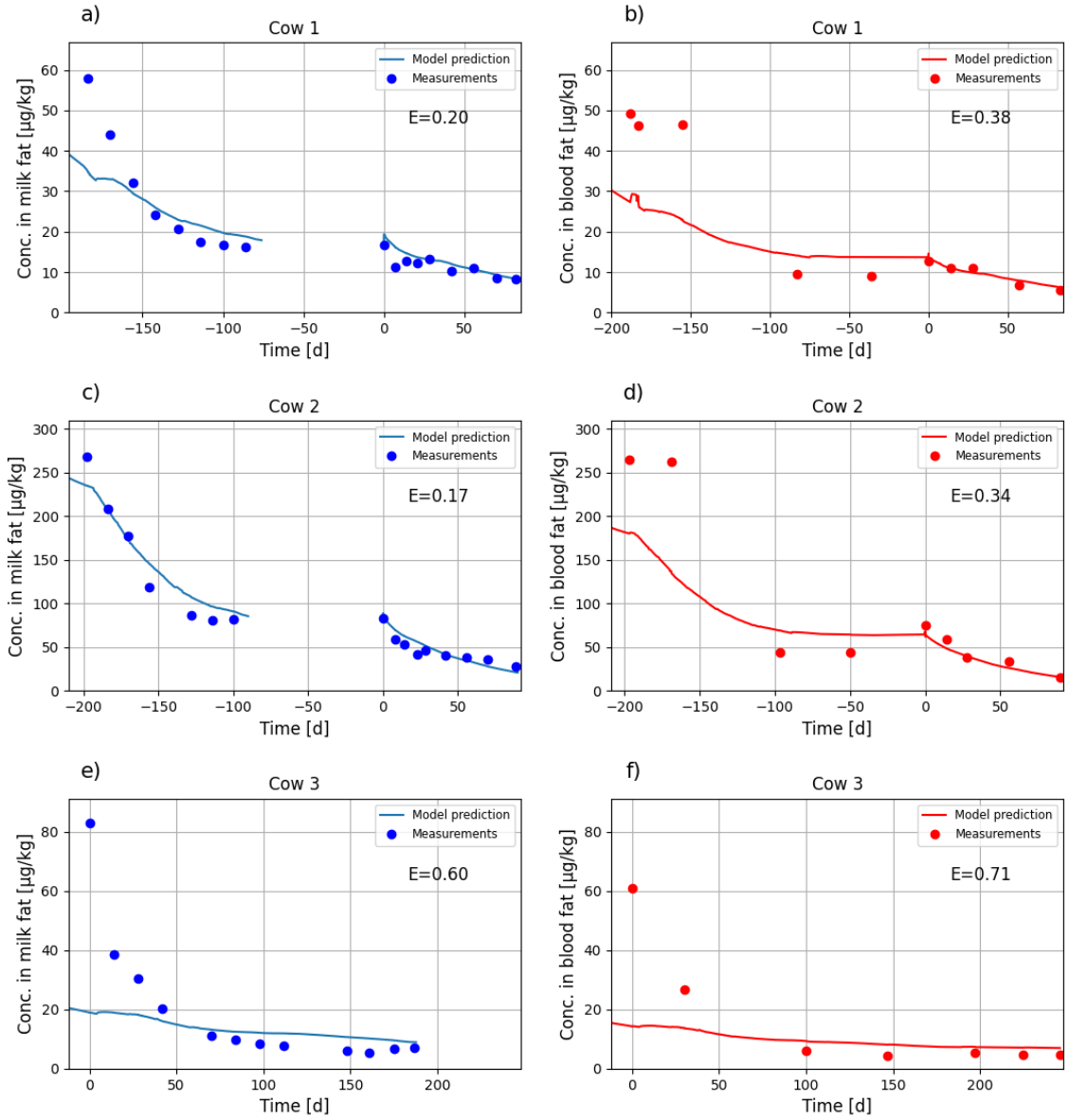

Figure S1: Ct-profile of ndl-PCB-153 in milk fat (a,c,e) and blood fat (b,d,f) of the three cows derived from the model (solid line) and from experimental data (dots). Cow 1 and 2 were impregnated at our site. The time $t = 0$ represents calving. Cow 3 was not pregnant. Here, the time $t = 0$ characterizes the day of arrival and the associated start of monitoring. Model accuracy is described via the root mean square error E of the log-concentrations (basis e).

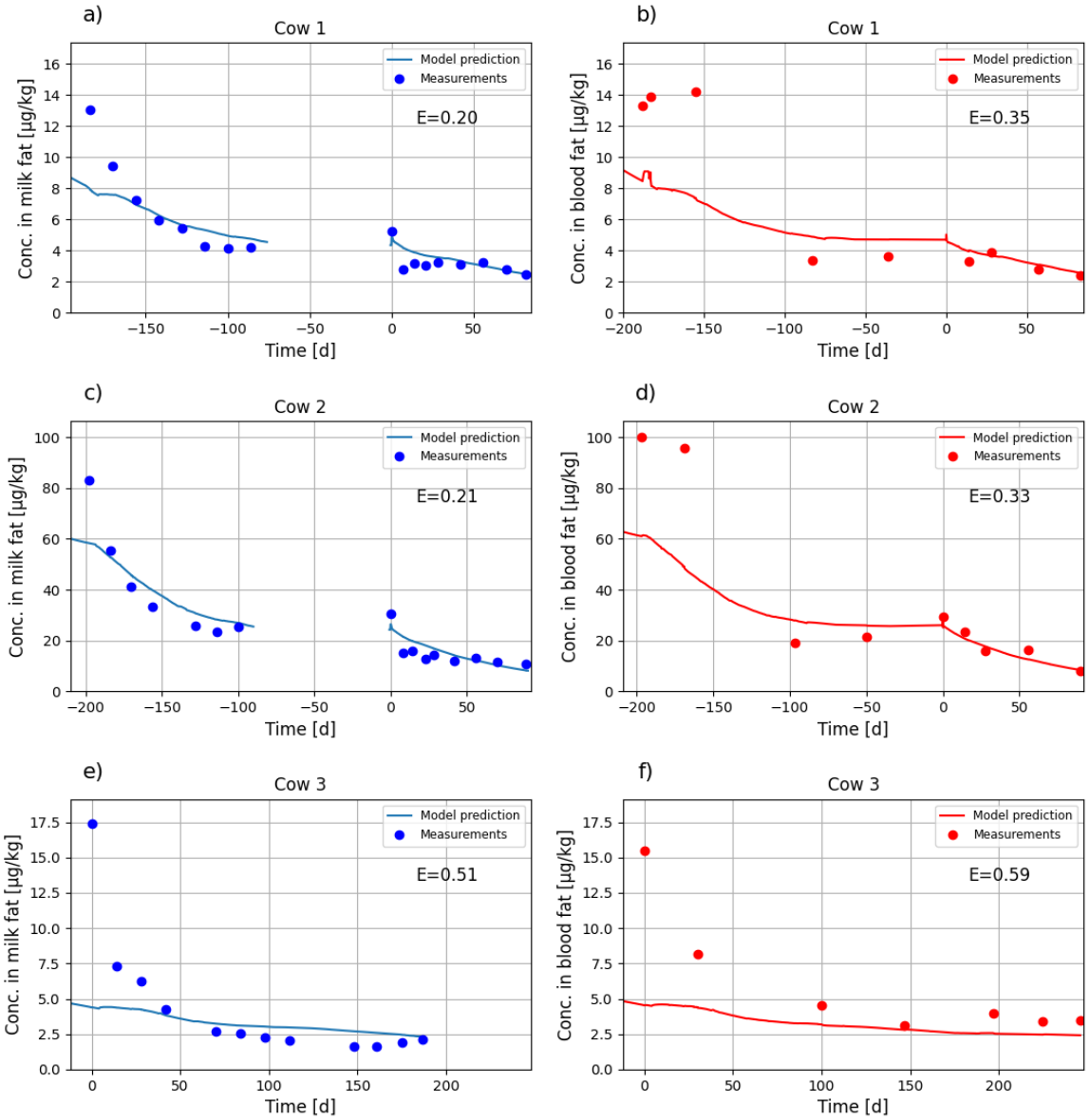

Figure S2: Ct-profile of ndl-PCB-180 in milk fat (a,c,e) and blood fat (b,d,f) of the three cows derived from the model (solid line) and from experimental data (dots). Cow 1 and 2 were impregnated at our site. The time $t = 0$ represents calving. Cow 3 was not pregnant. Here, the time $t = 0$ characterizes the day of arrival and the associated start of monitoring. Model accuracy is described via the root mean square error E of the log-concentrations (basis e).

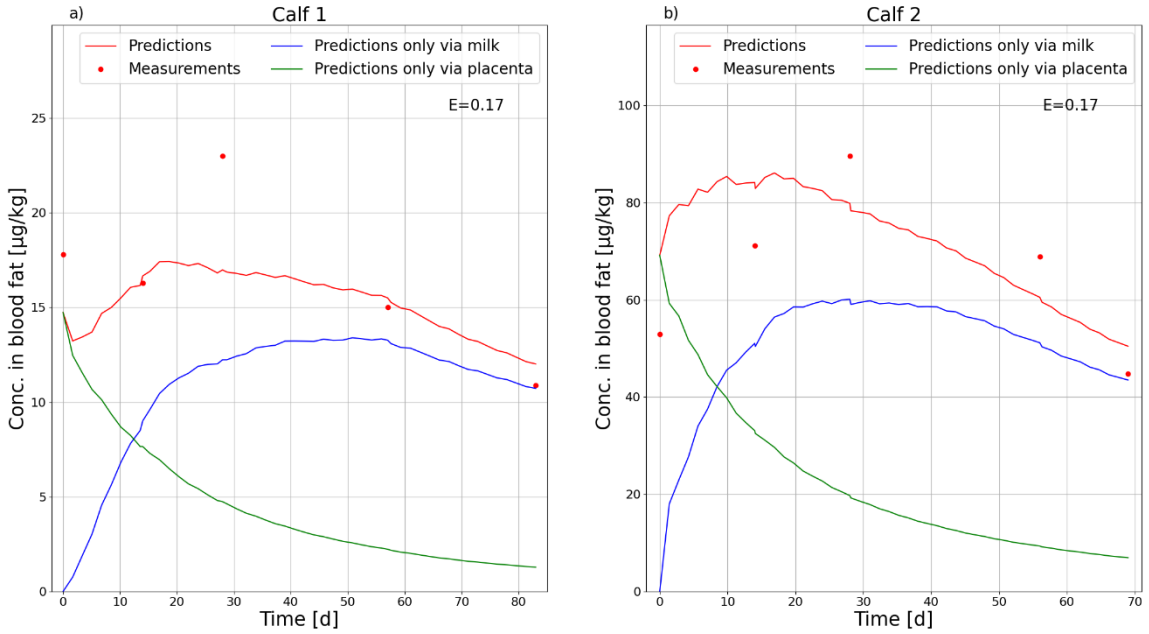

Figure S2: Ct-profile of ndl-PCB-153 in blood fat for the Calf 1 (a) and Calf 2 (b) derived from the model (solid line) and from the experimental data (dots). The input amounts via placenta or milk fat are from the simulations of the mother cow shown in Figure S2. In addition to the prediction of the total concentration (red line), the contributions from transfer via placenta (green line) and from consumed milk fat (blue line) are shown. Model accuracy is describe via the root mean square error E of the log-concentrations.

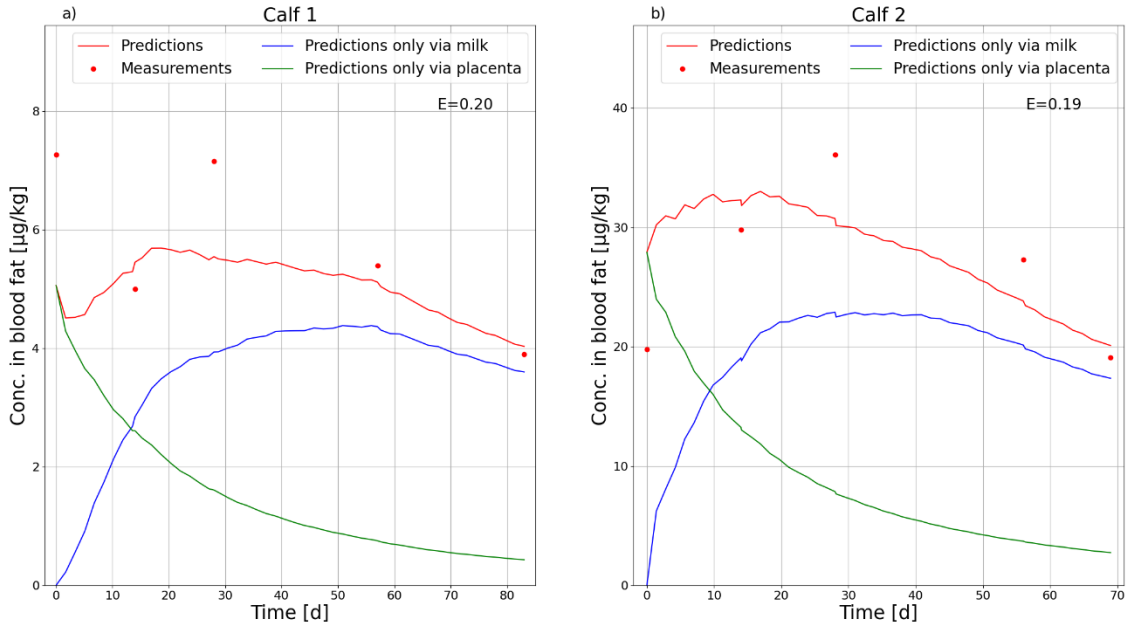

Figure S3 : Ct-profile of ndl-PCB-180 in blood fat for the Calf 1 (a) and Calf 2 (b) derived from the model (solid line) and from the experimental data (dots). The input amounts via placenta or milk fat are from the simulations of the mother cow shown in Figure S2. In addition to the prediction of the total concentration (red line), the contributions from transfer via placenta (green line) and from consumed milk fat (blue line) are shown. Model accuracy is describe via the root mean square error E of the log-concentrations.

Table S1: Comparison of the predicted and measured concentrations [µg/kg] of PCB-138 in all compartment's fats of the model.

	Cow 1		Cow 2		Calf 1		Calf 2	
	Observed	Predicted	Observed	Predicted	Observed	Predicted	Observed	Predicted
Liver	28.25	32.94	108.39	109.35	65.93	77.18	181.20	322.45
Adipose	10.03	11.65	42.55	40.39	23.78	18.76	67.34	77.01
Richly perfused	-	2.42	-	8.03	-	5.59	-	23.34
Slowly perfused	9.10	9.28	37.99	31.36	19.78	21.40	70.76	89.63
Udder	5.94	7.11	32.99	23.44	-	-	-	-

Table S2: Comparison of the predicted and measured concentrations [µg/kg] of PCB-153 in all compartment's fats of the model.

	Cow 1		Cow 2		Calf 1		Calf 2	
	Observed	Predicted	Observed	Predicted	Observed	Predicted	Observed	Predicted
Liver	20.89	29.55	72.76	100.90	65.93	57.35	181.20	240.72
Adipose	11.01	15.12	44.21	53.46	23.78	21.11	67.34	86.99
Richly perfused	-	3.74	-	12.77	-	7.16	-	30.04
Slowly perfused	10.54	12.80	43.72	44.37	19.78	24.44	70.76	102.77
Udder	6.21	8.33	39.12	38.29	-	-	-	-

Table S3: Comparison of the predicted and measured concentrations [µg/kg] of PCB-180 in all compartment's fats of the model

	Cow 1		Cow 2		Calf 1		Calf 2	
	Observed	Predicted	Observed	Predicted	Observed	Predicted	Observed	Predicted
Liver	7.61	10.24	34.84	42.81	20.58	16.31	59.54	81.25
Adipose	5.27	5.66	27.64	24.29	5.80	6.77	22.78	33.05
Richly perfused	-	1.84	-	7.68	-	2.88	-	14.36
Slowly perfused	4.59	4.78	21.73	20.21	6.19	7.49	23.90	37.32
Udder	2.27	2.49	19.08	10.36	-	-	-	-

Paper 3

Moenning, J.-L., et al., Toxicokinetic modeling of the transfer of polychlorinated biphenyls (PCBs) and polychlorinated dibenzo-p-dioxins and dibenzofurans (PCDD/Fs) into milk of high-yielding cows during negative and positive energy balance. Computational Toxicology, 2023: p. 100290

Supplementary Material

Toxicokinetic modeling of the transfer of polychlorinated biphenyls (PCBs), polychlorinated dibenzo-p-dioxins and dibenzofurans (PCDD/Fs) into milk of high-yielding cows during negative and positive energy balance

Jan-Louis Moenning[1], Julika Lamp[2], Karin Knappstein[2], Joachim Molkentin[2], Andreas Susenbeth[3], Karl-Heinz Schwind[4], Sven Dänicke[5], Peter Fürst[6], Hans Schenkel[7], Robert Pieper[1], Torsten Krause[2], Jorge Numata[1]

[1]Department Safety in the Food Chain, German Federal Institute for Risk Assessment (BfR), Max-Dohrn-Straße 8-10, 10589 Berlin, Germany

[2]Department of Safety and Quality of Milk and Fish Products, Max Rubner-Institut (MRI), Hermann-Weigmann-Str. 1, 24103 Kiel, Germany

[3]Institute of Animal Nutrition and Physiology, Kiel University (CAU), 24118 Kiel, Germany

[4]Department of Quality and Safety of Meat, Max Rubner-Institut (MRI), E.-C.-Baumann-Str. 20, 95326 Kulmbach, Germany

[5]Institute of Animal Nutrition, German Federal Research Institute for Animal Health, Friedrich-Loeffler-Institut (FLI), Bundesallee 37, 38116 Braunschweig, Germany

[6]Chemical and Veterinary Analytical Institute Münsterland-Emscher-Lippe (CVUA-MEL), Joseph-König-Straße 40, 48147 Münster, Germany

[7]Department of Animal Nutrition, University of Hohenheim, Emil-Wolff-Str. 10, 70599 Stuttgart, Germany

Estimation of transfer parameters

Half-lives

By application of the model half-lives can be derived with the transition matrix $M_{i,j}$ in equation (1). For this, the eigenvalues k_1,k_2,k_3<0 [1/d] of $M_{i,j}$ are determined and then the half-lives are given by

$$t_{1/2,i} = -\frac{ln(2)}{k_i} \text{ for i in } \{1,2,3\}. \quad (S1)$$

The longest is the β-half-life and the second longest is the α-half-life. The remaining shortest half-life will not be discussed further as it is practically unobservable.

Transfer rates

The transfer rate can be easily derived from the model parameter as they are simply given by the absorption fraction of feed and bolus respectively, i.e., feed and bolus lead to different transfer

rates. The *TR*s given in this paper always refer to the bolus, since feeds are only presented as background contamination, the concentration of which is often too low to be reliably estimated.

Time until steady state

The time until steady state (T_{ss}) is defined here as the time required to reach 90% of the steady state concentrations. T_{ss} was determined by simulating the concentration-time course of contamination in milk fat after constant dosing with a bolus until 90% of the steady-state concentration was reached.

Mean residence times

The mean residence time (MRE), i.e., the average time of a contaminant molecule in the cow's body before it is excreted in the milk, can be calculated using the following formula

$$MRT = \pi_{blood}\left(\int_0^{\infty} te^{M_{jt}}(1,0,0)^T dt\right) P_{Milk,j} CL_{Milk} \qquad (S2)$$

$$= \pi_{blood}(M_j{}^{-2}(1,0,0)^T) P_{Milk,j} CL_{Milk}, \qquad (S3)$$

where π_{blood} is canonical projection onto the blood compartment.

The MRT can then be used to calculate the MRT in each respective compartment k by multiplying it with the normalized (to the sum) vector containing the relative amounts in each compartment in steady state $\frac{A_{ss,k}}{sum(A_{ss})}$. The steady state is given by $A_{ss} = M^{-1}I$ with $I = (1,0,0)^T$.

Furthermore $\ln(2)$MRT also reflects in a certain sense the average half-life of the contaminant.

Transition times

The transition times represent the time that elapses from steady-state to reaching the beta phase of elimination during the depuration phase.

To calculate this parameter it is assumed that there are only 2 relevant half-lives, i.e. there exist A, B>0, so that

$A_{blood}(t) \approx Ae^{k_2 t} + Be^{k_3 t}$,

where $A_{blood}(t)$ describes the total amount of contaminant during depuration. Then the transition time $\hat{t}$ is defined as

$$\frac{d}{dt} Ae^{k_2 t}|_{t=\hat{t}} = \frac{d}{dt} Be^{k_3 t}|_{t=\hat{t}} \quad (S4)$$

$$\Leftrightarrow k_2 Ae^{k_2 \hat{t}} = k_3 Be^{k_3 \hat{t}} \quad (S5)$$

$$\Leftrightarrow \hat{t} = \frac{ln(\frac{k_2 A}{k_3 B})}{k_3 - k_2}. \quad (S6)$$

Thus only A/ B is unknown. This can be calculated as follows

$$A/B = \frac{AUC_{ss}^{\infty} + \frac{A_{blood,ss}}{k_3}}{AUC_{ss}^{\infty} + \frac{A_{blood,ss}}{k_2}}, \quad (S7)$$

where $A_{blood,ss}$ is the amount in blood at steady state and is given by

$$A_{blood,ss} = \pi_{blood}(M^{-1} I) \quad (S8)$$

and AUC_{ss}^{∞} is the area under the curve of the amounts in blood starting from steady state, i.e.

$$AUC_{ss}^{\infty} = \int_0^{\infty} e^{Mt} A_{blood,ss} dt = \pi_{blood}(M^{-2} I). \quad (S9)$$

Here $I = (dose, 0,0)^T$ is the input vector. Note that AUC_{ss}^{∞}, $A_{blood,ss} \propto dose$ and therefore A/B does not depend on the dose amount.

Wilcoxon test on Jackknife samples

To be able to use Wilcoxon signed rank test one needs at first a set of i.i.d. samples, which is not the case for the individual jackknife samples J_i given presumably by

$$J_i \approx \frac{1}{n-1}\sum_{j\neq i} x_j, \tag{S10}$$

where x_i are the i.i.d. samples of the parameter induced by each cow and n $(= 3)$ is the sample size. Therefore, the x_i are used instead but they cannot be derived directly, which is why they are reconstructed using these J_i and the fitted mean value across all cows $\bar{X} \approx \frac{1}{n}\sum x_i$. The individual samples x_i can then be calculated in the following way

$$x_i \approx n\bar{X} - (n-1)J_i. \tag{S11}$$

Note that theoretically theses samples x_i could also be reconstructed using only the jackknife samples J_i without the mean $\bar{X}$ but the main interest was the deviation from the mean and not the deviation on the individual jackknife samples themselves.
A second important requirement is the symmetric distribution of theses samples, which is not the case if

$$\hat{d} := \frac{x}{y}, \tag{S12}$$

where x and y i.i.d. (>0 a.s.). But it is the case for d:=ln(x)-ln(y).
If the jackknife method were perfect, it would not be possible for almost all parameters (except Transition Time) to be negative. But due to the imperfection of the Jackknife samples, equation (S11) sometimes produces negative values. Therefore,

Case 1: $x, y > 0$

$$d := \ln(x) - \ln(y) \tag{S13}$$

Case 2: $x \leq 0, y > 0$

$$d := -\infty \tag{S14}$$

Case 3: $x > 0, y \leq 0$

$$d := \infty \tag{S15}$$

Case 4: $x \leq 0, y \leq 0$

$$d := 0 \tag{S16}$$

So the Wilcoxon signed rank test is used on the now presumably symmetric i.i.d. d's.

Limit of Quantification (LOQ) values

Table S1: Limit of quantification (LOQ) values for the measurements in milk, feed and blood.

name	Milk [ng/kg fat]	Blood [pg/kg]	Feed [ng/kg 88% DM]
2378-TCDD	0.009	0.205	0.004
12378-PeCDD	0.019	0.414	0.008
123478-HxCDD	0.027	0.578	0.012
123678-HxCDD	0.028	0.608	0.012
123789-HxCDD	0.029	0.620	0.013
1234678-HpCDD	0.013	0.284	0.006
OCDD	0.020	0.439	0.009
2378-TCDF	0.009	0.196	0.004
12378-PeCDF	0.026	0.570	0.012
23478-PeCDF	0.026	0.567	0.011
123478-HxCDF	0.029	0.634	0.013
123678-HxCDF	0.027	0.592	0.012
123789-HxCDF	0.042	0.902	0.018
234678-HxCDF	0.031	0.682	0.014
1234678-HpCDF	0.023	0.491	0.010
1234789-HpCDF	0.020	0.432	0.009
OCDF	0.020	0.427	0.009
PCB-138	0.026	0.576	0.012
PCB-153	0.030	0.646	0.013
PCB-180	0.019	0.404	0.008
PCB-77	0.095	2.075	0.042
PCB-81	0.083	1.807	0.037
PCB-105	0.131	2.847	0.058
PCB-114	0.123	2.684	0.054
PCB-118	0.111	2.417	0.049
PCB-123	0.124	2.705	0.055
PCB-126	0.184	4.008	0.081
PCB-156	0.048	1.036	0.021
PCB-157	0.050	1.092	0.022
PCB-167	0.066	1.431	0.029
PCB-169	0.059	1.285	0.026
PCB-189	0.030	0.647	0.013

Animal age

Table S2: Age of each animal at the day of calving.

animal number	birthday	calving	age (days)	age (years)
3419	28.05.2013	30.10.2016	1251	3.4
3420	12.06.2013	30.03.2017	1387	3.8
3425	27.07.2013	03.11.2016	1195	3.3
3426	01.08.2013	08.11.2016	1195	3.3
3432	05.09.2013	25.02.2017	1269	3.5
3434	12.09.2013	07.11.2016	1152	3.2
3438	28.10.2013	05.02.2017	1196	3.3
3441	25.11.2013	16.02.2017	1179	3.2
3448	07.01.2013	06.03.2017	1519	4.2

Model parameters

Table S3: Parameters derived for the model for each contaminant in the NEB phase. Here $P_{i,Milk}^{-}$ are partition coefficients between blood and milkfat; $\hat{Q}_{i,Slow}^{-}$ are the effective blood flow rates into the slow turnover compartment; $\hat{V}_{i,Slow}^{-}$ and $\hat{V}_{i,Fast}^{-}$ are the relative the relative capacity of the slow and fast turnover compartments; and $F_{i,Dose}^{-}$ are the fractions absorbed.

name	$P_{i,Milk}^{-}$ [unitless]	$\hat{Q}_{i,Slow}^{-}$ [kg/d]	$\hat{V}_{i,Slow}^{-}$ [kg]	$\hat{V}_{i,Fast}^{-}$ [kg]	$F_{i,Dose}^{-}$ [%]
2378-TCDD	2.96E+02	1.19E+03	1.73E+04	3.45E+03	57
12378-PeCDD	2.90E+02	7.43E+02	1.73E+04	3.31E+03	52
123478-HxCDD	3.14E+02	3.56E+02	1.74E+04	3.88E+03	33
123678-HxCDD	1.64E+02	5.35E+02	1.72E+04	3.02E+03	38
123789-HxCDD	1.75E+02	3.35E+02	1.12E+04	1.99E+03	23
1234678-HpCDD	1.54E+02	1.16E+02	1.07E+04	2.74E+03	7
OCDD	6.05E+01	1.94E+02	7.05E+03	3.48E+02	0
2378-TCDF	5.10E+02	7.66E+01	2.72E+03	1.72E+03	4
12378-PeCDF	3.61E+02	6.85E+01	2.17E+03	1.29E+03	6
23478-PeCDF	3.77E+02	8.92E+02	2.25E+04	4.71E+03	53
123478-HxCDF	3.00E+02	3.76E+02	2.10E+04	3.76E+03	33
123678-HxCDF	1.68E+02	3.54E+02	1.35E+04	1.95E+03	30
123789-HxCDF	4.21E+02	1.78E+02	1.13E+04	2.48E+03	11
234678-HxCDF	3.05E+02	5.24E+02	2.21E+04	3.67E+03	27
1234678-HpCDF	8.53E+01	1.70E+02	3.49E+04	1.50E+03	5
1234789-HpCDF	2.28E+02	1.46E+02	9.27E+03	2.95E+03	6
OCDF	8.31E+01	5.63E+01	6.48E+04	1.07E+03	0
PCB-138	1.56E+02	4.05E+02	9.06E+03	1.29E+03	52

PCB-153	1.40E+02	3.48E+02	4.84E+03	1.09E+03	47
PCB-180	1.37E+02	1.89E+02	6.09E+03	1.07E+03	47
PCB-77	4.70E+01	1.73E+01	6.96E+04	2.20E+02	3
PCB-81	3.11E+02	3.36E+02	6.09E+03	1.34E+03	23
PCB-105	9.26E+01	3.78E+02	6.96E+04	5.15E+03	81
PCB-114	2.96E+02	1.02E+03	2.03E+04	3.73E+03	63
PCB-118	8.24E+01	3.75E+02	2.29E+04	6.38E+02	59
PCB-123	3.30E+02	1.11E+03	2.12E+04	4.10E+03	61
PCB-126	3.43E+02	1.07E+03	2.52E+04	3.55E+03	60
PCB-156	1.31E+02	3.31E+02	8.94E+03	1.05E+03	53
PCB-157	2.22E+02	6.33E+02	1.91E+04	2.35E+03	50
PCB-167	1.46E+02	3.14E+02	7.39E+03	1.27E+03	61
PCB-169	3.46E+02	7.79E+02	5.00E+04	3.36E+03	65
PCB-189	2.24E+02	3.33E+02	1.90E+04	2.04E+03	52

Table S4: Parameters derived for the model for each contaminant in the PEB phase. Here $P^{+}_{i,Milk}$ are partition coefficients between blood and milkfat; $\hat{Q}^{+}_{i,Slow}$ are the effective blood flow rates into the slow turnover compartment; $\hat{V}^{+}_{i,Slow}$ and $\hat{V}^{+}_{i,Fast}$ are the relative the relative capacity of the slow and fast turnover compartments; and $F^{+}_{i,Dose}$ are the fractions absorbed.

name	$P^{+}_{i,Milk}$ [unitless]	$\hat{Q}^{+}_{i,Slow}$ [kg/d]	$\hat{V}^{+}_{i,Slow}$ [kg]	$\hat{V}^{+}_{i,Fast}$ [kg]	$F^{+}_{i,Dose}$ [%]
2378-TCDD	2.48E+02	6.38E+02	1.03E+04	2.34E+03	45
12378-PeCDD	2.30E+02	3.25E+02	8.32E+03	2.01E+03	38
123478-HxCDD	2.57E+02	2.04E+02	9.37E+03	3.00E+03	26
123678-HxCDD	1.39E+02	1.15E+02	5.87E+03	1.45E+03	26
123789-HxCDD	1.43E+02	9.98E+01	3.45E+03	1.17E+03	16
1234678-HpCDD	1.45E+02	4.10E+01	3.52E+03	2.46E+03	4
OCDD	6.13E+01	1.15E+02	1.75E+03	5.46E+02	0
2378-TCDF	3.43E+02	6.14E+01	7.02E+02	5.19E+02	2
12378-PeCDF	2.96E+02	2.92E+01	8.29E+02	6.73E+02	3
23478-PeCDF	3.02E+02	6.45E+02	1.35E+04	3.00E+03	41
123478-HxCDF	2.65E+02	2.63E+02	1.10E+04	2.32E+03	22
123678-HxCDF	1.53E+02	1.38E+02	4.89E+03	1.38E+03	23
123789-HxCDF	3.16E+02	5.81E+01	1.63E+03	8.24E+02	6
234678-HxCDF	2.60E+02	2.22E+02	8.92E+03	2.33E+03	21
1234678-HpCDF	8.18E+01	7.19E+01	2.83E+04	1.10E+03	4
1234789-HpCDF	1.68E+02	5.95E+01	5.25E+03	1.76E+03	5
OCDF	6.61E+01	5.25E+01	4.60E+04	8.68E+02	0
PCB-138	1.46E+02	3.05E+02	9.38E+03	1.51E+03	58
PCB-153	1.20E+02	2.02E+02	6.04E+03	1.08E+03	52
PCB-180	1.32E+02	1.09E+02	5.02E+03	1.06E+03	51

PCB-77	5.27E+01	3.71E+01	6.91E+04	2.20E+02	2
PCB-81	2.84E+02	2.26E+02	3.74E+03	1.07E+03	15
PCB-105	6.48E+01	1.14E+02	5.59E+04	2.03E+03	46
PCB-114	2.73E+02	6.81E+02	1.73E+04	2.82E+03	57
PCB-118	4.57E+01	7.83E+01	1.49E+03	4.14E+02	48
PCB-123	2.87E+02	6.52E+02	1.62E+04	2.76E+03	50
PCB-126	2.81E+02	5.30E+02	1.38E+04	2.39E+03	54
PCB-156	1.45E+02	2.55E+02	9.71E+03	1.16E+03	55
PCB-157	2.01E+02	3.66E+02	1.31E+04	1.68E+03	45
PCB-167	1.33E+02	2.35E+02	8.54E+03	1.07E+03	59
PCB-169	2.79E+02	2.95E+02	1.63E+04	2.00E+03	53
PCB-189	1.84E+02	1.86E+02	1.09E+04	1.11E+03	47

Transfer parameters

*Table S5: Transfer rates (TR) into milk in both phase and the literature[1]. *marks the contaminants with significant difference ($p<0.05$) between both phases using a paired t-test.*

name	P-value	NEB [%]	PEB [%]	Literature [%]
2378-TCDD	1.25E-01	57.4±4.5	45.4±4.8	30.0
12378-PeCDD*	4.82E-02	51.9±3.7	37.8±2.7	31.5
123478-HxCDD*	3.54E-02	33.3±0.9	25.8±2.2	24.4
123678-HxCDD	5.67E-01	38.5±2.3	26.3±33.1	26.0
123789-HxCDD*	3.30E-02	23.0±2.0	16.2±1.9	18.0
1234678-HpCDD	8.11E-02	6.5±1.3	4.3±1.2	3.3
OCDD	8.87E-01	0.4±0.5	0.4±0.5	0.7
2378-TCDF*	2.83E-03	3.6±0.1	1.6±0.3	3.4
12378-PeCDF*	7.16E-03	6.0±0.4	2.9±0.2	3.9
23478-PeCDF	1.47E-01	52.8±1.1	41.0±10.7	30.7
123478-HxCDF*	2.04E-02	32.6±1.9	21.9±3.9	19.6
123678-HxCDF	1.03E-01	29.9±2.4	23.4±4.5	21.3
123789-HxCDF	6.93E-02	10.6±2.4	5.8±0.3	12.4
234678-HxCDF	1.18E-01	26.5±0.6	20.9±4.0	18.8
1234678-HpCDF	6.61E-01	5.5±1.2	4.0±5.1	3.8
1234789-HpCDF	3.57E-01	6.1±1.3	4.7±1.0	6.4
OCDF	7.76E-01	0.5±0.1	0.4±0.4	0.4
PCB-138	6.29E-01	52.4±19.2	58.3±18.8	38.0
PCB-153	8.52E-01	47.2±17.4	52.2±64.2	28.5
PCB-180	8.85E-01	46.7±9.0	51.3±46.4	35.0
PCB-77	1.41E-01	2.5±0.8	1.7±0.4	1.2
PCB-81*	2.85E-02	23.2±5.0	15.2±3.4	9.7

PCB-105	2.91E-01	81.1±73.3	45.9±45.1	9.4
PCB-114	1.21E-01	63.2±9.5	57.2±5.6	10.7
PCB-118	8.29E-01	58.9±35.3	48.1±64.1	19.3
PCB-123	1.15E-01	60.6±7.5	50.3±2.0	2.5
PCB-126	3.71E-01	59.8±7.8	54.3±13.6	31.4
PCB-156	9.43E-01	53.0±39.2	55.5±25.1	18.5
PCB-157	1.60E-01	49.7±7.8	45.1±11.8	21.6
PCB-167	7.86E-01	60.5±10.1	59.2±9.7	21.5
PCB-169	4.52E-01	65.0±19.0	53.1±8.3	35.8
PCB-189	2.96E-01	51.6±6.9	46.9±1.9	14.0

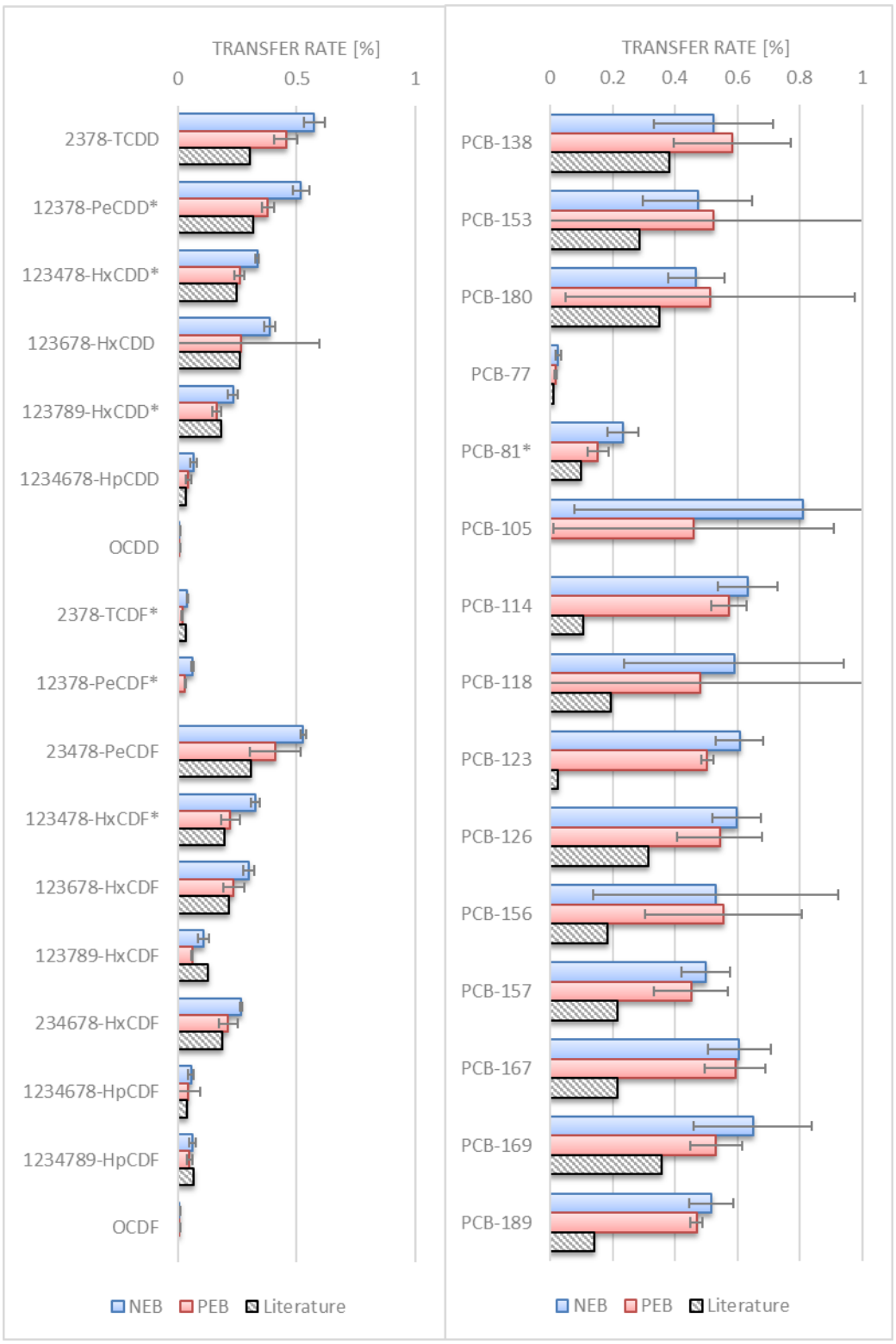

*Figure S1: Transfer rates (TR) in milk of all analyzed PCDD/Fs (left) and PCBs (right) divided into NEB (blue) and PEB (red) phase with error bars indicating the respective confidence interval. * marks the contaminants with significant difference ($p<0.05$) between both phases. Furthermore, in gray shaded are shown the median reported TRs in the literature according to Krause et al.* [1]

117 *Table S6: Blood mean residence times (BMRTs) in both phases. * marks the contaminants with statistically significant*
118 *difference (p<0.05) between both phases using a paired t-test.*

name	P-value	NEB [10^{-2} d]	PEB [10^{-2} d]
2378-TCDD	3.11E-01	5.7±0.7	6.7±1.3
12378-PeCDD	2.30E-01	5.8±2.3	7.3±0.7
123478-HxCDD	2.41E-01	5.3±1.1	6.5±0.7
123678-HxCDD	8.54E-02	10.2±0.3	12.0±1.4
123789-HxCDD*	4.69E-02	9.6±0.7	11.7±1.3
1234678-HpCDD	5.99E-01	10.9±1.1	11.6±2.9
OCDD	6.26E-01	27.6±15.3	27.3±14.5
2378-TCDF	7.95E-02	3.3±0.6	4.9±1.2
12378-PeCDF	7.26E-02	4.6±0.5	5.7±1.0
23478-PeCDF*	3.01E-02	4.4±0.4	5.5±0.7
123478-HxCDF	2.88E-01	5.6±1.0	6.3±0.4
123678-HxCDF	1.72E-01	10.0±0.4	10.9±0.6
123789-HxCDF	8.73E-02	4.0±0.3	5.3±0.7
234678-HxCDF	3.49E-01	5.5±1.4	6.4±0.4
1234678-HpCDF	5.40E-01	19.6±2.1	20.4±3.9
1234789-HpCDF*	3.20E-03	7.3±0.9	10.0±0.7
OCDF	6.71E-01	20.1±2.4	25.3±19.5
PCB-138	6.31E-01	10.7±1.5	11.4±3.2
PCB-153	1.61E-01	11.9±1.0	13.9±2.6
PCB-180	8.36E-01	12.2±2.0	12.6±5.7
PCB-77	6.53E-01	35.6±40.5	31.7±26.6
PCB-81	2.17E-01	5.4±1.2	5.9±1.3
PCB-105	3.41E-01	18.1±12.0	25.8±22.6
PCB-114	1.90E-01	5.6±0.9	6.1±0.4
PCB-118	1.66E-01	20.3±13.0	36.6±27.9
PCB-123	2.01E-01	5.1±0.5	5.8±0.4
PCB-126	2.58E-01	4.9±0.7	6.0±1.2
PCB-156	7.19E-01	12.7±1.0	11.6±4.7
PCB-157	1.76E-01	7.5±1.6	8.3±2.3
PCB-167	4.61E-01	11.5±2.2	12.6±4.2
PCB-169*	3.53E-02	4.8±1.1	6.0±0.9
PCB-189	1.58E-01	7.5±1.3	9.1±1.3

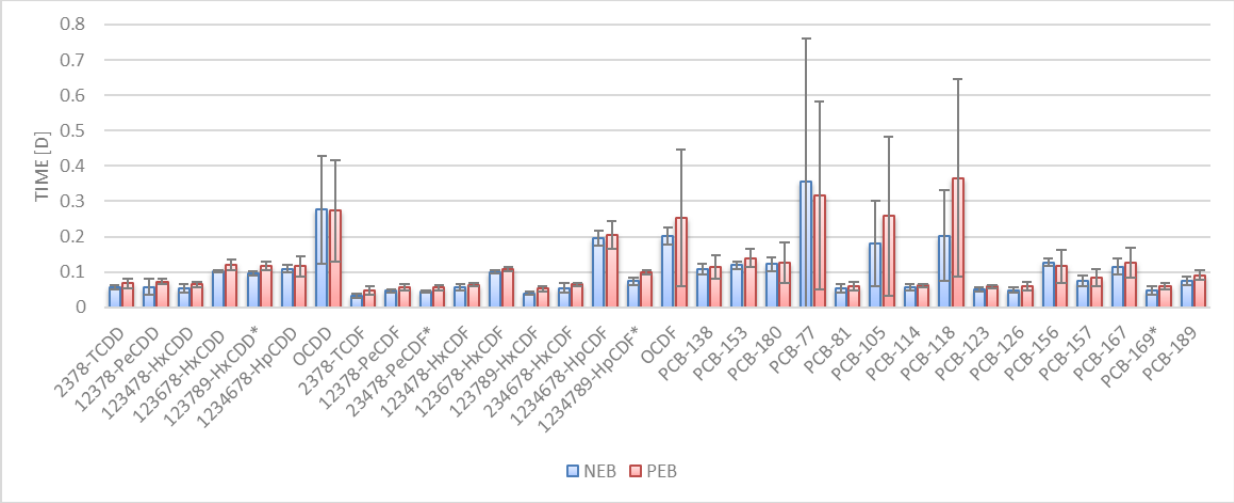

*Figure S2: Blood mean residence times (BMRTs) of all analyzed PCDD/Fs (left) and PCBs (right) divided into NEB (blue) and PEB (red) phase with error bars indicating the respective confidence interval. * marks the contaminants with significant difference ($p<0.05$) between both phases.*

125 *Table S7: Time until steady state (90%) (T_{ss}) in both phases.*

name	P-value	NEB [d]	PEB [d]
2378-TCDD	1.10E-01	109±15	84±10
12378-PeCDD*	2.93E-02	117±18	80±13
123478-HxCDD	3.37E-01	122±37	90±15
123678-HxCDD	8.50E-01	205±39	101±930
123789-HxCDD*	1.39E-02	131±23	61±7
1234678-HpCDD	6.75E-01	165±739	55±301
OCDD	8.94E-01	186±280	63±1328
2378-TCDF	1.38E-01	7±2	4±1
12378-PeCDF	6.08E-02	8±2	4±0
23478-PeCDF	5.14E-02	121±22	92±13
123478-HxCDF	3.98E-01	150±101	95±0
123678-HxCDF*	3.31E-02	153±21	77±18
123789-HxCDF	3.78E-01	60±90	6±4
234678-HxCDF	1.35E-01	159±67	82±10
1234678-HpCDF	8.33E-01	501±374	743±1889
1234789-HpCDF	8.40E-01	101±190	69±94
OCDF	9.52E-01	1415±1741	1498±1753
PCB-138	4.62E-01	105±84	128±35
PCB-153	7.78E-01	74±1057	105±867
PCB-180	9.35E-01	100±1374	89±1141
PCB-77	9.89E-01	2800±4819	2822±2327
PCB-81	1.39E-01	44±5	32±5
PCB-105	6.31E-01	1259±1363	1650±2407
PCB-114	5.65E-01	129±12	123±7
PCB-118	9.44E-01	65±1143	72±970
PCB-123	5.53E-01	122±10	112±31
PCB-126	1.27E-01	135±18	100±11
PCB-156	9.75E-01	128±420	135±70
PCB-157	3.71E-01	160±10	131±45
PCB-167*	2.23E-02	100±8	129±1
PCB-169	2.66E-01	244±155	128±27
PCB-189	1.01E-01	172±9	129±28

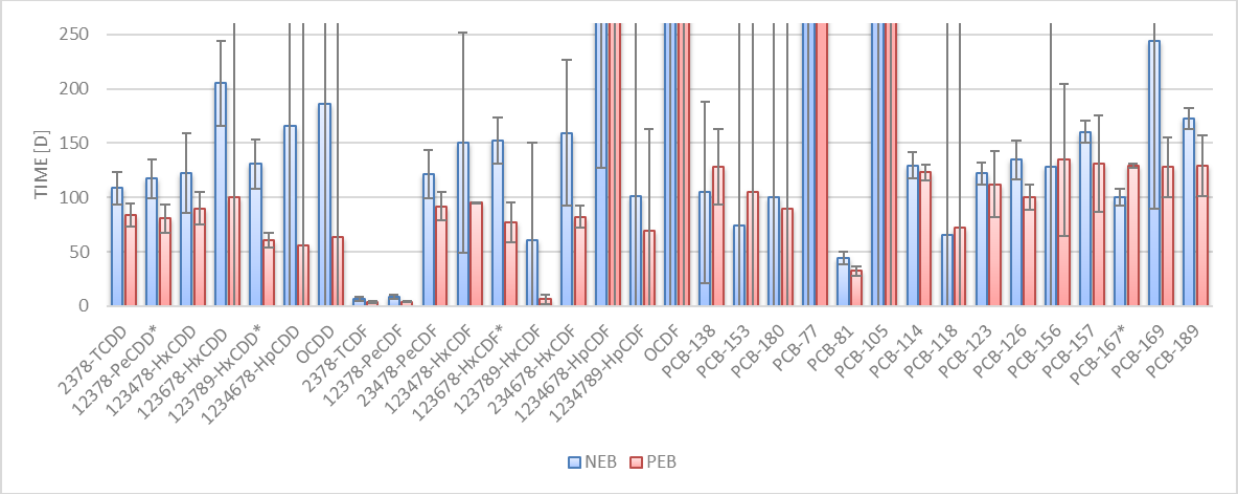

126

127 *Figure S3: Time until steady state (90%) (T_{ss}) of all analyzed PCDD/Fs (left) and PCBs (right) divided into NEB (blue)*
128 *and PEB (red) phase with error bars indicating the respective confidence interval.*

129

*Table S8: The distribution into the three different compartments during steady state for each contaminant. * marks the contaminants with significant difference (p<0.05) between both phases in the distribution into the slow turnover compartment using a paired t-test.*

name	P-value	slow-NEB [%]	slow-PEB [%]	fast-NEB [%]	fast-PEB [%]	blood-NEB [‰]	blood-PEB [‰]
2378-TCDD	5.44E-01	83.2±3.1	81.4±5.2	16.6±3.0	18.4±5.2	0.1±0.0	0.2±0.0
12378-PeCDD	2.91E-01	83.8±2.8	80.3±6.6	16.1±2.7	19.4±6.5	0.1±0.1	0.3±0.1
123478-HxCDD	2.16E-01	81.1±4.0	75.6±3.9	18.7±3.9	24.2±3.9	0.1±0.1	0.2±0.1
123678-HxCDD	5.98E-01	85.4±5.9	79.8±23.0	14.4±5.9	19.8±22.5	0.1±0.0	0.4±0.5
123789-HxCDD	9.16E-02	84.7±4.4	74.3±7.4	15.1±4.4	25.1±7.4	0.2±0.0	0.6±0.0
1234678-HpCDD	2.46E-01	79.2±21.5	58.6±38.2	20.6±21.2	40.9±37.8	0.2±0.3	0.5±0.4
OCDD	1.84E-01	94.5±18.5	75.3±0.6	5.1±17.3	23.5±0.6	0.4±1.6	1.2±0.0
2378-TCDF	7.46E-01	62.8±28.9	56.2±6.2	36.6±28.4	41.5±6.5	0.6±0.5	2.3±0.3
12378-PeCDF	5.60E-01	62.2±16.1	54.2±7.8	37.0±15.9	44.0±7.5	0.8±0.3	1.9±0.3
23478-PeCDF	4.82E-01	82.8±4.7	81.6±5.1	17.1±4.6	18.2±5.1	0.1±0.0	0.2±0.0
123478-HxCDF	6.98E-01	84.4±5.2	82.4±3.8	15.4±5.1	17.4±3.8	0.1±0.1	0.2±0.0
123678-HxCDF	2.29E-01	86.7±4.1	77.6±7.7	13.1±4.1	21.9±7.6	0.2±0.0	0.5±0.1
123789-HxCDF	5.31E-01	81.8±15.4	65.6±26.7	18.0±15.3	33.2±25.5	0.2±0.2	1.2±1.2
234678-HxCDF	1.66E-01	86.5±4.1	79.1±6.7	13.4±4.0	20.6±6.7	0.1±0.1	0.3±0.0
1234678-HpCDF	8.89E-01	93.6±6.3	96.2±32.0	6.2±6.2	3.7±30.9	0.1±0.1	0.1±1.1
1234789-HpCDF	9.62E-01	75.7±21.4	74.6±18.1	24.1±21.2	25.0±17.7	0.2±0.2	0.4±0.4
OCDF	9.90E-01	98.0±12.1	98.1±1.8	1.9±11.8	1.9±1.7	0.1±0.3	0.1±0.0
PCB-138	9.00E-01	86.5±9.8	85.9±3.3	13.2±9.5	13.9±3.2	0.3±0.3	0.3±0.1
PCB-153	1.13E-01	82.3±15.6	84.5±15.2	17.3±15.2	15.1±14.8	0.5±0.4	0.4±0.4
PCB-180	4.04E-01	85.4±12.6	82.2±18.0	14.3±12.2	17.4±17.5	0.4±0.4	0.5±0.5
PCB-77	9.95E-01	99.6±0.4	99.6±0.0	0.3±0.4	0.3±0.0	0.0±0.0	0.0±0.0
PCB-81	6.37E-01	81.4±9.6	77.3±5.3	18.3±9.6	22.1±5.3	0.4±0.1	0.6±0.1
PCB-105	4.86E-01	92.9±24.6	96.4±32.1	7.0±23.4	3.5±29.7	0.0±1.2	0.0±2.4
PCB-114	6.50E-01	84.5±3.6	85.9±4.1	15.4±3.5	14.0±4.1	0.1±0.0	0.1±0.0
PCB-118	4.01E-01	81.1±18.8	77.1±26.3	18.1±17.7	21.4±23.8	0.8±1.2	1.5±2.5
PCB-123	5.55E-01	83.7±2.3	85.3±4.6	16.2±2.3	14.5±4.6	0.1±0.0	0.1±0.0
PCB-126	5.39E-01	87.4±4.8	85.0±2.1	12.5±4.7	14.8±2.1	0.1±0.0	0.2±0.0
PCB-156	9.64E-01	89.2±8.2	89.1±4.5	10.5±8.0	10.6±4.5	0.3±0.3	0.3±0.0
PCB-157	8.04E-01	89.0±2.6	88.4±4.4	10.9±2.6	11.4±4.4	0.1±0.0	0.2±0.0
PCB-167	5.50E-01	84.8±8.7	88.6±2.9	14.8±8.6	11.1±2.9	0.3±0.1	0.3±0.1
PCB-169	2.56E-01	93.0±3.8	89.0±4.2	6.9±3.7	10.9±4.2	0.1±0.0	0.2±0.0
PCB-189	7.95E-01	90.1±1.6	90.6±1.7	9.8±1.5	9.2±1.7	0.1±0.0	0.2±0.0

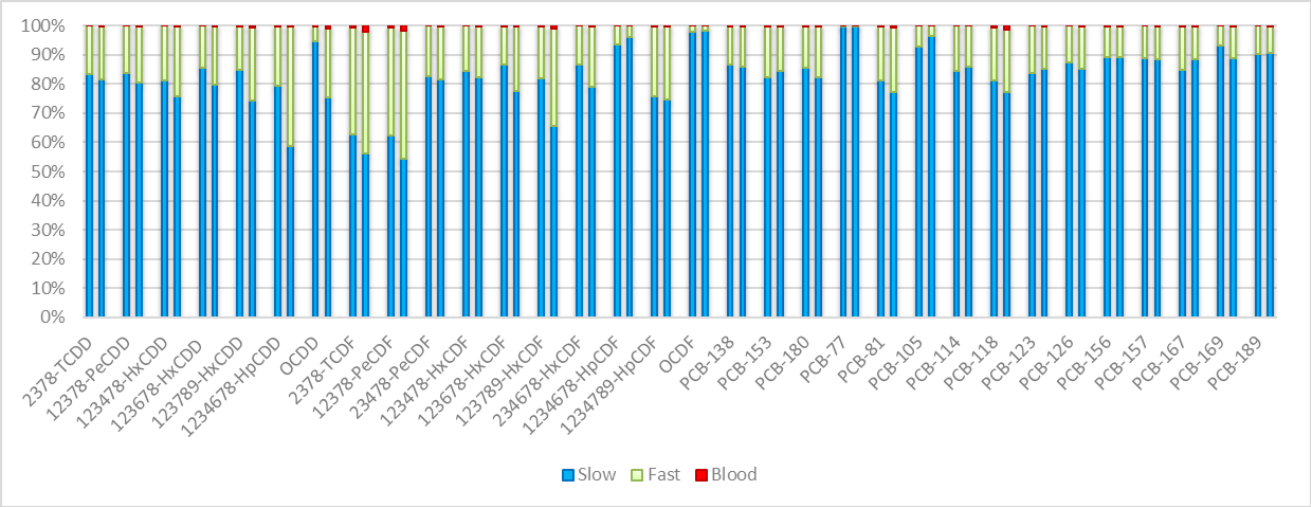

*Figure S4: The distribution into the three different compartments during steady state for each contaminant. It is distinguished between NEB (left column) and PEB phase (right column). *marks the contaminants where there is a statistically significant difference ($p<0.05$) between both phases regarding the distribution into the slow turnover compartment.*

Table S9: α-half-lives [d] in both phases and the literature[1]. Additionally, the confidence interval is given, which is not symmetric around the fitted value. If an upper limit is negative since the inverse normal distribution also has negative values, it is replaced by ∞.

name	NEB [d]	NEB range [d]	PEB [d]	NEB range [d]	Literature
2378-TCDD	1.31	1.21-1.43	1.43	1.18-1.83	3.51
12378-PeCDD	1.76	1.74-1.79	1.88	1.54-2.43	1.24
123478-HxCDD	2.95	2.52-3.56	3.17	2.64-3.95	5.00
123678-HxCDD	2.43	1.68-4.38	2.83	2.23-3.89	1.53
123789-HxCDD	2.11	1.64-2.95	2.35	1.90-3.06	1.50
1234678-HpCDD	4.96	3.78-7.22	5.91	5.73-6.10	
OCDD	0.86	0.26-∞	1.66	1.49-1.87	
2378-TCDF	1.29	0.89-2.34	0.59	0.49-0.73	
12378-PeCDF	1.33	0.93-2.36	0.91	0.84-0.99	
23478-PeCDF	2.02	1.66-2.58	1.70	1.34-2.34	1.86
123478-HxCDF	2.88	2.24-4.05	2.22	1.60-3.63	2.12
123678-HxCDF	2.05	1.52-3.15	2.37	1.90-3.14	1.27
123789-HxCDF	1.94	1.51-2.70	0.99	0.94-1.05	
234678-HxCDF	2.38	1.87-3.28	2.39	1.93-3.15	
1234678-HpCDF	3.29	2.90-3.81	3.68	3.50-3.88	
1234789-HpCDF	3.77	3.49-4.10	3.54	3.18-4.01	
OCDF	3.83	3.64-4.04	3.76	2.89-5.36	
PCB-138	1.30	1.09-1.61	1.84	1.58-2.21	
PCB-153	1.23	0.65-12.41	1.81	1.31-2.95	
PCB-180	1.74	0.96-9.40	2.20	1.56-3.76	1.04
PCB-77	1.77	1.09-4.63	1.36	0.95-2.37	
PCB-81	1.07	0.77-1.73	1.04	0.84-1.35	
PCB-105	6.48	1.21-∞	6.30	1.82-∞	
PCB-114	1.60	1.33-2.00	1.64	1.16-2.78	
PCB-118	0.80	0.40-∞	1.82	1.26-3.28	
PCB-123	1.59	1.36-1.93	1.62	1.28-2.21	
PCB-126	1.44	0.98-2.71	1.60	1.44-1.80	2.19
PCB-156	1.29	0.95-2.04	1.59	1.24-2.23	
PCB-157	1.57	1.32-1.93	1.63	1.38-1.98	
PCB-167	1.52	0.89-5.31	1.60	1.27-2.16	
PCB-169	1.69	1.31-2.39	1.80	1.51-2.23	
PCB-189	1.97	1.60-2.56	1.56	1.38-1.80	

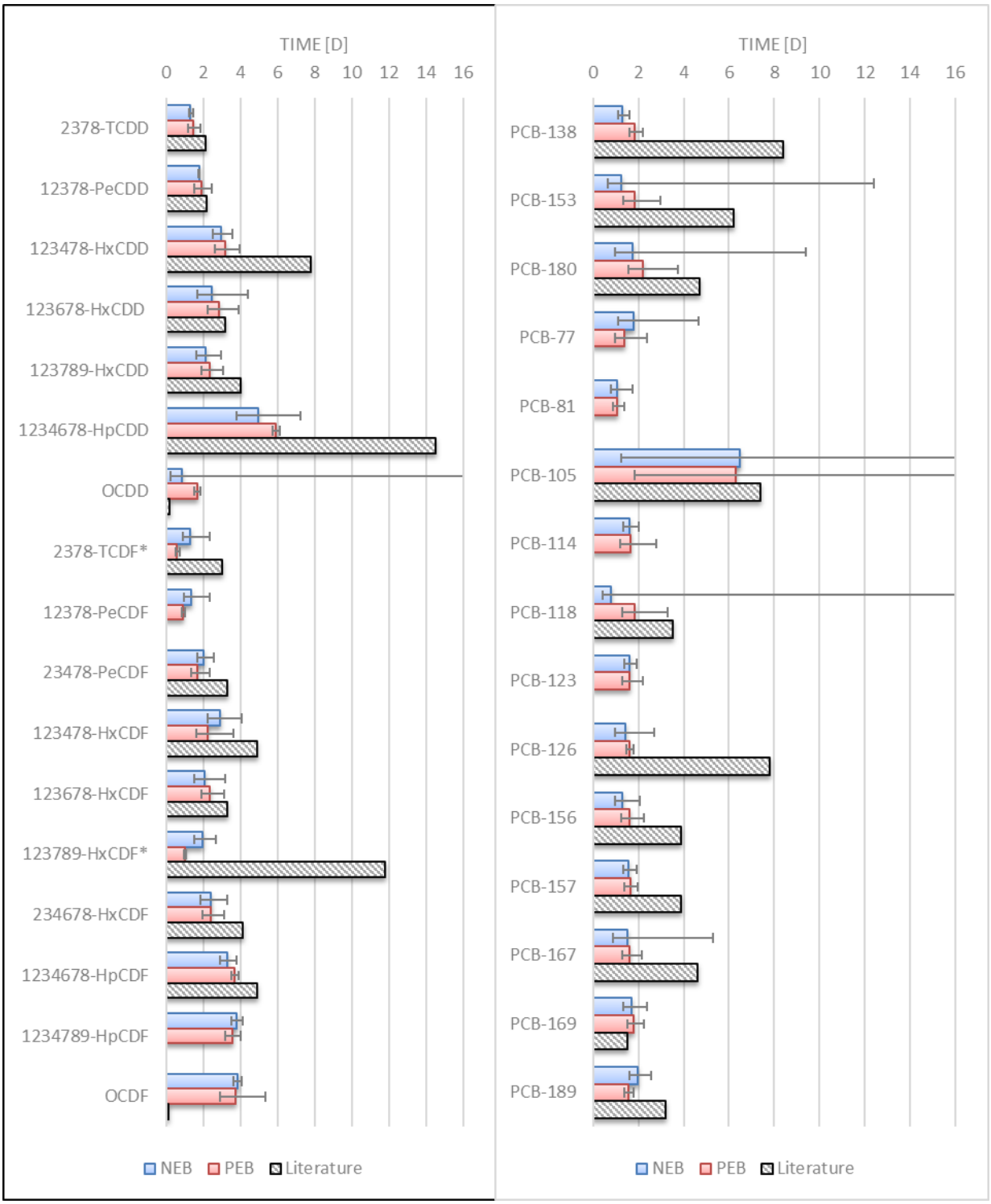

144

145 *Figure S5: α-half-lives [d] of all analyzed PCDD/Fs (left) and PCBs (right) divided into NEB (blue) and PEB (red)*
146 *phase with error bars indicating the respective confidence interval.*

147

148

149 *Table S10: β-half-lives [d] in both phases and the literature[1]. Additionally, the confidence interval is given, which is not*
150 *symmetric around the fitted value. If an upper limit is negative since the inverse normal distribution also has negative*
151 *values it is replaced by ∞.*

name	P-value	NEB [d]	NEB range [d]	PEB [d]	NEB range [d]	Literature
2378-TCDD	1.87E-01	37.2	32.3-44.0	30.6	27.0-35.3	53.4
12378-PeCDD	6.89E-02	43.2	37.1-51.6	34.2	29.4-40.9	53.0
123478-HxCDD	5.00E-01	56.6	44.2-78.8	48.2	41.1-58.2	99.2
123678-HxCDD	7.24E-01	72.7	61.9-88.1	53.8	24.4-∞	65.7
123789-HxCDD*	4.72E-03	51.6	43.5-63.5	34.8	30.3-41.0	90.0
1234678-HpCDD	5.00E-01	93.1	42.1-∞	70.4	35.0-∞	29.6
OCDD	3.34E-01	67.9	18.1-∞	24.3	23.9-24.7	63.0
2378-TCDF	1.09E-01	29.3	17.4-91.1	8.8	5.3-27.4	0.8
12378-PeCDF	3.83E-01	24.5	16.4-48.8	20.9	14.5-37.6	
23478-PeCDF	8.42E-02	45.3	36.6-59.4	34.9	29.1-43.8	43.4
123478-HxCDF	1.72E-01	68.0	41.6-186.1	47.1	38.8-59.9	63.4
123678-HxCDF	1.46E-01	59.3	51.8-69.5	38.9	30.5-53.4	77.0
123789-HxCDF	6.43E-02	55.3	28.6-861.2	21.6	17.0-29.8	598.0
234678-HxCDF	1.41E-01	65.3	45.1-118.2	43.1	35.5-54.7	63.0
1234678-HpCDF	6.11E-01	202.5	106.3-2126.0	414.9	93.5-∞	45.8
1234789-HpCDF	7.22E-01	61.9	31.5-1756.8	74.6	50.5-143.1	55.3
OCDF	9.91E-01	932.2	109.2-∞	891.6	616.2-1612.4	14.1
PCB-138	4.55E-01	38.7	24.0-101.0	49.7	41.7-61.6	196.5
PCB-153	2.00E-01	27.3	13.7-3571.9	43.1	21.8-2192.2	165.0
PCB-180	7.18E-01	44.0	21.0-∞	48.3	23.2--593.2	195.0
PCB-77	6.80E-01	3382.5	784.3-∞	1822.4	1596.7-2122.4	
PCB-81	2.17E-01	20.9	18.0-24.9	17.3	15.9-19.0	
PCB-105	4.73E-01	440.1	18.7-∞	695.6	19.0-∞	610.5
PCB-114	8.97E-01	45.4	41.0-51.0	46.0	43.7-48.5	
PCB-118	1.82E-01	21.9	9.9-∞	28.6	12.5-∞	205.0
PCB-123	9.64E-01	42.8	38.5-48.3	42.6	34.7-55.0	
PCB-126	1.71E-01	48.4	44.0-53.9	39.9	36.6-43.7	196.4
PCB-156	6.51E-01	48.3	25.4-470.6	55.4	37.3-107.2	352.0
PCB-157	5.61E-01	58.9	53.9-64.8	53.1	40.7-76.5	281.0
PCB-167*	4.15E-02	38.5	34.5-43.6	53.0	50.7-55.4	274.5
PCB-169	1.79E-01	95.3	56.1-316.4	63.2	48.3-91.6	38.8
PCB-189	2.95E-01	75.0	69.8-80.9	65.8	53.2-86.0	241.0

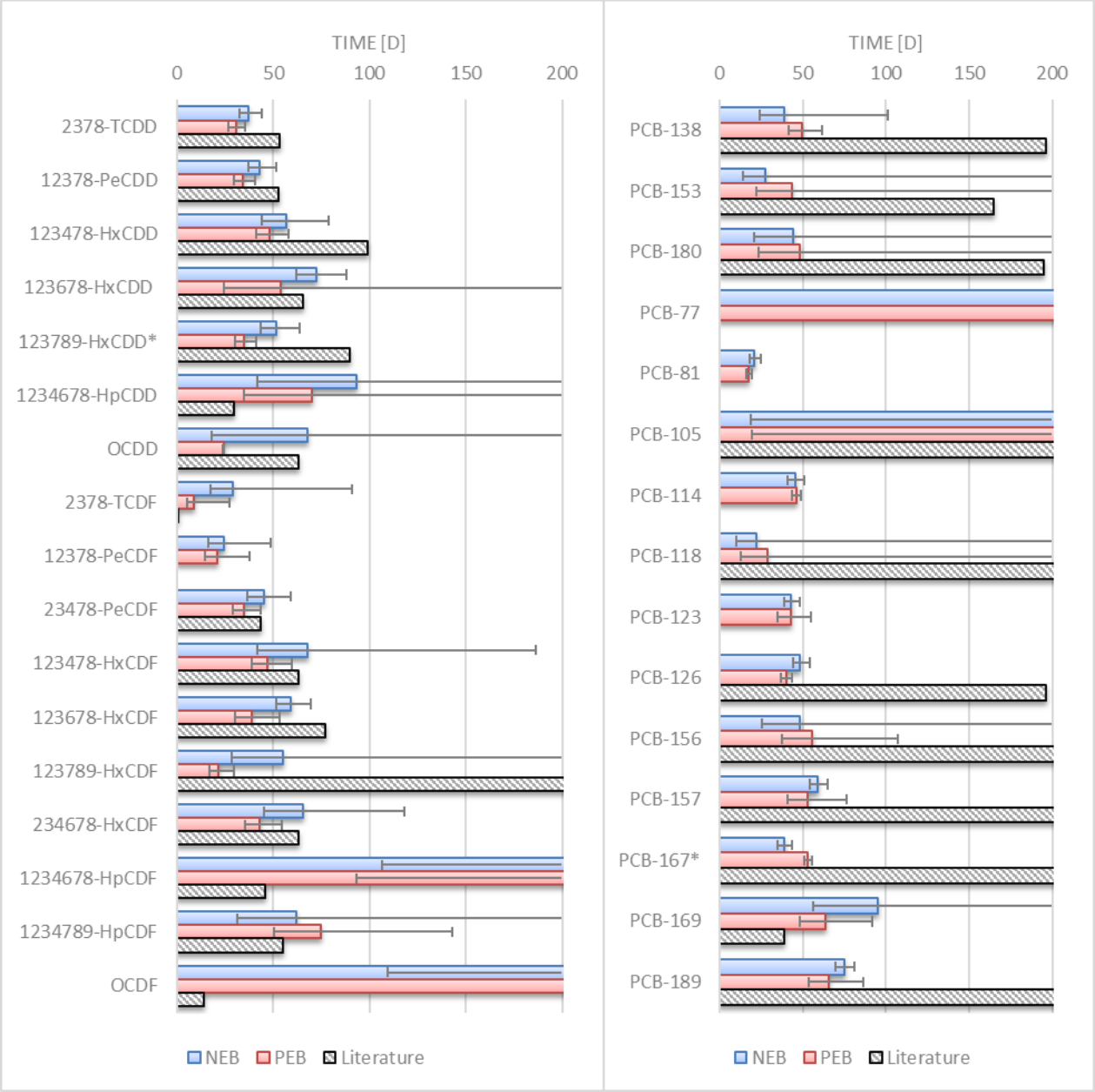

Figure S6: β-half-lives [d] of all analyzed PCDD/Fs (left) and PCBs (right) divided into NEB (blue) and PEB (red) phase with error bars indicating the respective confidence interval.

156 *Table S11: Transition times (TTs) in both phases.*

name	P-Value	NEB [d]	PEB [d]
2378-TCDD	2.89E-01	4.3±0.7	5.2±0.3
12378-PeCDD	1.43E-01	6.8±0.4	8.2±0.7
123478-HxCDD	5.78E-01	14.3±2.8	16.0±2.3
123678-HxCDD	2.84E-01	9.2±1.8	15.1±5.4
123789-HxCDD	1.88E-01	9.2±1.9	12.3±1.2
1234678-HpCDD*	1.46E-02	27.1±11.2	37.8±13.4
OCDD	8.66E-01	4.6±14.4	5.8±11.3
2378-TCDF	1.19E-01	10.6±4.4	4.4±1.6
12378-PeCDF	4.00E-01	10.1±4.0	8.1±0.9
23478-PeCDF	3.01E-01	7.8±1.8	6.6±2.2
123478-HxCDF	1.07E-01	14.4±4.6	11.6±4.8
123678-HxCDF	2.75E-01	9.2±2.2	11.8±1.8
123789-HxCDF	1.90E-01	13.5±4.0	7.8±2.6
234678-HxCDF	6.49E-01	11.2±2.8	12.4±1.6
1234678-HpCDF	1.12E-01	18.8±1.1	28.7±5.4
1234789-HpCDF	3.59E-01	20.9±4.4	24.2±7.6
OCDF	9.41E-01	35.6±19.1	33.9±18.0
PCB-138	2.19E-01	5.4±1.4	8.0±1.3
PCB-153	8.06E-01	4.6±28.1	8.2±6.6
PCB-180	7.65E-01	8.6±21.4	12.2±8.3
PCB-77	4.07E-01	23.2±11.7	15.8±3.4
PCB-81	9.54E-01	5.3±2.7	5.4±0.8
PCB-105	5.69E-01	30.8±29.5	42.5±34.4
PCB-114	5.78E-01	5.8±1.1	6.8±1.6
PCB-118	9.32E-01	2.4±88.3	6.9±8.8
PCB-123	4.81E-01	5.6±1.3	6.8±1.2
PCB-126	5.29E-01	5.8±2.9	7.0±0.3
PCB-156	1.16E-01	5.9±4.1	8.0±4.1
PCB-157	3.36E-01	6.9±1.4	8.0±0.6
PCB-167	7.15E-01	6.4±5.5	7.9±1.5
PCB-169	5.62E-01	9.1±3.9	10.5±1.1
PCB-189	5.20E-01	10.7±2.7	9.7±1.1

157

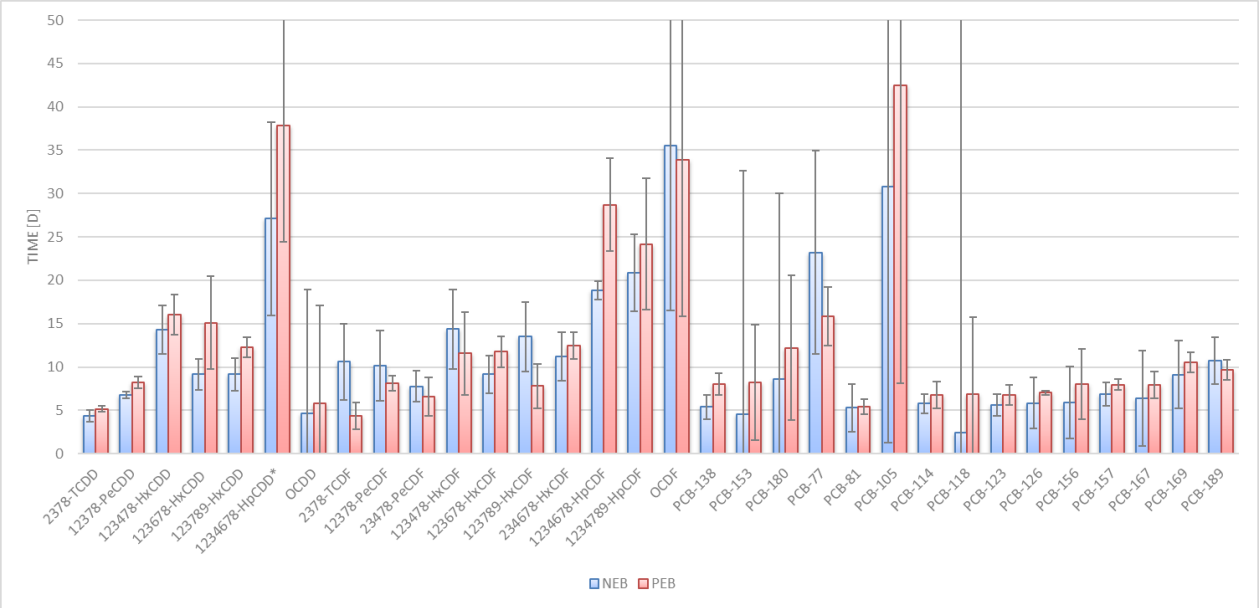

Figure S7: Transition times (TTs) [d] of all analyzed PCDD/Fs (left) and PCBs (right) divided into NEB (blue) and PEB (red) phase with error bars indicating the respective confidence interval.

Simulation

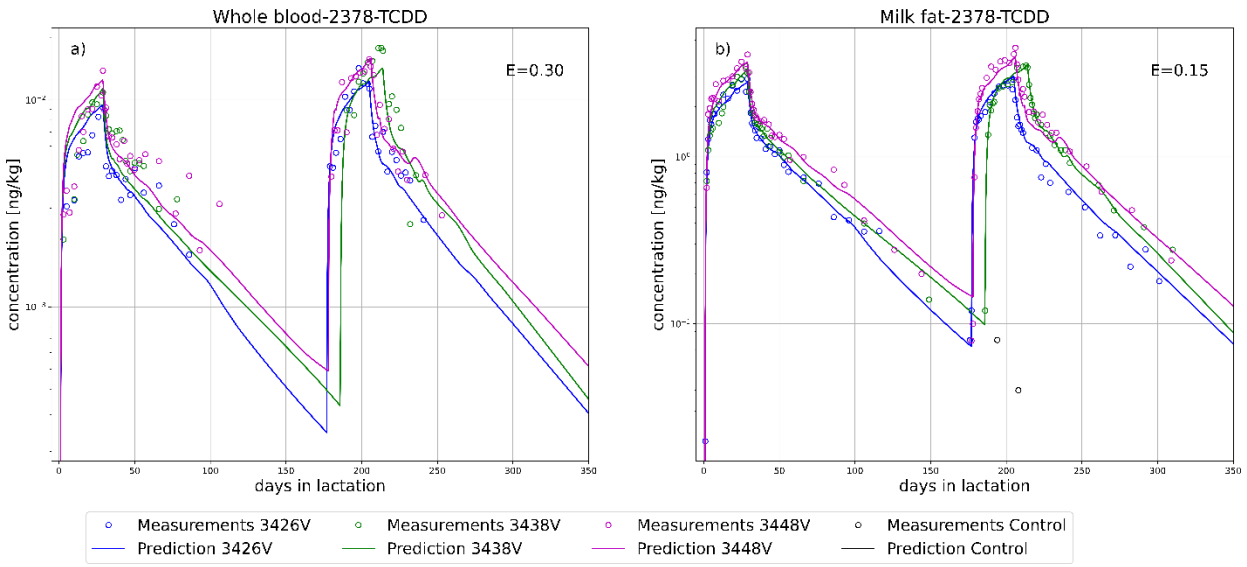

Figure S8: Concentration-time profiles of 2378-TCDD in blood and in milk fat of all 6 cows, which were considered for modeling. The dots represent the measured data and the lines model predictions. E describes the weighted log error of equation (4) for the respective data set. The concentration of the control cows is assumed to be 0.

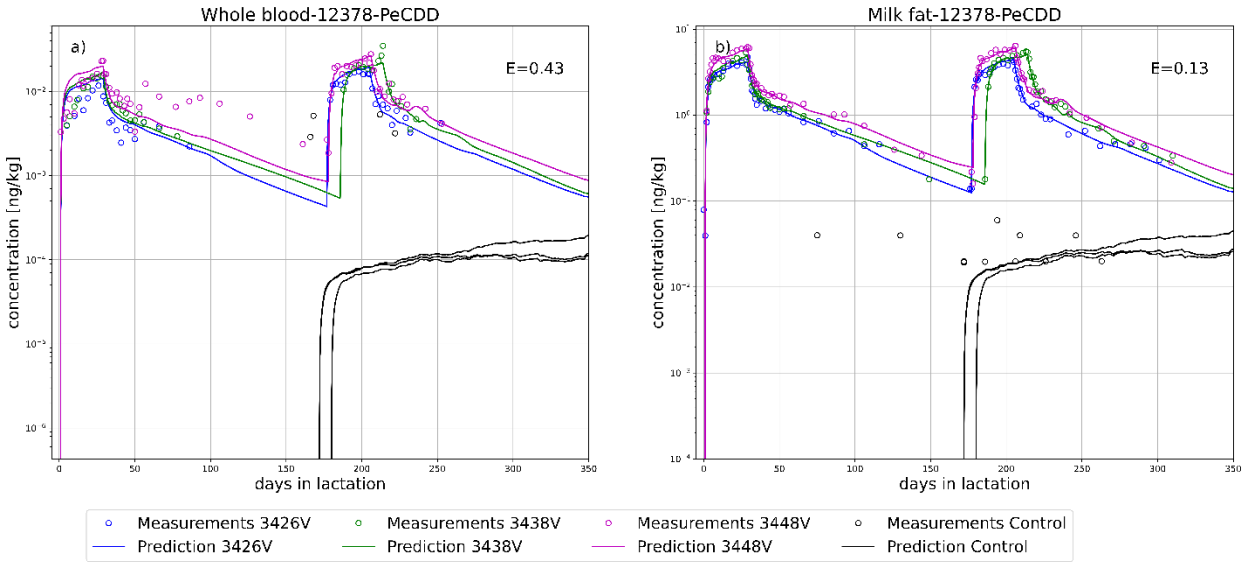

Figure S9: Concentration-time profiles of 12378-PeCDD in blood and in milk fat of all 6 cows, which were considered for modeling. The dots represent the measured data and the lines model predictions. E describes the weighted log error of equation (4) for the respective data set. The concentrations of the control cows in NEB phase are assumed to be 0.

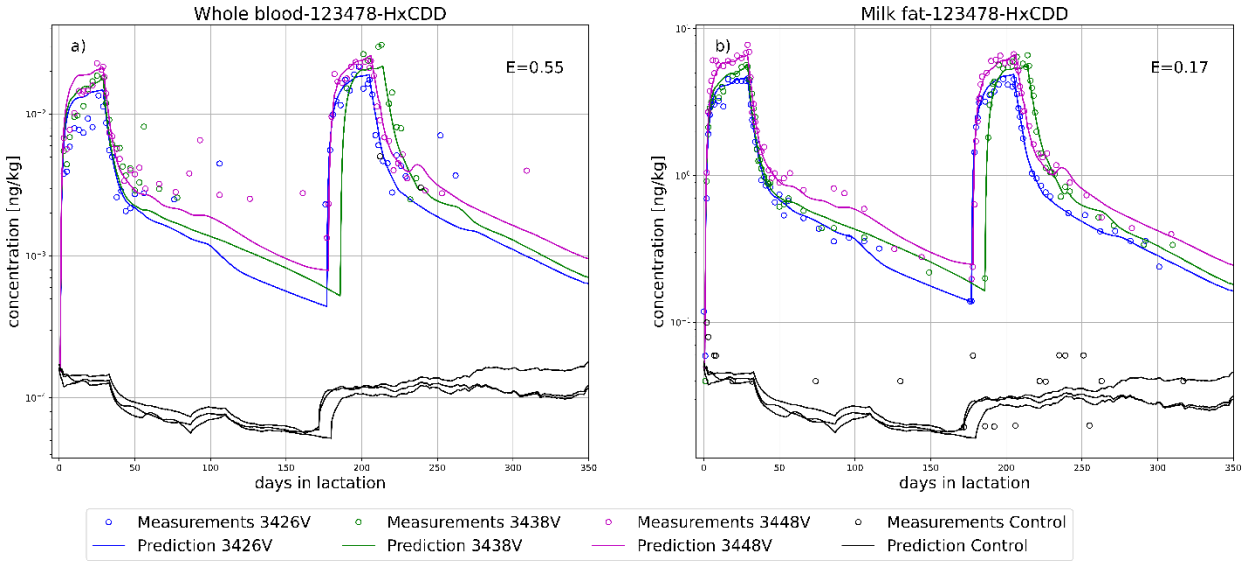

Figure S10: Concentration-time profiles of 123478-HxCDD in blood and in milk fat of all 6 cows, which were considered for modeling. The dots represent the measured data and the lines model predictions. E describes the weighted log error of equation (4) for the respective data set.

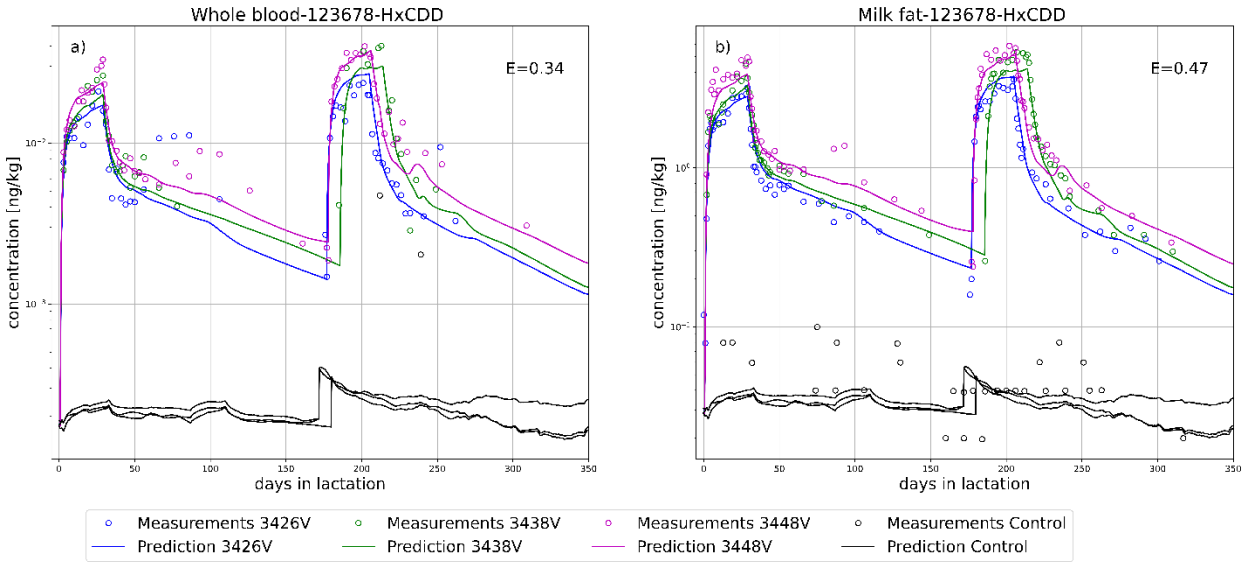

Figure S11: Concentration-time profiles of 123678-HxCDD in blood and in milk fat of all 6 cows, which were considered for modeling. The dots represent the measured data and the lines model predictions. E describes the weighted log error of equation (4) for the respective data set.

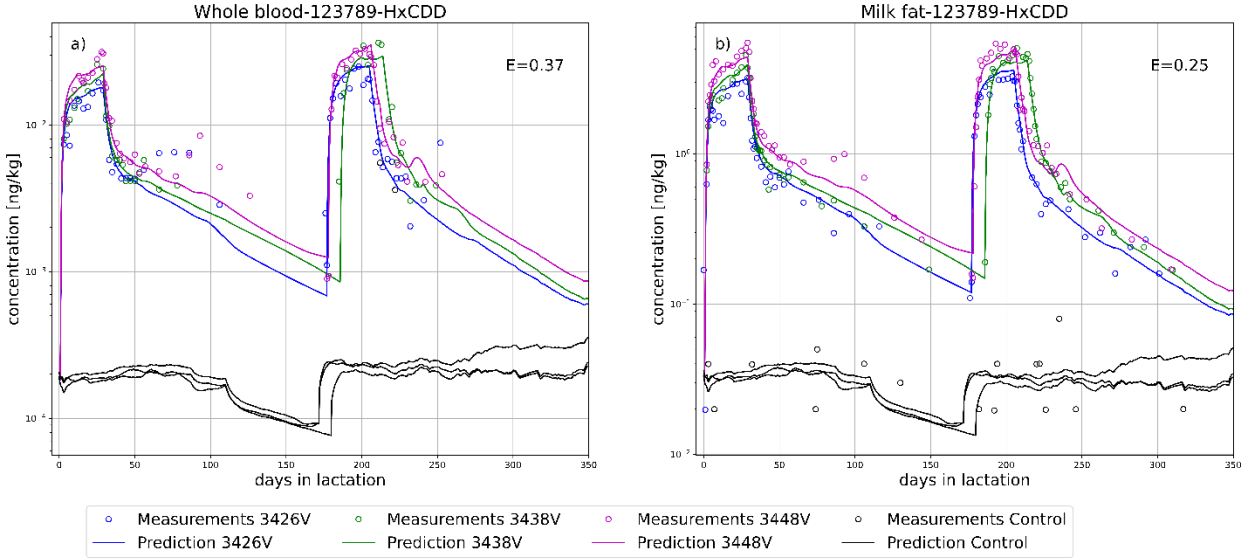

Figure S12: Concentration-time profiles of 123789-HxCDD in blood and in milk fat of all 6 cows, which were considered for modeling. The dots represent the measured data and the lines model predictions. E describes the weighted log error of equation (4) for the respective data set.

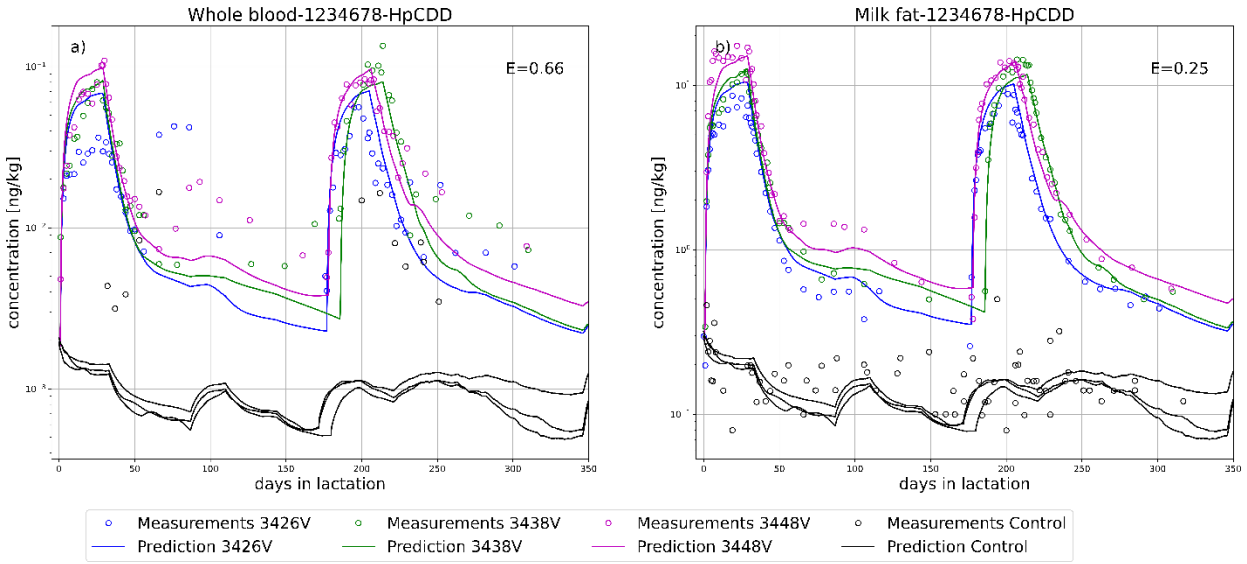

183

184 *Figure S13: Concentration-time profiles of 1234678-HpCDD in blood and in milk fat of all 6 cows, which were*
185 *considered for modeling. The dots represent the measured data and the lines model predictions. E describes the*
186 *weighted log error of equation (4) for the respective data set.*

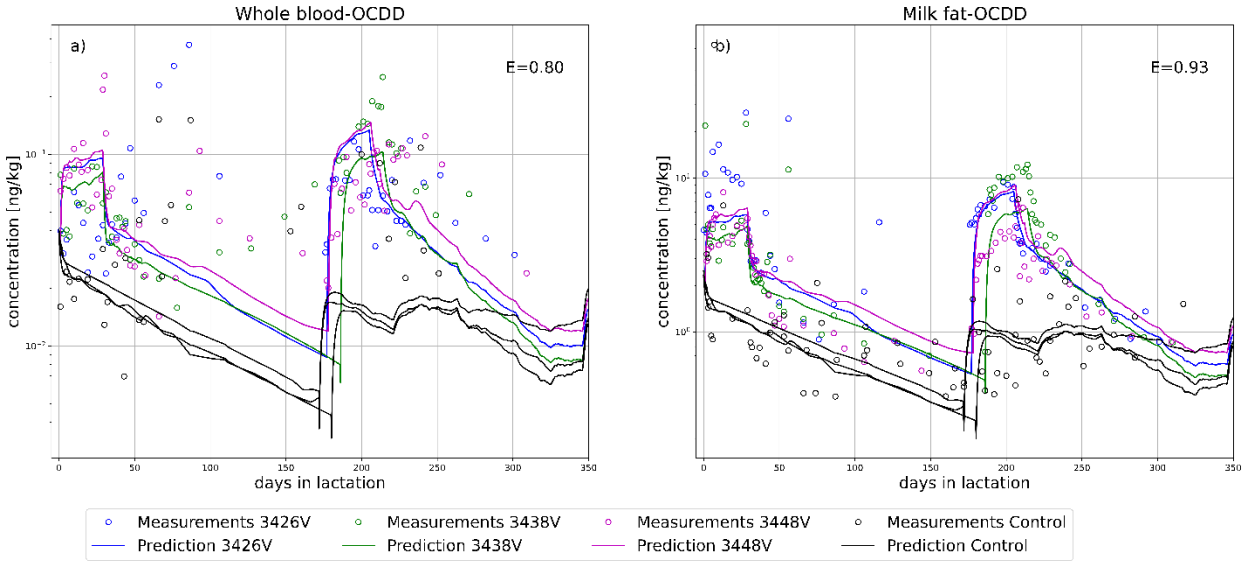

187

188 *Figure S14: Concentration-time profiles of OCDD in blood and in milk fat of all 6 cows, which were considered for*
189 *modeling. The dots represent the measured data and the lines model predictions. E describes the weighted log error*
190 *of equation (4) for the respective data set.*

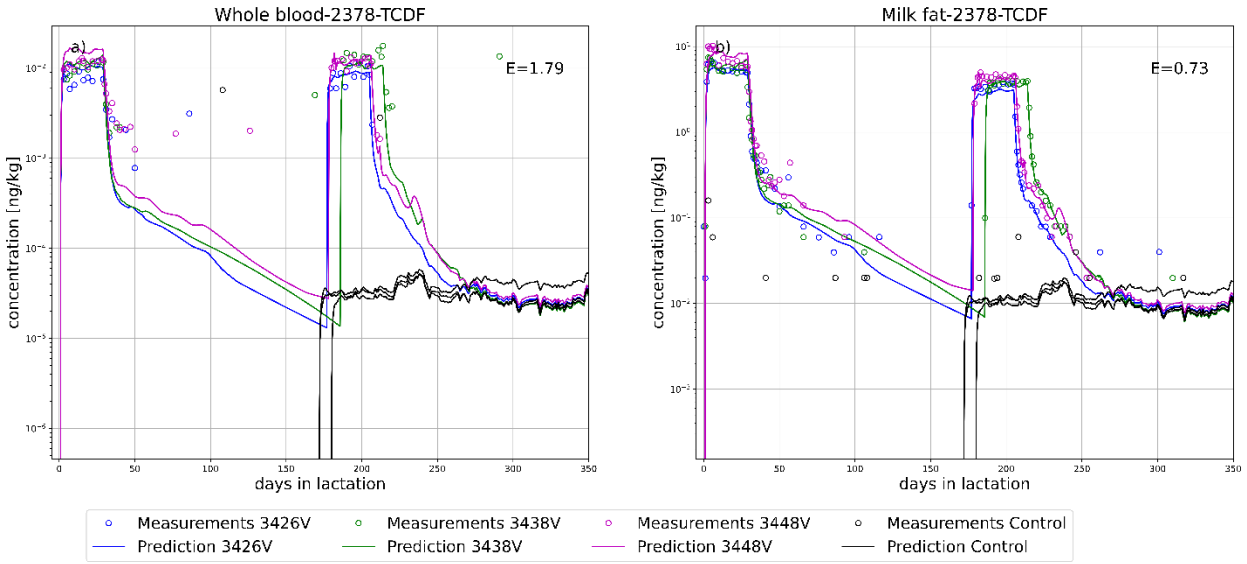

Figure S15: Concentration-time profiles of 2378-TCDF in blood and in milk fat of all 6 cows, which were considered for modeling. The dots represent the measured data and the lines model predictions. E describes the weighted log error of equation (4) for the respective data set. The concentration of the control cows in NEB phase are assumed to be 0.

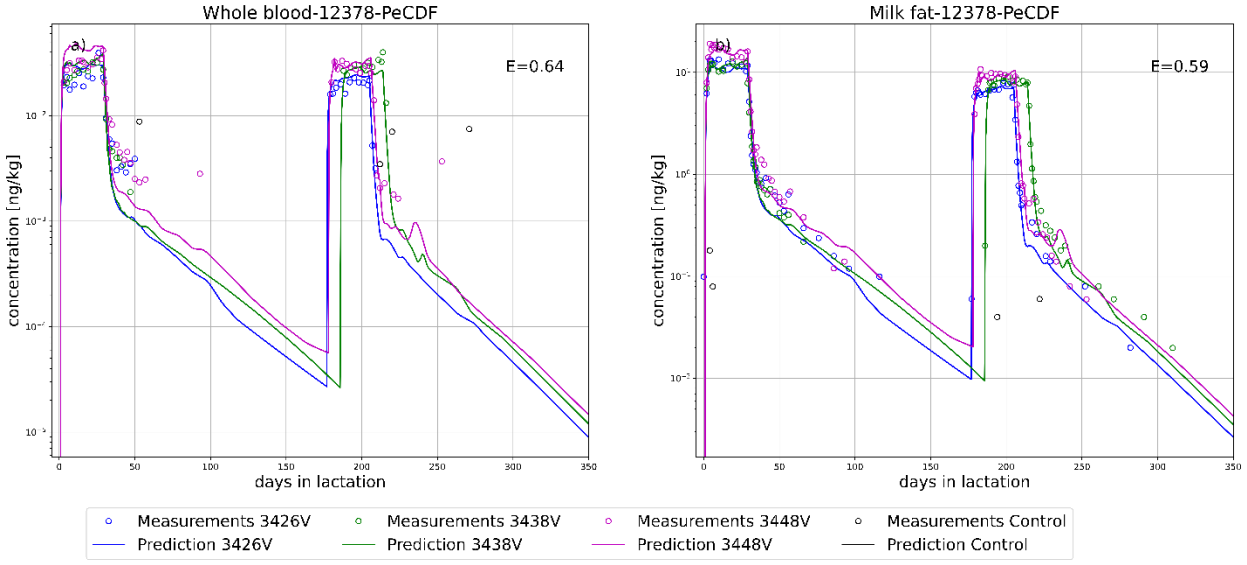

Figure S16: Concentration-time profiles of 12378-PeCDF in blood and in milk fat of all 6 cows, which were considered for modeling. The dots represent the measured data and the lines model predictions. E describes the weighted log error of equation (4) for the respective data set. The concentration of the control cows are assumed to be 0.

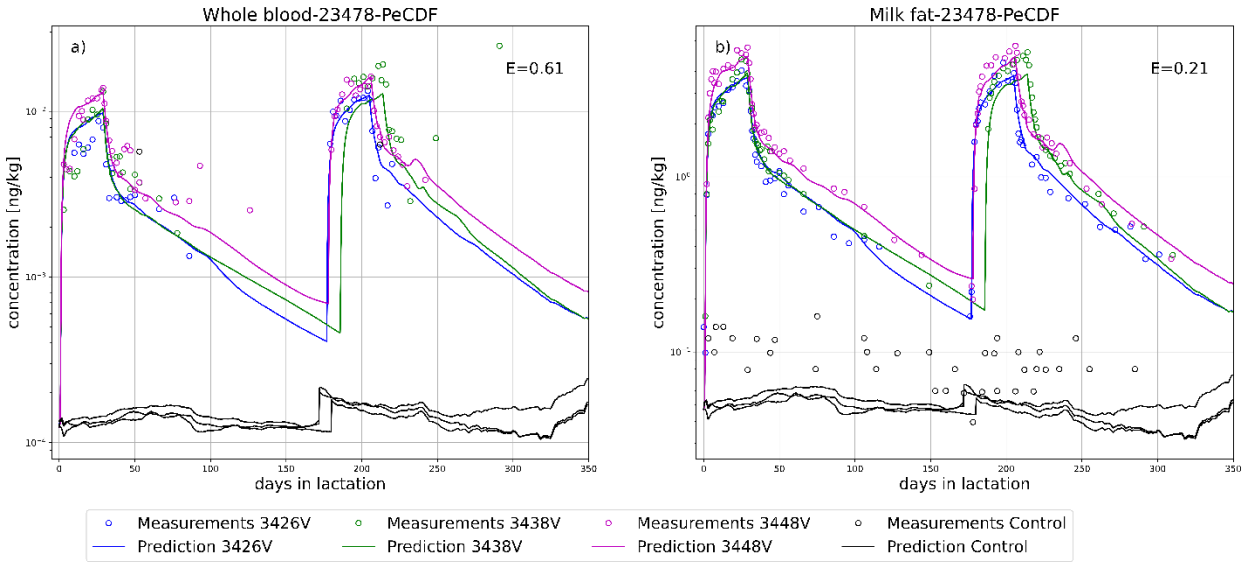

201

202 *Figure S17: Concentration-time profiles of 23478-PeCDF in blood and in milk fat of all 6 cows, which were considered*
203 *for modeling. The dots represent the measured data and the lines model predictions. E describes the weighted log*
204 *error of equation (4) for the respective data set.*

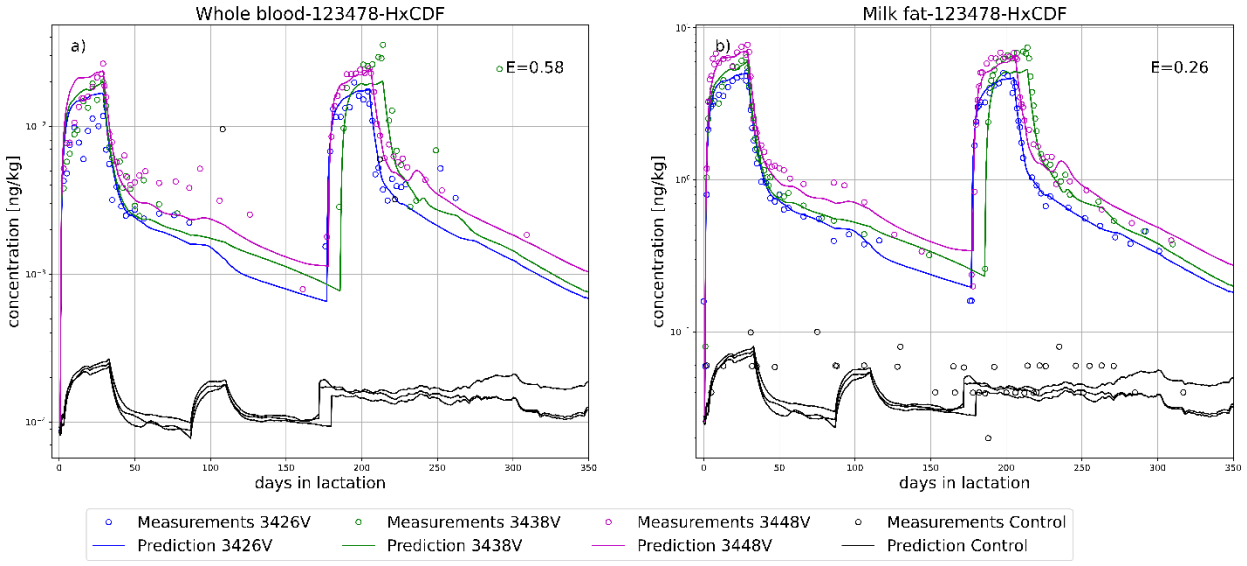

205

206 *Figure S18: Concentration-time profiles of 123478-HxCDF in blood and in milk fat of all 6 cows, which were*
207 *considered for modeling. The dots represent the measured data and the lines model predictions. E describes the*
208 *weighted log error of equation (4) for the respective data set.*

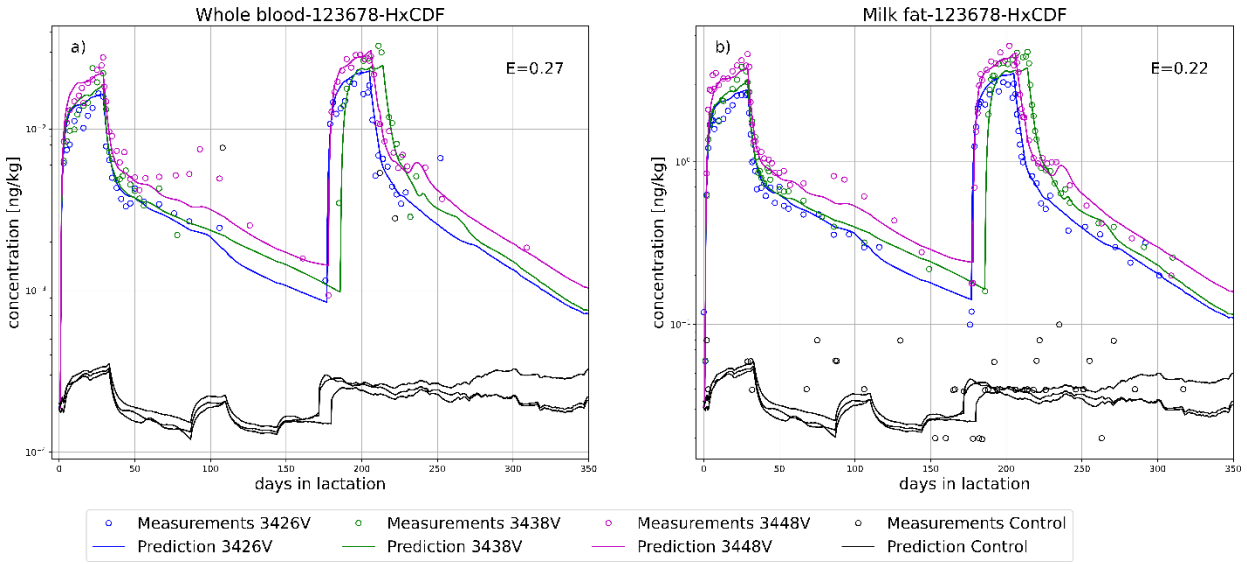

Figure S19: Concentration-time profiles of 123678-HxCDF in blood and in milk fat of all 6 cows, which were considered for modeling. The dots represent the measured data and the lines model predictions. E describes the weighted log error of equation (4) for the respective data set.

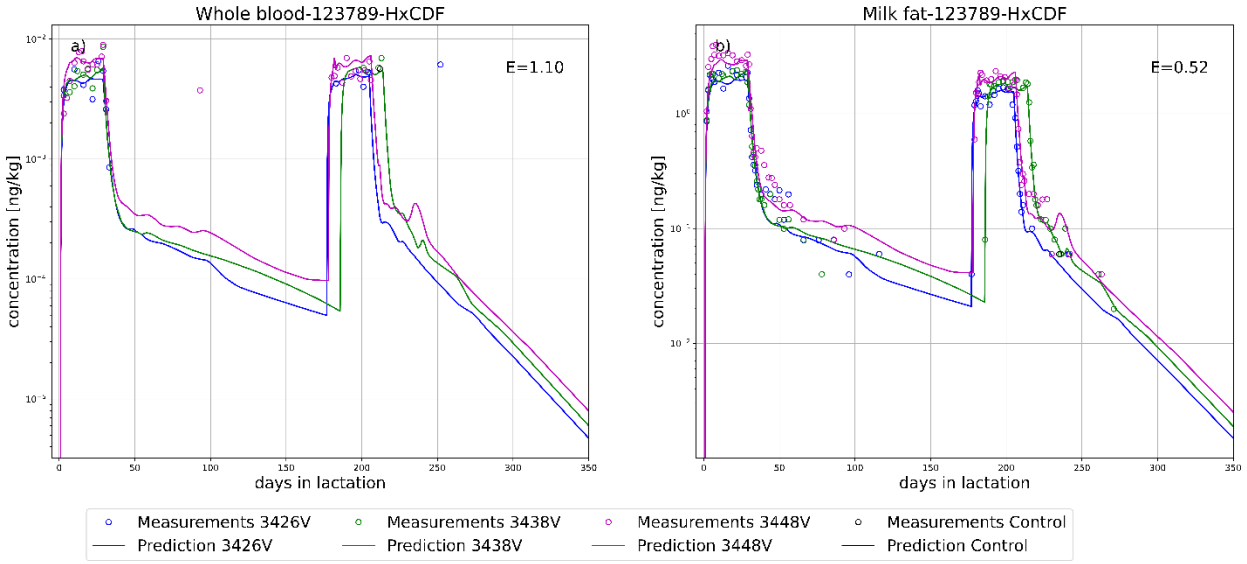

Figure S20: Concentration-time profiles of 123789-HxCDF in blood and in milk fat of all 6 cows, which were considered for modeling. The dots represent the measured data and the lines model predictions. E describes the weighted log error of equation (4) for the respective data set. The concentrations of the control cows are assumed to be 0.

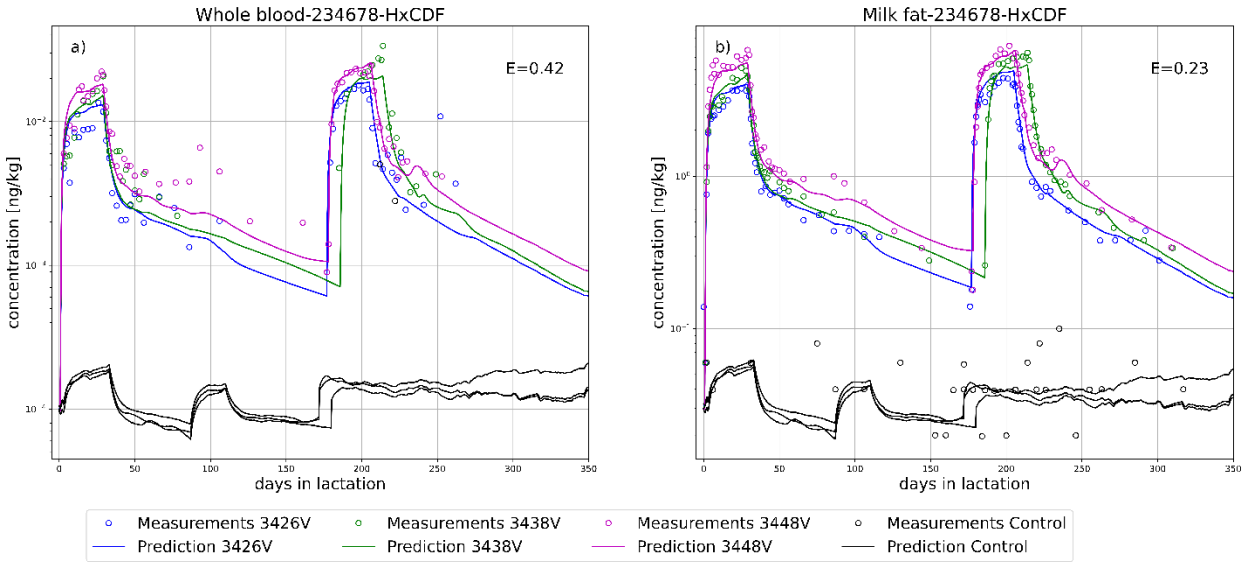

Figure S21: Concentration-time profiles of 234678-HxCDF in blood and in milk fat of all 6 cows, which were considered for modeling. The dots represent the measured data and the lines model predictions. E describes the weighted log error of equation (4) for the respective data set.

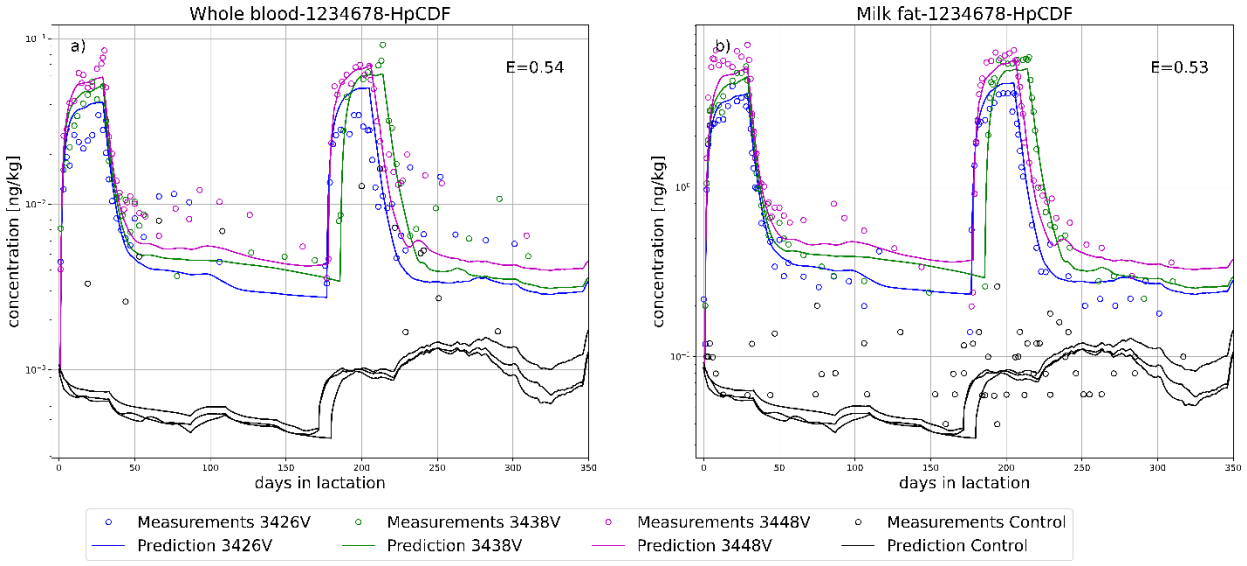

Figure S22: Concentration-time profiles of 1234678-HpCDF in blood and in milk fat of all 6 cows, which were considered for modeling. The dots represent the measured data and the lines model predictions. E describes the weighted log error of equation (4) for the respective data set.

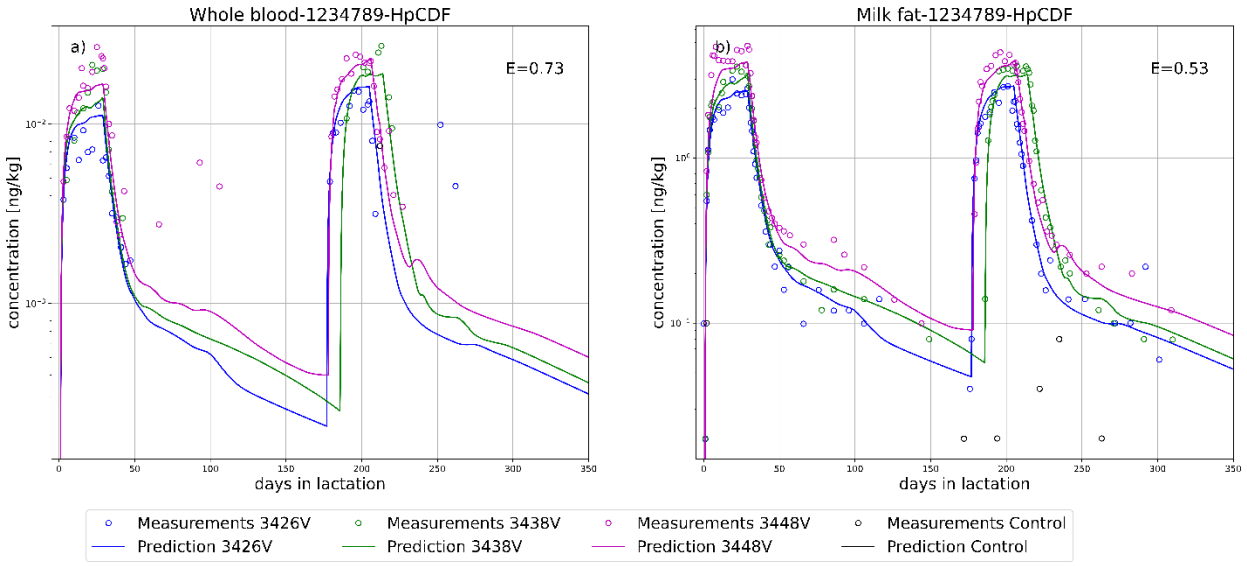

Figure S23: Concentration-time profiles of 1234789-HpCDF in blood and in milk fat of all 6 cows, which were considered for modeling. The dots represent the measured data and the lines model predictions. E describes the weighted log error of equation (4) for the respective data set. The concentrations of the control cows are assumed to be 0.

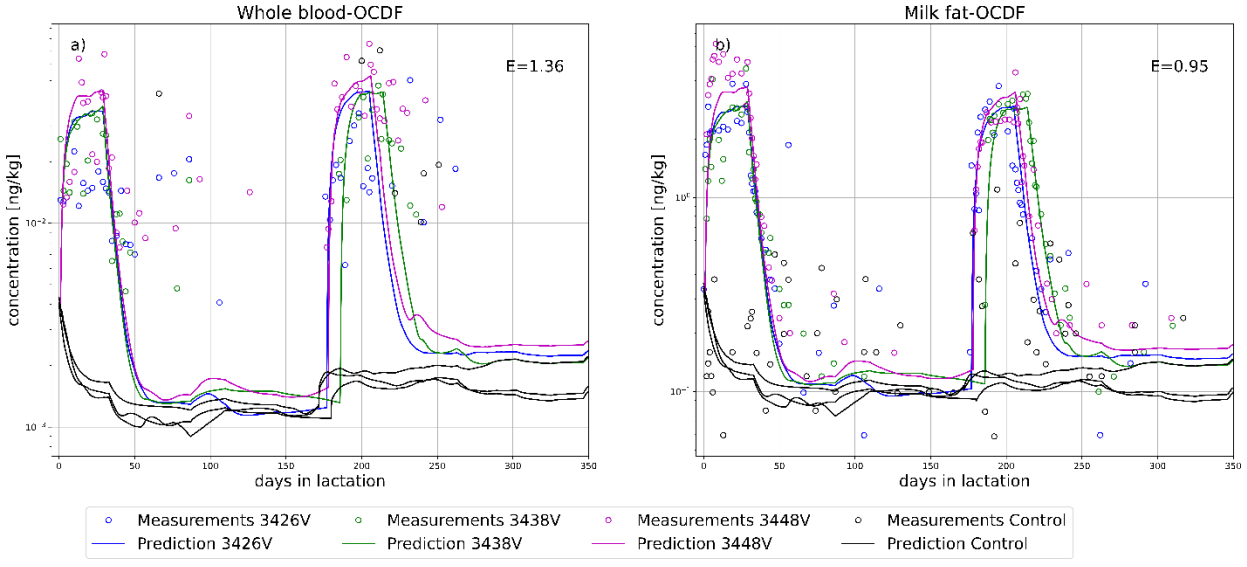

Figure S24: Concentration-time profiles of OCDF in blood and in milk fat of all 6 cows, which were considered for modeling. The dots represent the measured data and the lines model predictions. E describes the weighted log error of equation (4) for the respective data set.

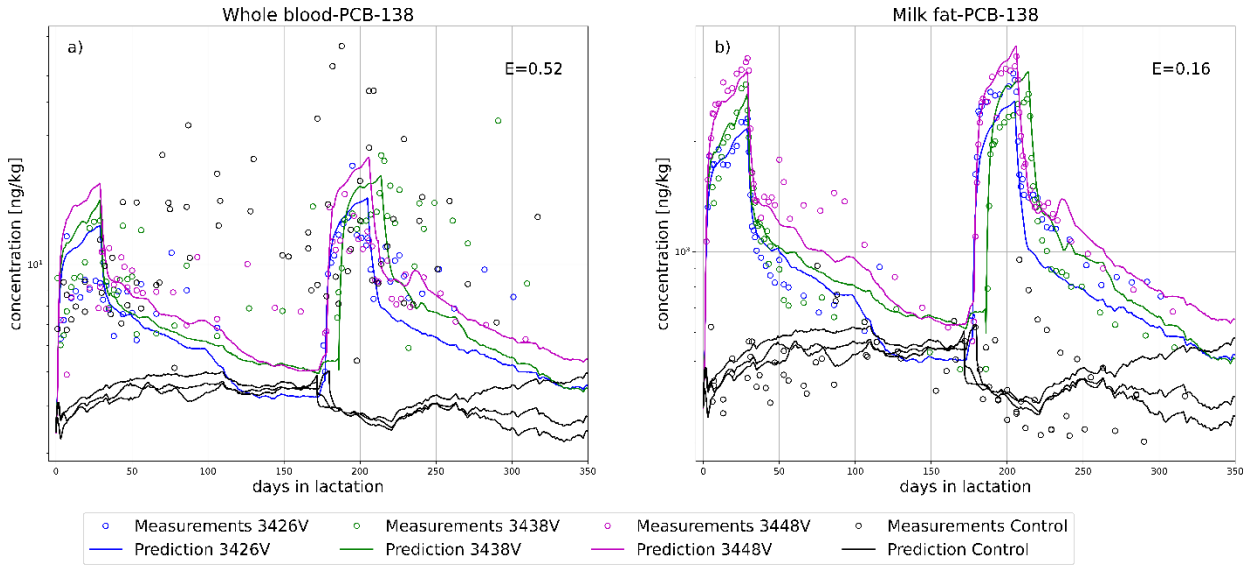

Figure S25: Concentration-time profiles of PCB-138 in blood and in milk fat of all 6 cows, which were considered for modeling. The dots represent the measured data and the lines model predictions. E describes the weighted log error of equation (4) for the respective data set.

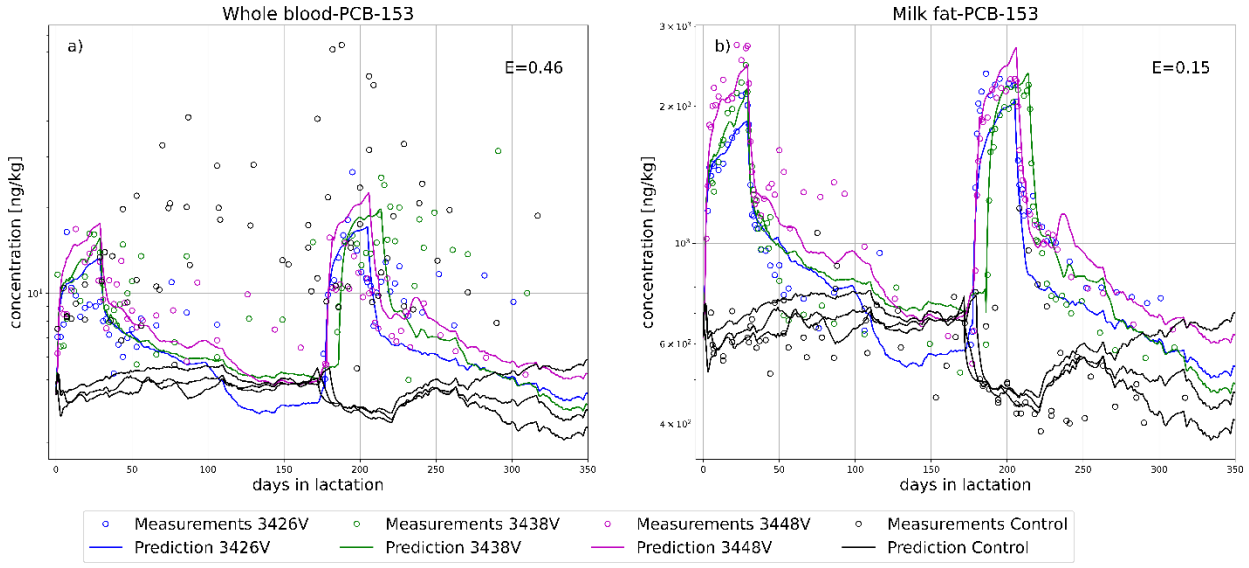

Figure S26: Concentration-time profiles of PCB-153 in blood and in milk fat of all 6 cows, which were considered for modeling. The dots represent the measured data and the lines model predictions. E describes the weighted log error of equation (4) for the respective data set.

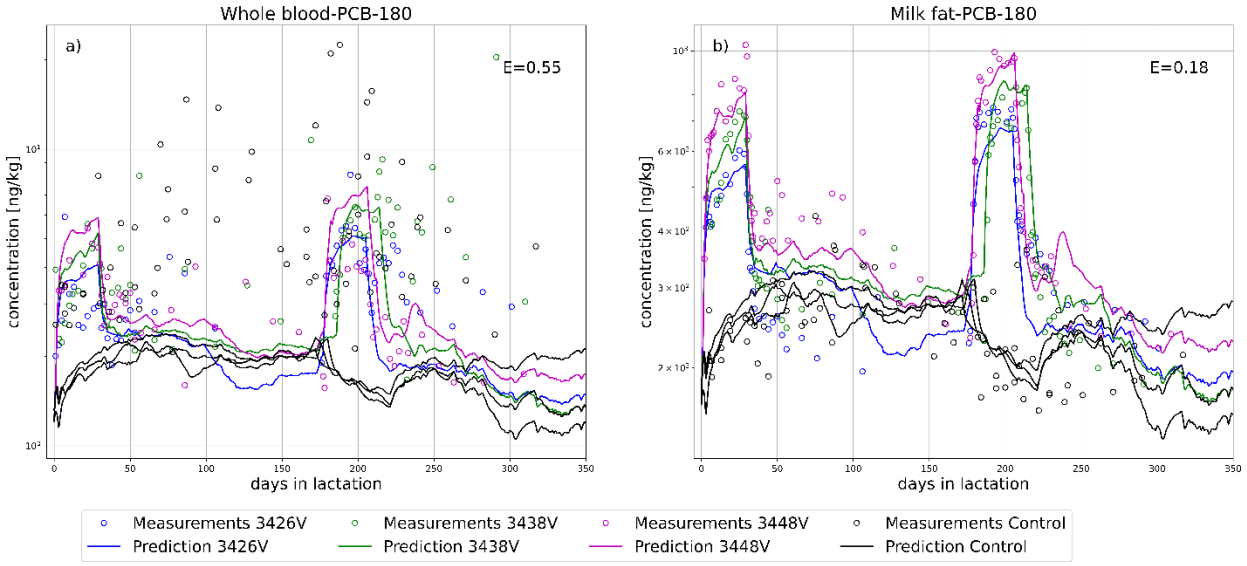

Figure S27: Concentration-time profiles of PCB-180 in blood and in milk fat of all 6 cows, which were considered for modeling. The dots represent the measured data and the lines model predictions. E describes the weighted log error of equation (4) for the respective data set.

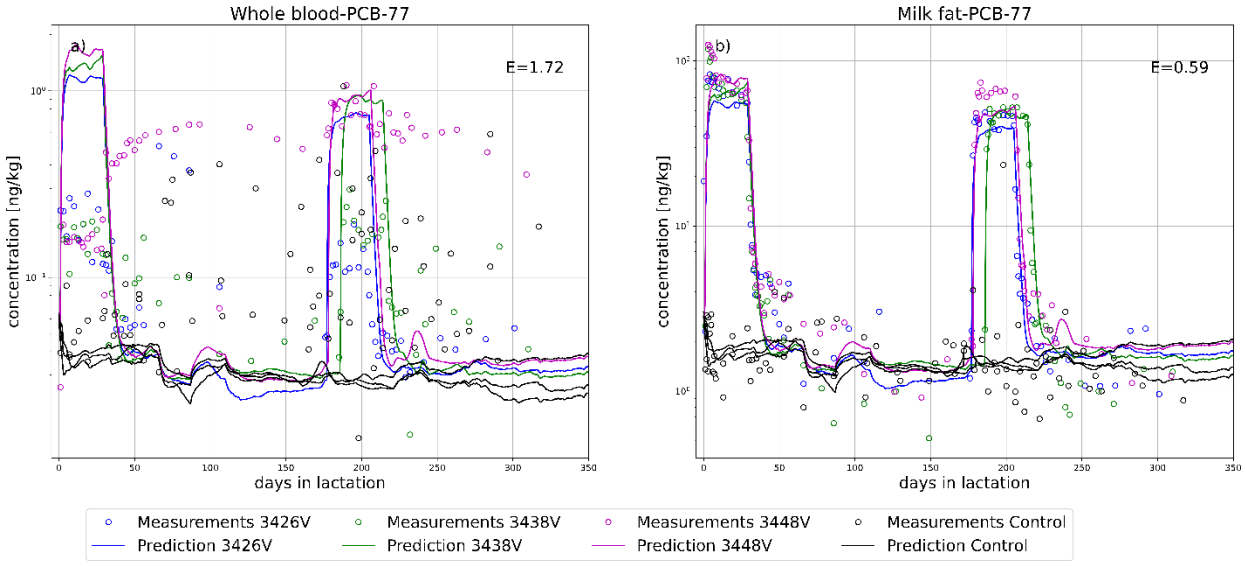

Figure S28: Concentration-time profiles of PCB-77 in blood and in milk fat of all 6 cows, which were considered for modeling. The dots represent the measured data and the lines model predictions. E describes the weighted log error of equation (4) for the respective data set.

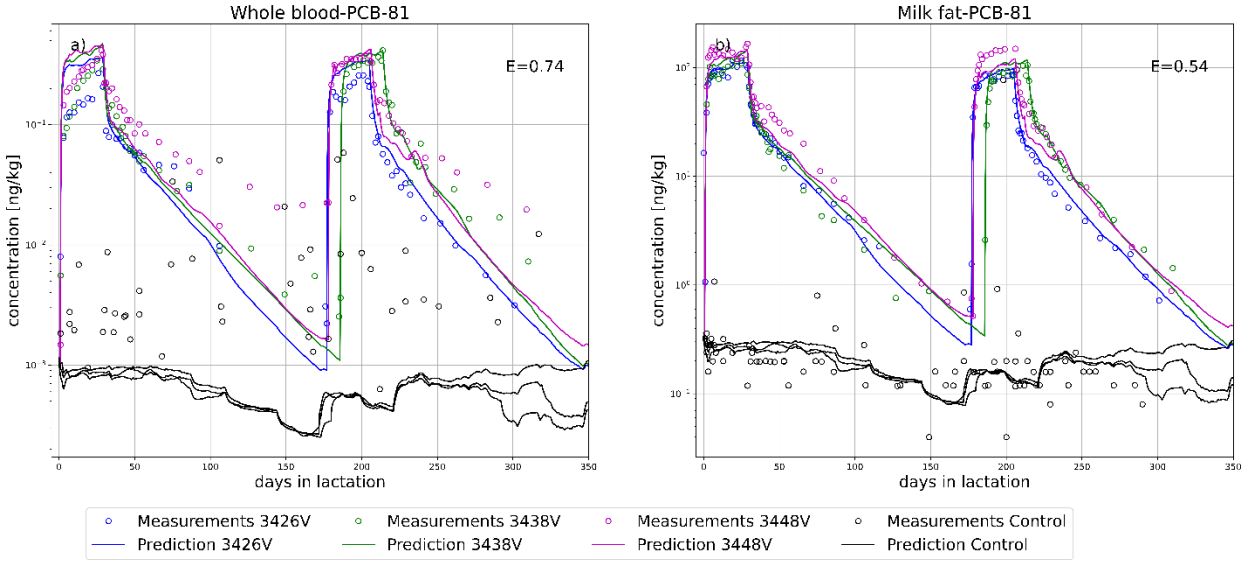

251

252 *Figure S29: Concentration-time profiles of PCB-81 in blood and in milk fat of all 6 cows, which were considered for*
253 *modeling. The dots represent the measured data and the lines model predictions. E describes the weighted log error*
254 *of equation (4) for the respective data set.*

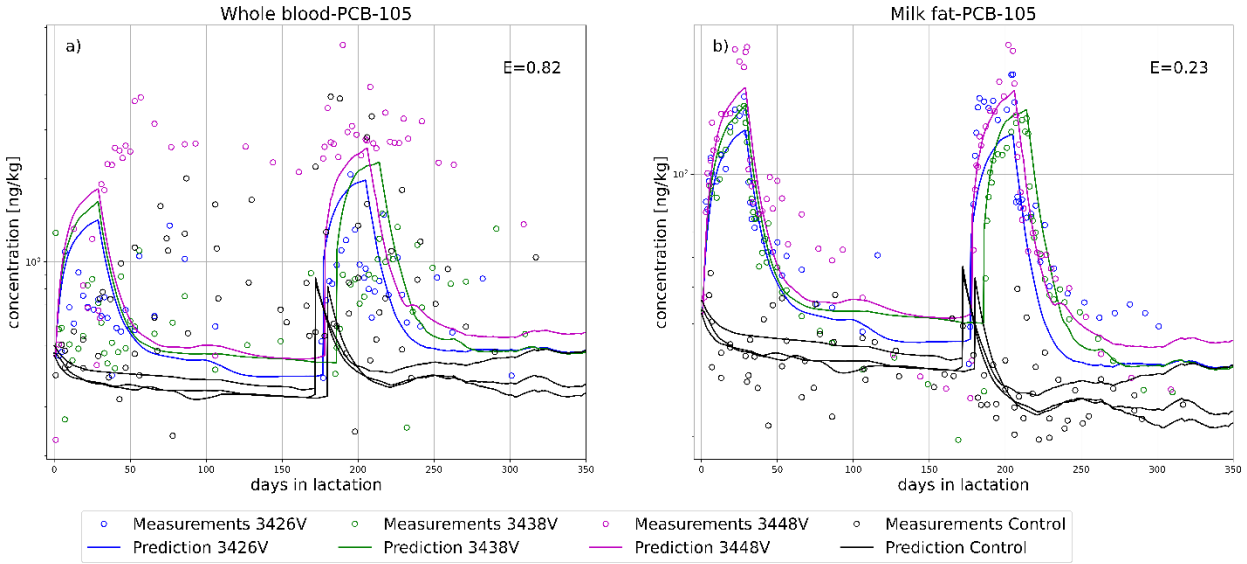

255

256 *Figure S30: Concentration-time profiles of PCB-105 in blood and in milk fat of all 6 cows, which were considered for*
257 *modeling. The dots represent the measured data and the lines model predictions. E describes the weighted log error*
258 *of equation (4) for the respective data set.*

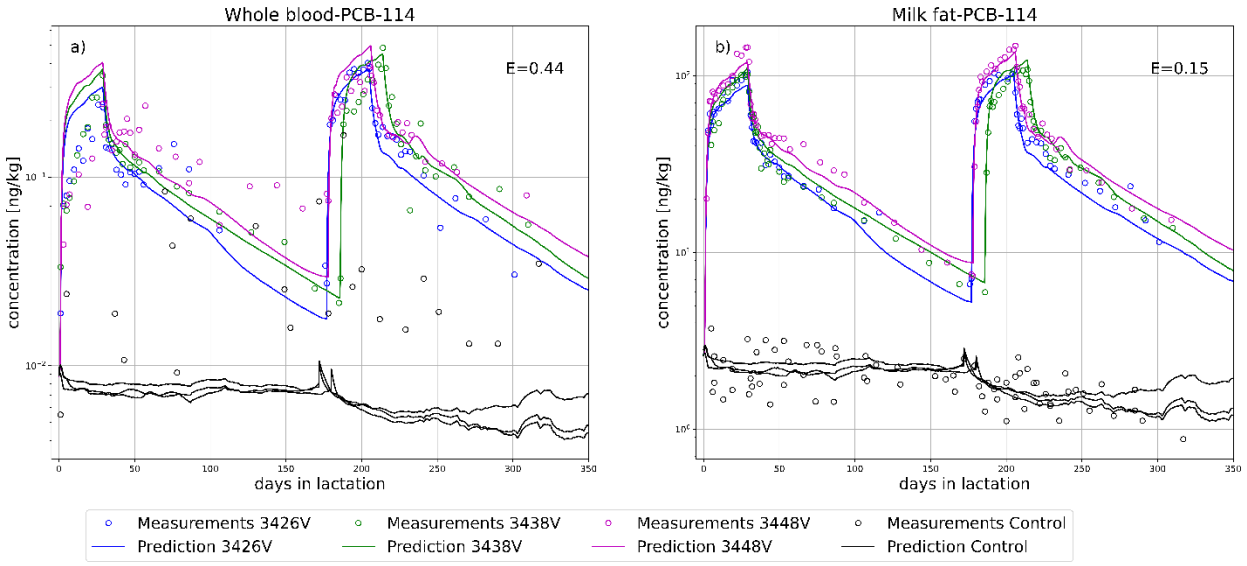

Figure S31: Concentration-time profiles of PCB-114 in blood and in milk fat of all 6 cows, which were considered for modeling. The dots represent the measured data and the lines model predictions. E describes the weighted log error of equation (4) for the respective data set.

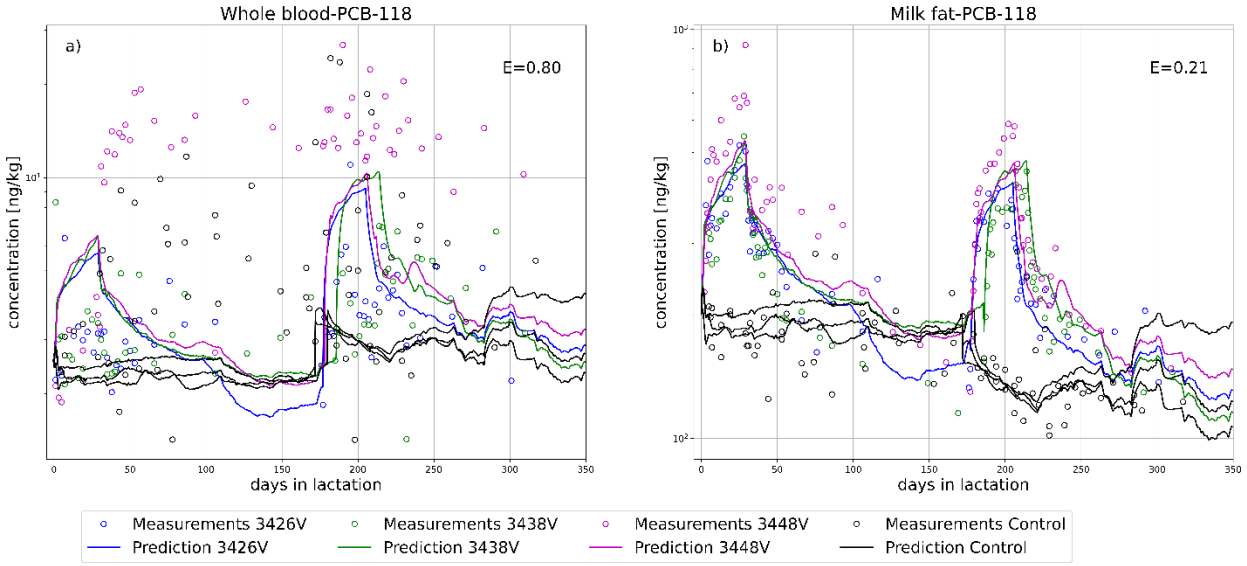

Figure S32: Concentration-time profiles of PCB-118 in blood and in milk fat of all 6 cows, which were considered for modeling. The dots represent the measured data and the lines model predictions. E describes the weighted log error of equation (4) for the respective data set.

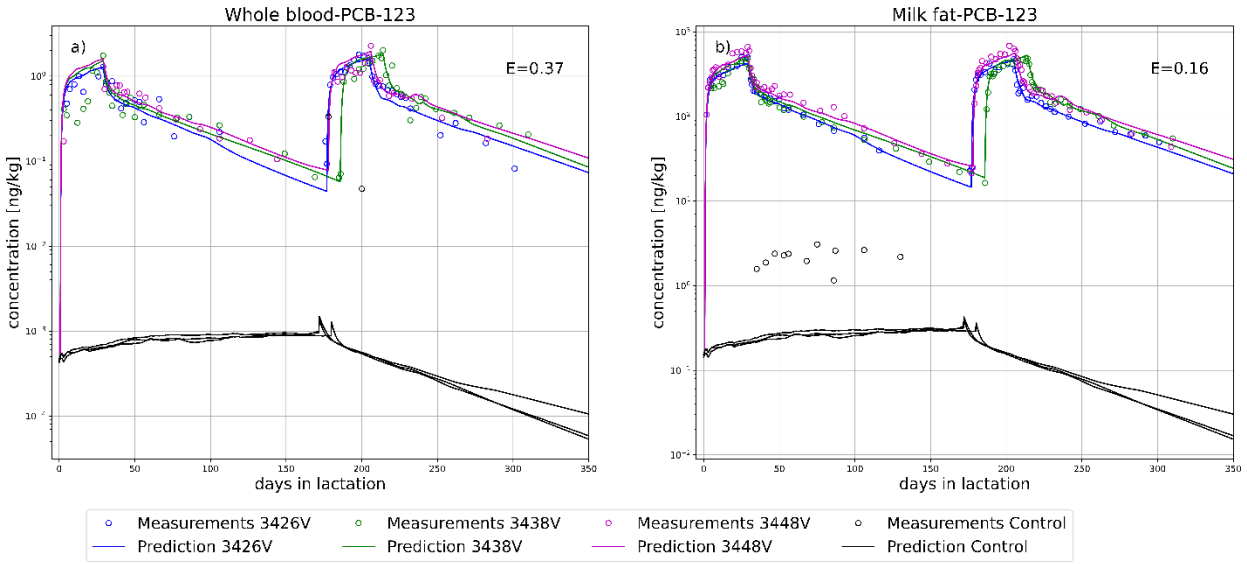

267

268 *Figure S33: Concentration-time profiles of PCB-123 in blood and in milk fat of all 6 cows, which were considered for*
269 *modeling. The dots represent the measured data and the lines model predictions. E describes the weighted log error*
270 *of equation (4) for the respective data set.*

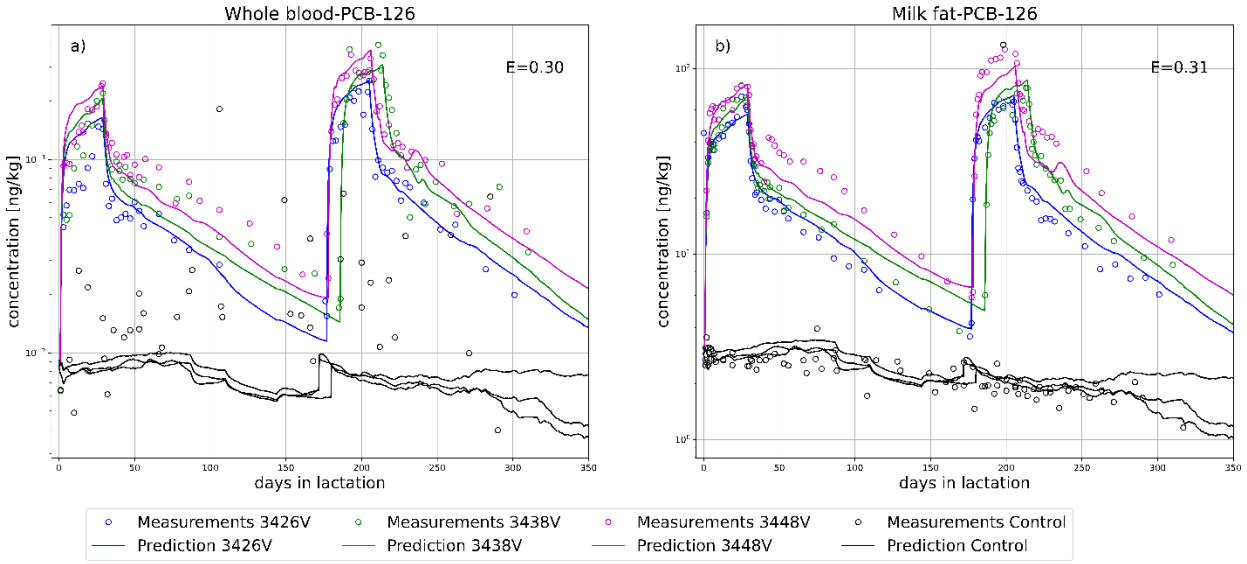

271

272 *Figure S34: Concentration-time profiles of PCB-126 in blood and in milk fat of all 6 cows, which were considered for*
273 *modeling. The dots represent the measured data and the lines model predictions. E describes the weighted log error*
274 *of equation (4) for the respective data set.*

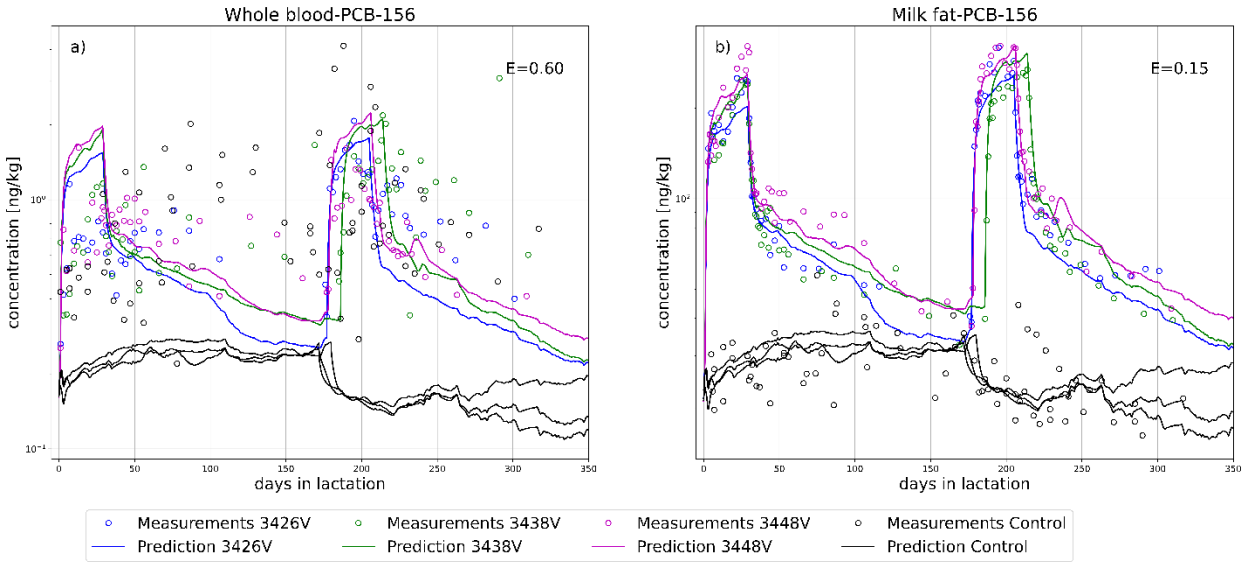

275

276 *Figure S35: Concentration-time profiles of PCB-156 in blood and in milk fat of all 6 cows, which were considered for*
277 *modeling. The dots represent the measured data and the lines model predictions. E describes the weighted log error*
278 *of equation (4) for the respective data set.*

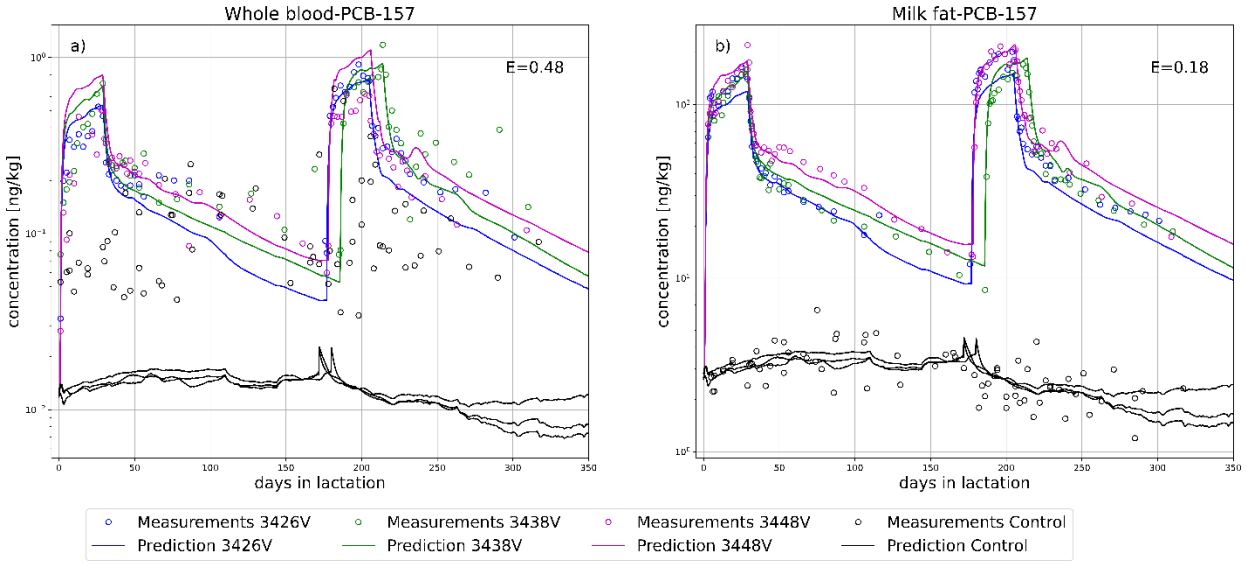

279

280 *Figure S36: Concentration-time profiles of PCB-157 in blood and in milk fat of all 6 cows, which were considered for*
281 *modeling. The dots represent the measured data and the lines model predictions. E describes the weighted log error*
282 *of equation (4) for the respective data set.*

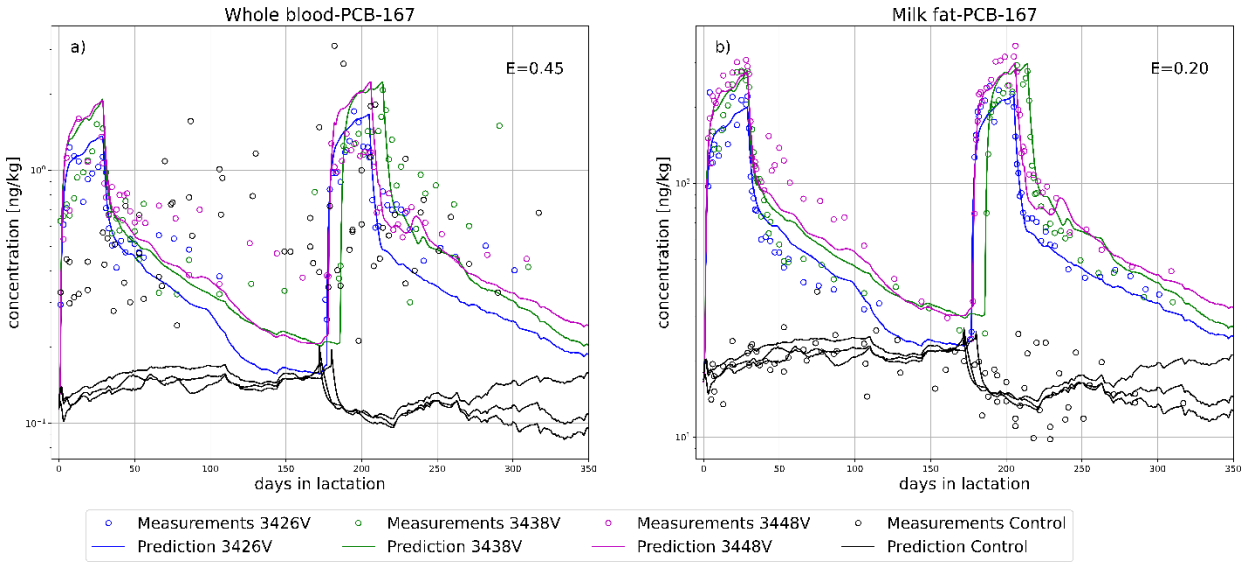

283

284 *Figure S37: Concentration-time profiles of PCB-167 in blood and in milk fat of all 6 cows, which were considered for*
285 *modeling. The dots represent the measured data and the lines model predictions. E describes the weighted log error*
286 *of equation (4) for the respective data set.*

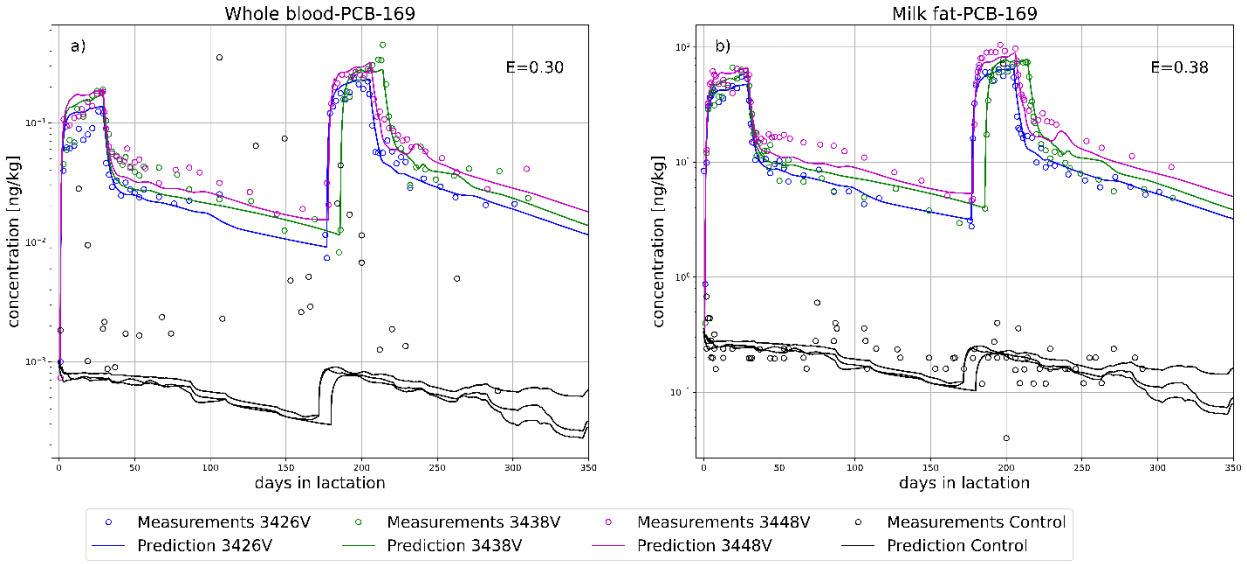

287

288 *Figure S38: Concentration-time profiles of PCB-169 in blood and in milk fat of all 6 cows, which were considered for*
289 *modeling. The dots represent the measured data and the lines model predictions. E describes the weighted log error*
290 *of equation (4) for the respective data set.*

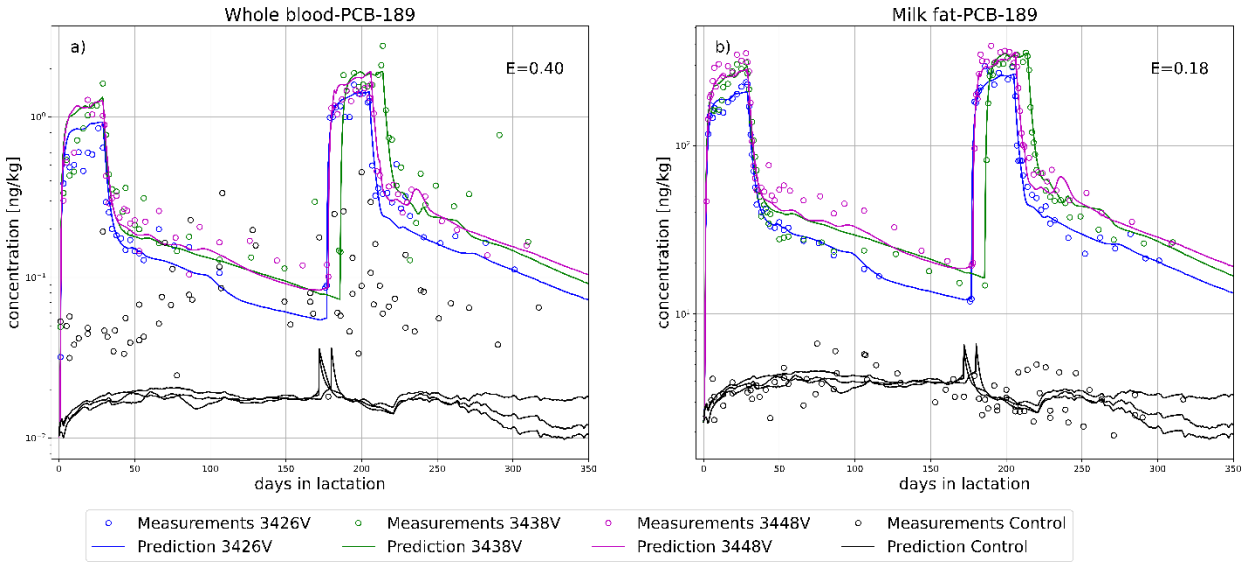

Figure S39: Concentration-time profiles of PCB-189 in blood and in milk fat of all 6 cows, which were considered for modeling. The dots represent the measured data and the lines model predictions. E describes the weighted log error of equation (4) for the respective data set.

References

(1) Krause, T.; Moenning, J.-L.; Lamp, J.; Maul, R.; Schenkel, H.; Fürst, P.; Pieper, R.; Numata, J. Transfer of Polychlorinated Dibenzo-p-dioxins and Dibenzofurans (PCDD/Fs) and Polychlorinated Biphenyls (PCBs) from Feed into Cow's Milk - Part 1: State of Knowledge and Uncertainties. *Nutrition Research Reviews* **2022**

Paper 4

Moenning, J.-L., et al., Toxicokinetic modelling of the transfer of non-dioxin like polychlorinated biphenyls from feed into edible tissues of pigs. Science of The Total Environment, 2023: p. 164539

Supplementary Material: Toxicokinetic modelling of the transfer of non-dioxin like polychlorinated biphenyls from feed into edible tissues of pigs

Jan-Louis Moenning, Britta Ohlhoff, Mariko Yamamoto, Anke Jährmann, Anne Jahnke, Anja Lüth, Robert Pieper, Jorge Numata

1 Relevance of the biexponetial behaviour in the peripheral compartment

To prove that the initial depuration phase is less relevant in the peripheral compartment of a standard two compartment model, note that the solution to a standard two compartment model under constant feeding conditions can always be described as

$$\dot{A}(t) = MA(t) + I. \tag{S1}$$

Where $A(t) = (A_C(t), A_P(t))^T \in \mathbb{R}^2_{+,0}$ is the amount vector containing the amounts of contaminants in both compartments at time t. $I = ((I_C), 0)^T \in \mathbb{R}^2_{+,0}$ is the input vector and $M \in \mathbb{R}^{2\times 2}$ is the transition matrix given by

$$M = \begin{pmatrix} -(a+b) & c \\ b & -c \end{pmatrix} \tag{S2}$$

for some $a, b, c \in \mathbb{R}_+$.
A solution to S1 during depuration phase, i.e. $I \equiv 0$, has always the form

$$A(t) = e^{\lambda_1 t} \begin{pmatrix} p_1^1 \\ p_2^1 \end{pmatrix} + e^{\lambda_2 t} \begin{pmatrix} p_1^2 \\ p_2^2 \end{pmatrix} \tag{S3}$$

with $p_1^1, p_1^2, p_2^1, p_2^2 \in \mathbb{R}$ and $\lambda_1 < \lambda_2 \in \mathbb{R}_-$ being the elimination speed, where λ_1 is associated to the early depuration phase and λ_2 to the late depuration phase. Therefore to show that the fast depuration phase is less influence in the peripheral compartment it is sufficient to show that

$$\frac{|p_2^1|}{|p_2^2|} < \frac{|p_1^1|}{|p_1^2|}. \tag{S4}$$

For simplicity, to prove S4 it is assume that the system start from steady state, i.e.

$$A(0) = -M^{-1} \begin{pmatrix} I_C \\ 0 \end{pmatrix} \tag{S5}$$

with $I_C > 0$. Furthermore to prove this statement it has to be assumed that

$$p_1^1 > 0. \tag{S6}$$

This assumption seems to be reasonable for the investigated congener as $p_1^1 \leq 0$ would result in a initial slower or equal elimination (longer half life) than in latter phases of the depuration in the central compartment, which would contradict the behaviour reported in the literature.

Theorem 1. *For any solution of equation S1 during depuration ($I \equiv 0$) of the form S3 inequality S4 holds true assuming the system started in steady state (S5) and S6.*

Proof. A solution of S1 is given by

$$A(t) = e^{Mt} A(0) \tag{S7}$$

The first factor can be explicitly written out as

$$e^{Mt} = \frac{1}{\lambda_2 - \lambda_1} \begin{pmatrix} (\lambda_2 + c)e^{\lambda_2 t} - (\lambda_1 + c)e^{\lambda_1 t} & ce^{\lambda_2 t} - ce^{\lambda_1 t} \\ be^{\lambda_2 t} - be^{\lambda_1 t} & (-\lambda_1 - c)e^{\lambda_2 t} - (-\lambda_2 - c)e^{\lambda_1 t} \end{pmatrix} \tag{S8}$$

with

$$\lambda_1 := \frac{1}{2}(-\sqrt{(a+b+c)^2 - 4ac} - a - b - c), \tag{S9}$$

$$\lambda_2 := \frac{1}{2}(\sqrt{(a+b+c)^2 - 4ac} - a - b - c). \tag{S10}$$

Due to linearity of equation S1 w.l.o.g. it can be assumed $I_C = a(\lambda_2 - \lambda_1)$, then the second factor can be explicitly written out as

$$A(0) = \frac{1}{a} \begin{pmatrix} 1 & 1 \\ \frac{b}{c} & \frac{a+b}{c} \end{pmatrix} \begin{pmatrix} a(\lambda_2 - \lambda_1) \\ 0 \end{pmatrix} \tag{S11}$$

$$= (\lambda_2 - \lambda_1) \begin{pmatrix} 1 \\ \frac{b}{c} \end{pmatrix}. \tag{S12}$$

Next from the definitions of λ_1 and λ_2 (S9,S10) follows

$$p_1^1 = -\lambda_1 - c - b \tag{S13}$$

$$= \lambda_2 + a \overset{S6}{>} 0, \tag{S14}$$

$$p_1^2 = \lambda_1 + c + b \tag{S15}$$

$$= -\lambda_1 - a > 0 \tag{S16}$$

and

$$p_2^1 = -b - (-\lambda_2 - c)\frac{b}{c} \tag{S17}$$

$$= \lambda_2 \frac{b}{c} < 0, \tag{S18}$$

$$p_2^2 = b + (-\lambda_1 - c)\frac{b}{c} \tag{S19}$$

$$= -\lambda_1 \frac{b}{c} > 0. \tag{S20}$$

Therefore

$$\frac{|p_2^1|}{|p_2^2|} = \frac{\lambda_2}{\lambda_1} \tag{S21}$$

$$< \frac{\lambda_2 + a}{\lambda_1 + a} \tag{S22}$$

$$= \frac{|p_1^1|}{|p_1^2|}, \tag{S23}$$

because $0 > \lambda_k + a > \lambda_k$ for both $k \in \{1, 2\}$ and $\lambda_1 < \lambda_2 < 0$. □

Remark 1. *Note that $p_2^1 < 0$ for any standard two compartment model. This means that at the start of depuration phase the elimination rate in the peripheral compartment is always slower (longer half life) than at the end of depuration phase.*

Remark 2. *Note that* $\frac{|p_2^1|}{|p_2^2|}$ *can be directly calculated if the elimination rates* λ_k *are know, which means that the shape of the depuration phase function can already be derived knowing only the two elimination rates* λ_k*.*

2 Convergence of the transfer parameters

To prove that the transfer parameters used in this article we assume that the compartments T-total; F-fat; L-liver grow as follows:

$$V_T = r_T t + a_T, \tag{S24}$$
$$V_F = V_T f_F t, \tag{S25}$$
$$V_L = r_L V_T + a_L, \tag{S26}$$

and that the amount of contaminant given increases linear, i.e.

$$Dose^i = (r_S t + a_S) C_S, \tag{S27}$$

for some $r_T, r_S, r_L, f_F, C_S \in \mathbb{R}_+$ and $a_T, a_S, a_L \in \mathbb{R}$.

Theorem 2. *Assuming eq S24-S27 hold true for a pig, then*

$$TF_F = \frac{\varphi}{1 + \frac{k_{eli}}{\xi}} \tag{S28}$$

with

$$\varphi := \frac{r_S F_{abs}}{r_F 2}, \tag{S29}$$
$$\phi := \frac{r_F 2}{\tilde{r}_L} P_{FL}, \tag{S30}$$
$$r_F := f_F r_T, \tag{S31}$$
$$\tilde{r}_L := r_L r_T. \tag{S32}$$

Proof. Combining equation S24 and S25 yields

$$V_F = r_F t^2 + a_F t \tag{S33}$$

for $r_F := f_F r_T$ and $a_F := f_F a_T$.
Similar combining equation S24 and S26 yields

$$V_L = \tilde{r}_L t + \tilde{a}_F \tag{S34}$$

for $\tilde{r}_L := r_L r_T$ and $\tilde{a}_F := r_L a_T + a_L$.
Next note that due to $C_F = C_L P_{FL}$ and $V_F \in \Theta(t^2)$, $V_L \in \Theta(t)$ it holds true that

$$\lim_{t\to\infty} C_F = \lim_{t\to\infty} \frac{A_T}{V_F} \tag{S35}$$

Using L'Hôpital's rule yields than

$$\lim_{t\to\infty} C_F = \lim_{t\to\infty} \frac{A_T}{V_F} \tag{S36}$$

$$= \lim_{t\to\infty} \frac{\dot{A}_T}{\dot{V}_F} \tag{S37}$$

$$= \lim_{t\to\infty} \frac{-k_{eli}A_T}{(1+\frac{V_F}{V_L}P_{FL})\dot{V}_F} + \frac{I}{\dot{V}_F} \tag{S38}$$

$$= \lim_{t\to\infty} \frac{A_T}{V_F}\frac{-k_{eli}}{(1+\frac{V_F}{V_L}P_{FL})\frac{\dot{V}_F}{V_F}} + \frac{I}{\dot{V}_F}. \tag{S39}$$

For the second term can be easily simplfied to

$$\lim_{t\to\infty} \frac{I}{\dot{V}_F} = \lim_{t\to\infty} \frac{C_S r_S F_{abs} t + o(1)}{r_F t2 + o(1)} \tag{S40}$$

$$= \frac{C_S r_S F_{abs}}{r_F 2} \tag{S41}$$

$$=: C_S\varphi. \tag{S42}$$

Next note that

$$\frac{\dot{V}_F}{V_F} = \frac{2r_F t + o(1)}{r_F t^2 + o(t)} \tag{S43}$$

and

$$\frac{V_F}{V_L} = \frac{r_F t^2 + o(t)}{\tilde{r}_L t + o(1)}. \tag{S44}$$

Combining equations S43 and S44 yields

$$\lim_{t\to\infty} (1+\frac{V_F}{V_L}P_{FL})\frac{\dot{V}_T}{V_T} = \lim_{t\to\infty} o(t-1) + \frac{r_F^2 2t^3 + o(t^2)}{r_L r_F t^3 + o(t^2)}P_{FL} \tag{S45}$$

$$= \frac{r_F 2}{\tilde{r}_L}P_{FL} \tag{S46}$$

$$=: \xi \tag{S47}$$

Inserting S47 and S42 in equation S39 yields

$$\lim_{t\to\infty} C_F = \frac{-k_{eli}}{\xi}\lim_{t\to\infty}\frac{A_T}{V_F} + C_S\varphi \tag{S48}$$

$$\overset{eq.S35}{=} \frac{-k_{eli}}{\xi}\lim_{t\to\infty} C_F + C_S\varphi \tag{S49}$$

$$\Leftrightarrow \lim_{t\to\infty} C_F = C_S\frac{\varphi}{1+\frac{k_{eli}}{\xi}} \tag{S50}$$

From this follows

$$TF_F = \lim_{t\to\infty}\frac{C_F}{C_S} = \frac{\varphi}{1+\frac{k_{eli}}{\xi}}. \tag{S51}$$

□

Lemma 1. *Assuming eq S24-S27 hold true for a pig, then*

$$TF_L = \frac{TF_F}{P_{FL}} \tag{S52}$$

Proof. Due to $C_F = C_L P_{FL}$ it holds true

$$TF_L = \lim_{t\to\infty} \frac{C_L}{C_S} \tag{S53}$$

$$= \lim_{t\to\infty} \frac{C_F}{C_S P_{FL}} \tag{S54}$$

$$= \frac{TF_F}{P_{FL}}. \tag{S55}$$

□

Lemma 2. *Assuming eq S24-S27 hold true for a pig, then*

$$TR = TF_F \frac{r_F}{r_S} \tag{S56}$$

Proof.

$$TR = \lim_{t\to\infty} \frac{A_T}{\int_0^t I(\tilde{t})d\tilde{t}} \tag{S57}$$

$$= \lim_{t\to\infty} \frac{V_F}{\int_0^t r_S\tilde{t} + a_S d\tilde{t}} \lim_{t\to\infty} \frac{A_T}{V_F C_S}. \tag{S58}$$

It then follow due to theorem 2 and equation S35 it follows

$$TR = TF_F \lim_{t\to\infty} \frac{V_T}{\int_0^t r_S\tilde{t} + a_S d\tilde{t}} \tag{S59}$$

$$= TF_F \lim_{t\to\infty} \frac{r_F t^2 + o(1)}{r_S t^2 + o(1)} \tag{S60}$$

$$= TF_F \frac{r_F}{r_S}. \tag{S61}$$

□

3 Sensitivity analysis

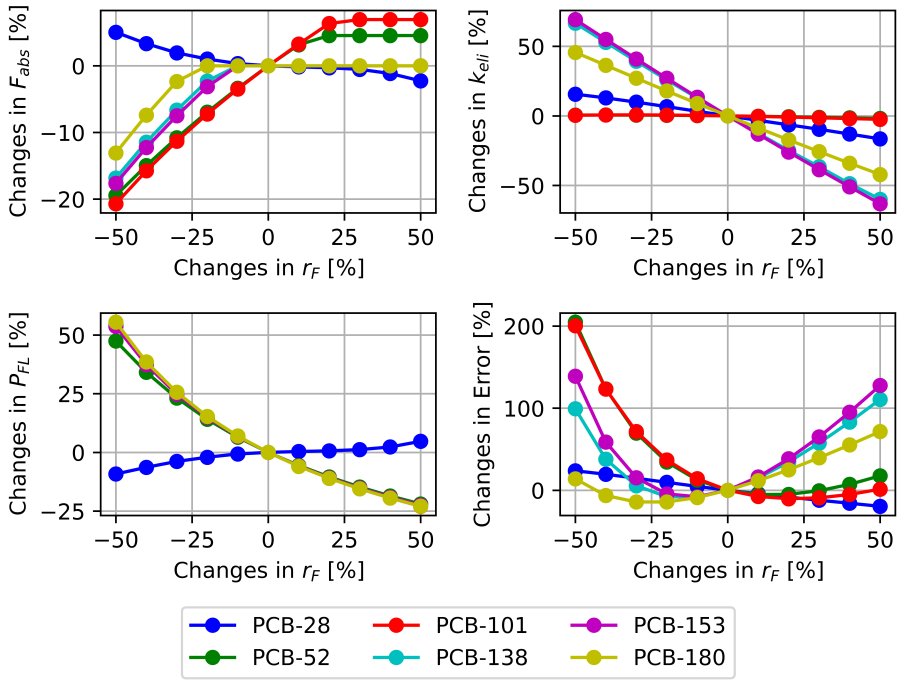

Figure S1: Sensitivity analysis of the model parameters and log square error when varying the fat growth rate r_{Fat} up tp ±50% in intervals of 10%.

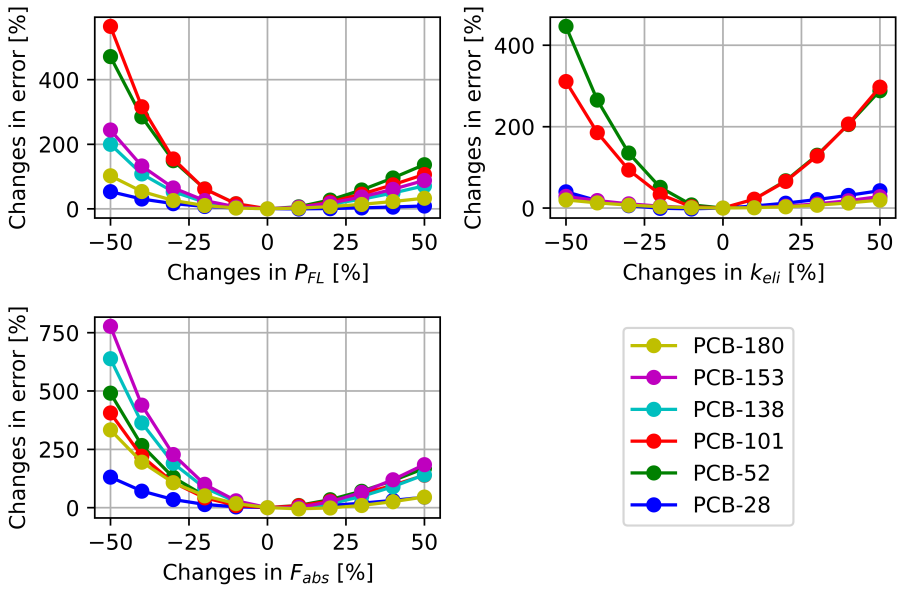

Figure S2: Sensitivity analysis on the log square error when varying only one of the contaminant dependent parameters up to ±50% in intervals of 10%.

4 Animal and feeding data

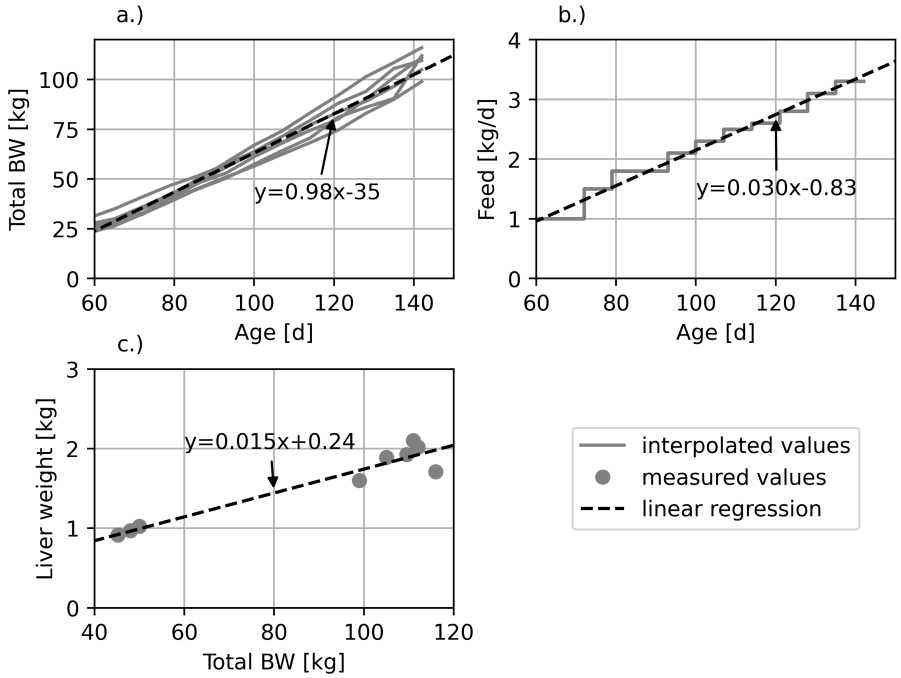

Figure S3: Interpolated values of the total body weight (BW) (a) and daily feed intake (b) (solid grey line) of the pigs as well as the measured weights of the livers (c) (grey dots). The black dashed line represents the estimated linear function for total BW (a), daily feed intake (b) and liver weight (c) of an average pig derived via linear regression.

5 Concentrations in tissues

Table S1: Measured concentration in the liver [μg/kg ww] at the day of slaughter.

Group	PCB-28	PCB-52	PCB-101	PCB-138	PCB-153	PCB-180
Control	7.16E-04	1.98E-03	3.59E-03	6.60E-03	6.00E-03	2.14E-03
Control	1.64E-03	2.53E-03	2.14E-03	7.06E-03	4.33E-03	2.68E-03
Control	1.52E-03	2.20E-03	1.49E-03	5.87E-03	4.14E-03	2.35E-03
Control	8.90E-04	6.18E-03	4.56E-03	1.10E-02	9.21E-03	4.71E-03
Control						
Control	8.24E-04	4.12E-03	4.10E-03	2.49E-02	7.17E-03	6.32E-03
A	1.73E-02	2.38E-01	3.48E-01	9.21E-01	9.74E-01	7.39E-01
A	3.12E-02	2.63E-01	1.98E-01	9.78E-01	1.09E+00	8.37E-01
A	1.63E-02	2.58E-01	2.90E-01	1.07E+00	1.19E+00	9.00E-01
B	5.34E-04	5.26E-03	1.91E-02	1.34E-01	1.54E-01	7.57E-02
B	1.29E-03	1.88E-02	1.07E-02	1.97E-01	2.37E-01	1.07E-01
B	5.76E-04	1.76E-02	2.34E-02	2.30E-01	2.26E-01	1.18E-01
C	2.28E-02	1.25E-01	1.97E-01	5.64E-01	5.10E-01	5.37E-01
C	2.62E-02	1.42E-01	2.15E-01	5.29E-01	5.63E-01	5.83E-01
C	6.15E-03	6.62E-02	7.63E-02	2.55E-01	2.54E-01	2.49E-01

Table S2: Measured concentrations in the muscle [μg/kg fat] at the day of slaughter.

Group	PCB-28	PCB-52	PCB-101	PCB-138	PCB-153	PCB-180
Control	9.99E-03	2.44E-02	4.09E-02	1.44E-01	1.04E-01	6.75E-02
Control	2.81E-02	3.26E-02	3.72E-02	1.39E-01	1.04E-01	6.12E-02
Control	2.01E-02	3.90E-02	3.88E-02	1.79E-01	1.41E-01	1.12E-01
Control	4.16E-02	6.96E-02	7.58E-02	2.09E-01	1.63E-01	1.18E-01
Control						
Control	9.60E-03	4.69E-02	4.77E-02	1.70E-01	1.30E-01	9.68E-02
A	3.05E-01	3.50E+00	7.01E+00	2.12E+01	1.69E+01	1.99E+01
A	4.11E-01	3.37E+00	4.60E+00	1.88E+01	1.56E+01	1.53E+01
A	3.39E-01	3.32E+00	5.79E+00	2.14E+01	1.71E+01	1.68E+01
B	1.37E-02	7.98E-02	4.22E-01	3.76E+00	3.07E+00	3.13E+00
B	1.18E-02	2.25E-01	2.66E-01	5.73E+00	4.73E+00	5.06E+00
B	5.62E-03	1.77E-01	4.03E-01	4.47E+00	3.68E+00	3.82E+00
C	1.62E-01	1.11E+00	1.89E+00	4.42E+00	3.88E+00	3.52E+00
C	1.34E-01	1.16E+00	2.17E+00	5.50E+00	4.41E+00	3.90E+00
C	1.17E-01	8.64E-01	1.48E+00	3.55E+00	2.99E+00	2.83E+00

Paper 5

Engel, A.M., et al., Investigations on the transfer of quinolizidine alkaloids from Lupinus angustifolius into the milk of dairy cows. Journal of Agricultural and Food Chemistry, 2022. **70**(37): p. 11749-11758.

Supporting information

Investigations on the transfer of quinolizidine alkaloids from *Lupinus angustifolius* into the milk of dairy cows

Anna Maria Engel[†], Fenja Klevenhusen[†], Jan-Louis Moenning[†], Jorge Numata[†], Carola Fischer-Tenhagen[‡], Benjamin Sachse[§], Bernd Schäfer[§], Hildburg Fry[†], Oliver Kappenstein[†], Robert Pieper*[†]

[†]German Federal Institute for Risk Assessment, Department Safety in the Food Chain, Max-Dohrn-Strasse 8-10, 10589 Berlin, Germany

[‡]German Federal Institute for Risk Assessment, Department Experimental Toxicology and ZEBET, Alt-Marienfelde 17-21, 12277 Berlin, Germany

[§]German Federal Institute for Risk Assessment, Department Food Safety, Max-Dohrn-Strasse 8-10, 10589 Berlin, Germany

*Email: Robert.Pieper@bfr.bund.de

Table of contents

1 LC-MS/MS Chromatograms

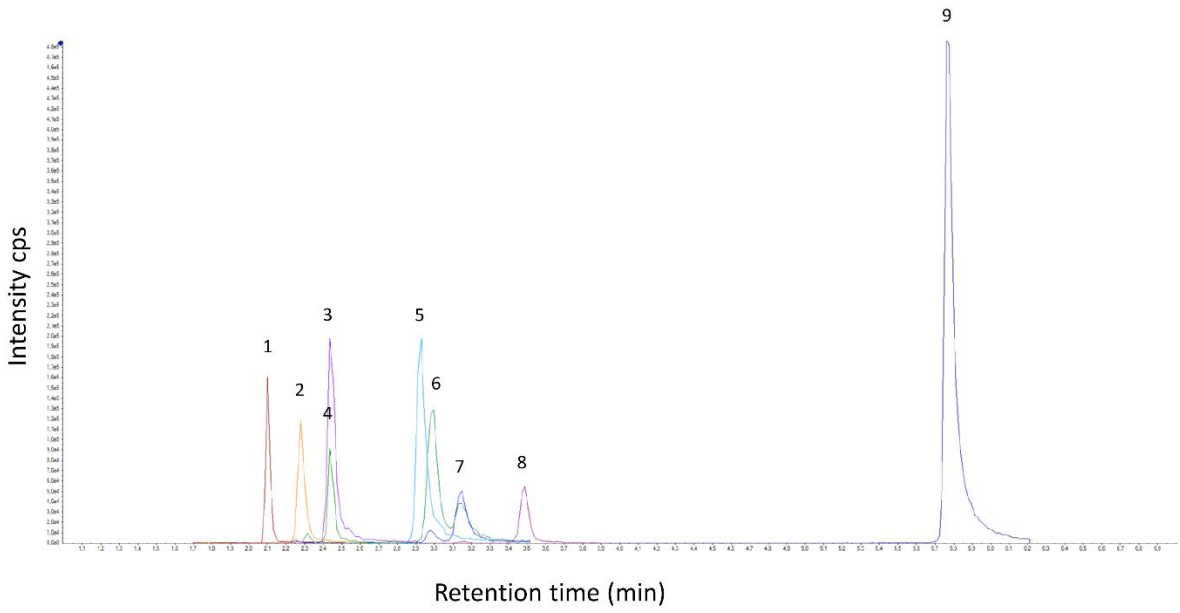

Figure S1. Overlay LC-MS/MS chromatogram of the quantifier MRM transitions of nine QAs in a standard solution with a concentration of 2.5 ng/ml each (1. cytisine (Rt = 2.1 min), 2. lupinine (Rt = 2.3 min), 3. thermopsine (Rt = 2.45 min), 4. 13-hydroxylupanine (Rt = 2.45 min), 5. multiflorine (Rt = 2.95 min), 6. lupanine (Rt = 6.0 min), 7. iso-lupanine (Rt = 3.15 min), 8. angustifoline (Rt = 3.5 min), 9. sparteine (Rt = 5.8 min).

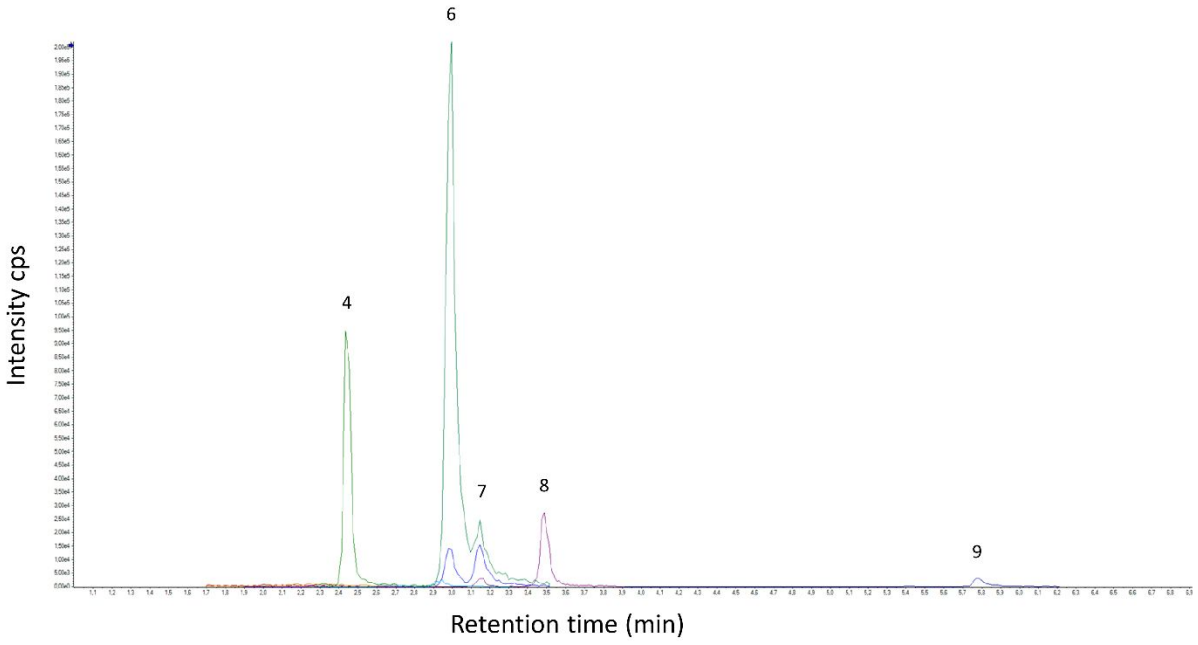

Figure S2. Overlay LC-MS/MS chromatogram of the quantifier MRM transitions of five QAs analysed in lupin seeds (whole grain, untoasted) used for feeding (4. 13-hydroxylupanine 3.6 ng/ml (715 mg/kg), 6. lupanine 3.8 ng/ml (765 mg/kg), 7. iso-lupanine 0.7 ng/ml (140 mg/kg), 8. angustifoline 156 ng/ml (156 mg/kg), 9. sparteine < LOD; Dilution 1:8000).

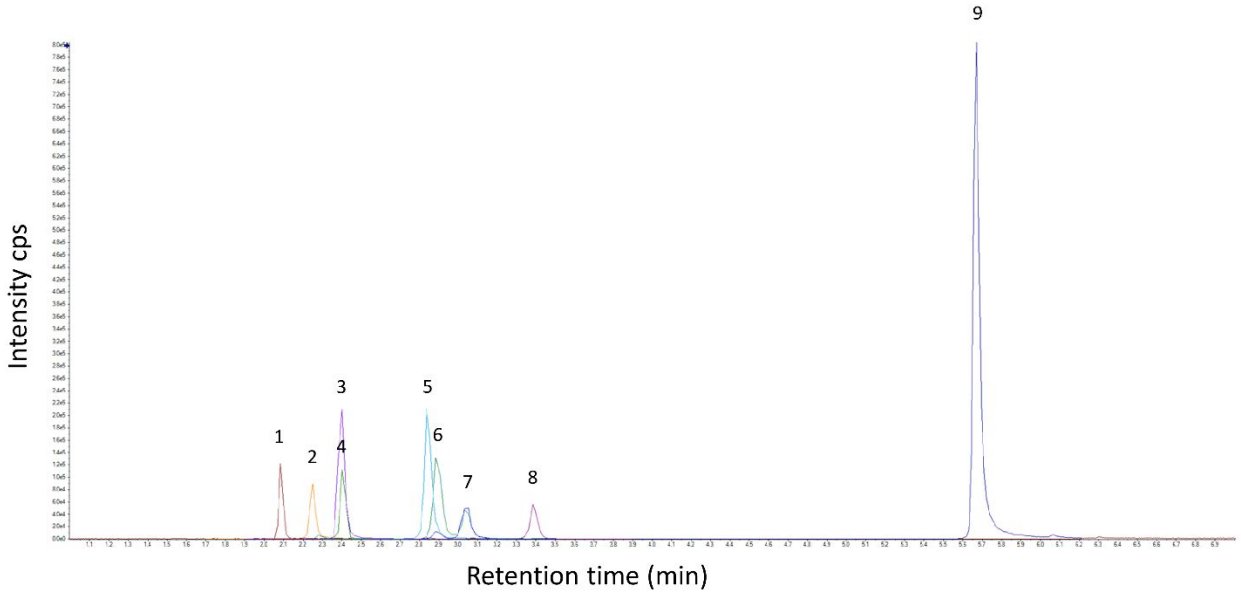

Figure S3. Overlay LC-MS/MS chromatogram of the quantifier MRM transitions of nine QAs in a matrix matched calibration by utilizing cow milk (dilution 1:20) fortified at a level of 2.5 ng/ml (substances and Rt see figure 1).

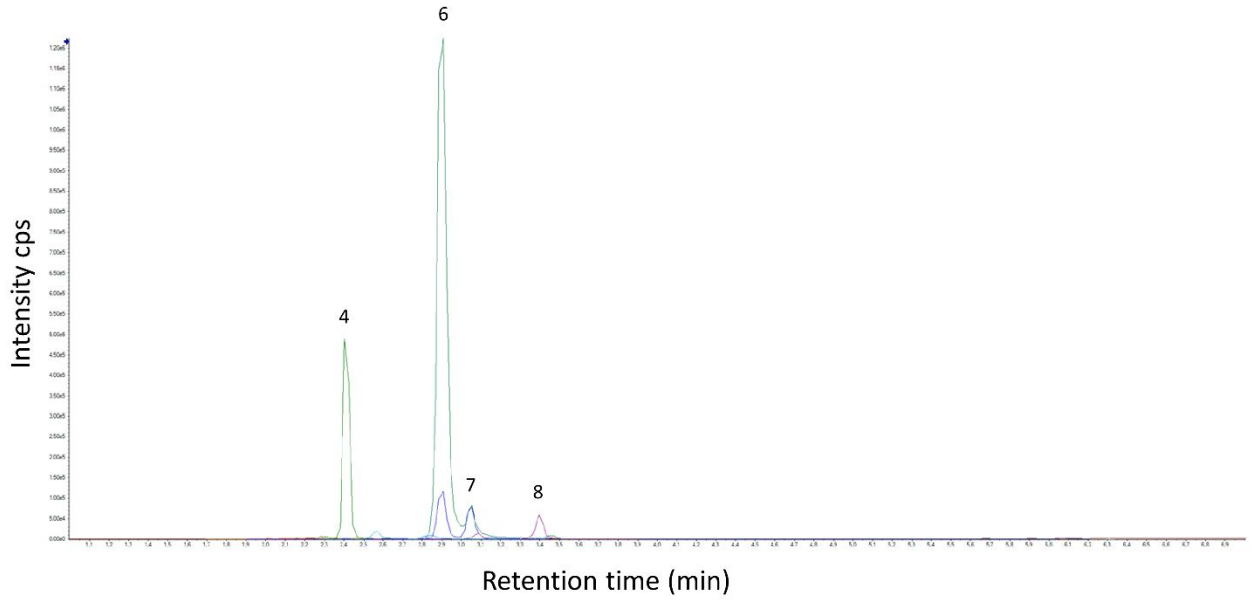

Figure S4. Overlay LC-MS/MS chromatogram of the quantifier MRM transitions of four QAs analysed in a cow milk sample (dilution 1:20) 4. 13-hydroxylupanine and 6. lupanine (both shown QAs are outside of the linear range), 7. iso-lupanine 3.5 ng/ml (117 µg/kg), 8. angustifoline 2.9 ng/ml (97 µg/kg).

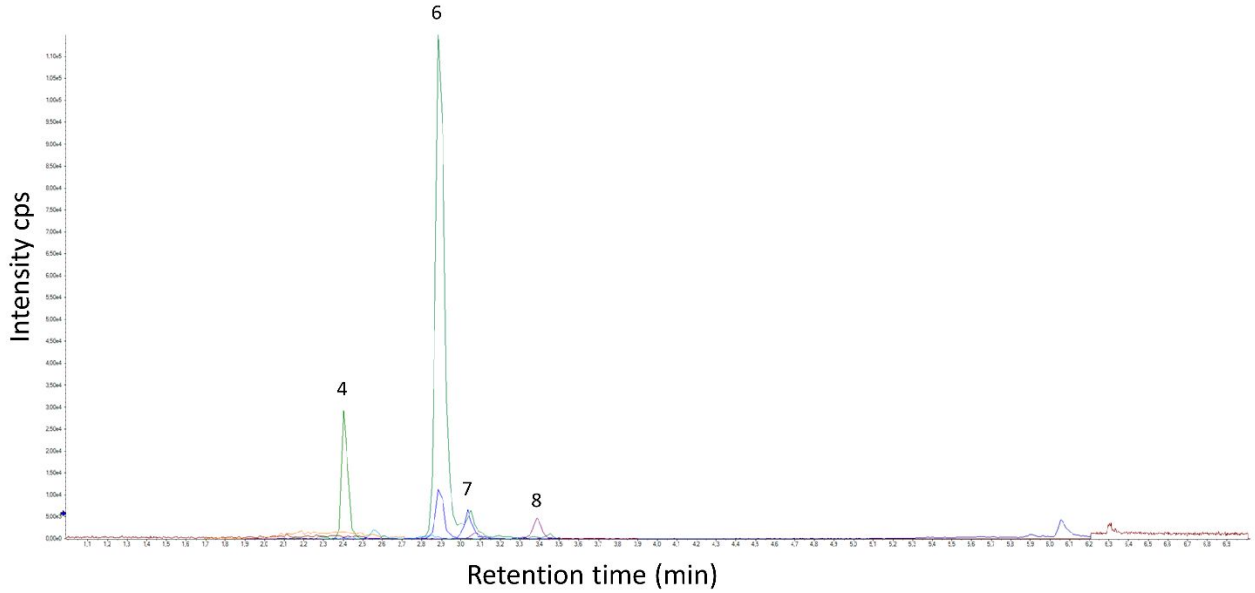

Figure S5. Overlay LC-MS/MS chromatogram of the quantifier MRM transitions of four QAs analysed in a cow milk sample (dilution 1:200) 4. 13-hydroxylupanine 1.2 ng/ml (404 µg/kg), 6. lupanine 1.9 ng/ml (642 µg/kg).

2 Calculations of transfer parameters

2.1 Transfer rates (TR)

The steady state transfer rates were approximated by assuming that a constant feeding period with the same daily intake D[ng/d] (for simplicity D=1 ng/d). Then, the total output via milk at the 100th day M_{100}[ng] was derived via simulating the system until the 100th day, whereupon the transfer rate is given by

$$TR = \frac{M_{100}}{D} 100\% \quad \text{(S1)}$$

2.2 Half-lives

The half-lives of the model are derived analytically. The amount of QA excreted at the n'th morning milk can be described by the following equation

$$X_{n,\,mor} = (\underbrace{e^{M14/24} I_l e^{M10/24} \mathrm{I_l}}_{=:\mathrm{A}})^n X_{0;mor} \tag{S2}$$

for a given starting vector $X_{0;\,\mathrm{mor}}$ at the 0'th morning milk. Here, M is the transition matrix of the PBTK model and I_l is the matrix describing the milking process, i.e.

$$I_l = \begin{pmatrix} 1 & 0 & 0 \\ 0 & 0 & 0 \\ 0 & 0 & 1 \end{pmatrix} \tag{S3}$$

Note that I_l only induces two non-zero eigenvalues (1 with multiplicity 2) and $e^{M14/24}$; $e^{M10/24}$ are both invertible, which is why A induces two non-zero eigenvalues λ_1, λ_2. Assuming $\lambda_1 \neq \lambda_2$, then A can be expressed as

$$A = D \begin{pmatrix} \lambda_1 & 0 & 0 \\ 0 & 0 & 0 \\ 0 & 0 & \lambda_2 \end{pmatrix} D^{-1} \tag{S4}$$

for some invertible matrix D. Furthermore, it follows

$$A^{\mathrm{n}} = D \begin{pmatrix} \lambda_1 & 0 & 0 \\ 0 & 0 & 0 \\ 0 & 0 & \lambda_2 \end{pmatrix}^n D^{-1} \tag{S5}$$

$$= D \begin{pmatrix} e^{ln(\lambda_1)} & 0 & 0 \\ 0 & 0 & 0 \\ 0 & 0 & e^{ln(\lambda_2)} \end{pmatrix}^n D^{-1} \tag{S6}$$

Therefore, the half-lives induced by *A* are given by

$$\tau_\alpha = \frac{\ln(2)}{-\ln(\lambda_1)} \quad \text{(S7)}$$

$$\tau_\beta = \frac{\ln(2)}{-\ln(\lambda_2)} \quad \text{(S8)}$$

Finally, note that the amount in each compartment at the evening milking time of the n'th day can be expressed as follows

$$X_{n,\,eve} = e^{M10/24} I_n X_{n,mor} \quad \text{(S9)}$$

Therefore, morning and evening milk have the same half-lives and

so does the whole milk of the day as

$$X_{n,\,tot} = X_{n,\,mor} + X_{n.\,eve} \quad \text{(S10)}$$

2.3 Relative transition amount (RTA)

The relative transition amount describes the amount relative to a steady state at which the decay (starting from steady state) of the amount of QA excreted with milk is better described by the τ_β rather than the τ_α. The decay is described by a biexponential function (except for the first day), i.e.,

$$A(t) = C_1 e^{\lambda_1 t} + C_2 e^{\lambda_2 t} \quad \text{(S11)}$$

Note that A(t) is the continuous expansion of the QA excretion function, as this only makes sense in a discrete setting, i.e., $A|_{\mathbb{N}}(t) = \pi_{Udder}(X_{t;tot})$ with π_{Udder} being the projection onto the udder compartment. The time point at which this happens can be expressed by $\tilde{t}$

$$\frac{d}{dt} C_1 e^{\lambda_1 t}\big|_{t\,=\,\tilde{t}} = \frac{d}{dt} C_2 e^{\lambda_2 t}\big|_{t\,=\,\tilde{t}} \quad \text{(S12)}$$

$$\Leftrightarrow \lambda_1 C_1 e^{\lambda_1 \tilde{t}} = \lambda_2 C_2 e^{\lambda_2 \tilde{t}} \quad \text{(S13)}$$

$$\Leftrightarrow \tilde{t} = \frac{ln\left(\frac{\lambda_1 C_1}{\lambda_2 C_2}\right)}{\lambda_2 - \lambda_1} \quad \text{(S14)}$$

Thus, knowing the half-lives (section 1.2), only C_1; C_2 are unknown. To derive these, the function A(t) is solved for two different time points, i.e. for simplicity t0 = 0 and t10=10. This can be done by simulating the 101th and the 111th day assuming a 100 day feeding period. Note that the 101st day is chosen as the start of A instead of the 100th, due to the partial influence of the feeding on the decay of the first day of the depuration phase. Then C_1 and C_2 can be calculated as follows

$$C_1 = A(0) - C_2 \tag{S15}$$

$$C_2 = \frac{A(10) - A(0)e^{\lambda_1 10}}{e^{\lambda_2 10} - e^{\lambda_1 10}} \tag{S16}$$

Together with equations (S11) and (S14), the amounts at the transition time can now be calculated. Then the relative transition amount (RTA) is given by

$$RTA = \frac{A(\tilde{t})}{A_{ss}} 100\% \tag{S17}$$

where A_{ss} are the amounts excreted during steady state.

3 Transfer parameters

Table S1. α-half-lives τ_α of the simulated QA. The mean value was derived via fitting the model to the four experimental cows and the confidence interval (α=0.05) was derived using the delete-one jackknife method.

	Mean (d)	95% confidence interval (d)
Hydroxylupanine	0.28	0.26 - 0.31
Lupanine	0.26	0.25 - 0.28
Isolupanine	0.26	0.23 - 0.29
Angustifoline	0.27	0.24 - 0.29

Table S2. *β*-half-lives τ_β of the simulated QAs. The mean value was derived via fitting the model to all four cows and the confidence interval (α=0.05) was derived using the delete-one jackknife method.

	Mean (d)	95% confidence interval (d)
Hydroxylupanine	3.51	2.66 – 5.41
Lupanine	3.04	2.00 – 5.93
Isolupanine	2.48	2.17 – 2.95
Angustifoline	5.18	2.85 – 25.79

Table S3. The relative transition amount from alpha into beta phase of the simulated QA. The mean value was derived via fitting the model to all four cows and the confidence interval (α=0.05) was derived using the delete-one jackknife method.

	Mean (%)	95% confidence Interval (%)
Hydroxylupanine	0.14	0.11 - 0.17
Lupanine	0.11	0.01 - 0.17
Isolupanine	0.34	0.19 - 048
Angustifoline	0.14	0.10 – 0.18

4 Complete toxicokinetic model

The PBTK model (Fig 2) between milking events can be described by a linear equation system of the form

$$\dot{\boldsymbol{A}}(t) = \boldsymbol{MA}(t) + \boldsymbol{I}(t) \tag{S18}$$

where M is the transition Matrix given by

$$\mathbf{M} = \begin{pmatrix} -(k_{CP} + k_{CU} + k_{CE}) & k_{UC} & k_{PC} \\ k_{CU} & -k_{UC} & 0 \\ k_{CP} & 0 & -k_{PC} \end{pmatrix}. \tag{S19}$$

Here the model parameters k_{ij} represent the transition rates from compartment i to compartment j for the following compartments: i,j=C, Central; i,j=P, Peripheral; i,j=U , Milk

and i,j=E, Eliminated (conceptually lumping any metabolization and excretion). Alternatively, the same model can be written as the system of differential equations

$$\dot{A}_C(t) = -(k_{CP} + k_{CU} + k_{CE})A_C(t) + k_{UC}A_U(t) + k_{PC}A_P(t) \quad \text{(S20)}$$

$$\dot{A}_U(t) = k_{CU}A_C(t) - k_{UC}A_U(t) \quad \text{(S21)}$$

$$\dot{A}_P(t) = k_{CP}A_C(t) - k_{PC}A_P(t) \quad \text{(S22)}$$

4.1 Periodic milking

The last piece of the model is the implementation of the periodic milking or emptying of the udder at each milking time, which is calculated algorithmically as follows:

$X = (0,0,0)^T$ #Initialization

MilkList=[] #Intialzing the array containing the milk data

for i=0:numberOfExperimentHours-1:

if [i,i+1] is feeding time:

$I=(\frac{daily\ dose}{10},0,0)^T$

else:

$I=(0,0,0)^T$

$x^* = -M^{-1}I$

$X = x^* + e^M(X - x^*)$

if i+1 is milking time:

MilkList.append(X["Udder"])

$X = I_l X$

Here MilkList contains the QA amount excreted at each milking time, thereby alternating between morning and evening milk. The feeding times and milking times follow the experimental schedule for fitting the data, and can be fixed for a predictive model for the

general case. The total QA amount excreted per day can be calculated by adding the amounts for morning and evening milking, as is done for the predictive model included as code. The best-fit values for the model parameters in eq S19 are reproduced in Table S4.

Table S4. Optimized model parameters k_{ij} for each of the modeled QAs.

	k_{CP} (1/d)	k_{PC} (1/d)	k_{CU} (1/d)	k_{UC} (1/d)	k_{CE} (1/d)
Hydroxylupanine	$5.40*10^{-3}$	$2.00*10^{-1}$	$6.57*10^{-2}$	1.69	2.41
Lupanine	$4.87*10^{-3}$	$2.28*10^{-1}$	$2.24*10^{-1}$	6.25	2.61
Isolupanine	$1.44*10^{-2}$	$2.81*10^{-1}$	$2.87*10^{-1}$	6.12	2.67
Angustifoline	$4.65*10^{-3}$	$1.34*10^{-1}$	$1.05*10^{-1}$	6.59	2.59

5 Semilogarithmic plot to show biphasic behavior during depuration

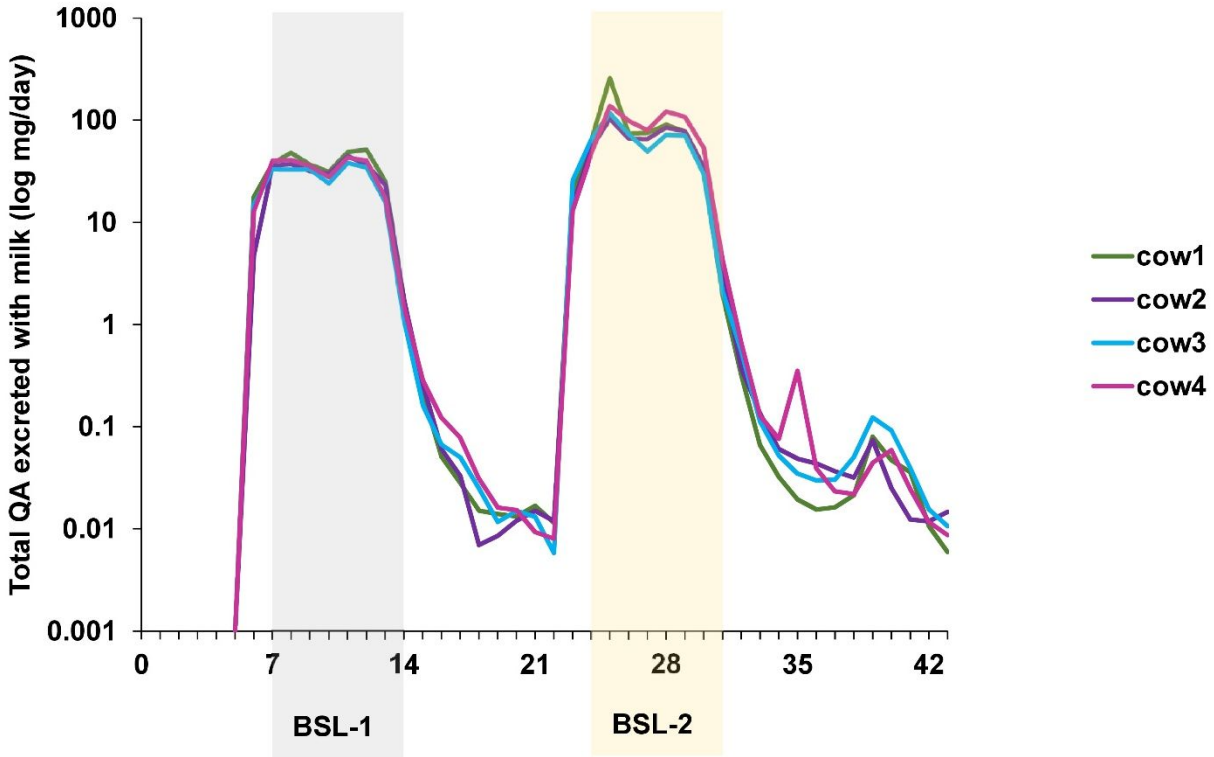

Figure S6. Logarithmic plot of total QA excreted with milk daily in mg/d. The depuration periods following BSL–1 (blue sweet lupine 1 kg/d) and BSL–2 (blue sweet lupine 2 kg/d) show a biphasic behavior: an initial fast α-phase and a later slow β-phase.

Acknowledgments

I would like to take this opportunity to thank all the people who have supported me during my Ph.D. studies. First and foremost, I would like to express my sincere gratitude to my supervisor, Dr. Jorge Numata, for his constant guidance, motivation and stimulating discussions. His encouragement and mentorship have been of immense importance to my scientific development. I would also like to thank Prof. Dr. Max von Kleist for accepting and supporting me as a Ph.D. student at the Institute of Bioinformatics at the Free University of Berlin.

I am also very grateful to Dr. Robert Pieper, the head of my department, who has always supported me and given me the opportunity to pursue my research goals. In addition, I owe special thanks to Dr. Kirsten Schulz and Dr. Torsten Krause for their invaluable advice and support throughout the development of this thesis. I would also like to extend my gratitude to Daria Savvateeva for her constant willingness to discuss toxicokinetic issues with me. Furthermore, I want to sincerely thank Dr. Hans Mielke for insightful discussions on mathematical modelling and statistics, and for sharing his valuable opinions on my work and Dr. Matthew Salewski for helpful discussions on model implementation.

I am incredibly grateful for the support of my colleagues in the department, who have helped me to gain a better understanding of farm animal physiology and nutrition, topics about which I previously had limited knowledge.

The collegial atmosphere, especially during our enlightening lunchtime discussions, made this work enjoyable.

Many thanks also to my friends outside the office for counterbalancing the scientific efforts.

Finally, I would like to thank my parents for always supporting me and believing in me, even in the most difficult times.

Zusammenfassung

Im Rahmen dieser kumulativen Dissertation wurden physiologisch-basierte toxikokinetische (PBTK) Modelle erstellt, die zur Vorhersage der Konzentration spezifischer Kontaminanten in Lebensmitteln tierischen Ursprungs auf der Grundlage der Konzentration im Futter verwendet werden können, um die Risikobewertung zu unterstützen. Der erste Teil der Dissertation befasst sich mit dem Transfer von Dioxinen (polychlorierte Dibenzo-*p*-Dioxine (PCDDs) und Dibenzofurane (PCDFs)), sowie polychlorierten Biphenylen (PCBs) in die Milch von Kühen. Zuerst wurde ein Literaturreview durchgeführt um einen Überblick über den aktuellen Stand der Forschung zu bekommen. Dabei zeigte sich, dass zwar viele Modellierungsansätze existieren, diese aber oft nur auf eingeschränkten Datensätze beruhen. Im Rahmen dieser Arbeit wurden zwei Modelle erstellt, die auf komplexere Datensätze basieren und valide Vorhersagen ermöglichen. Das erste Modell wurde von Daten aus einem PCB-Kontaminationsfall abgeleitet und beschreibt den Verbleib von drei nicht-dioxinähnlichen (ndl) PCBs in verschiedenen Geweben und der Milch einer erwachsenen Kuh während zweier Laktationen und einer Trockenperiode, sowie in ihrem Kalb. Hierbei konnte auch zwischen dem Transfer via Milch und Plazenta in das Kalb unterschieden werden. Es zeigte sich, dass 10-14 % der Menge an Kongenere in den Kälbern bei der Schlachtung auf den plazentaren Transfer zurückzuführen sind. Das zweite entwickelte Modell basiert auf einer Fütterungsstudie, in der Kühe in unterschiedlich metabolischen Phasen (positive und negative Energiebilanz) mit einem Gemisch aus Dioxinen und PCBs dosiert wurden. Damit konnten die Konzentrations-Zeit-Profile der einzelnen untersuchten Kongenere in Milch und Blut valide vorhersagt werden. Ein Vergleich der Parameter aus den unterschiedlichen metabolischen Phasen ergab, dass insbesondere die Transferrate in der positiven Energiebilanzphase signifikant erhöht war. Im zweiten Teil der Doktorarbeit wurden die Erkenntnisse aus den vorangegangenen Modellierungsansätzen mit Dioxinen und PCB genutzt, um ein Modell für den Transfer in Mastschweinen zu entwickeln. Besonders im Vordergrund standen hier die für den die Verbraucher relevanten Gewebe Leber und Muskelfleisch (auf Basis von Fett). Es wurden verschiedene Transferparameter abgeleitet, wie z.B. eine modifizierte Version der Transferrate, die das Ausmaß des Transfers dieser Schadstoffe in diese Gewebe unter realistisch wechselnden Fütterungsbedingungen und dem Wachstum der Tiere ermöglicht. Die niedrigste Transferrate zeigte PCB-28 mit 9,57%, die höchste PCB-153 mit 77,2%.

Im letzten Teil dieser hier vorliegenden Arbeit wurde auf Grundlage einer Fütterungsstudie an Milchkühen der Transfer von Chinolizidin-Alkaloide (QAs) aus Lupinen in die Milch untersucht. Es wurde ein Modell entwickelt, das den Transfer der QAs in Milch gut beschreibt. Auch hier wurden mehrere Parameter zur Risikobewertung abgeleitet, darunter Transferraten und α-Halbwertszeiten. Die niedrigste Transferrate wurde für Angustifolin (1.05%) errechnet, die höchste für Isolupanin (2,92 %). Die α-Halbwertszeiten liegen alle im engen Bereich von 0,26 d (Lupanin) bis 0,28 d (Hydroxylupanin). Eine Untersuchung zur Dosisabhängigkeit lieferte kein eindeutiges Ergebnis.

Selbstständigkeitserklärung

Hiermit versichere ich, dass ich die vorliegende Arbeit selbstständig verfasst habe und alle dabei verwendeten Hilfsmittel und Quellen angegeben habe. Geistiges Eigentum anderer Autoren wurde als entsprechend gekennzeichnet. Ebenso versichere ich, dass ich an keiner anderen Stelle ein Prüfungsverfahren beantragt bzw. die Dissertation in dieser oder anderer Form an keiner anderen Fakultät als Dissertation vorgelegt habe.

Berlin, 30.01.2024